Final Report to the Earthquake Commission

on Project 60PR/1A-"Evaluating New Zealand models for short-term earthquake probability".

Thessa Tormann, Martha K. Savage and Mark Stirling

11 January 2007

LAYMAN'S ABSTRACT

The possibility that a moderate earthquake may be followed by a larger one (foreshock probability) increases the hazard in its immediate vicinity for a short time by an order of magnitude or more. Similarly, damaging aftershocks often occur after large events. Yet previously, these fluctuations in hazard have not been included in the New Zealand seismic hazard model.

We combine the current average background New Zealand seismic hazard model with a new model for foreshock probability and an established model of aftershock probability to create a dynamic seismic hazard model for New Zealand. This model calculates the chances of a damaging earthquake with peak ground acceleration over 0.05g, and changes daily to reflect the increased or decreased hazards depending on recent events.

We develop a method to test these ground motion forecasts against 40 years of strong motion observations in New Zealand. The standard background model underestimates the hazard at 0.05g level for the time period and locations in the dataset by a factor of two. The new dynamic seismic hazard model provides a closer match to the strong motion records, but with some overestimation (factor of three) of hazard on days of high probability and underestimation (factor of six) on days of low probability forecasts.

TECHNICAL ABSTRACT

A new dynamic seismic hazard model for New Zealand is created to add the effects of short-term hazard fluctuations due to earthquake triggering to the current Poissonian probability from the national probabilistic seismic hazard model.

Prospective foreshock probability decay is modeled as a function of origin time and epicentral distance from the potential foreshock, and the magnitude difference between foreshock-mainshock pairs. We calculate the probability of an initial earthquake (a foreshock) being followed by a mainshock in New Zealand, considering the parameters of elapsed time and distance and magnitude differences between foreshock and mainshock. We use non-aftershock events between 1964 and 2003, with magnitude ≥ 3.8 and shallower than 40 km, separating the catalogue into events within and outside the Taupo Volcanic Zone (TVZ). We provide a model for the probability P' that at time t after a potential foreshock of magnitude Mfs, and at distance r, a mainshock with magnitude Mfs+δM will occur:

$$P'(t,r,\delta M) = P(t=1,r=10,\delta M=0) * 10(-B*\delta M) * 1/(t+ct)texp * 10rexp/(r+cr)rexp$$

We find (1) foreshock probabilities are independent of foreshock magnitude, (2) foreshock probabilities decrease with increasing inter-event time with texp significantly larger than one (2.5±0.5 (TVZ) and 1.7±0.2 elsewhere), (3) foreshock probabilities decrease with increasing epicentral distance with rexp of 2.6±0.2 (non-TVZ) and 3.66±0.2 (TVZ) and (4) the mainshock magnitude distribution follows the Gutenberg-Richter relationship with a significantly higher than normal b-value (B=1.4±0.1 (Non-TVZ) and 1.8±0.2 (TVZ)).

The behaviour of these foreshock probabilities with time and distance differs from the behaviour of aftershock probabilities as modeled by previous workers, suggesting that there may be a different triggering mechanism for foreshocks than for aftershocks.

Combining a previous, similar foreshock model with a generic aftershock model, fluctuating daily hazard maps for New Zealand are calculated, showing the regional probability distribution for peak ground accelerations of 0.05g or more being observed.

A methodology has been developed to test these ground motion forecasts against 40 years of strong motion observations in New Zealand. The Poissonian model underestimates the hazard at 0.05g level for the time period and locations in the dataset by a factor of two. The new dynamic seismic hazard model provides a closer match to the strong motion records, but with some overestimation (factor of three) of hazard on days of high probability and underestimation (factor of six) on days of low probability forecasts.

Contents:

Publications relating to this project:

Please note: Thessa Tormann changed her name from Thessa Rudolf when she got married in 2004.

Masters' thesis:

Tormann, Thessa. Dynamic seismic hazard model for New Zealand, submitted February 2005, 238 pp.

Submitted Article:

Tormann, Thessa, Martha Kane Savage, Mark Williamson Stirling, Time, distance and magnitude dependent foreshock probability model for New Zealand, submitted to Bulletin of the Seismological Society of America, September 2006.

Abstracts:

T. Tormann, M. K. Savage, M. W. Stirling, A. Christophersen, and J. Zhuang , Time, distance and magnitude dependence of foreshocks in New Zealand, to be presented at New Zealand Geophysical Society/GEOLOGICAL SOCIETY OF NEW ZEALAND 36th ANNUAL CONFERENCE, Massey University, Palmerston North New Zealand, 4-7 December 2006, abstract, Geological Society of New Zealand Miscellaneous Publication 122 A ISBN N0 0-908678-05-3, p. 87.

Tormann T, Savage M K, Stirling M, Dynamic Seismic Hazard Model of New Zealand, European Geophysical Union presentation, Vienna, Austria, EGU05-A-08890, 2005.

Tormann T, Savage M K, Stirling M, Dynamic Seismic Hazard Model for New Zealand, Eos Trans. AGU, 85(47), Fall Meet. Suppl., Abstract S13A-1029, 2004.

Other presentations: Tormann, T. MSc presentation, Dynamic Seismic Hazard Model for New Zealand, presented at Victoria University of Wellington, December 2004.

Time, distance and magnitude dependent foreshock probability model for New Zealand

by

Thessa Tormann, VUW, now at ETH Zurich, thessa.tormann@sed.ethz.ch

Martha Kane Savage, VUW, Martha.Savage@vuw.ac.nz

Mark Williamson Stirling, GNS, m.stirling@gns.cri.nz

Abstract

The possibility that a moderate earthquake may be followed by a larger one (foreshock probability) increases the hazard in its immediate vicinity for a short time by an order of magnitude or more. Thus, foreshock probabilities are of interest for time dependent seismic hazard forecasts. We calculate the probability of an initial earthquake (a foreshock) being followed by a mainshock in New Zealand, considering the parameters of elapsed time and distance and magnitude differences between foreshock and mainshock. We use non-aftershock events between 1964 and 2003, with magnitude ≥ 3.8 and shallower than 40 km, separating the catalogue into events within and outside the Taupo Volcanic Zone (TVZ). We provide a model for the probability P' that at time t after a potential foreshock of magnitude Mfs, and at distance r, a mainshock with magnitude Mfs+δM will occur:

$$P'(t,r,\delta M) = P(t=1,r=10,\delta M=0) * 10^{(-B*\delta M)} * 1/(t+ct)^{texp} * 10^{rexp}/(r+cr)^{rexp}$$

We find (1) foreshock probabilities are independent of foreshock magnitude, (2) foreshock probabilities decrease with increasing inter-event time with texp significantly larger than one (2.5±0.5 (TVZ) and 1.7±0.2 elsewhere), (3) foreshock probabilities decrease with increasing epicentral distance with rexp of 2.6±0.2 (non-TVZ) and 3.66±0.2 (TVZ) and (4) the mainshock magnitude distribution follows the

Gutenberg-Richter relationship with a significantly higher than normal b-value (B=1.4±0.1 (Non-TVZ) and 1.8±0.2 (TVZ)).

The behaviour of these foreshock probabilities with time and distance differs from the behaviour of aftershock probabilities as modeled by previous workers, suggesting that there may be a different triggering mechanism for foreshocks than for aftershocks.

Introduction

Located on a plate boundary with complex tectonic setting, New Zealand experiences frequent moderate sized earthquakes (Fig. 1a). As the analysis of "linked events" (e.g. foreshocks-mainshocks-aftershocks, stress triggering) is of increasing interest for the development of time dependent seismic hazard forecasting methodologies, this paper addresses the questions of how the probabilities for future larger events vary with increasing time and distance from the potential foreshock, as well as probability dependence on foreshock magnitude and magnitude differences between foreshock and mainshock. We develop equations that allow calculation of the probability for a mainshock of a certain magnitude at a certain time after, and distance from, a potential foreshock. We show that the rates of decay of foreshock probability with time and space are more rapid in New Zealand than in other regions of the world.

Previous Studies

Jones (1985) was the first author to investigate prospective foreshock probabilities, i.e. the probability that an event might be followed by an equal or larger event within a certain time and space window. Jones studied the Southern Californian catalogue and found that 6±0.5% of $M \geq 3$ events are followed by an equal or larger event within 5 days and 30 km, i.e. qualify as foreshocks.

Applying Jones' empirical technique, Savage and DePolo (1993) obtained similar results for Eastern California and Western Nevada. With slightly changed windows of 5 days and 10 km search radius they found the same 6% chance for a $M \geq 3$ event to be followed by an equal or larger one in the Nevada region. For the volcanic Mammoth/Mono region the probabilities reach 10%.

Reasenberg (1999) used a time window of 10 days and an epicentral search radius of 75 km for the analysis of global foreshock probabilities in two worldwide catalogues. He observed worldwide probabilities that are about twice as high as the Californian values from Jones' generic model. He also found a significant dependency of foreshock probabilities on the mainshock's focal mechanism, thrust earthquakes being the most frequent to have foreshocks.

Ogata et al. (1994) and Maeda (1996) considered relationships between foreshock clusters and significantly larger mainshocks as a function of magnitude, temporal and spatial distribution in the cluster.

Jones et al. (1999) suggested and tested the hypothesis that foreshocks might be mainshocks whose aftershocks happen to be big and therefore could be modeled and predicted using aftershock relationships. The authors concluded that no separate mechanism is needed to explain foreshock-mainshock sequences. However, for the analysed Italian catalogue (1975-1996), the fraction of earthquakes that triggered larger events (6%) was only half of the prediction based on aftershock rates (11%). Similarly, for the Southern Californian catalogue the aftershock rates predict 10.5% of events with larger earthquakes following them, while the actual foreshock probability is only 6%.

Felzer et al. (2004) analysed the global CMT and NEIC catalogues as well as the local Californian CNSS catalogue to argue that one single physical triggering mechanism can explain the occurrence of foreshocks, aftershocks and multiplets, i.e. clusters of earthquakes are the result of an initial earthquake triggering subsequent ones, and the magnitude of the triggering earthquake is independent of the magnitude of the triggered events. They found that the number of foreshock and multiplets observations is a fixed fraction of the number of aftershock observations as estimated by the Gutenberg-Richter relationship with b=1. The Gutenberg-Richter relation (1944) is given by $\log10(N) = a-bM$, where N is the cumulative number of earthquakes equal to or greater than magnitude M and the productivity rate a and slope b are constants.

The two most recent foreshock probability studies of New Zealand data were carried out by (1) Savage and Rupp (2000) who applied Jones' and Savage and DePolo's methodology (with windows of 5 days and 30 km) and obtained average foreshock probabilities for $M \geq 5$ earthquakes of 4.5±0.4% and (2) Merrifield et al. (2004) who used the same windows and analysed regional differences in foreshock probability for $M \geq 4$ events. Merrifield et al. (2004) found that the Taupo Volcanic Zone (TVZ) shows a significantly higher foreshock probability (9.6±1.7%) than the rest of New Zealand (6.3±0.47%). The TVZ, sometimes called the Central Volcanic Region, is a region of high heat flow and volcanism that is interpreted as back-arc extension that represents the southern end of the Lau-Havre Trough (e.g., Stern et al. (2006)) (Fig.1a).

Data & Methodology

The foreshock probabilities are calculated from the $M \geq 3.8$ and shallower than 40 km non-aftershock events between 1964 and 2003 from the New Zealand earthquake catalogue available from the GeoNet websites

(www.geonet.org.nz). According to Smith (1981) the catalogue is complete to magnitude 4.0; referring to Figure 1b, which shows the frequency magnitude plot for M≥3, we feel comfortable using all events with M≥3.8.

Declustering the catalogue is a necessary step as otherwise pairs from within aftershock sequences could match the searching criteria and artificially increase the foreshock probability values considerably (e.g. Jones (1985)). We use the Gardner & Knopoff (1974) algorithm with time and distance windows modified for New Zealand, as published by Savage and Rupp (2000). The algorithm applies simple, magnitude-dependent windows in time and space to remove aftershocks from the catalogue. The catalogue is examined in chronological order, and after each event, any further event of smaller magnitude within the appropriate distance and time window is removed from the catalogue. Equal or larger events will be left in the catalogue, and will begin their own search windows.

Examining the declustered catalogue in chronological order, we count all earthquakes that have been followed by an equal or bigger one on the first day, on the second, on the third, etc., to the 5^{th} day, and within 10 km epicentral distance, 10-20 km, and so on to 40-50 km. We do not treat multiple foreshock sequences separately, so we include a maximum of one foreshock per mainshock.

We modify the probability calculations first proposed by Jones (1985) by using the beta distribution (e.g. Mendenhall et al. (1994)). This distribution is useful in statistical analyses because it avoids zero probability values when no observations are made. If N is the number of earthquakes tested (potential foreshocks) and n is the number of events that qualified as foreshocks, we calculate the foreshock probability as:

$$P = (\alpha+n)/(\alpha+\beta+N)$$

where $\alpha=0.05$ and $\beta=0.95$. This choice of parameters guarantees a positive minimum value in the case of n=0, and, for n>0, calculates probabilities P that agree to at least three decimal places with straightforwardly calculated probabilities P*=n/N. The standard deviation σ is given by

$$\sigma = (((\alpha+n)*(\beta-n+N))/((\alpha+\beta+N)^2*(\alpha+\beta+N+1)))^{0.5}$$

We analyse the foreshock probabilities as a function of (1) foreshock magnitude – testing only potential foreshocks of a certain magnitude bin at a time and comparing the results for different foreshock magnitude bins, (2) mainshock magnitude – what are the chances for same sized mainshocks, 0.1 magnitude units larger, 0.2, etc. up to 2.0 units of magnitudes between foreshock and mainshock, (3) time between foreshock and mainshock – testing how the probabilities decrease with increasing time on a daily basis and (4) epicentral distance between foreshock and mainshock – testing how much more likely events follow in the direct vicinity of the foreshock compared to greater distances.

Because Merrifield et al. (2004) find differences in foreshock probabilities between seismicity in the TVZ and outside, we treat the subcatalogue of potential foreshocks located in the TVZ separately. We define earthquakes to be in the TVZ if their epicenters lie in the triangle between (longitude/latitude) points (175.85 / -37.0), (175.55 / -39.29), and (177.4 / -37.5).

To allow for enough events for statistical analysis, we bin the data in several ways. In time, we consider integer days after the foreshock time. We start the count at the exact foreshock time (e.g., if the event occurred at 09:13 UT on day 247, the first time interval ends at 09:12:59 on day 248). In space, we consider rings of 10 km radius. To account for the fact that the area increases with the radius of the ring, we consider spatial probabilities in terms of the number of events per unit area. In magnitude, we consider bins of 0.1 magnitude unit. We display the foreshock probabilities as a function of time and epicentral distance in the middle of each bin and as a function of mainshock magnitude at the edge of the bin (tenth of units of magnitude) (Figures 3-5).

We fit the data points using nonlinear regression (software from www.graphpad.com) for a least squares fit to equations that have been used in previous foreshock calculations. We use the Gutenberg-Richter relation (1944) for the mainshock magnitude dependence, the modified Omori law (Utsu (1995)) for temporal decay, and consider spatial decay as a power law decay. Two sets of parameters are determined, applicable for TVZ and non-TVZ seismicity.

Results

The initial catalogue had 13,087 events, reduced to 3474 when the aftershocks were removed. In the remaining, declustered catalogue, 187 are located in the TVZ, 42 of which are identified as foreshocks. Out

of the 3287 events outside the TVZ, 222 are followed by bigger events close in time and space. This translates into an overall 6.7±0.4% foreshock probability for non-TVZ events, which is a close reproduction of Merrifield et al.'s (2004) results, and a 22±3% probability for TVZ events, which is about twice the value that Merrifield et al. (2004) determined. The difference can be explained by the different definitions of TVZ seismicity used in the two studies: we cut the New Zealand catalogue into two parts, the TVZ subcatalogue and the rest of the country. To reduce boundary effects, we only require the foreshock to be situated within the borders of the TVZ. We then search for all events in the New Zealand earthquake catalogue that fulfill the foreshock-mainshock search criteria. Merrifield et al. (2004) analyse the New Zealand earthquake catalogue by using a lattice of 0.1 degree spacing and for each knot searching for foreshock-mainshock pairs within a circle of 100 km radius. As the TVZ is only about up to 50 km wide and 250 km long, nearly all lattice points within that area are assigned probability values dominated by outside TVZ activity, smearing the high values from within the zone.

Foreshock magnitude dependence

The analysis of foreshock probabilities for different foreshock magnitude bins shows no significant differences for smaller or larger initial events (Tables 1 and 2). Note that the bins are not used to determine whether an event is a foreshock. Mainshocks are still required to have magnitude equal or higher than the "true" foreshock. E.g., bin 4.0 includes foreshocks of magnitudes 3.8 to 4.2, but a magnitude 4.1 event is only considered a foreshock to a magnitude 4.1 or higher event.

Mainshock magnitude dependence

Plotted on a logarithmic scale the cumulative observed probabilities for different magnitude differences show a remarkably linear decay up to magnitude differences of 1.8 units (Non-TVZ) and 1 unit (TVZ) (above there is not enough data to consider the change of slope to be significant) (Fig. 2). The linear decay suggests that the magnitude distribution of foreshock-mainshock pairs may be similar to the Gutenberg-Richter relation (1944): log10(N) = a-bM, where N is the cumulative number of earthquakes equal to or greater than magnitude M and the productivity rate a and slope b are constants. Accordingly, the data can be fitted through a function of the type:

$$P'(\delta mag) = 10^{A-B*(Mfs+\delta mag)}$$

where δmag is the difference in magnitude between the foreshock and the subsequent mainshock. A can be calculated by taking the observed probability for δmag=0, i.e. the probability for same sized mainshocks within 5 days and 50km radius, which has been calculated from the catalogue (0.019 for Non-TVZ and 0.075 for TVZ). For simplicity reasons it is assumed to have no errors. Substitution gives the model equation:

$$P'(\delta mag) = A*10^{-B*\delta mag}$$

The fit function therefore depends on the parameter B only, which is related to the b-value from the Gutenberg-Richter relationship but is not equivalent. The nonlinear regression optimises the fit for B(TVZ)=1.8±0.2 and B(Non-TVZ)=1.4±0.1. Figures 3a and 3b show data and models on a linear scale in probability and in a non-cumulative sense, with their 95% confidence bands for Non-TVZ and TVZ, respectively. For example, the point at (0.1, 0.011) on the Non-TVZ plot means that 1.1% of the foreshock events were followed by mainshocks with 0.1 units of magnitude larger than the foreshock.

Distance dependence

Plotting the probability data against epicentral distance shows a decay of probabilities with increasing distance whose shape suggests a decay dominated by 1/r (Figures 4a and 4b). Here the probability shown is the probability per unit area (i.e., the proportion of events divided by the area of the ring) that an event will be followed within 5 days by an equal or larger event within the specified distance ring. The character of the fit function is

$$P'(r)=a/(r+cr)^{rexp}$$

with a being a scaling factor to take into account the probability measured in the distance bin closest to the foreshock: $a=P(r=10)*10^{rexp}$. The least square fit was minimized for cr(TVZ)=5.007±0.005 and rexp(TVZ)=3.66±0.02, cr(Non-TVZ)=4.9±0.1 and rexp(NonTVZ)=2.6±0.2 (see Figures 4a and 4b).

The same exponents (within the error bars) were determined when the data was broken into smaller subsets with different magnitude ranges and fitted for separate exponents (For example, considering only

potential foreshock events between magnitudes 4 and 5, or between 4.5 and 5, etc), so it appears to be a robust parameter (Tormann (2005)).

Time dependence

Foreshock probabilities decay rapidly with time (Figures 5a and 5b). We fit the data to the modified Omori law (Utsu et al. (1995))

$$P'(t) = d/(t+ct)^{texp}$$

where d is the scaling factor to approximate the initial probabilities that are observed for the first day d=P(t=1), t is the time since the potential foreshock in days and ct is a constant that avoids a singularity for t=0.

The data can be modeled by the fit function with ct(TVZ)=0.5±0.03, texp(TVZ)=2.5±0.5, ct(NonTVZ)=0.51±0.03, and texp(NonTVZ)=1.7±0.2 as shown in Figures 5a and 5b.

Discussion & evaluation

Foreshock magnitude independence

As in previous studies (e.g. Jones (1985)) we conclude that foreshock probabilities are independent of the foreshock magnitude, i.e. a M=4.0 earthquake is as likely to be a foreshock as a M=6.0 event.

Mainshock magnitude dependence

The B-values of 1.8 for the TVZ and 1.4 for the rest of New Zealand are somewhat unexpected: they are significantly higher than the b-value from the Gutenberg-Richter relationship for New Zealand, which is about 1.1 (Figure 1b). The B-values found in this study are also more than twice the values found in previous studies in California and Nevada, where B of 0.73 and 0.72 were determined, respectively (Jones (1985), Savage & DePolo (1993)). However, as seen for the volcanic Mammoth/Mono region (0.89) compared to the non-volcanic Nevada region (0.72) (Savage and DePolo (1993)), we find a higher B-value for the Taupo Volcanic Zone than for the rest of New Zealand. In the TVZ a high occurrence of earthquake swarms of small to moderate magnitudes is observed while the region does not feature faults capable of

producing very large events. This explains the steeper slope of the magnitude frequency distribution, i.e. a higher b-value in the TVZ.

Distance dependence

Decay of foreshock probability with distance was not determined directly in the studies of Jones (1985) and Savage & DePolo (1993), but examining their plots suggests the vast majority of foreshocks occur within 1 or 5 km of the mainshock location, respectively. In Jones' plot, the decay with distance appears to be slightly slower than the temporal decay, (i.e., the exponent in the distance dependence appears smaller than the exponent in the temporal dependence) while in Savage & DePolo's plots the spatial decay is faster than the temporal one, as we see for the New Zealand data in this study.

Abercrombie et al. (1996), suggested that foreshocks in California occur in a larger volume around mainshocks than expected from the size of the mainshock "preparation zone", i.e. the critical slip distance over which laboratory studies of frictional sliding observe pre-seismic slip before unstable dynamic failure.

Felzer et al. (2004) used earthquakes $M \geq 2.2$ in California that have been followed by a larger one within two days and found that, up to about 10 km distance from the mainshock, foreshock incidences decrease roughly as a power-law decay. At greater distances the foreshock incidences become erratic, and observed seismicity is dominated by background seismicity.

Analysing foreshock sequences in Japan, Ogata et al. (1994), found an approximate inverse power law of foreshock intensity (i.e. expected number of events per unit area) decreasing with distance from the mainshock with exponent of 1.32 for $1 \leq r \leq 35$ km.

Thus, different regions may yield different distance decay parameters. The stronger localisation in the TVZ compared to the rest of New Zealand may be caused by the high seismic attenuation in the TVZ (e.g. Salmon et al. (2002), Eberhart-Phillips and McVerry (2003)). If the mainshocks are caused by dynamic triggering from the foreshocks (e.g., Anderson et al. (1994), Jaumé (1999)), then the higher attenuation would likely limit the triggering to shorter distances than in the rest of the country.

Dynamic stress changes associated with propagating waves from earthquakes are expected to fall off slightly less rapidly than $1/r^2$ (Anderson et al. (1994)), while static stress changes in an infinite medium fall off as $1/r^3$ (Stein et al. (1992)). Thus, our results for the TVZ could be consistent with either dynamic or

static stress triggering, with attenuation providing the rest of the variation. However, the results for the rest of New Zealand suggest that dynamic stress triggering is more likely. For simplicity, we prefer to consider that the same mechanism, dynamic stress triggering, occurs in both regions, but with the influence of attenuation making a stronger falloff.

Time dependence

The exponents of 2.5±0.5 for the TVZ and 1.7±0.2 for non-TVZ as determined for the time decay in this study are unexpected, since previous studies that looked into foreshock probability decay over time after an event find that probability behaviour is similar to the frequency decay of an aftershock sequence, modeled by a modified Omori's law $1/(t+c)^p$ (Utsu et al. (1995)) where c is small and p very close to one. Jones (1985) and Savage and DePolo (1993) determined p for Southern Californian and Western Nevada's foreshock probabilities, and obtained values of 0.9 and 1.0, respectively. Possible explanations for this difference are a regional variation in parameters.

According to Eberhart-Phillips (1998), New Zealand aftershock probabilities do not show a different falloff behaviour compared to other regions in the world. She analysed 17 New Zealand aftershock sequences and although the parameter values varied greatly between the individual sequences, the median values turned out to be very similar to the generic California values as determined by Reasenberg and Jones (1989). Of special interest for comparison with this foreshock probability analysis are the parameters b from the Gutenberg-Richter equation, found to be 0.91 in California and 0.98 in New Zealand, and the temporal decay parameter p from the modified Omori's law, found to be 1.08 in California and 1.05 in New Zealand.

The finding that New Zealand's foreshock probabilities do not follow this generic law, at least not with the generally observed decay exponent, suggests that possibly foreshocks are not just mainshocks whose aftershocks happen to be bigger, i.e. the proposed single triggering mechanism for foreshocks, multiplets and aftershocks (Felzer et al. (2004)) cannot explain the New Zealand data.

Model equations

Jones (1985) analysed the Southern Californian foreshock data for mainshock magnitude distribution and time differences between foreshock and mainshock and described her findings in an equation which

calculates the probability P(Mms,t) that a mainshock of M≥Mms will occur within one hour after time t in hours after an earthquake of M=Mfs as

$$P(Mms,t)=A*10^{B*(Mms-Mfs)}*(t+1)^{-p}$$

She determined A=0.016, B=-0.75, and p=0.9.

Savage and DePolo (1993) modelled the data with the same equation as introduced by Jones (1985) and obtain the best fit for A=0.012 (Nevada), A=0.019 (Mammoth/Mono), B=-0.72 (Nevada), B=-0.89 (Mammoth/Mono) and p=1.0 for both regions.

We analyse New Zealand foreshock probabilities and find equations to model their decay behaviour with magnitude difference, time and distance. Multiplying the three separate equations gives a model that calculates the probability P' that at time t after an event and distance r from the potential foreshock a mainshock with magnitude Mfs+δmag will occur as:

$$P'(t,r,\delta mag)=P(t=1,r=10,\delta mag=0)*10^{-B*\delta mag}*1/(t+ct)^{texp}*10^{rexp}/(r+cr)^{rexp}$$

with two parameter sets for the TVZ and the rest of New Zealand (Table 3).

Conclusion

Temporal, spatial and magnitude dependent analysis of New Zealand foreshock probability data shows unexpected decay properties that do not agree with the idea of foreshocks and aftershocks being results of the same triggering mechanism.

Acknowledgements

We thank the New Zealand Earthquake Commission for funding this study and Euan Smith, David Vere-Jones, and David Rhoades for helpful discussions. John Townend and Stefan Wiemer provided comments on the thesis on which this work is based. The plots were produced using GMT, ZMAP and GraphPad Prism version 4.03 for Windows, GraphPad Software, San Diego California, USA, www.graphpad.com.

References

Abercrombie, R.E., and Mori, J. (1996). Occurrence patterns of foreshocks to large earthquakes in the Western United States. *Nature*, **381**, 303-307

Anderson, J.G. et al. (1994). Seismicity in the Western Great Basin apparently triggered by Landers, California, earthquake, 28 June 1992. *Bulletin of the Seismological Society of America*, **84(3)**, 863-891

Eberhart-Phillips, D. (1998). Aftershock Sequence Parameters in New Zealand. *Bulletin of the Seismological Society of America*, **88(4)**, 1095-1097

Eberhart-Phillips, D. and McVerry, G. (2003). Estimating slab earthquake response spectra from a 3D Q model. *Bulletin of the Seismological Society of America*, **93(6)**, 2649-2663

Felzer, K.R., Abercrombie, R.E., and Ekström, G. (2004). A common origin for aftershocks, foreshocks, and multiplets. *Bulletin of the Seismological Society of America*, **94(1)**, 88-98

Gardner, J. and Knopoff, L. (1974). Is the sequence of earthquakes in Southern California, with aftershocks removed, Poissonian? *Bulletin of the Seismological Society of America*, **64(5)**, 1363-1367

Gutenberg, B. and Richter, C.F. (1944). Frequency of earthquakes in California. *Bulletin of the Seismological Society of America*, **34**, 185-188

Jaumé, S.C. (1999). Stress transfer, dynamic triggering, and stress correlations: how earthquake occurrence affects the timing and slip of subsequent earthquakes. *in ACES Inaugural Workshop Proceedings*

Jones, L.M. (1985). Foreshocks and time-dependent earthquake hazard assessment in Southern California. *Bulletin of the Seismological Society of America*, **75(6)**, 1669-1679

Jones, L.M., Console, R., Di Lucio, F. et al. (1999). Are foreshocks mainshocks whose aftershocks happen to be big? In press *Bulletin of the Seismological Society of America*

Maeda, K. (1996). The use of foreshocks in probabilistic prediction along the Japan and Kuril Trenches. *Bulletin of the Seismological Society of America*, **86(1A)**, 242-254

Mendenhall, A., Wackerly, D.D., and Scheaffer, R.L. (1994). Mathematical Statistics with Applications. *Duxbury Press, Belmont, California, fourth edition.*

Merrifield, A., Savage, M.K., and Vere-Jones, D. (2004). Geographical distributions of prospective foreshock probabilities in New Zealand. *New Zealand Journal of Geology and Geophysics*, **47**, 327-339

Ogata, Y., Utsu, T., and Katsura, K. (1994). Statistical features of foreshocks in comparison with other earthquake clusters. *Geophysical Journal International*, **121**, 233-254

Reasenberg, P.A., and Jones, L.M. (1989). Earthquake hazard after a mainshock in California. *Science*, **243**, 1173-1176

Reasenberg, P.A. (1999). Foreshock occurrence before large earthquakes. *Journal of Geophysical Research*, **104(B3)**, 4755-4768

Salmon, M., Bannister, S., Savage, M.K. et al. (2002). Seismic attenuation in the central North Island, New Zealand. Poster at *2002 Western Pacific Geophysics Meeting*

Savage, M.K., and DePolo, D.M. (1993). Foreshock probabilities in the Western Great- Basin, Eastern Sierra Nevada. *Bulletin of the Seismological Society of America*, **83(6)**, 1910-1938

Savage, M.K., and Rupp, S.H. (2000). Foreshock probabilities in New Zealand. *New Zealand Journal of Geology and Geophysics*, **43**, 461-469

Smith, E.G.C. (1981). Foreshocks of shallow New Zealand earthquakes. *New Zealand Journal of Geology and Geophysics*, **24**, 579-584

Stein, R.S., King, G.C.P., and Lin, J. (1992). Change in failure stress on the southern San Andreas fault system caused by the 1992 magnitude = 7.4 Landers earthquake. *Science*, **258**, 1328-1332

Stern, T.A., Stratford, W.R. and M.L. Salmon (2006). Subduction at a continental margin: kinematics and dynamics of the central North Island, New Zealand. *Reviews of Geophysics* , in press, March 2006

Tormann, T. (2005). Dynamic seismic hazard model for New Zealand. Thesis, Master of Science, Victoria University of Wellington.

Utsu, T., Ogata, Y., and Matsu'ura, R.S. (1995). The centenary of the Omori formula for a decay law of aftershock activity. *Journal of the Physics of the Earth*, **43**, 1-33

Tables

Foreshock bin	Total prob (%)	Max prob (%)	Total number
All	0.22±0.03	0.12±0.02	187
4.0	0.24±0.04	0.14±0.03	122
4.5	0.21±0.06	0.08±0.04	48
5.0	0.20±0.1	0.20±0.1	11
5.5	0.01±0.04	0.01±0.04	4
6.0	0.03±0.09	0.03±0.09	1

Table 1: Foreshock probability values observed for different foreshock magnitude bins (TVZ). Magnitude bin 4.0 includes magnitudes 3.8 to 4.2, bin 4.5 includes 4.3 to 4.7, etc. "Total prob" refers to the total foreshock probability observed within five days and 50 kilometers. "Max prob" is the highest probability observed within the single time and distance bins (which is always on the first day after and within 10km of the potential foreshock).

Foreshock bin	Total prob	Max prob	Total number
All	0.067±0.004	0.021±0.002	3287
4.0	0.068±0.006	0.017±0.003	2100
4.5	0.071±0.009	0.027±0.006	787
5.0	0.05±0.01	0.03±0.01	289
5.5	0.09±0.03	0.03±0.01	75

6.0	0.05±0.05	0.05±0.05	20

Table 2: Foreshock probability values observed for different foreshock magnitude bins (Non-TVZ). Magnitude bin 4.0 includes magnitudes 3.8 to 4.2, bin 4.5 includes 4.3 to 4.7, etc. "Total prob" refers to the total foreshock probability observed within five days and 50 kilometers. "Max prob" is the highest probability observed within the single time and distance bins (which is always on the first day after and within 10km of the potential foreshock).

	TVZ	NonTVZ
P	0.0375	0.0049
B	1.8±0.2	1.4±0.1
CT	0.5±0.03	0.51±0.03
CR	5.007±0.005	4.9±0.1
Texp	2.5±0.5	1.7±0.2
Rexp	3.66±0.02	2.6±0.2

Table 3: Foreshock probability model parameters as determined in this study for the TVZ seismicity and the rest of New Zealand

Figures

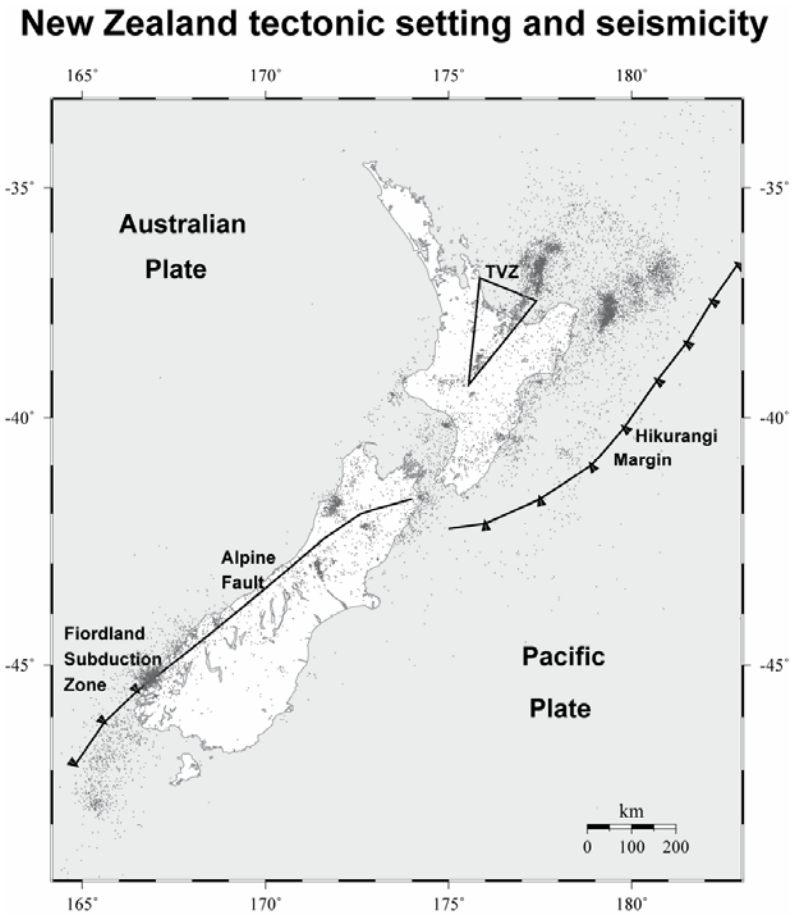

Fig.1a: New Zealand plate tectonic setting:

Subducting Pacific Plate under the Australian Plate (Hikurangi Subduction Zone)

in the North, subducting Australian Plate under the Pacific Plate (Fiordland Subduction Zone) in the South.

The Alpine Fault (South Island) accommodates most of the strike slip motion and is capable of producing large earthquakes. The Taupo Volcanic Zone (TVZ) on the North Island is an extensional geothermally active volcanic area with frequent small to moderate earthquake swarms.

The dots represent the recorded New Zealand seismicity (GeoNet catalogue) between 1964 and 2003 for magnitudes equal to or greater M=3.8

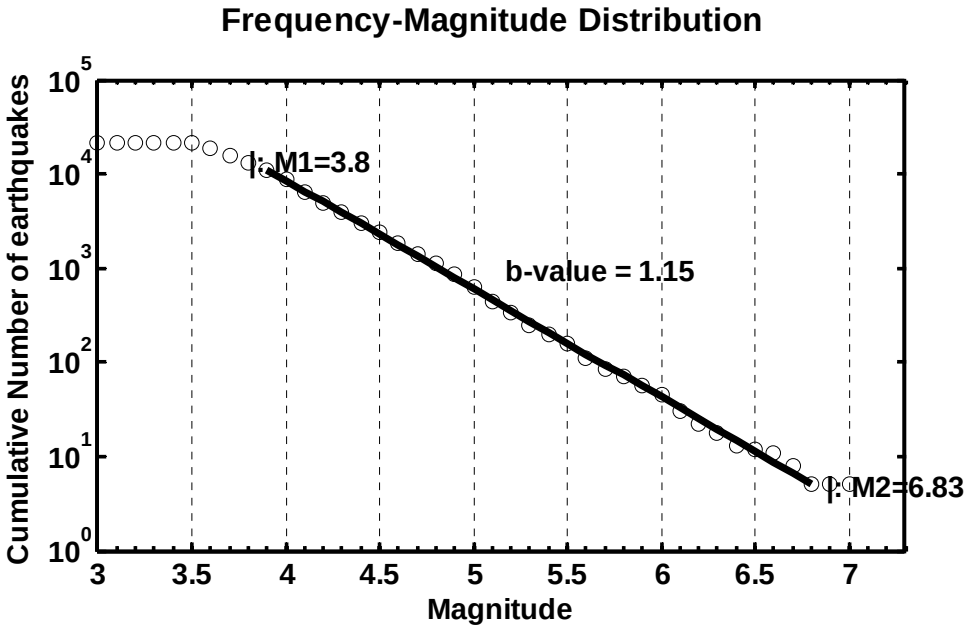

Fig.1b: Frequency magnitude distribution of New Zealand seismicity data between 1964 and 2003, depth ≤ 40km. The slope has been manually fit.

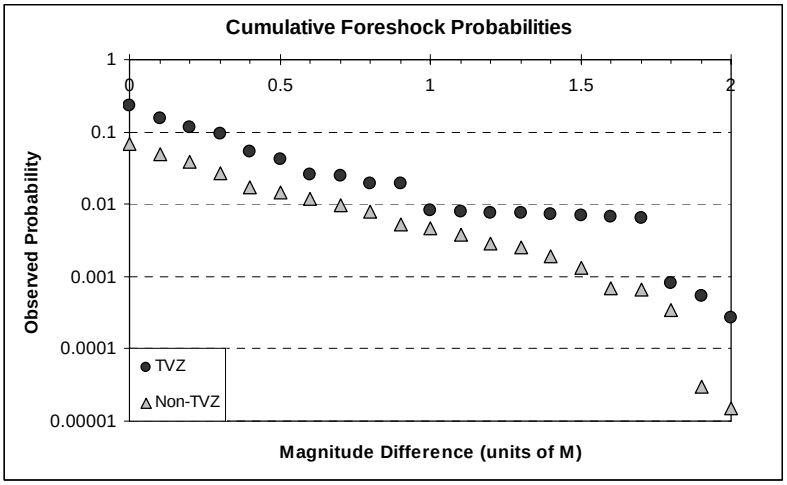

Fig. 2: Cumulative foreshock probabilities with increasing magnitude differences between foreshock and mainshock, for TVZ and Non-TVZ.

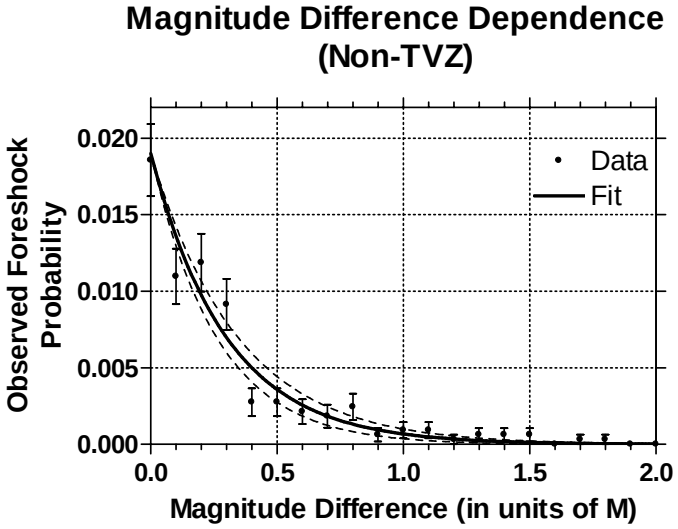

Fig.3a: Foreshock probability dependence on magnitude differences between foreshock and mainshock (Non-TVZ). The model is a least square fit to the data, using the fit function with a B-value of 1.4±0.1. The dotted line is the 95% confidence for the fit.

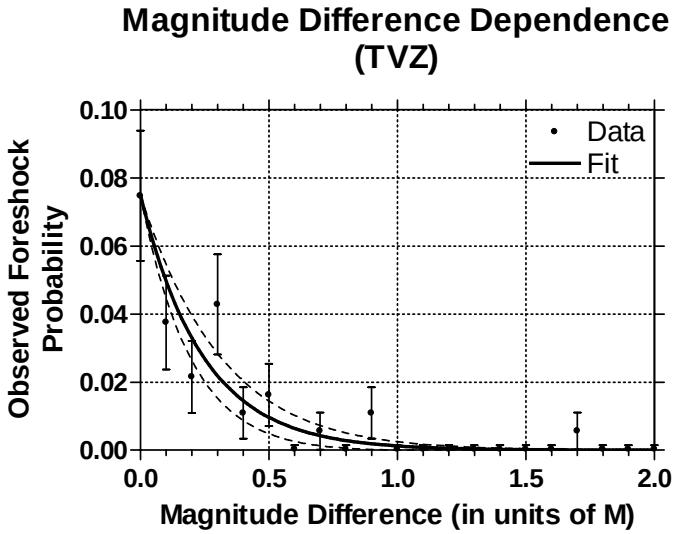

Fig.3b: Foreshock probability dependence on magnitude differences between foreshock and mainshock (TVZ). The model is a least square fit to the data, using the fit function with a B-value of 1.8±0.2. The dotted line is the 95% confidence for the fit.

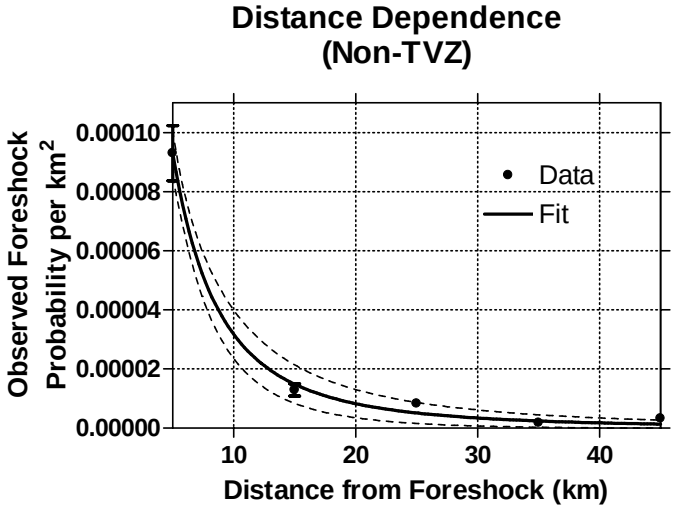

Fig.4a: Foreshock probability dependence on distance between foreshock and mainshock (Non-TVZ). The model is the least square fit to the data, using the fit function with an exponent of 2.6±0.2. The dotted line is the 95% confidence band for the fit.

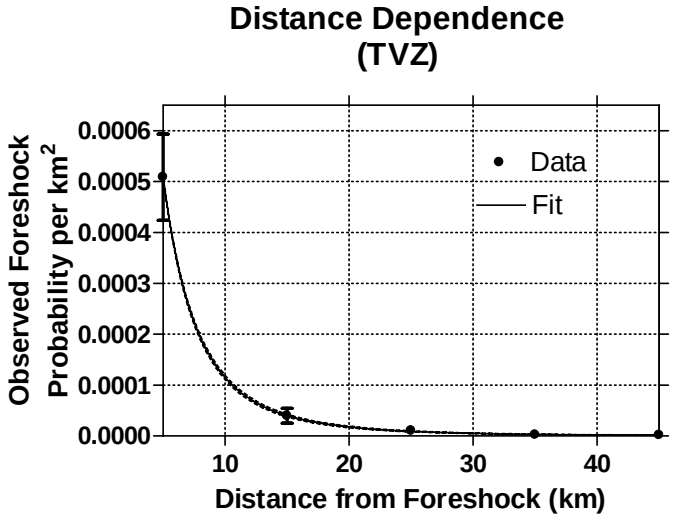

Fig.4b: Foreshock probability dependence on distance between foreshock and mainshock (TVZ). The model is the least square fit to the data, using the fit function with an exponent of 3.66±0.03. The dotted line (nearly too narrow to see) is the 95% confidence band for the fit.

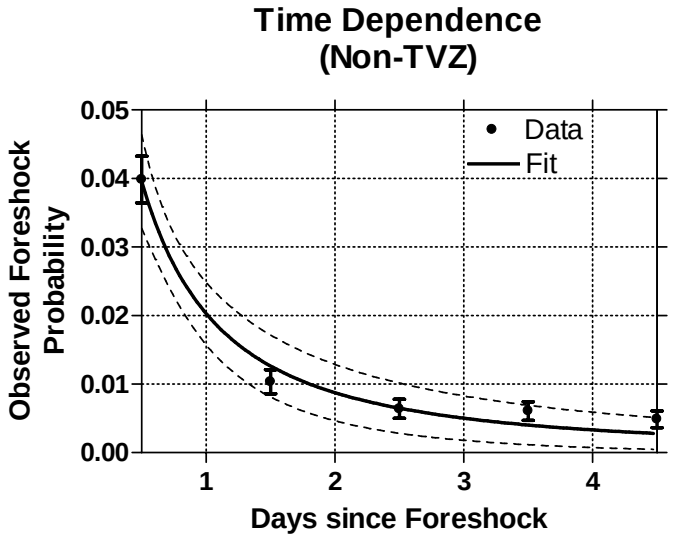

Fig.5a: Foreshock probability dependence on time differences between foreshock and mainshock (Non-TVZ). The model is the least square fit to the data, using the fit function with an exponent of 1.7±0.2. The dotted line is the 95% confidence band for the fit.

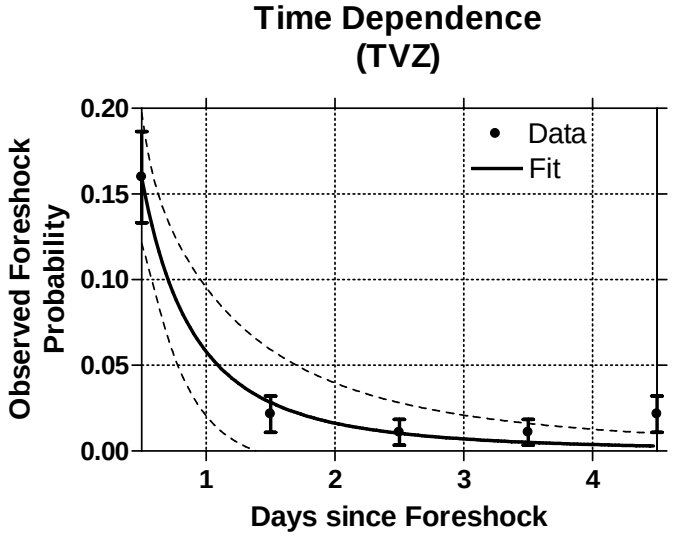

Fig.5b: Foreshock probability dependence on time differences between foreshock and mainshock (TVZ). The model is the least square fit to the data, using the fit function with an exponent of 2.5±0.5. The dotted line is the 95% confidence band for the fit.

Affiliations and addresses of the authors

Thessa Tormann
Institute of Geophysics, Victoria University of Wellington, New Zealand
Now at:
Swiss Seismological Service
ETH Zurich, HPP P3
Schaffmattstrasse 30
CH-8093 Zurich
Switzerland
e-mail: thessa.tormann@sed.ethz.ch

Martha Kane Savage
Institute of Geophysics
Victoria University of Wellington
Box 600, Wellington
New Zealand
e-mail: Martha.Savage@vuw.ac.nz

Mark Williamson Stirling
GNS Science
PO Box 30368, Lower Hutt
New Zealand
e-mail: m.stirling@gns.cri.nz

Victoria University of Wellington

School of Earth Sciences

Dynamic Seismic Hazard Model for New Zealand

Thessa Tormann

A thesis

in partial fulfilment of the
requirements for the degree of

Master of Science
in Geophysics

February 2005

Technical Abstract

A new dynamic seismic hazard model for New Zealand is created to add the effects of short-term hazard fluctuations due to earthquake triggering to the current Poissonian probability from the national probabilistic seismic hazard model.

Prospective foreshock probability decay is modelled as a function of origin time and epicentral distance from the potential foreshock, and the magnitude difference between foreshock-mainshock pairs. Across the country, the distribution of mainshock magnitudes in the set of foreshock-mainshock pairs follows the Gutenberg-Richter relationship with a b-value of 1.3. In the Taupo Volcanic Zone (TVZ), a region characterised by crustal extension and volcanism, the foreshock probability decreases with approximately $1/t^{2.4\pm0.5}$ and $1/r^{3.62\pm0.03}$. Elsewhere in the country, the decay with time and distance is smaller, at $1/t^{1.6\pm0.2}$ and $1/r^{2.7\pm0.2}$. This is consistent with the higher attenuation of seismic energy likely to be experienced in an area of active volcanism. Combining this information with a generic aftershock model, fluctuating daily hazard maps for New Zealand are calculated, showing the regional probability distribution for peak ground accelerations of 0.05g or more being observed.

A methodology has been developed to test these ground motion forecasts against 40 years of strong motion observations in New Zealand. The Poissonian model underestimates the hazard at 0.05g level for the time period and locations in the dataset by a factor of two. The new dynamic seismic hazard model provides a closer match to the strong motion records, but with some overestimation (factor of three) of hazard on days of high probability and underestimation (factor of six) on days of low probability forecasts.

Acknowledgements

This is the place to thank everyone who played a part in the successful completion of this project and in this fabulous second year that I spent in Wellington.

My first thanks go to my supervisors Martha Savage and Mark Stirling for their enormous input throughout this thesis. You found a great way to combine being supervisors with being mates.

I was always impressed by the helpfulness of so many Vic and GNS staff. In particular, I would like to thank Euan Smith and David Vere-Jones – I don't know how I could have mastered the statistics part without your tutoring sessions. Also, I would like to thank Graeme McVerry and Jim Cousins for their great cooperation.

My thanks go to the Earthquake Comission for partly funding this project.

Annemarie, I greatly enjoyed our work and fun meetings, the intense discussions, the cooking, the evenings out, and last but not least our phenomenal time in San Francisco.

J.A.M.E.S., this second year with you was as great as the first – we will never forget our Kiwi family! We hope to be with you many more times.

The year 2004 was overwhelming and unforgettable in many ways. On 31 July at little Matiu Somes Island, Martin, we made it unique in our lives. I have never been happier and I am looking forward to all those years ahead of us, together.

Contents

List of Figures

List of Tables

Thesis Outline

Goal

The goal of this thesis is to develop and implement a first time dependent seismic hazard model for New Zealand that is theoretically capable of calculating the expected hazard due to triggering effects on a daily basis. A method is designed to test the model's forecasts against strong ground motion observations.

Structure

This thesis consists of four parts, each divided into several chapters.

- In **Part I** I describe the development of a new foreshock probability model for the country that will later be used to estimate the foreshock triggering impact in the seismic hazard calculations. It provides more detailed information about time, distance and magnitude dependence of foreshock probabilities in New Zealand than earlier models.

- In **Part II** I discuss studies on aftershock probabilities and describe the model I chose to use for the hazard calculations.

- In **Part III** I describe the methodology of seismic hazard analysis and give a full account of how I apply the foreshock and aftershock probability models to calculate daily seismic hazard. I display the results in form of one day hazard maps on the one hand and time series for a fixed site on the other hand.

- In **Part IV** I describe the testing algorithm I developed for ground motion testing and present the results I obtained for New Zealand's data.
- In the **Appendix** I list detailed probability tables from the foreshock study, background information on the strong motion stations and their triggers used for the ground motion test, and additional test results.

Part I

Foreshock Probability Model

Chapter 1

Introduction

This introductory chapter motivates why many people are interested in knowing foreshock probabilities, and gives definitions of terms widely used in literature dealing with earthquake statistics. Their meaning differs between different authors so I state how they are used in this thesis.

1.1 Motivation

Earthquakes are scary for most people. They are afraid of the "big one" and get very worried when they feel smaller ones, fearing that they could trigger a damaging earthquake.

For rescue services it would be a fundamental step forward to know whether an event will be – or what the chances are that it might be – followed by more events, especially by larger magnitude ones.

Are the people's worries appropriate? Are small or moderate earthquakes likely to be precursors to damaging ones? Scientists have been trying to answer those questions by studying the recorded earthquake activity around the world. Many analyses have been designed during the last 50 years to reveal and better understand earthquake interaction, looking at chances for events being followed by bigger ones as well as smaller ones over different periods of time. Those studies suggest earthquake triggering mechanisms and derive parameters to describe the different phenomena. But no reliable formal methods of earthquake forecasting have been developed to date, thus many questions still need answering.

1.2 Definitions

In the course of studying earthquake interactions a categorisation of events into foreshocks, mainshocks and aftershocks as well as earthquake swarms has been established. Hence, different studies use the above terms in slightly different ways, so the following definitions clarify the meaning that has been adopted for this thesis.

Definition 1.1 *An **earthquake sequence** is a set of earthquakes which are presumed to be physically related because of their spatial and temporal closeness. (**Smith, 1981**) [54]*

Definition 1.2 *A **mainshock** is the largest event of a sequence whenever a largest*

*event is readily identifiable. (**Smith, 1981**) [54]*

Definition 1.3 *A **foreshock** is an event preceding a larger or equal in magnitude mainshock in an earthquake sequence close enough in time and space, such that the two events can be considered physically related. (**Smith, 1981**) [54]*

Definition 1.4 *An **aftershock** is a smaller event following a mainshock in an earthquake sequence within a limited interval of time and space. (**Reasenberg and Jones, 1989**) [42]*

Definition 1.5 *Long series of small and large shocks with no one particular outstanding principal event, are called **earthquake swarms**. (**Richter, 1958**) [46]*

Definition 1.6 *A **triggered event** is any earthquake that has been caused by an earlier event, whether or not it qualifies as an aftershock.*

Definition 1.7 ***Retrospective foreshock probabilities** are the proportions of mainshocks that have had foreshocks.*

Definition 1.8 ***Prospective foreshock probabilities** are the proportions of events that have been followed by bigger ones close in time and space, i.e. events that have been foreshocks.*

In the course of this thesis the symbol '*' stands for multiplication.

Unless otherwise mentioned, error bars are used as one standard deviation.

Chapter 2

Previous Work

Much effort has been put into revealing and understanding foreshock relationships in New Zealand and elsewhere. Catalogues have been statistically analysed to derive retrospective as well as prospective foreshock probabilities for different regions in the world. Theories have been developed to explain the physics of earthquake triggering.

2.1 The physics of earthquake triggering

In the course of this thesis, I deal with statistical analyses of earthquake clustering. But in addition to statistical studies of triggering phenomena, numerous studies have been and are still looking for physical explanations for the observations. It is beyond the scope of this thesis to give a full account of the findings of the various scientists working on this hot topic of current earthquake research. Here I provide a summary of some of the more major results presented in recent studies.

Laboratory observations suggest that the strength of a fault is dependent on the slip rate and the fault's displacement history. One set of equations that has been derived to describe a variety of different sliding behaviours of faults is called the "rate-and-state" friction model (**Dieterich and Kilgore, 1996** [10]). It depends on the sliding speed and a state variable that can be interpreted to represent the effects of contact time between the two surfaces of a fault (**Harris, 2000** [21]). In this formulation, an earthquake occurs when the sliding speed increases above a critical value, i.e. to speeds in the order of centimeters per second. **Dieterich and Kilgore, 1996** [10] have shown that earthquake nucleation times are sensitive to very small stress perturbations, such as occur in the vicinity of prior earthquakes.

Earthquakes result from failure of a fault surface under shear and normal stress and therefore change the static stress field in the region around the area of rupture. These stress changes, usually only a fraction of the stress drop during an earthquake, are often quantified as a change in the Coulomb failure function (ΔCFF), (e.g. **Stein, 1999** [56])

$$\Delta CFF = \Delta\tau - \mu(\Delta\sigma - \Delta p) \tag{2.1}$$

where $\Delta\tau$ is the change in the shear stress due to the event, $\Delta\sigma$ the change in normal stress, Δp the change of pore fluid pressure and μ is the coefficient of friction. It is suggested that the static stress change due to an earthquake can move other faults

toward or away from failure, changing the probability of potential earthquakes on these faults (**Hardebeck, 2004** [20]).

Spatial patterns of aftershocks are in some cases found to correlate strongly with "predictions" from ΔCFF. Aftershocks tend to concentrate in areas of increased Coulomb static stress (positive ΔCFF) and earthquake activity is observed to reduce in areas where ΔCFF is negative, in so called stress shadows (**Harris, 2000** [21]). **Stein, 1999** [56] for example observes that 65% of the seismicity rate changes after the 1994 Northridge, California, earthquake ($M_w = 6.7$) are correlated with the calculated Coulomb stress change.

Parsons, 2002 [40] finds that about 61% of modelled earthquakes after magnitude seven or above events in the Harvard CMT catalogue are associated with calculated shear stress increases. The seismicity rate's decay obeys the Omori law (which states that the number of earthquakes decays as $1/t$, where t is the time of the mainshock. **Omori, 1894** [36]) and it takes about 7-11 years for the rate of triggered earthquakes to return to background rates. The remaining 39% of aftershocks occur in areas of decreased shear stress and are probably triggered by different mechanisms, possibly dynamic stress changes (see below). Their rate only takes one to two years to return to the background level. **Parsons, 2002** [40] also demonstrates that the Coulomb failure function strongly depends on the choice of the friction coefficient. For the 2001 El Salvador ($M_w = 7.7$) shock he finds that using different values for the friction coefficient can change the $M_w = 6.6$ earthquake that was recorded shortly after the mainshock to be located either in zones of calculated Coulomb stress increase or decrease (e.g. $\mu = 0.75$ and $\mu = 0.0$, respectively).

Since the 1992 Landers, California, earthquake ($M_w = 7.3$) the possibility of long-distance triggering has been raised (e.g. **Anderson et al., 1994** [2]). Earthquakes not only change the static stress field, but also induce dynamic stress changes during the passage of large amplitude seismic waves. This can also effect the timing of subsequent earthquakes, especially in the far field, and is referred to as "dynamic triggering"

(**Jaumé, 1999** [22]). The seismicity changes due to the 1999 Hector Mine, California, (M_w = 7.1) (e.g. **Gomberg et al., 2001** [18]) and the 1999 Izmit, Turkey, (M_w = 7.4) (e.g. **Brodsky et al., 2000** [5]) earthquakes appear to be better explained by the dynamic stress field than by the static stress change. (**Voisin et al., 2004** [63])

Dieterich and Kilgore, 1996 [10] propose and model two different possible causes of foreshocks. One model assumes that small to moderate earthquakes redistribute the static stress field, which triggers other parts of the same fault or different faults to rupture in similar sized, or larger events. As the triggered events are presumed to obey the Gutenberg-Richter frequency distribution of earthquake magnitudes, some of these triggered events will be of larger magnitude, classifying the triggering earthquake as foreshock. The other model assumes that foreshocks are driven by the strain changes of the mainshock nucleation process. Both models show a comparable fit to the data, so no one physical model for foreshock occurrence has been defined.

2.2 International work on foreshock probabilities

Attention was drawn to foreshocks when studies of different earthquake catalogues showed that a considerable proportion of moderate and large events are preceded by smaller magnitude earthquakes. Depending on the tectonic setting and definition of a foreshock, the proportions vary between five percent (**Bowman and Kisslinger, 1984**) [4] and fifty percent (**Mogi, 1969**) [33]. In Southern California **Jones** found thirty-five per cent of events greater than or equal to magnitude five being preceded by foreshocks within 1 day and 5 km distance (**Jones, 1984**) [24]. All these values are derived in retrospect, counting large events, and checking whether they have been preceded by smaller events.

The relatively high probability defined in these previous studies has provided a possibility for undertaking hazard forecasts based on this feature. For a warning application it is not sufficient to reveal afterwards that a mainshock has been preceded by a foreshock, so it becomes necessary to determine the probability for a given earthquake

to be a foreshock.

In 1975 **Papazachos** [39] analysed foreshock sequences in Greece and found that the time distribution, τ_1, between the mainshock and the largest foreshock follows a statistical law of the form

$$N = c - \kappa log(\tau_1) \tag{2.2}$$

where N is the probability that the largest foreshock will occur τ_1 days before the mainshock or sooner. Through least-square fitting he determined the values for $c = 0.59$ and $\kappa = 0.31$. Differentiating gives the frequency distribution to be

$$n(\tau_1) = \frac{const}{\tau_1} \tag{2.3}$$

where n is the rate of earthquakes. This supports the idea that the time distribution of foreshocks follows a statistical law similar to that followed by the time distribution of aftershocks.

Jones, 1985 [25] was the first author to investigate prospective foreshock relationships. She worked on the Southern Californian catalogue, defining a foreshock as an event of magnitude three or larger that is followed by a stronger earthquake within five days and a distance of ten kilometers. Considering all mainshocks for potential foreshocks of at least magnitude three, the resulting foreshock probability was 6 ± 0.5 per cent, independent of the magnitude of the foreshock. It reduced to less than one per cent if the mainshock was required to be at least magnitude five, which led in many cases to a mainshock much larger than the foreshock. Looking only at foreshocks of magnitude five and more that were followed by at least magnitude five mainshocks, the probabilities are again around six per cent. She found that the magnitudes of the mainshocks followed a normal b-value distribution above the magnitude of the foreshock with a b-value of 0.75.

Although the time window for a foreshock is defined to be five days, the mainshock is most likely to occur during the first few hours after the foreshock and the probability decreases approximately inversely with time. **Jones, 1985** [25] finds that 26% of the mainshocks occur within the first hour. After that the rate of mainshock occurrence decays with $1/t^{0.9}$, where t is the time after the foreshock.

The author combines her results in an equation which calculates the probability $P(M_m)$ that an earthquake of $M \geq M_m$ will occur within 1 hour after time t in hours after an earthquake of $M = M_f$ as

$$P(M_m, t) = 0.016 * 10^{-0.75*(M_m - M_f)} * (t+1)^{-0.9} \tag{2.4}$$

With this study, **Jones** showed that the probability increase for larger events after an earthquake of $M \geq 3.0$ in California in the small time space window is 500 times more than the background level for the whole region.

Applying this empirical technique of **Jones, 1985** [25], **Savage and DePolo, 1993** [49] obtained similar results for Eastern California and Western Nevada. The probabilities of a magnitude three event there to be followed by a larger one within five days and ten kilometers vary between six per cent in the Nevada region and ten per cent in the Mammoth/Mono region. If the mainshock is required to be at least one magnitude larger, the probabilities decrease to one to two per cent each.

Savage and DePolo (1993) find that 20% of the mainshocks follow within the first hour, and derive two equations for the two regions, following the notation used by **Jones, 1985** [25] (see above):

$$P(M_m, t) = 0.012 * 10^{-0.72*(M_m - M_f)} * (t+1)^{-1.0} \quad (Nevada) \tag{2.5}$$

$$P(M_m, t) = 0.019 * 10^{-0.89*(M_m - M_f)} * (t+1)^{-1.0} \quad (Mammoth/Mono) \tag{2.6}$$

For Nevada, the occurrence of a magnitude five event increases the empirical chances for another magnitude five or higher earthquake to 500 times the background level. For

a magnitude six event following the magnitude five foreshock the likelihood increases to 1200 times more than the background seismicity rates. For the Mammoth/Mono region, the values are 1600 and 1200 for a magnitude five or six mainshock, respectively.

In 1991 **Agnew and Jones** expanded the earlier mentioned study (**Jones, 1985**) [25] in deriving probabilities for characteristic earthquakes on major faults if a potential foreshock occurs near such a structure. They found a dependence for the occurence of a mainshock after a small foreshock on the rate of background seismicity along the fault segment, the long-term probability of the characteristic earthquake occurrence, and the rate at which the mainshocks are preceded by foreshocks. They applied the method to the San Andreas fault system and derived values for the probability that small events there might be precursors to large plate-boundary earthquakes. (**Agnew and Jones, 1991**) [1]

In 1999 **Reasenberg** analysed two worldwide catalogues to derive global foreshock probabilities. (**Reasenberg, 1999**) [44] Using a slightly different definition of foreshocks – he takes the time window to be ten days and an epicentral radius of 75 km – **Reasenberg** observed that worldwide rates are about twice as high as those derived for California using the generic model from **Jones, 1985** [25].

In his study **Reasenberg** also analysed subsets of earthquakes defined by the same focal mechanisms. He found a significant pattern: the foreshock rate before magnitude six and greater thrust mainshocks is twice the corresponding rate before strike-slip mainshocks. Thus, the low rates estimated from the Californian catalogue could imply that the regional model significantly underestimates the conditional probabilities following potential megathrust foreshocks in Cascadia. Still, for the vast majority of Californian earthquakes, originating in the active strike-slip plate boundary, the generic model can be considered to be "correct" for most of California. There might also be certain other regions in the world where sufficient seismological data are available and a regionally determined generic clustering model might provide a better basis for esti-

mating short-term earthquake probabilities. The world generic model, however, better represents worldwide foreshock-related conditional probabilities. (**Reasenberg, 1999**) [44]

Ogata et al., 1995 [35] studied the relationships between clusters of earthquakes and later significantly larger events. They analysed the chances for those earthquake clusters to be foreshock clusters as a function of magnitude, temporal and spatial distribution in the cluster.

Jones et al., 1999 [26] suggested and tested the hypothesis that foreshocks might be mainshocks whose aftershocks happen to be big and therefore could be modelled and predicted using aftershock relationships. The authors conclude that no separate mechanism is needed to explain foreshock-mainshock sequences. However, for the analysed Italian catalogue between 1975 and 1996, the fraction of earthquakes that triggered larger events (6%) was only half of the prediction based on aftershock rates (11%). Similarly, for the Southern Californian catalogue the aftershock rates predict 10.5% of events with larger earthquakes following them, while the actual foreshock probability is only 6%.

2.3 Foreshock probability studies for New Zealand

Investigation of New Zealand's prospective foreshock probabilities started with **Savage and Rupp, 2000** [50], who applied and modified **Savage and DePolo's, 1993** [49] methodology. **Savage and Rupp's** definition of a foreshock in New Zealand has since been used for subsequent regional studies.

Definition 2.1 *A foreshock is an event that is followed by a mainshock within five days and a maximal epicentral distance of 30 km.*

The varied tectonic setting of New Zealand suggested that the probabilities could vary for different classes of earthquakes depending on their epicentral depth. The

intervals were chosen to be 0 to 50 km, 50 to 100 km and deeper than 100 km, and it was found that deep events produce surprisingly high foreshock probabilities for low magnitude foreshocks and show a strong dependence on the foreshock magnitude.

Savage and Rupp found the New Zealand foreshock probability range to be roughly between zero and 20 per cent. With increasing foreshock magnitude the values decrease exponentially.

Savage and Rupp, 2000 [50] additionally assessed the normal background seismicity rate and compared it with the probabilities obtained for foreshocks.

They also found that for shallow events (less than 40 km) the foreshock probabilities are independent of foreshock magnitude as well as aftershock-removal windows and different time periods. This does not hold for deeper events, whose probabilities show a clear dependence on all three factors.

Merrifield spent his Master's Thesis on the examination of regional distributions of prospective foreshock probabilities in New Zealand. (**Merrifield, 2000**) [31] He carried out an intense statistical analysis of the New Zealand earthquake catalogue, investigating foreshock probability dependencies on depth, foreshock magnitude, foreshock-mainshock magnitude differences, foreshock location, and declustering algorithms and their parameters. (**Merrifield et al., 2004** [32]) **Merrifield** also discusses the variation in probabilities as a function of the spatial and temporal windows used for New Zealand foreshocks, which were defined by **Savage and Rupp, 2000** [50] as 30 km and five days, respectively.

As **Smith, 1981** [54] stated, the development of New Zealand's seismic recording network produced earthquake data throughout the years that vary greatly in quality, i.e. in the completeness regarding small magnitude events. Only since 1960 can the catalogue be assumed to be complete down to magnitudes of four. Hence this is the basis for **Merrifield's** and other following studies.

Vere-Jones, Turnovsky and Eiby, 1964 [62], observed differing behaviour between deep and shallow events, the first of which do not necessarily have foreshocks preceding them. In his study **Merrifield** therefore divided all events into three depth categories, following the classification of **Savage and Rupp, 2000** [50]: *shallow earthquakes:* 0 to 40 km, *medium earthquakes:* 40 to 120 km, *deep earthquakes:* greater than 120 km.

The temporal window is commonly used. It was first introduced and justified by **Jones, 1985** [25]: mainshocks occur most frequently in the first day after the foreshock and the rate of occurrence decays rapidly, so a five day window will adequately capture foreshock-mainshock pairs.

The spatial window needs much more attention as it varies between different seismic regions. **Jones, 1985** [25] used an epicentral radius of only ten kilometers for California, since she observed most of the mainshocks to occur even within one kilometer. For the worldwide catalogue **Reasenberg, 1999** [44] uses the significantly wider range of 75 km and **Savage and Rupp, 2000** [50] chose a compromise of 30 km for New Zealand, justifying that decision with the more diffuse seismicity and poorer location accuracy of the New Zealand catalogue compared to that of California. **Merrifield** corroborates this choice after calculating foreshock probabilities for different spatial windows. Assuming that he would miss related events if he chooses too small a window and capture unrelated events if the window gets too big, he plotted the calculated probabilities against the applied radius, which allowed him to examine trends. He found the expected rise of probability with increasing radius, but no distinct feature that would suggest a certain preferrable distance. To maintain consistency he stayed with the formerly used 30 km radius.

In the **Merrifield et al., 2004** [32] study, the foreshock probabilities for New Zealand are calculated for shallow events with foreshock magnitudes equal to or greater

than four. Average probability turns out to be 6.39% ± 0.47% that an earthquake will be followed by a larger one within five days and 30 km. The probabilities are independent of the foreshock magnitude, but decrease significantly if the mainshock is required to be 0.5 or one magnitude larger than the potential foreshock. Intermediate depth earthquakes are less likely to be foreshocks, and for events greater than magnitude five the probability is estimated as close to zero. Deep earthquakes seem to also behave differently in terms of foreshock probabilities. The analysis suggests that deep earthquakes are more likely to be followed by larger ones than shallow or medium events.

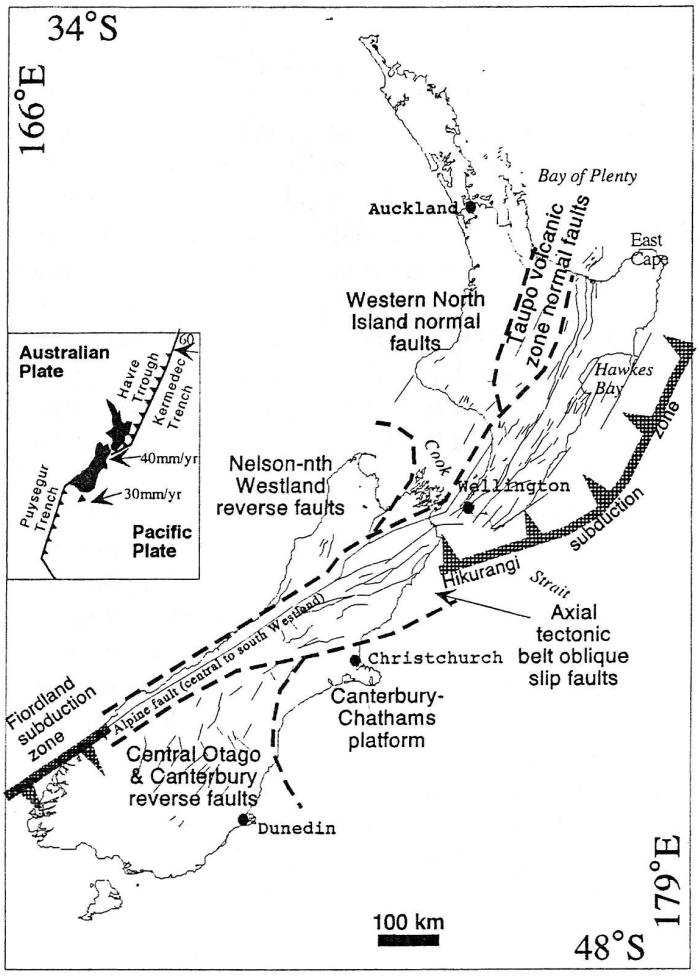

Figure 2.1: The plate tectonic setting of New Zealand. The country is divided into the tectonic provinces identified by **Berryman and Beanland, 1988** [3]. (Figure 1 in **Stirling et al., 2002** [58])

The main regional feature for foreshock probability differences turns out to be the Taupo Volcanic Zone (TVZ), a triangular area on the North Island, covering the geothermally active vicinities of Taupo and Rotorua (see Fig. 2.1). Here, the chances that a magnitude four or greater earthquake will be followed by another of equal or greater size are as high as $9.6\% \pm 1.7\%$. Although a number of zones with different seismic properties can be distinguished in New Zealand, the foreshock probabilities vary significantly only between the TVZ and the rest of the country.

Merrifield et al., 2004 [32] found that the foreshock activity and the resulting probabilities vary significantly for this region compared to the rest of the country, for which they are considerably uniform. According to that study, a small earthquake in the TVZ is much more likely to be a foreshock than elsewhere. On the other hand, larger events (magnitudes 5.5 or higher) are hardly observed in that area and have not yet been foreshocks to larger ones.

2.4 Why a new model?

As summarised above, several studies have investigated foreshock relations to different degrees of detail. **Jones, 1985** [25] and **Savage and DePolo, 1993** [49] derived functions of magnitude and time to calculate California's and Nevada's foreshock probabilities. But New Zealand models have not studied local foreshock properties to such detail. **Merrifield et al., 2004** [32] displayed regional and magnitude dependencies but did not investigate temporal or spatial decay.

To include foreshock triggering probabilities into hazard estimates properly, the spatiotemporal distribution after an event needs to be known.

The new model develops equations that allow calculation of the probability for a mainshock of a certain magnitude occuring at a certain time after and distance from the foreshock.

Chapter 3

Time, Distance, and Magnitude Dependent Foreshock Model

A new foreshock probability model for New Zealand is developed, investigating dependencies on temporal and spatial distance from the potential foreshock, as well as the magnitude distribution for the mainshocks.

3.1 Data

For the foreshock probability calculations I use the New Zealand earthquake catalogue available from the GeoNet web site (www.geonet.org.nz). As New Zealand earthquake recordings can be considered to be complete down to magnitude 4.0 from 1964, that is the starting point of my dataset. It goes through to September 2003.

I eliminated all events of magnitudes less than 3.8 and deeper than 40 km. Even if 3.8 and 3.9 are below completeness in the first few years of the catalogue, it is helpful to have a lower threshold, because when binning magnitudes to half magnitude steps, 3.8 and 3.9 are rounded towards 4.0 and can, with caution, still be used (see section 3.3.2).

The depth cutoff is chosen for two reasons. First, **Vere-Jones, Turnovsky and Eiby, 1964** [62] found differing behaviour between shallow and deep earthquakes, the latter of which do not necessarily have foreshocks preceding them. New Zealand foreshock studies as **Savage and Rupp, 2000** [50] and **Merrifield, 2000** [31] therefore divided all events into three depth categories, the shallowest of which is 0 to 40 km. Intermediate depth earthquakes are classified as going down to 120 km and deep events happen below that. Secondly, I only consider shallow events, because I am interested in hazard changes in terms of ground motions on the surface of the earth. Those are mainly influenced by the first 40 km, because for deeper events the spherical spreading and attenuation over the longer distances has more effect and reduces the contribution of these ruptures to any ground motions on the surface. Nevertheless, large to great deep earthquakes could have a significant effect on the hazard estimates, but are, for simplicity reasons, not included in this model.

Foreshock statistics must be calculated on a declustered catalogue: that is, a catalogue without any aftershocks in it. The reason is: within aftershock sequences, there might be numerous aftershock pairs that could be misinterpreted as foreshock-mainshock pairs because the temporal and spatial conditions are fulfilled. That would lead to a major overestimation of foreshock probabilities.

Several algorithms have been developed to decluster earthquake catalogues. Using different approaches of how to cluster earthquake data into aftershock sequences, they vary significantly in the number of events classified as aftershocks. Two widely known methods are the Gardner & Knopoff (1974) [15] and Reasenberg (1985) [43] algorithms.

The Gardner & Knopoff (1974) algorithm reads the catalogue in chronological order, considers the very first event as a potential mainshock, tests subsequent earthquakes to see whether they are aftershocks of that potential mainshock according to the specified time-space window, eliminates all that match the criteria, and then considers non-aftershock events to be new potential mainshocks until the end of the catalogue is reached.

Reasenberg, 1985 [43] suggests that the Gardner & Knopoff method probably overestimates the aftershock population in nearly all cases, as it does not allow for the variation in spatial and temporal extents of different aftershock sequences. His model identifies aftershocks by modelling an interaction zone about each earthquake in the catalogue. These zones are modelled dynamically with one spatial and one temporal parameter. The former is based on an estimate of the stress redistribution in the vicinity of each earthquake; the latter is determined using a probabilistic model. An event is marked as an aftershock of a potential mainshock, if its hypocentral and origin time differences are less than the spatial and temporal extent of the interaction zone modelled for the chosen event.

Savage and DePolo, 1993 [49] compared the Gardner & Knopoff (1974) algorithm with the Reasenberg (1985) declustering method and found that the latter was more difficult to apply to a heterogeneous earthquake catalogue and the results were still close to the ones obtained with the Gardner & Knopoff algorithm. Therefore **Savage and Rupp, 2000** [50] adopted the Gardner & Knopoff (1974) algorithm for New Zealand (using different time-space windows adapted to the regional seismic situation).

Following **Savage and Rupp, 2000** [50] I use the Gardner & Knopoff (1974) algorithm for my analysis of New Zealand foreshock probabilities. Table 3.1 gives the temporal and spatial windows that have been used to eliminate the aftershocks from the raw catalogue.

Magnitude	Distance (km)	Time (days)
4.0	35.5	22
4.5	44.5	42
5.0	52.5	83
5.5	63	155
6.0	79.4	510
6.5	100	790
7.0	125.9	1737
7.5	151.4	3981

Table 3.1: Time and distance windows used to decluster the New Zealand catalogue using the Gardner & Knopoff (1974) Algorithm

The basis for my foreshock probability model for New Zealand are therefore the country's non-aftershock events since 1964 above magnitude 3.8 and shallower than 40 km. I call this the "declustered" catalogue.

3.2 Methodology

The principle of determining generic foreshock probabilities from the declustered catalogue is very simple. I count all earthquakes that have been followed by bigger ones within a given time and distance. But in contrast to former studies in New Zealand, I do not choose an upper time and distance bound and treat everything within those bounds uniformly. Instead, I count all events that are followed within one day, all those that are followed on the second day, third day, and so on. Similarly I split the area into concentric rings, the first being a 10 km radius circular area, the second reaching

from 10 to 20 km, the next from 20 to 30 km, and so on. Doing that, I do not get cumulative probabilities, but discrete values that I can not only compare easily but also use afterwards just as they are.

As **Merrifield et al., 2004** [32] stated a difference in foreshock activity in the TVZ compared to the rest of New Zealand, I analyse this area separately. To minimise boundary effects, I put the regional constraint on the potential foreshock only. The mainshocks can be located in the same region as the foreshock (TVZ or non-TVZ) or in the other one.

One more parameter that I study is the magnitude difference between foreshock and associated mainshock and its relevance for foreshock probabilities. When counting pairs I therefore keep track of the overall number of pairs as well as the number of pairs of magnitude differences of 0.0, 0.1, 0.2, 0.3, and so on, up to 2.0 units of magnitude difference.

I search the catalogue in chronological order, taking the first event to be a potential foreshock and determine whether the next events fulfil the spatial and temporal conditions. If I do not find any mainshocks, I go on to the second event in the catalogue, take it to be a potential foreshock, look for mainshocks, and so on. If I do find an event that happened within the time and space window of a potential foreshock event, I count the pair and go on to the next potential foreshock. I do not look at whether there might be more than one event per foreshock fulfilling the conditions. That is because if I did, I could overestimate the probabilities in case of increasing magnitude sequences. If, for example, a potential foreshock of magnitude 4.2 is followed by a magnitude 4.3 the next day and a magnitude 4.5 the day after, I would count three foreshock-mainshock pairs with only three earthquakes (4.2-4.3, 4.2-4.5, 4.3-4.5). Even worse, if there was a fourth event of 4.6 the next day, I would count six pairs from four events (additionally 4.2-4.6, 4.3-4.6, 4.5-4.6). That seems unreasonable, so I cut

my count and get probabilities for at least one earthquake following a foreshock but allow "mainshocks" following a foreshock to be potential foreshocks themselves (i.e. in the above example I would count the three foreshock-mainshock pairs 4.2-4.3, 4.3-4.5, 4.5-4.6).

Parallel to counting the actual pairs, I keep track of how many potential foreshocks I have been testing (this could be either all events in the catalogue or only those of a certain magnitude bin).

To treat the TVZ separately, I run the calculations twice, once looking only at potential foreshocks located in the TVZ (mainshock anywhere within the concentric rings), the next time counting only the complement, the potential foreshock events located outside the TVZ (again, the mainshock does not need to be outside, as long as it is located within the foreshock-mainshock search area).

The straightforward way to give probabilities p_{m_f} for a given earthquake of magnitude bin m_f would then be to just divide the number of foreshocks n found in that magnitude bin by the number of all potential foreshocks N_{m_f}, i.e. all events of magnitude bin m_f.

$$p_{m_f}(n_{m_f}|N_{m_f}) = \frac{n_{m_f}}{N_{m_f}} \tag{3.1}$$

The associated approximate standard error $s.e.$ for that count is then

$$s.e.(p_{m_f}) = \sqrt{\frac{p_{m_f}(1-p_{m_f})}{N_{m_f}}} \tag{3.2}$$

The problem with this simple approach is that in case of no successful observations the probability turns out to be zero. But associating a zero probability to future events means asserting that these events will not be followed by a bigger one. We cannot do that, because we do not know whether it is true. We just have not observed any such pairs yet. This problem is especially concerning for high magnitudes, where we have few data.

The beta distribution (e.g **Mathematical Statistics with Applications** [30]) is therefore used; it yields positive values everywhere. This distribution modifies the probabilities to the following formulas:

$$P_{m_f}(n_{m_f}|N_{m_f}) = \frac{\alpha + n_{m_f}}{\alpha + \beta + N_{m_f}} \tag{3.3}$$

The associated standard deviation σ is

$$\sigma = \sqrt{\frac{(\alpha + n_{m_f})(\beta - n_{m_f} + N_{m_f})}{(\alpha + \beta + N_{m_f})^2(\alpha + \beta + N_{m_f} + 1)}} \tag{3.4}$$

The probabilities derived from the two methods were tested on the whole dataset. With $\alpha = 0.05$ and $\beta = 0.95$, parameters were found for which the probabilities P calculated from equation 3.3 agree with the probabilities p derived from equation 3.1 to at least three decimal places. The same holds for the error bounds. The data cannot distinguish changes of higher order, so equations 3.3 and 3.4 are used to calculate the new New Zealand foreshock probability model.

I estimated the probabilities from the whole catalogue between 1964 and 2003, and also split the data in half (1964 to 1984 and 1985 to 2003) to derive probability values from each of the subcatalogues. This is one way to check whether they can be assumed to be constant over time and therefore independent of the period of the catalogue used for the estimate.

In order to find a mathematical description for each of the time, distance, and magnitude-dependent decay behaviour of foreshock probabilities, I use a nonlinear regression program (**GraphPad Prism 4 Demo** available from www.graphpad.com) to calculate least square fits for the data. For each dependence I require the program to use a certain type of equation (that is consistent with the literature) and the program provides the best least square fit parameters for that model including some statistical tests to help accept or reject the results. The most valuable test parameter for this application is the coefficient of determination, R^2, which quantifies the goodness of

fit. R^2 is a fraction between negative one and one with no unit which is computed as follows:

$$R^2 = 1 - \frac{SLS}{SHS} \tag{3.5}$$

where SLS is the sum of the squares of the distances of the data points from the model curve, and SHS is the sum of the squares of the distances between the data points and a horizontal line through the mean of the data points. If the model fits the data well, SLS will be small, and much smaller than SHS. Therefore the fraction of SLS/SHS will become small and R^2 close to one. For a value of one, the model fits the data exactly, with all data points lying on the best-fit curve. For a value of zero, the model fits the data no better than a horizontal line through the mean of the data points. Should the model fit the data even less than the horizontal line through the mean, R^2 will be negative. However, the parameter R^2 only evaluates the mathematical fit, i.e. the absolute distances between data and model. It cannot tell whether the fit is reasonable in other ways, i.e. whether best-fit parameters have sensible values. Therefore R^2 alone cannot accept or reject models, it can just be used as an indicator of how well the chosen parameters fit the data. (**Motulsky and Christopoulus, 2003** [34])

3.3 Results

3.3.1 Some catalogue statistics

Out of the 3474 events in the declustered catalogue, 187 were located in the TVZ, 42 of these being identified as foreshocks. Out of the 3287 events outside the TVZ, 222 were followed by bigger events close in time and space.

Table 3.2 and Fig. 3.1 (Non-TVZ) and 3.2 (TVZ) summarise the absolute numbers of potential and actual foreshock events found for different foreshock magnitudes. The distribution is shown for three different periods of the catalogue. As expected there are fewer events for higher magnitudes.

	Whole catalogue (1964-2003)		First part (1964-1984)		Second part (1985-2003)	
	TVZ	non-TVZ	TVZ	non-TVZ	TVZ	non-TVZ
Total number of events	187	3287	112	1822	75	1465
Total number of foreshocks	42	222	29	131	13	91
Potential FS in bin 4.0	122	2100	71	1137	51	963
FS in bin 4.0	30	143	23	84	7	59
Potential FS in bin 4.5	48	787	32	465	16	322
FS in bin 4.5	10	56	5	37	5	19
Potential FS in bin 5.0	11	289	5	169	6	120
FS in bin 5.0	2	15	1	6	1	9
Potential FS in bin 5.5	4	75	4	35	0	40
FS in bin 5.5	0	7	0	4	0	3
Potential FS in bin 6.0	1	20	0	9	1	11
FS in bin 6.0	0	1	0	0	0	1
Potential FS in bin 6.5	1	12	0	5	1	7
FS in bin 6.5	0	0	0	0	0	0

Table 3.2: Numbers of potential and actual foreshock events counted in different FS (=foreshock) magnitude bins (MS (=mainshock) within 5 days and 50 km). Results shown for three periods of the New Zealand catalogue, and distinguishing between TVZ and Non-TVZ

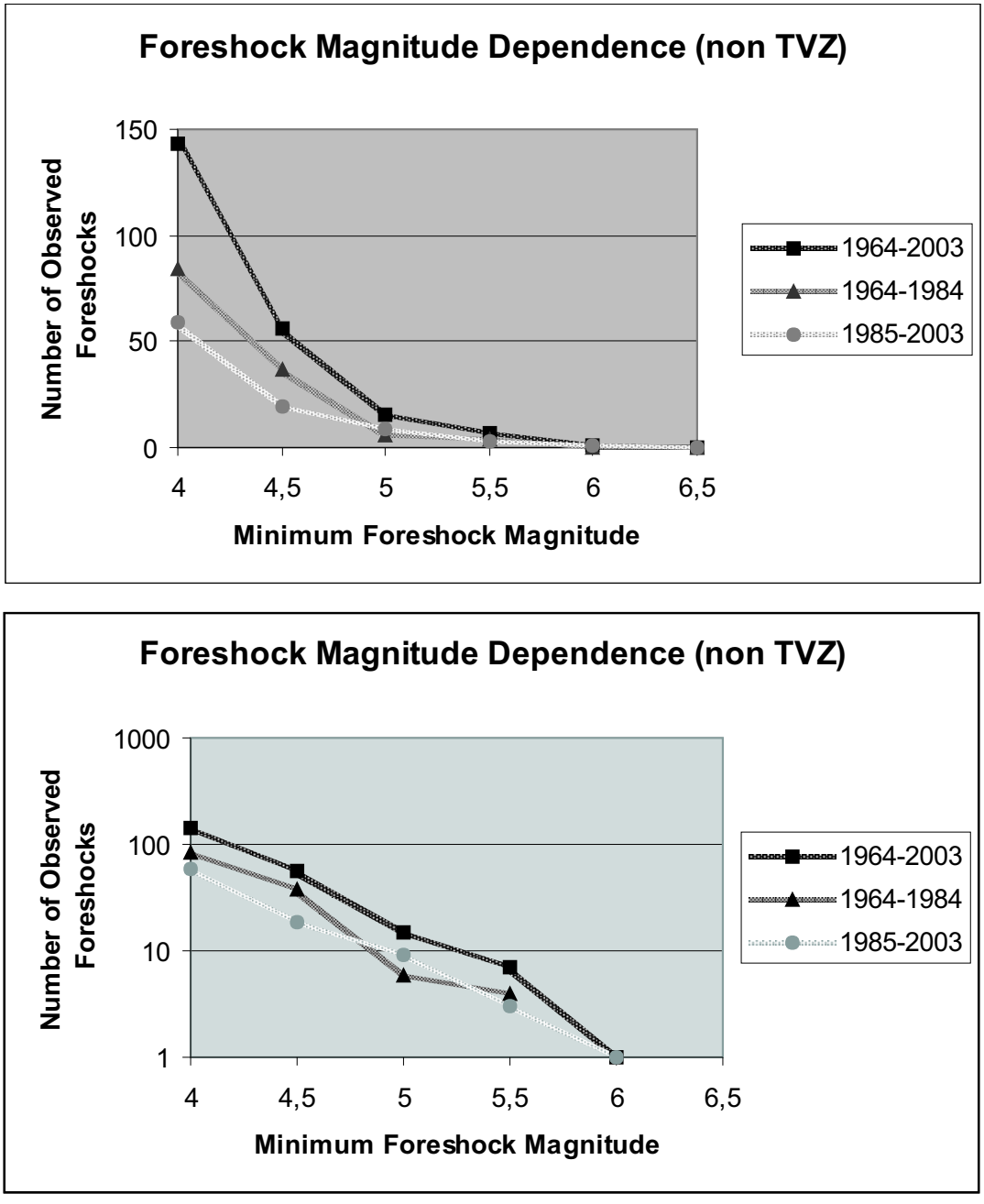

Figure 3.1: Absolute numbers of foreshock events outside the TVZ counted for different magnitude bins, plotted with linear (top) and logarithmic scaling (bottom).

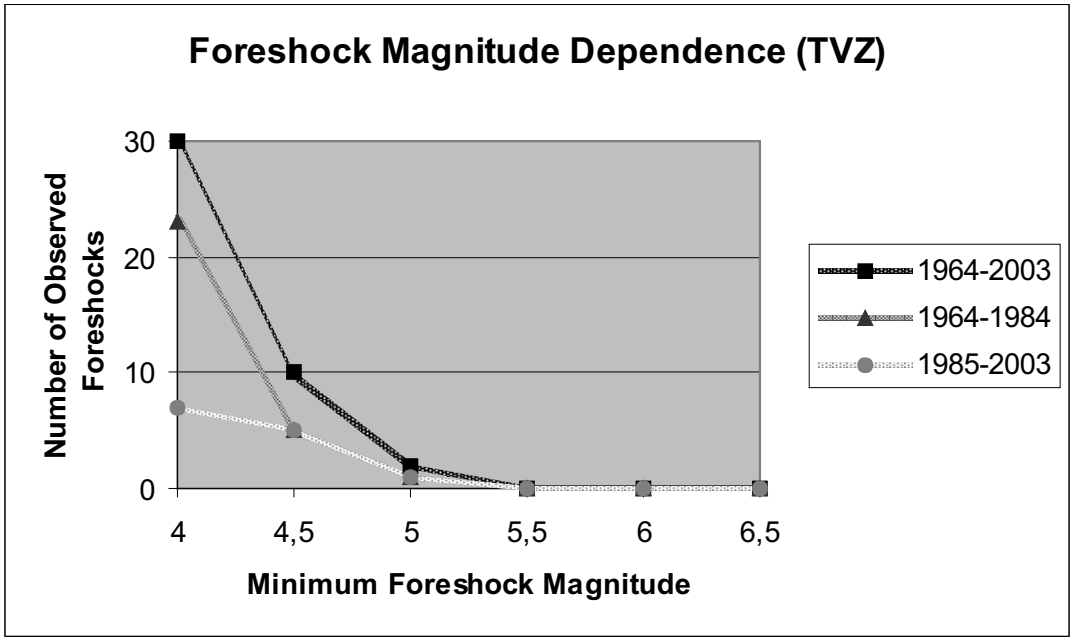

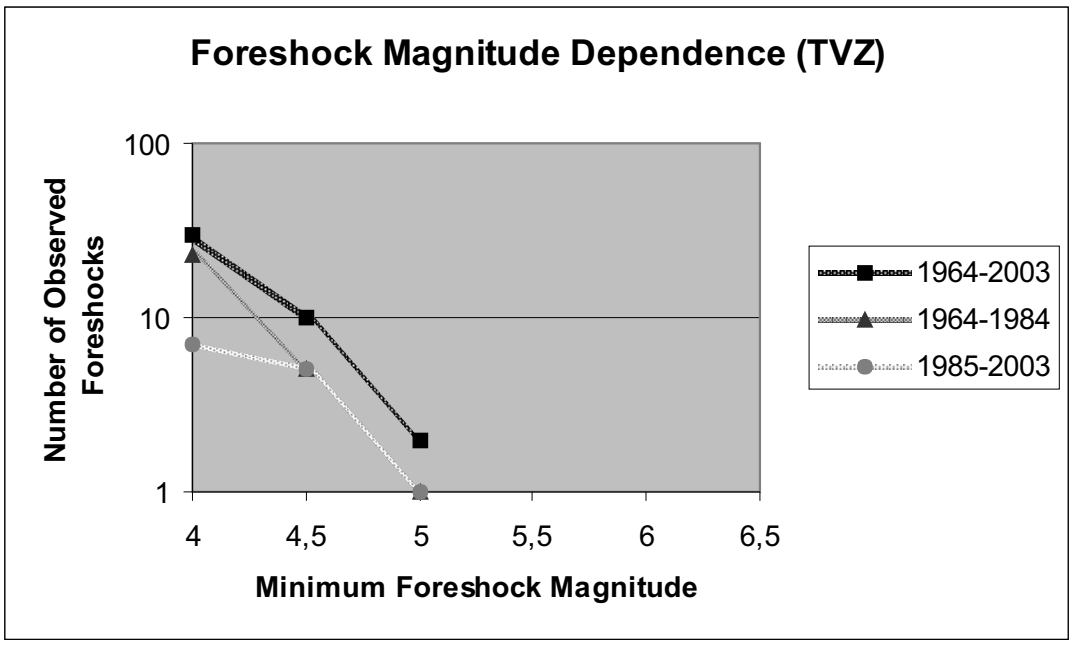

Figure 3.2: Absolute numbers of foreshock events in the TVZ counted for different magnitude bins, plotted with linear (top) and logarithmic scaling (bottom).

Tables 3.3 and 3.4 and Fig. 3.3 and 3.4 show, for all three periods of the catalogue, that foreshock-mainshock incidences decrease sharply with increasing time and epicentral distance between the two earthquakes.

	Whole catalogue (1964-2003)		First part (1964-1984)		Second part (1985-2003)	
	TVZ	non-TVZ	TVZ	non-TVZ	TVZ	non-TVZ
Total number of events	187	3287	112	1822	75	1465
Total number of foreshocks	42	222	29	131	13	91
MS on 1st day	30	131	20	82	10	49
MS on 2nd day	4	34	3	18	1	16
MS on 3rd day	2	21	2	12	0	9
MS on 4th day	2	20	1	9	1	11
MS on 5th day	4	16	3	10	1	6

Table 3.3: Number of foreshock-mainshock pairs counted in different time bins (MS within 50 km, all magnitudes)

	Whole catalogue (1964-2003)		First part (1964-1984)		Second part (1985-2003)	
	TVZ	non-TVZ	TVZ	non-TVZ	TVZ	non-TVZ
Total number of events	187	3287	112	1822	75	1465
Total number of foreshocks	42	222	29	131	13	91
MS in 0-10 km	30	96	19	46	11	50
MS in 10-20 km	7	40	7	29	0	11
MS in 20-30 km	3	43	2	33	1	10
MS in 30-40 km	1	13	0	7	1	6
MS in 40-50 km	1	30	1	16	0	14

Table 3.4: Number of foreshock-mainshock pairs counted in different distance bins (MS within 5 days, all magnitudes)

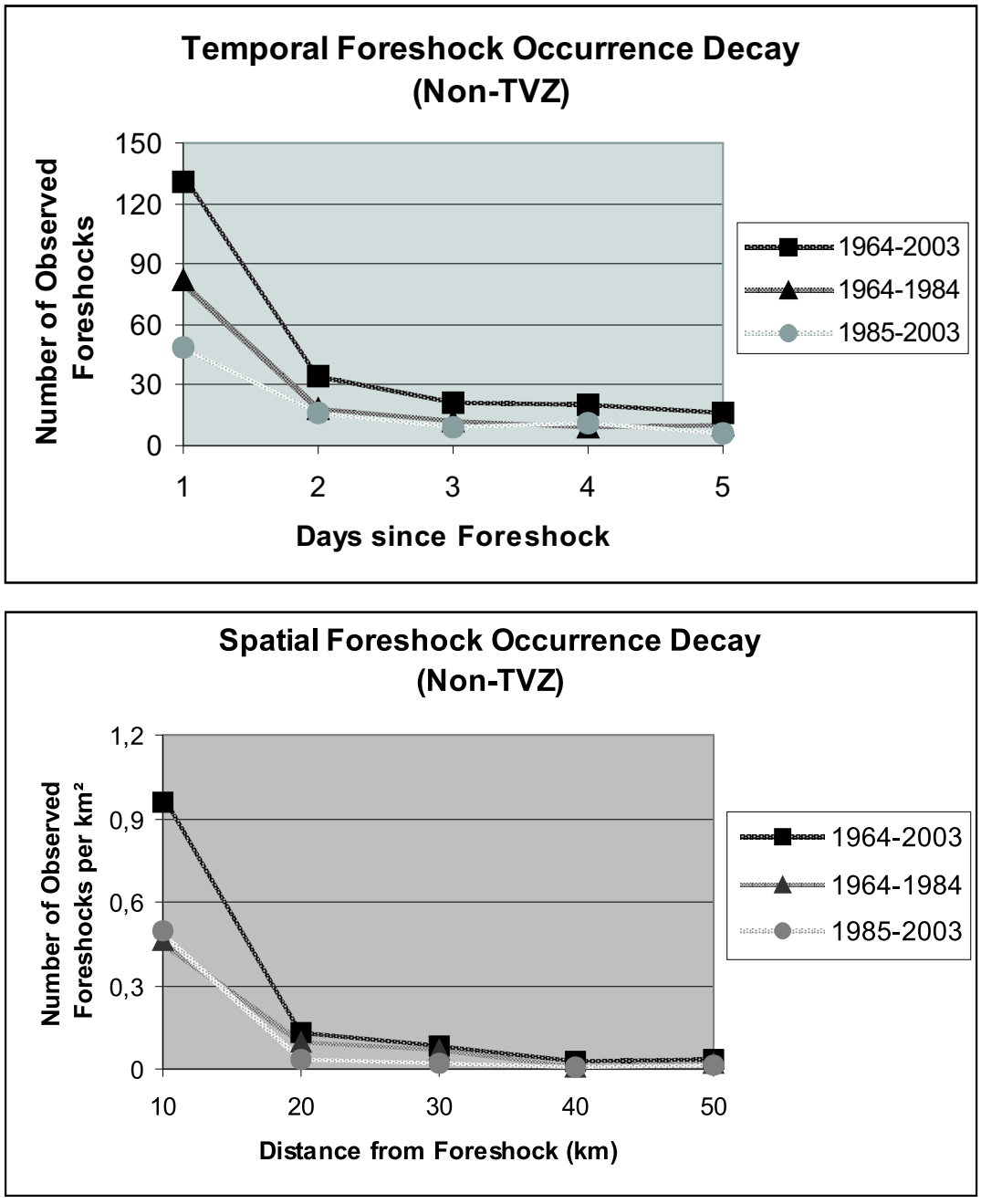

Figure 3.3: Numbers of foreshock-mainshock pairs outside the TVZ as a function of time summed over distance and magnitude (top) and as a function of distance summed over time and magnitude (bottom)

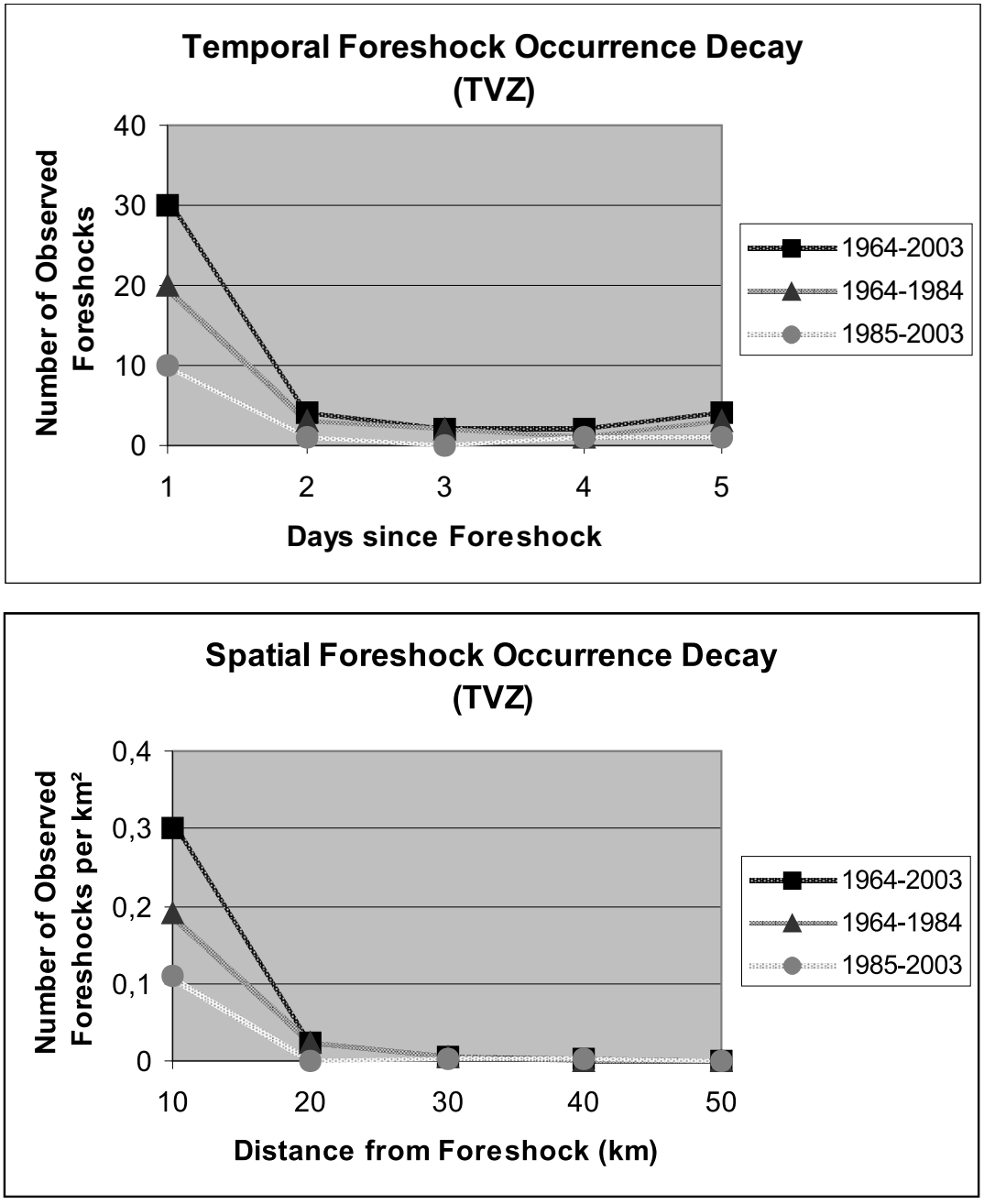

Figure 3.4: Numbers of foreshock-mainshock pairs in the TVZ as a function of time summed over distance and magnitude (top) and as a function of distance summed over time and magnitude (bottom)

The analysis of New Zealand's foreshock probability data is presented in the next few sections. Some tables of probability values found within different categories are in Appendix A.

3.3.2 Foreshock magnitude dependence

Surprisingly, most foreshock studies have found that the probabilities for an earthquake to be followed by an equal or larger one are the same whether the first is small or large (e.g. **Jones, 1985** [25]). I test this foreshock magnitude independence for the decay behaviour in time and space.

To study the probability behaviour as a function of different foreshock magnitudes I associate all potential foreshocks with certain magnitude bins of half magnitude steps. All magnitudes get counted for the bin of the closest half magnitude, i.e. .8, .9, .0, .1, .2 are counted for .0, and .3, .4, .5, .6, .7 are counted for .5. To maintain enough events in the single bins, I start with bin 4.0 and go up to bin 6.5, which then includes all events greater than or equal to magnitude 6.3. This could lead to overestimates for high magnitudes, so the definition needs to be kept in mind when interpreting the data. I do not replace the real magnitudes by the values of the appropriate bin, so that the real magnitude is used in all analysis steps. For example, for magnitude bin 4.5, I include all the magnitude 4.3 events that were followed by $M \geq 4.3$, all the magnitude 4.4 events followed by $M \geq 4.4$, and so on up through magnitude 4.7 events followed by $M \geq 4.7$.

I set up a series of calculations, putting constraints on the magnitudes of potential foreshocks and counting all foreshock-mainshock pairs whose foreshocks fulfilled the magnitude limits, i.e. I looked for events with magnitudes between 3.8 and 4.2 (magnitude bin 4.0) that turned out to be foreshocks, in the next count those with magnitude bin 4.5, then 5.0, and so on. There are few events above magnitude bin 5.5, so the data will be dominated by single observations and should not be taken too seriously.

The data (Fig.3.5 and Fig.3.6) show a very similar probability decay with increasing time and distance, for all different foreshock bins, both inside and outside the TVZ. The higher magnitude bins are more variable due to the smaller number of events used in the calculation. The few data explain the apparent exception of the general decay trend for foreshock magnitude bin 4.5 in the TVZ (bottom left plot in Fig. 3.5) and

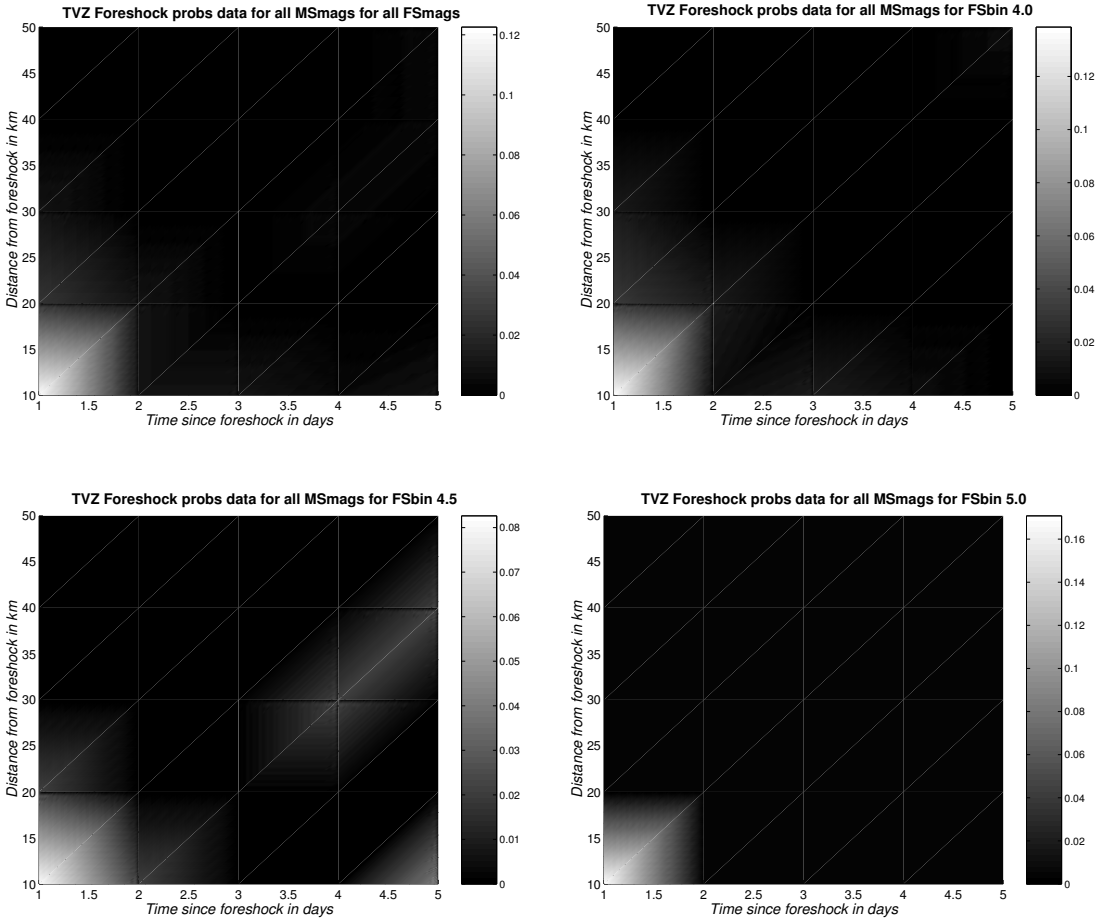

Figure 3.5: Foreshock magnitude dependence of foreshock probabilities in the TVZ (New Zealand catalogue 1964-2003): all FS (top left), FS bin 4.0 (top right), FS bin 4.5 (bottom left), FS bin 5.0 (bottom right). The plots show the temporal (x-axis) and spatial (y-axis) probability decay with increasing time and distance from the foreshock (origin). Probability values are represented by gray scale, with the gray scale bar used shown at the side of each graph. The plots are based on values for each full day and multiples of ten kilometers. Everything in between is linearly interpolated.

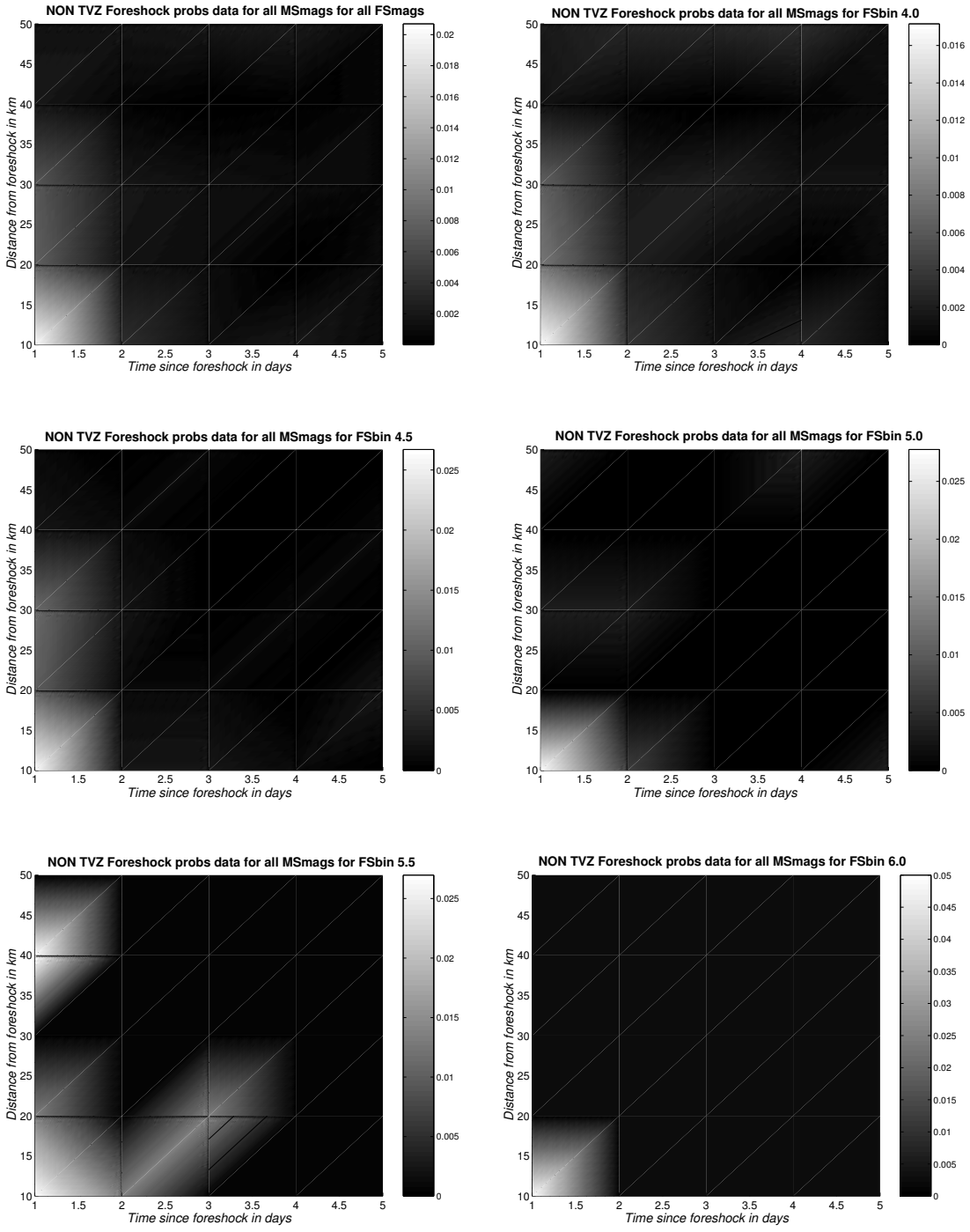

Figure 3.6: Foreshock magnitude dependence of foreshock probabilities outside the TVZ (New Zealand catalogue 1964-2003): All FS (upper left hand corner), FS bin 4.0 (upper right hand corner), FS bin 4.5 (middle on the left), FS bin 5.0 (middle on the right), FS bin 5.5 (lower left hand corner), and FS bin 6.0 (lower right hand corner). The plots show the temporal (x-axis) and spatial (y-axis) probability decay with increasing time and distance from the foreshock (origin). Probability values are represented by gray scale, with the gray scale bar used shown at the side of each graph. The plots are based on values for each full day and multiples of ten kilometers. Everything in between is linearly interpolated.

foreshock magnitude bin 5.5 for the Non-TVZ (bottom left plot in Fig. 3.6). The diagonal patterns of higher probability away from the foreshock in time and space are artifacts caused by single events in a very small number of observations.

Furthermore, the probability values turn out to be of similar order for different foreshock magnitudes, as shown in Table 3.5 and 3.6.

Foreshock bin	Total probability (5 days, 50km, all δmag)	Maximum probability (1^{st} day, 10km, δmag=0)	Total number of events
all	0.22 ± 0.03	0.12 ± 0.02	187
4.0	0.24 ± 0.04	0.14 ± 0.03	122
4.5	0.21 ± 0.06	0.08 ± 0.04	48
5.0	0.2 ± 0.1	0.2 ± 0.1	11
5.5	0.01 ± 0.04	0.01 ± 0.04	4
6.0	0.03 ± 0.09	0.03 ± 0.09	1

Table 3.5: Maximum probability values observed for different foreshock magnitudes (TVZ)

Foreshock bin	Total probability (5 days, 50km, all δmag)	Maximum probability (1^{st} day, 10km, δmag=0)	Total number of events
all	0.067 ± 0.004	0.021 ± 0.002	3287
4.0	0.068 ± 0.006	0.017 ± 0.003	2100
4.5	0.071 ± 0.009	0.027 ± 0.006	787
5.0	0.05 ± 0.01	0.03 ± 0.01	289
5.5	0.09 ± 0.03	0.03 ± 0.02	75
6.0	0.05 ± 0.05	0.05 ± 0.05	20

Table 3.6: Maximum probability values observed for different foreshock magnitudes (Non-TVZ)

3.3.3 Mainshock magnitude dependence

Another property of foreshock probabilities that has been studied before is the dependence on the magnitude difference between foreshock and mainshock. The suggestion is that it is much more likely that similar sized events follow than much larger ones.

Recent work e.g. from **Jones et al., 1999** [26] states that there is only one physi-

cal triggering process and whether foreshock-mainshock pairs or mainshock-aftershock pairs are observed is just random, following the Gutenberg-Richter relationship of magnitude frequency distributions (**Gutenberg, 1944** [19]). Therefore the magnitude distribution of mainshocks for foreshock-mainshock pairs should follow Gutenberg-Richter as well. **Jones, 1985** [25] and **Savage and DePolo, 1993** [49] used the Gutenberg-Richter relationship to model foreshock probability decay with increasing magnitude between the events in Southern California and Western Nevada, respectively. They found b-values of slightly less than one described the data best.

In this section I analyse the data from the New Zealand earthquake catalogue in order to reveal the probability distribution with increasing magnitude differences and see whether it can be modelled, especially whether it follows the Gutenberg-Richter relationship. Since it has been shown in the previous section that foreshock probabilities are independent of the foreshock magnitude, further analyses do not distinguish between foreshock magnitude. Their bases are all foreshocks that have been observed. Furthermore, for this analysis I take all pairs observed within the maximum radius of 50km and maximum time window of 5 days.

Fig.3.7 to 3.10 show the observed probabilities for different magnitude differences on a logarithmic scale, i.e. what proportion of earthquakes is followed by an event of the same magnitude, 0.1 magnitude higher, 0.2, and so on, up to 2.0 magnitude units higher. The decay is remarkably linear on the logarithmic plot for cumulative magnitude difference up to magnitude differences of 1.6 units (above that is not enough data to consider the change of slope significant) and therefore confirms the assumption that the Gutenberg-Richter relation applies to the magnitude distribution in foreshock-mainshock pairs in New Zealand, too. The probabilities are directly proportional to the number of events.

The character of the fit function is determined by the suggestion that the magnitude distribution of triggered events should follow the Gutenberg-Richter relation.

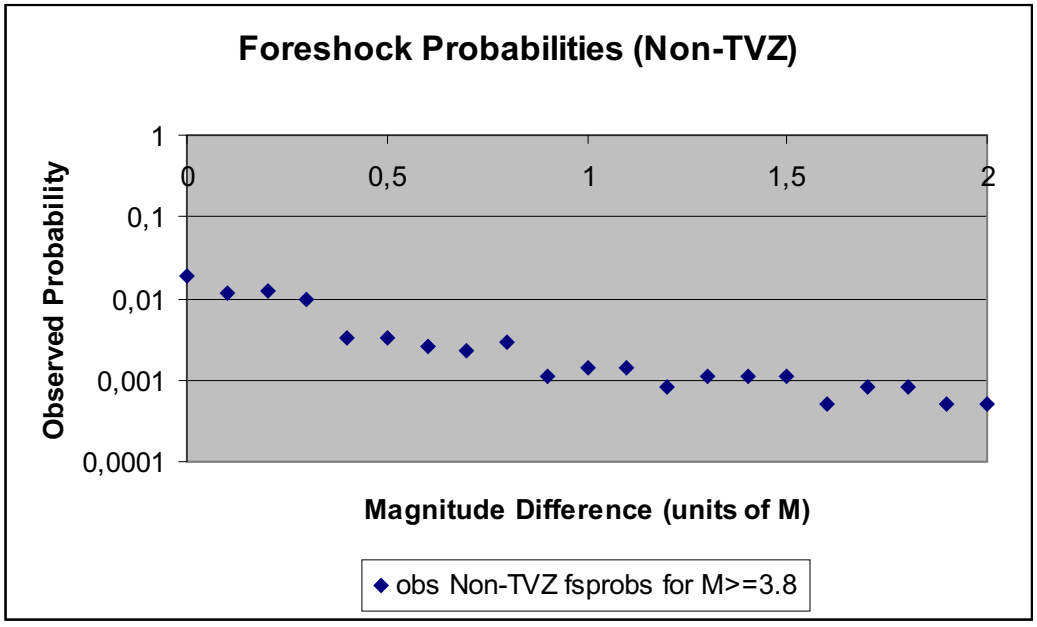

Figure 3.7: Foreshock probabilities with increasing magnitude differences between foreshock and mainshock (Non-TVZ)

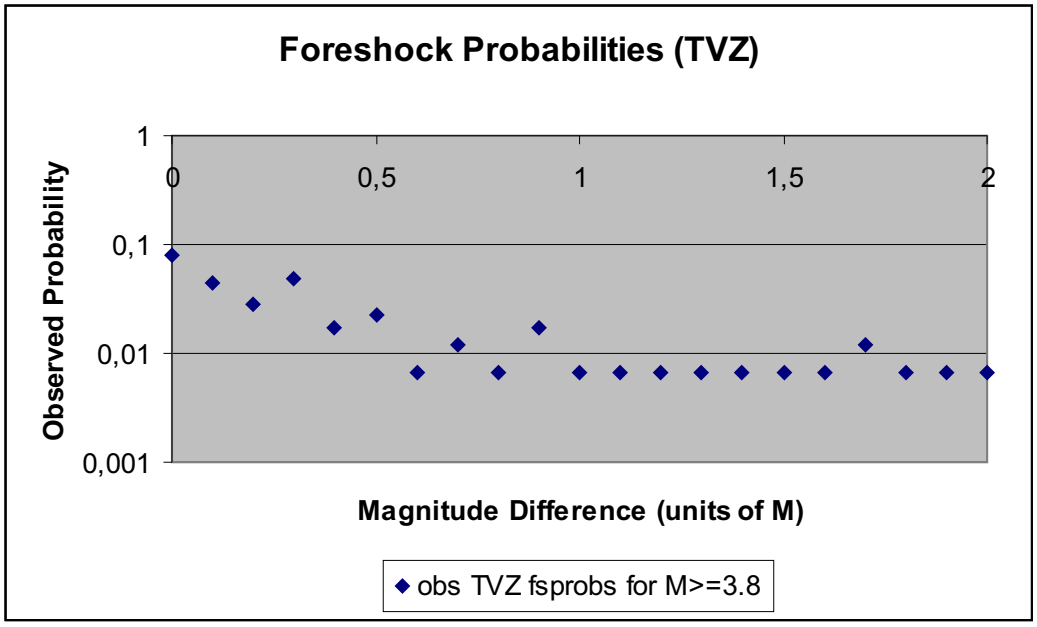

Figure 3.8: Foreshock probabilities with increasing magnitude differences between foreshock and mainshock (TVZ)

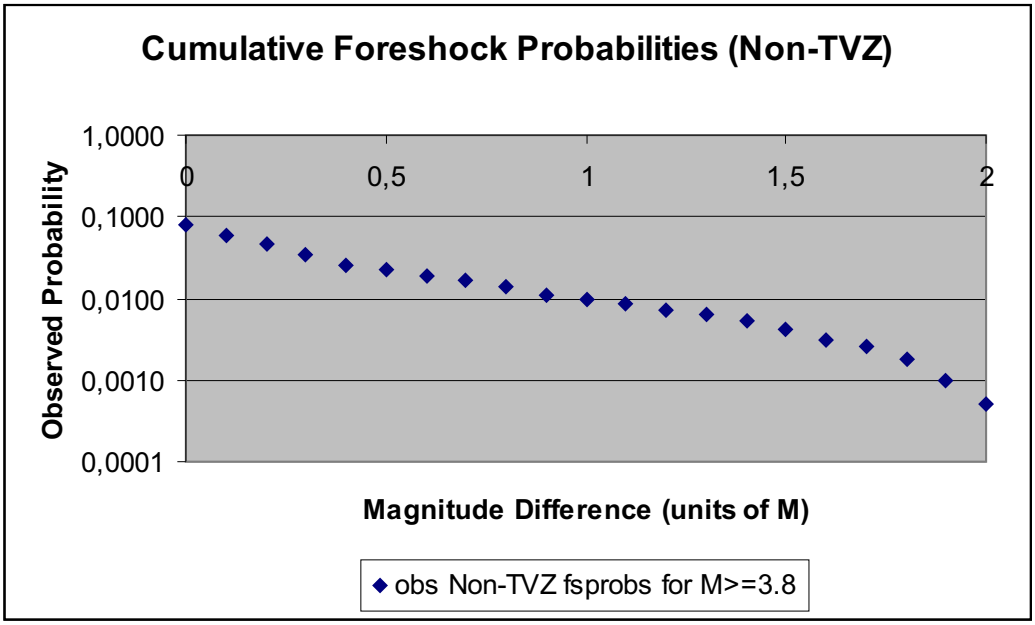

Figure 3.9: Cumulative foreshock probabilities with increasing magnitude differences between foreshock and mainshock (Non-TVZ)

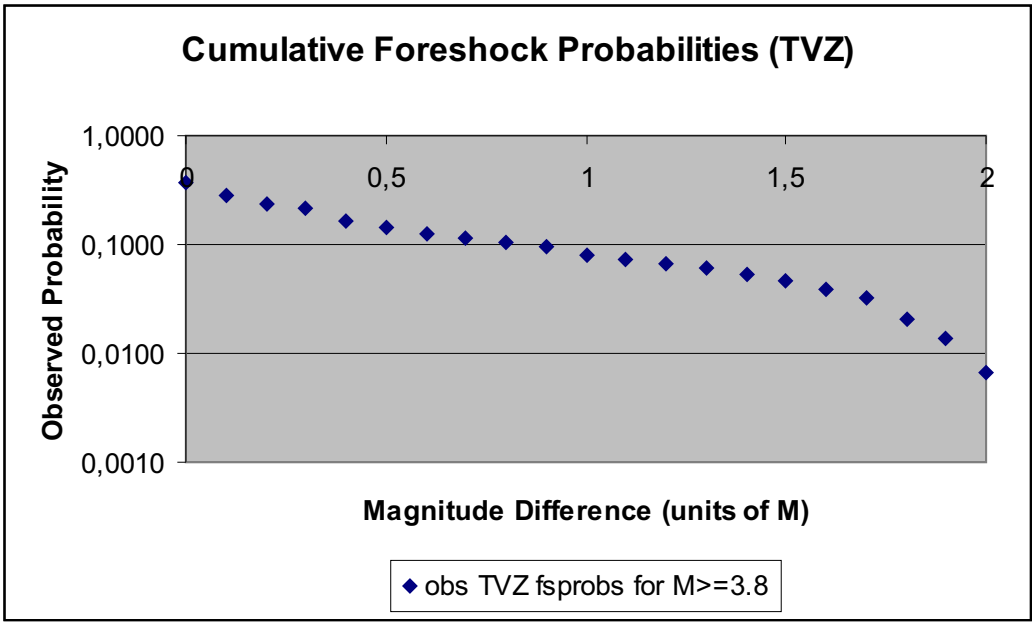

Figure 3.10: Cumulative foreshock probabilities with increasing magnitude differences between foreshock and mainshock (TVZ)

That law calculates the number of earthquakes of magnitude M or greater as follows (**Gutenberg, 1944** [19]):

$$log(N \geq M) = a - bM \tag{3.6}$$

Therefore the number of mainshocks with certain magnitude differences δmag from the foreshock is described by

$$N \geq (M_{fs} + \delta mag) = 10^{a-b(M_{fs}+\delta mag)} \tag{3.7}$$

Accordingly the data should be fitted through the fit function:

$$fitdata(\delta mag) = 10^{a-b(M_{fs}+\delta mag)} \tag{3.8}$$

a and b are parameters: a is the scaling factor describing the total number of pairs and b is the slope of the data line in the logarithmic plot, usually close to 1.

a can be calculated by taking the observed probability for $\delta mag = 0$ and solving equation 3.8 for a:

$$\begin{aligned} P(n|N, t = 1, r = 10, \delta mag = 0) &= 10^{a-bM_{fs}} \\ log(P(n|N, t = 1, r = 10, \delta mag = 0)) &= a - bM_{fs} \\ log(P(n|N, t = 1, r = 10, \delta mag = 0)) + bM_{fs} &= a \end{aligned} \tag{3.9}$$

Substitution into equation 3.8 gives

$$\begin{aligned} fitdata(\delta mag) &= 10^{log(P(n|N,t=1,r=10,\delta mag=0))+bM_{fs}-b(M_{fs}+\delta mag)} \\ &= 10^{log(P(n|N,t=1,r=10,\delta mag=0))-b*\delta mag} \\ &= P(n|N, t = 1, r = 10, \delta mag = 0)10^{-b*\delta mag} \end{aligned} \tag{3.10}$$

$P(n|N, t = 1, r = 10, \delta mag = 0)$ has been calculated from the catalogue (0.0046 for Non-TVZ, 0.0375 for the TVZ) and is for simplicity reasons assumed to have no errors, so the fit function depends on the parameter b only. Minimising the least square error

$$err = \sum_{i=1}^{k} (data(i) - fitdata(i))^2 \tag{3.11}$$

where k is the number of magnitude steps ($k = 21$), for different values of b, the above mentioned nonlinear regression program determined the best fit for

$$\begin{aligned} b_{TVZ} &= 1.3 \pm 0.2 \\ b_{Non-TVZ} &= 1.3 \pm 0.1 \end{aligned}$$

Fig. 3.11 shows data and models with their 95% confidence bands for Non-TVZ and TVZ.

The statistical test for this fit calculated the coefficient of determination, R^2, to be 0.8 for the TVZ and 0.94 for the Non-TVZ and therewith indicates a good approximation of the data.

The apparent misfit for $\delta mag > 1.0$ especially for the TVZ data (bottom plot in Fig. 3.11) is not significant: the uniform probability values for these magnitude differences are artifacts produced by the beta distribution (equation 3.3). There have been no observations in these categories and instead of probability zero suggested by the data set the artificial value of 0.00675 has been calculated with the beta distribution. The underestimation of this value by the model is therefore closer to the data themselves and should not be rejected as it stays positive, too.

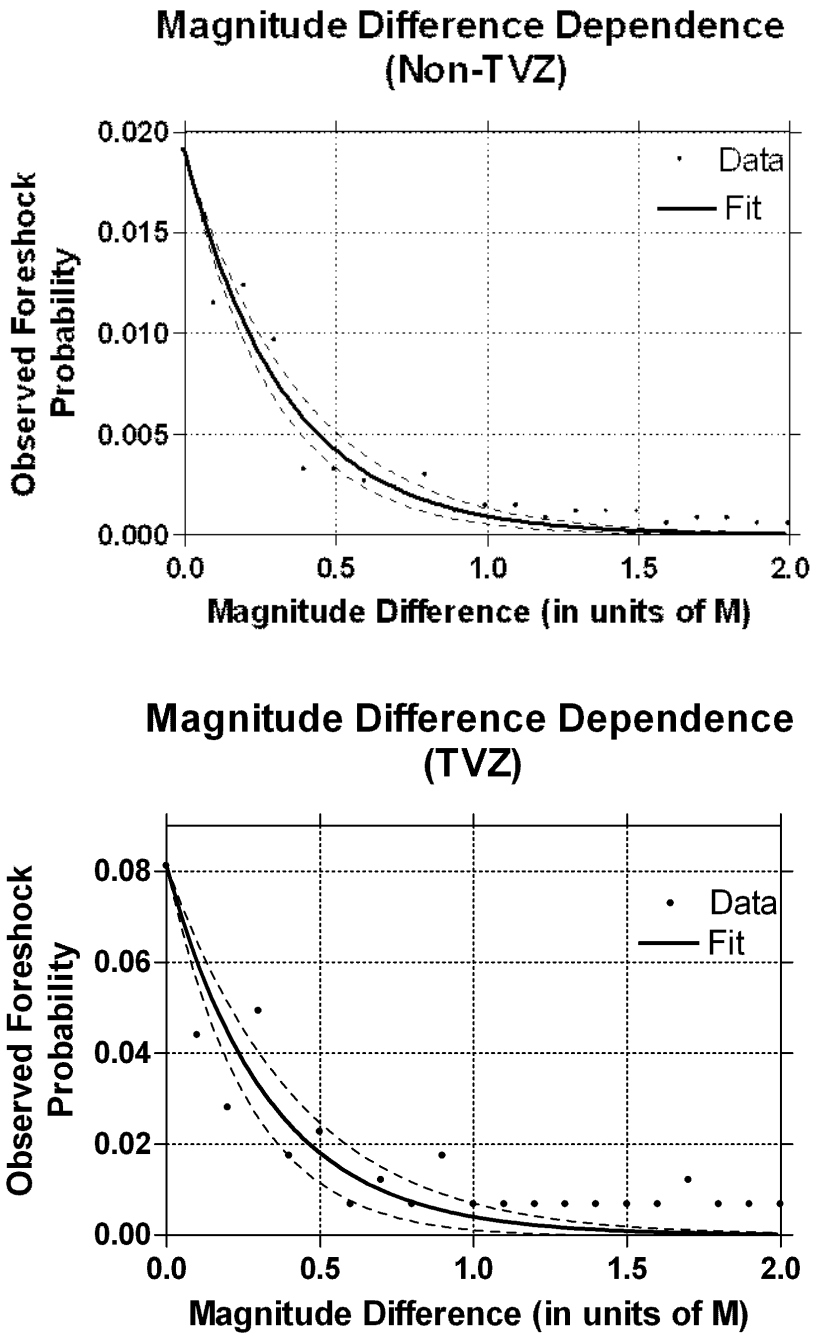

Figure 3.11: Foreshock probability dependence on magnitude differences between foreshock and mainshock (top: Non-TVZ, bottom: TVZ). The model is a least square fit to the data, using the fit function 3.10 with a b-value of 1.3 The dotted line is the 95% confidence band for the fit.

3.3.4 Distance dependence

The grey scale plots presented earlier to demonstrate foreshock magnitude independence (Fig. 3.5 and 3.6) showed a strong decay of foreshock probability with increasing distance and time between foreshock and mainshock. This section and the following are concerned with investigating the spatial and temporal decay.

As justified above, New Zealand foreshock probabilities can be assumed to be independent of the foreshock magnitude. Further calculations can therefore be done without separating the foreshock magnitudes. However, the difference between foreshock magnitude and mainshock magnitude is significant in that similar sized pairs are more likely than pairs with large magnitude differences. So relationships for spatial and temporal decay have to be verified for different foreshock- mainshock magnitude differences.

Figure 3.12 shows that the foreshock probabilities decrease with distance for all different categories of magnitude difference between foreshock and mainshock (represented by different colours). The black line is the total foreshock probability, when not separating magnitudes. The probabilities shown are those per square kilometer for the full five day period.

There are several possibilities to display the data: in the middle of each bin, at the point of the average position within the bin, or, as I chose to use, at the edge of each bin, i.e. the data collected within 0-10 km, 10-20 km, etc are shown at 10 km, at 20 km, etc.

The plots show that foreshock probabilities decrease with increasing distance between triggering and triggered event. The shape of the decay seems to be very similar for all magnitude differences, even though the few data for large magnitude differences limits interpretations.

The shape of the decay suggests that the decay is dominated by 1/distance. Therefore the function that I used to fit to the data was

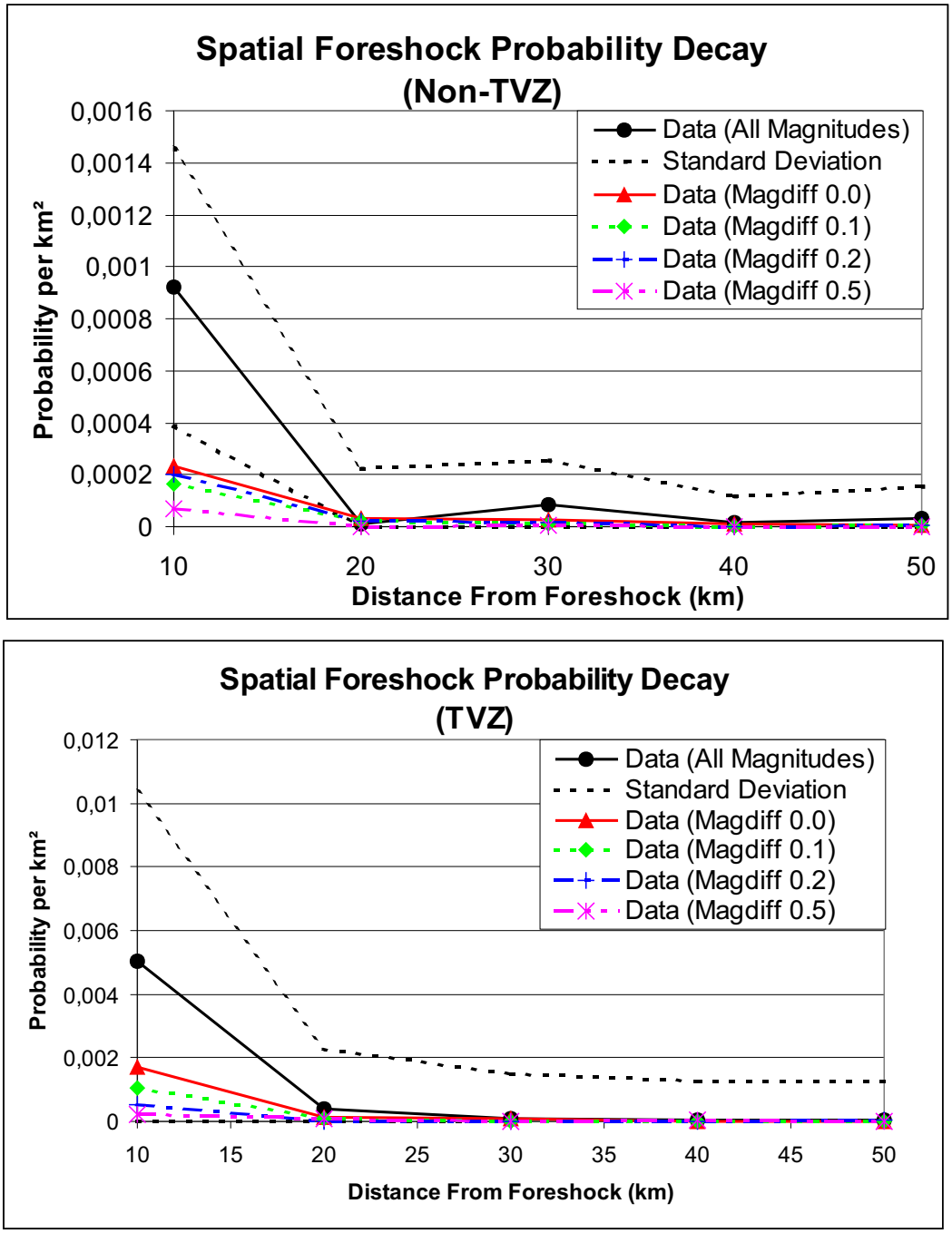

Figure 3.12: Spatial decay of foreshock probabilities for varying magnitude differences (top: Non-TVZ, bottom: TVZ). The black line is the total foreshock probability when not separating magnitudes (dashed is the standard deviation). The other coloured lines show the data for magnitude differences 0.0 (red), 0.1 (green), 0.2 (blue), and 0.5 (magenta)

$$fitdata(r) = \frac{a}{r^{rexp}} \tag{3.12}$$

$$a = P(n|N, r = 10) * 10^{rexp} \tag{3.13}$$

a is the scaling factor taking into account the probability observed closest to the foreshock. Again, a is treated without errors. The factor 10 has come in because units of r are kilometers not tens of kilometers. The least square fit was minimised for

$$rexp_{TVZ} = 3.63 \pm 0.02$$

$$rexp_{NonTVZ} = 2.7 \pm 0.2$$

Figures 3.13 and 3.14 show data and models with their 95% confidence bands for Non-TVZ and TVZ. The fit is extremly good in both cases. This is also strengthened by very high coefficients of determination: $R^2 = 1$ for both, the TVZ and Non-TVZ fits.

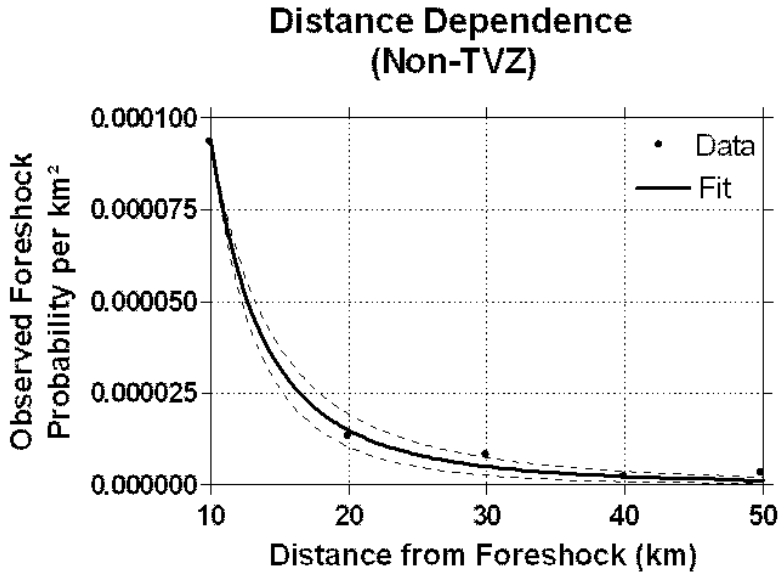

Figure 3.13: Foreshock probability dependence on distance between foreshock and mainshock (Non-TVZ). The model is a least square fit to the data, using the fit function 3.13 with an exponent of 2.7. The dotted line is the 95% confidence band for the fit.

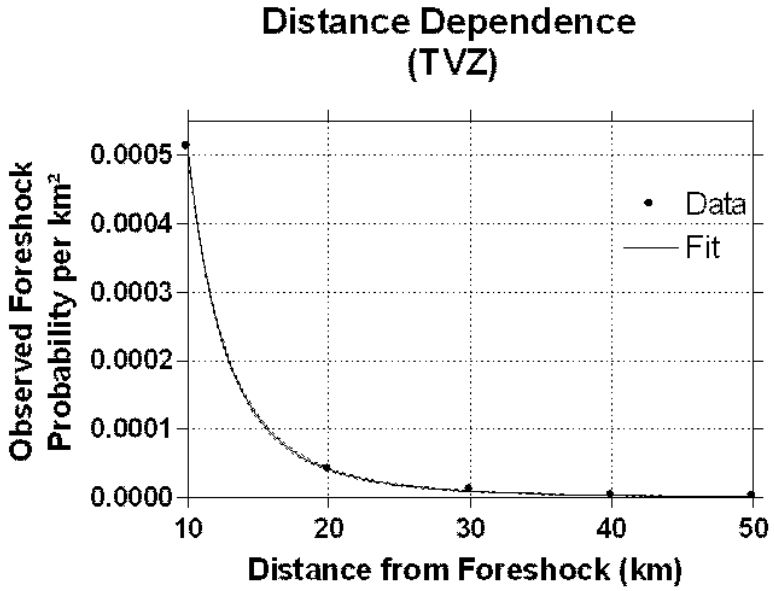

Figure 3.14: Foreshock probability dependence on distance between foreshock and mainshock (TVZ). The model is a least square fit to the data, using the fit function 3.13 with an exponent of 3.6. The dotted line is the 95% confidence band for the fit.

Figures 3.15 to 3.19 show the high degree of fit of the probabilities for some foreshock-mainshock magnitude differences. The fit is equally good for other magnitude differences, not shown here.

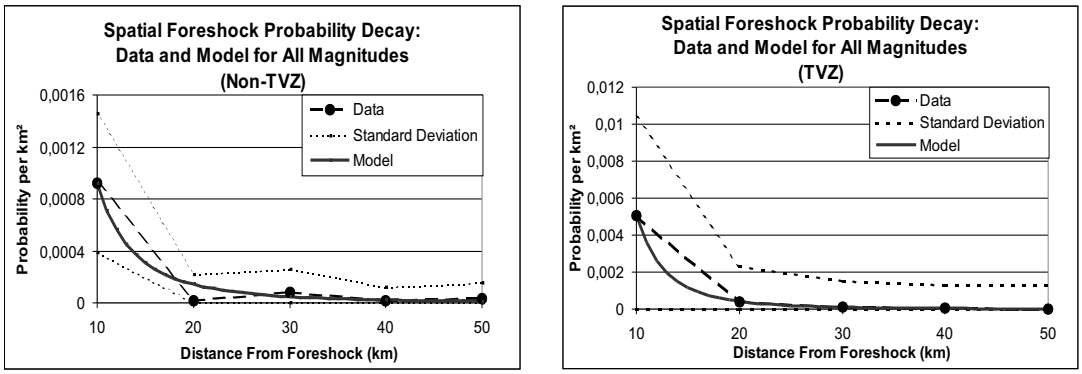

Figure 3.15: Comparison between data and model for all magnitudes (Non-TVZ left, TVZ right)

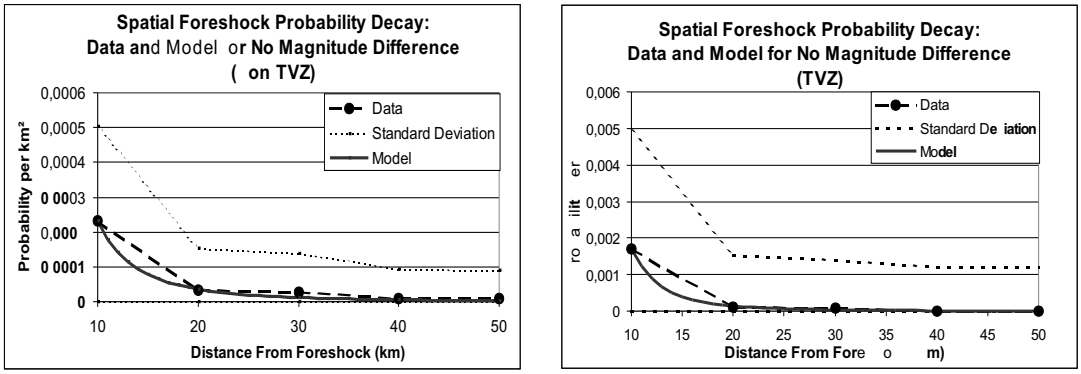

Figure 3.16: Comparison between data and model for no magnitude difference between foreshock and mainshock (Non-TVZ left, TVZ right)

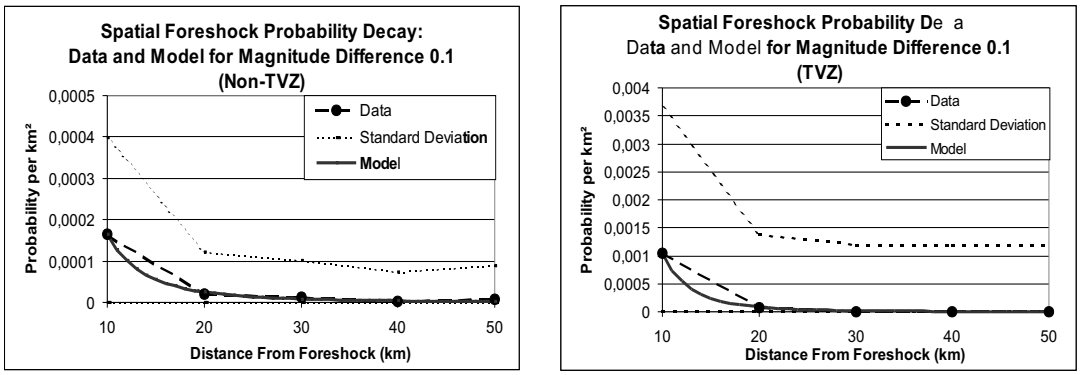

Figure 3.17: Comparison between data and model for 0.1 magnitude difference between foreshock and mainshock (Non-TVZ left, TVZ right)

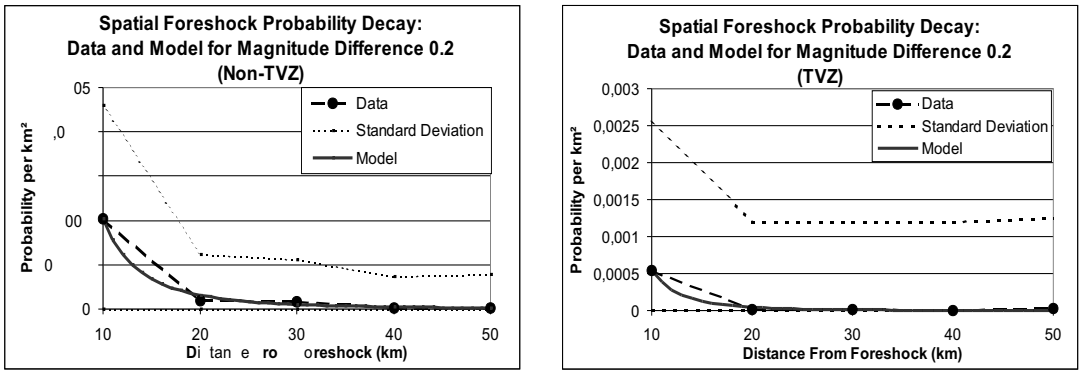

Figure 3.18: Comparison between data and model for 0.2 magnitude difference between foreshock and mainshock (Non-TVZ left, TVZ right)

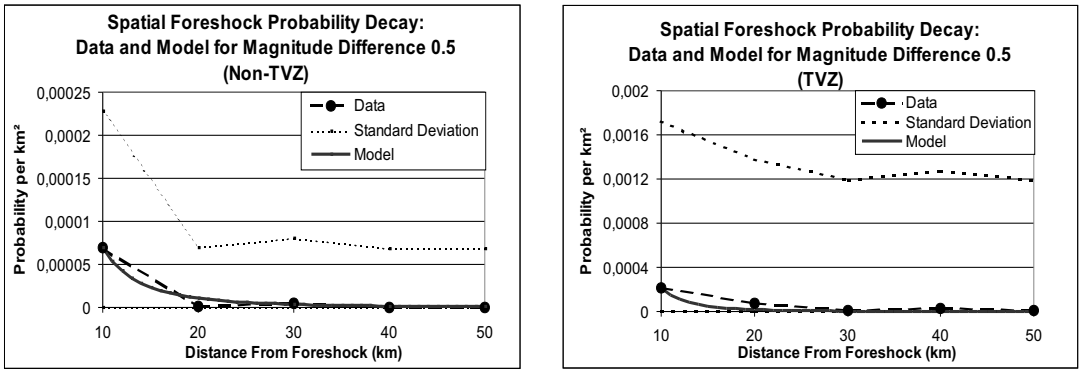

Figure 3.19: Comparison between data and model for 0.5 magnitude difference between foreshock and mainshock (Non-TVZ left, TVZ right)

The fit shown in the figures is calculated with always the same exponent (from the least square fit result) and changing scaling factor a with δmag.

The data from these plots suggest that there is no magnitude dependence in the spatial decay, i.e. the spatial decay is independent of the magnitude distribution.

3.3.5 Time dependence

As in the spatial behaviour, the temporal decay patterns of foreshock probabilities are studied without distinguishing different foreshock magnitudes, but with considering magnitude differences between the paired events.

In order to reveal foreshock variability with time I counted all foreshock-mainshock pairs that happened within 24 hours, between 24 and 48 hours, between 48 and 72 hours, and so on, up to five days. The maximum time of five days is consistent with former definitions of foreshocks for New Zealand. I counted events over a longer period, but the trend observable during the first five days continued and the absolute numbers were so small already, that it seems well justified to keep the New Zealand standard definition.

From the number of events, I calculated the daily probabilities following the method described earlier.

The following plots (Fig. 3.20 and 3.21) show an overview of the calculated foreshock probabilities for the first five days after the triggering event in the TVZ and outside. They include all identified pairs in the region, i.e. whose events were closer than 50 kilometer apart.

The differently coloured lines represent the data collected for different magnitude ranges between foreshock and mainshock. I plotted magnitude differences of 0, 0.1, 0.2, 0.5 magnitudes in order to give an idea of the general pattern. The other magnitude differences show the same behaviour.

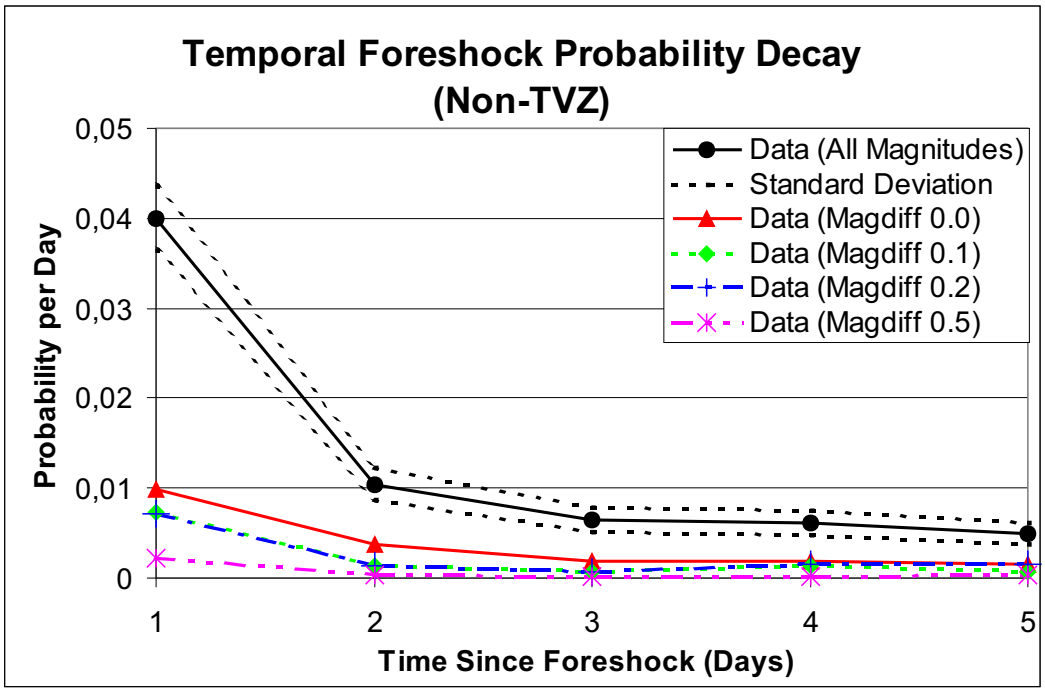

Figure 3.20: Temporal decay of foreshock probabilities for varying magnitude differences (Non-TVZ). The black line is the total foreshock probability when not separating magnitudes (dashed is the standard deviation). The other coloured lines show the data for magnitude differences 0.0 (red), 0.1 (green), 0.2 (blue), and 0.5 (magenta)

The black line is the sum of all foreshocks over the different mainshock magnitudes. It is shown with the associated standard deviation (dotted lines).

As described earlier, here, too, the data are plotted on the edge of the bin, i.e. all events that happened within the first 24 hours are plotted at 1 day, between 24 and 48 hours at day 2, etc.

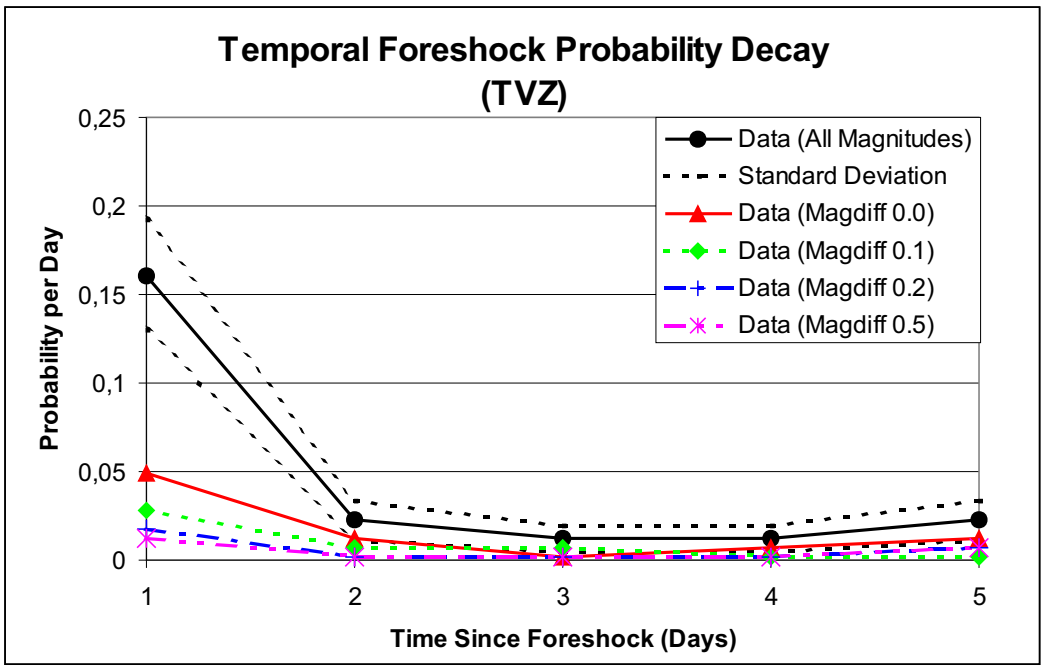

Figure 3.21: Temporal decay of foreshock probabilities for varying magnitude differences (TVZ). The black line is the total foreshock probability when not separating magnitudes (dashed is the standard deviation). The other coloured lines show the data for magnitude differences 0.0 (red), 0.1 (green), 0.2 (blue), and 0.5 (magenta)

The data agrees with former studies (e.g. **Jones, 1985** [25], **Savage and DePolo, 1993** [49]), which show that foreshock probabilities decrease approximately inversely with time.

The character of the fit function is therefore:

$$fitdata(t) = \frac{d}{(t+c)^{texp}} \tag{3.14}$$

$$d = P(n|N, t=1) \tag{3.15}$$

where t is the time since the potential foreshock in days and d is a scaling factor to

approximate the initial probabilities that are observed for the first day. c is a constant that helps avoid a singularity for $t = 0$.

The best-fit values have been computed to be

$$\begin{aligned} c_{TVZ} &= 0.001 \pm 0.03 \\ texp_{TVZ} &= 2.4 \pm 0.5 \\ c_{NonTVZ} &= 0.005 \pm 0.03 \\ texp_{NonTVZ} &= 1.6 \pm 0.2 \end{aligned}$$

Figures 3.22 and 3.23 show data and models with their 95% confidence bands for Non-TVZ and TVZ.

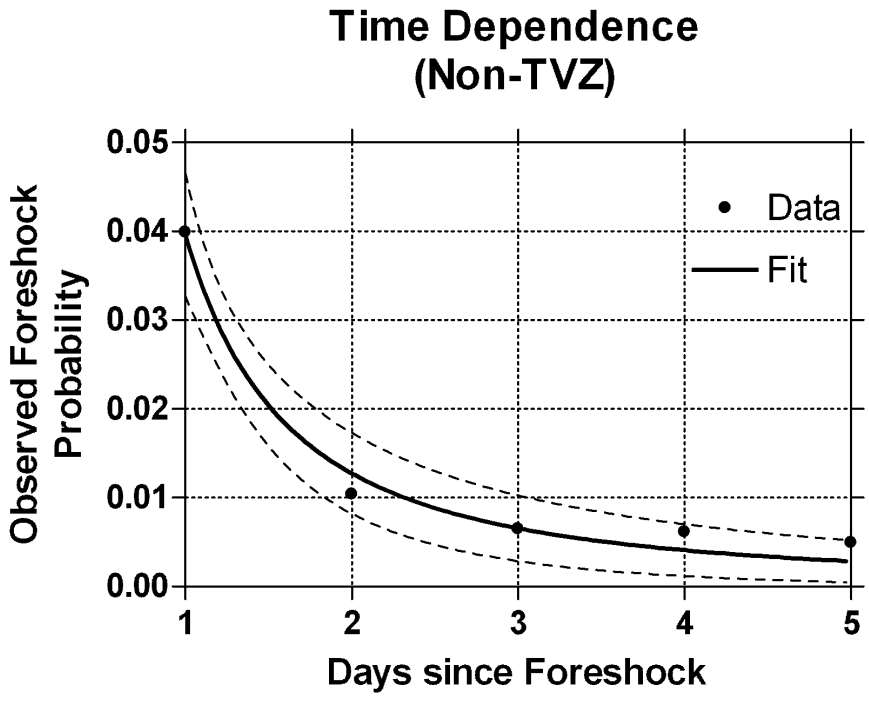

Figure 3.22: Foreshock probability dependence on time differences between foreshock and mainshock (Non-TVZ). The model is a least square fit to the data, using the fit function 3.15 with an exponent of 1.6. The dotted line is the 95% confidence band for the fit.

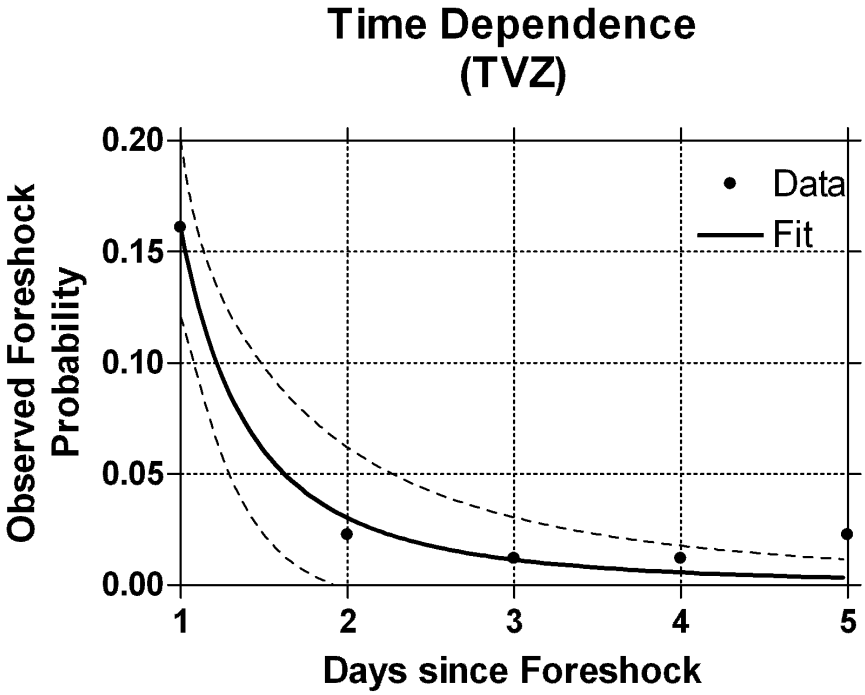

Figure 3.23: Foreshock probability dependence on time differences between foreshock and mainshock (TVZ). The model is a least square fit to the data, using the fit function 3.15 with an exponent of 2.4. The dotted line is the 95% confidence band for the fit.

The coefficients of determination, R^2 indicate a good result for both regions:

$$R^2_{NonTVZ} = 0.98$$
$$R^2_{TVZ} = 0.97$$

Figures 3.24 to 3.28 show how well the least square fit function, developed on the dataset of all foreshock-mainshock pairs, describes the subsets of pairs with certain magnitude differences.

As previously shown for distance dependence, I use the same exponent and move the intercept up or down to match the data for the particular magnitude difference.

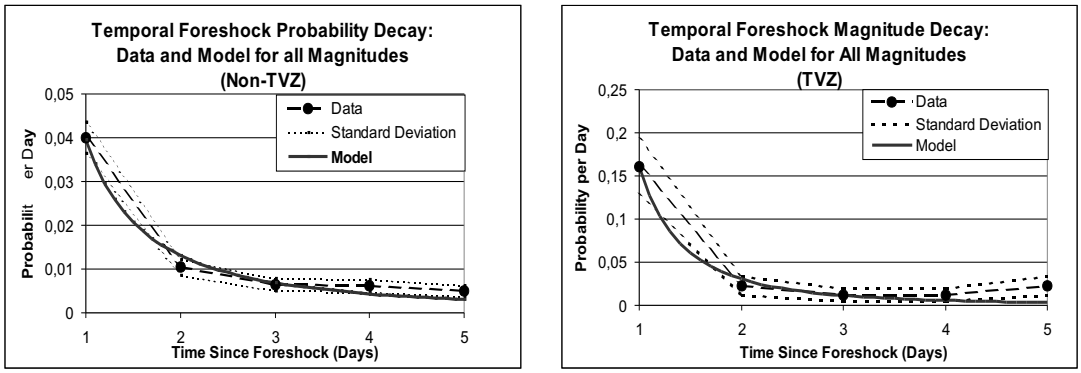

Figure 3.24: Comparison between data and model for all magnitudes (Non-TVZ left, TVZ right)

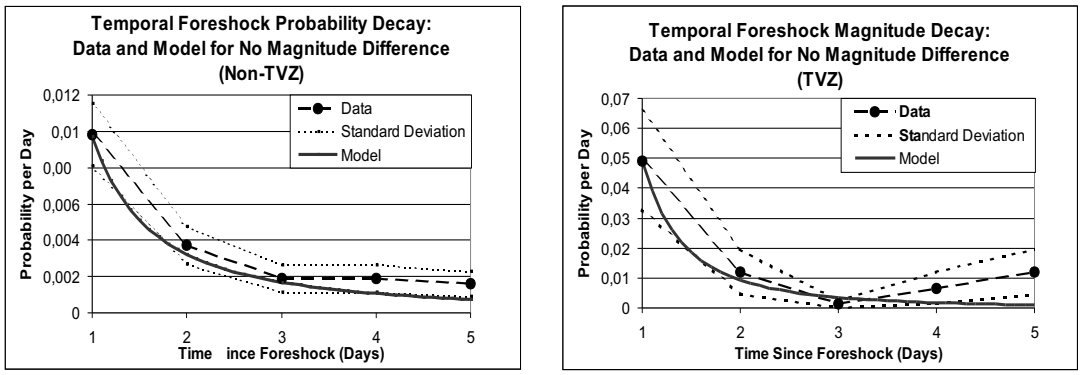

Figure 3.25: Comparison between data and model for no magnitude difference between foreshock and mainshock (Non-TVZ left, TVZ right)

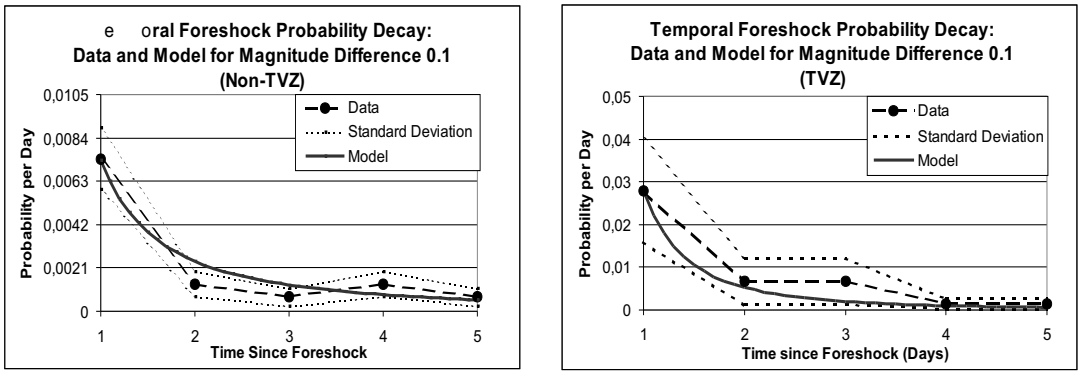

Figure 3.26: Comparison between data and model for 0.1 magnitude difference between foreshock and mainshock (Non-TVZ left, TVZ right)

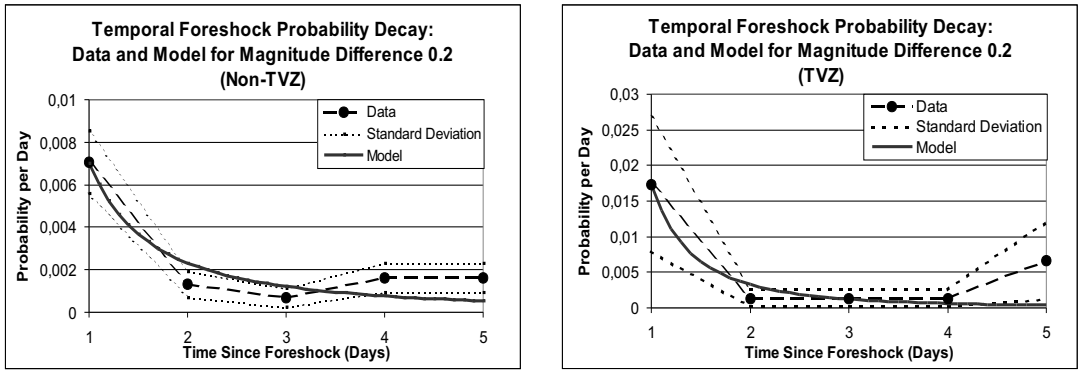

Figure 3.27: Comparison between data and model for 0.2 magnitude difference between foreshock and mainshock (Non-TVZ left, TVZ right)

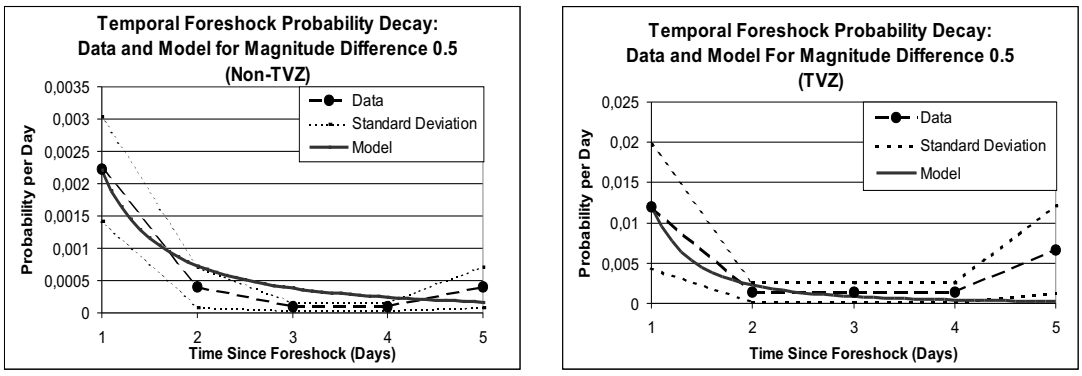

Figure 3.28: Comparison between data and model for 0.5 magnitude difference between foreshock and mainshock (Non-TVZ left, TVZ right)

3.3.6 Are foreshock probabilities constant over time?

This question is not easy to answer, because by reducing the time span looked at to achieve more resolution in the temporal dimension, the amount of data gets rapidly reduced. Still, as long as we assume that there are no periodic changes, or too small changes to resolve, it is possible to give an idea of whether foreshock probabilities are sensitive to the choice of different time periods of the catalogue. Therefore I split the catalogue in halves and ran the programs on each of the parts and compared the two and both with the results from the whole catalogue (Fig. 3.29 and 3.30).

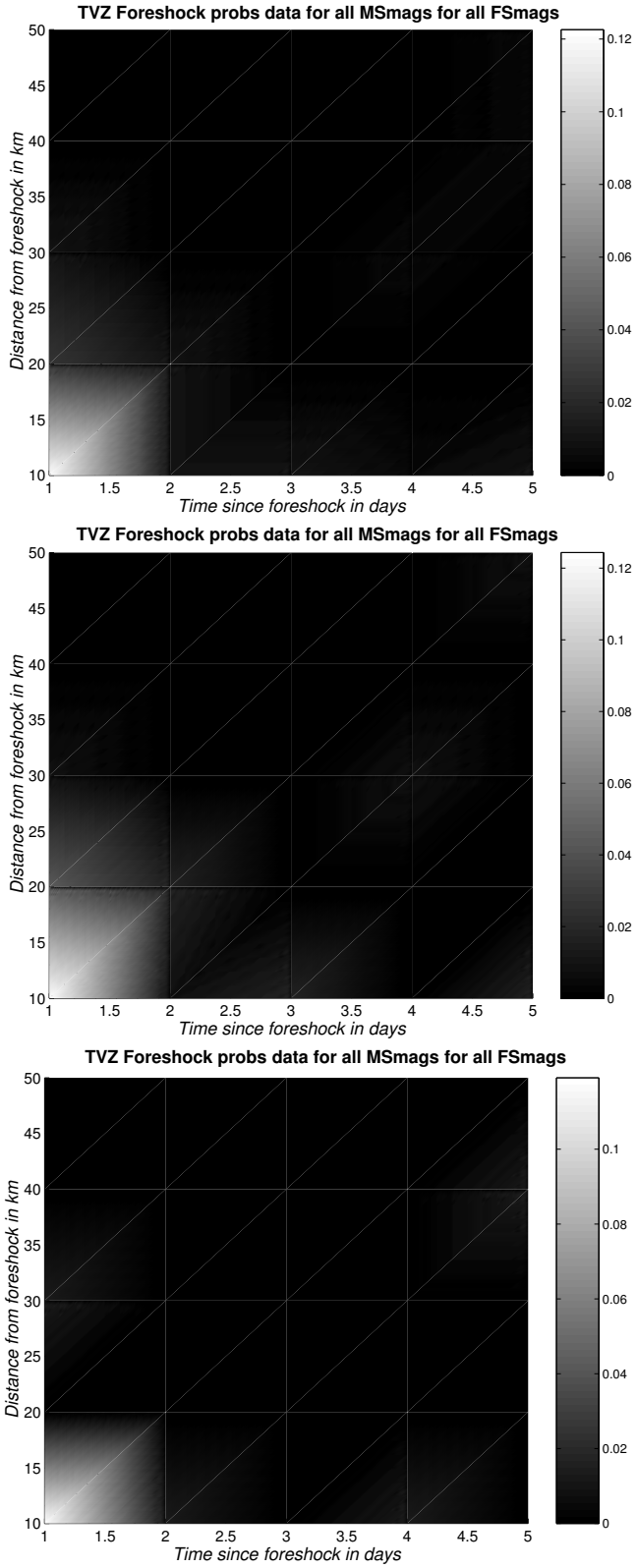

Figure 3.29: Variability in foreshock probabilities for different catalogue subsets (TVZ). Top: New Zealand catalogue 1964-2003, middle: New Zealand catalogue 1964-1984, bottom: New Zealand catalogue 1985-2003

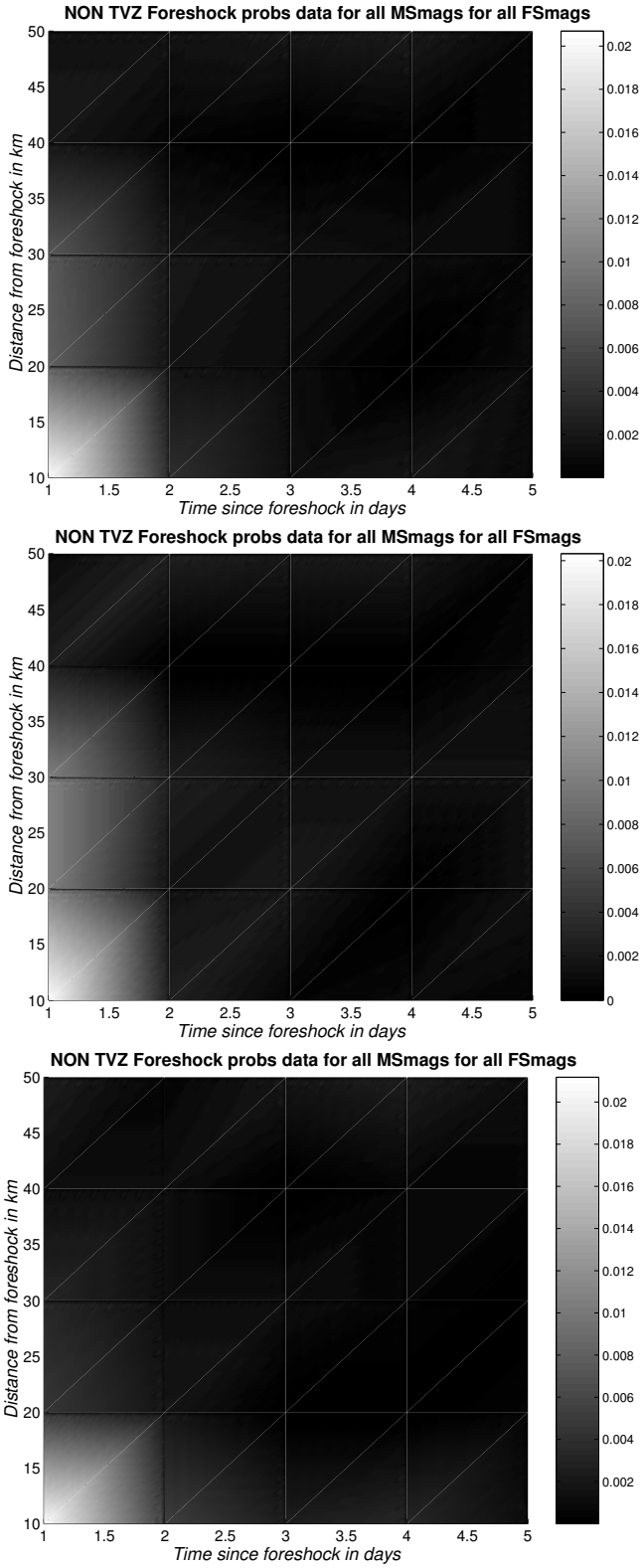

Figure 3.30: Variability in foreshock probabilities for different catalogue subsets (Non-TVZ). Top: New Zealand catalogue 1964-2003, middle: New Zealand catalogue 1964-1984, bottom: New Zealand catalogue 1985-2003

The similarities in the behaviour for the different subsets and the whole of the catalogue are strong. They suggest that foreshock probabilities could be constant over time, i.e. independent of the part of the catalogue they are derived from. Also, the maximum observed probabilities are similar:

Catalogue	Total probability (5 days, 50km, all δmag)	Maximum probability (1^{st} day, 10km, δmag=0)
1964-2003	0.22 ± 0.03 (TVZ)	0.12 ± 0.02 (TVZ)
	0.068 ± 0.004 (Non-TVZ)	0.021 ± 0.002 (Non-TVZ)
1964-1984	0.26 ± 0.04 (TVZ)	0.12 ± 0.03 (TVZ)
	0.072 ± 0.006 (Non-TVZ)	0.02 ± 0.003 (Non-TVZ)
1985-2003	0.17 ± 0.04 (TVZ)	0.12 ± 0.04 (TVZ)
	0.062 ± 0.006 (Non-TVZ)	0.021 ± 0.004 (Non-TVZ)

Table 3.7: Maximum probability values observed for different parts of the catalogue

The similarities of the probabilities for different catalogue subsets indicate time independence in the probabilities. However, the short duration of the catalogue places some limitations on that conclusion.

3.4 Discussion and evaluation

New Zealand earthquake data from the last 40 years have been statistically analysed to develop predictive relations that describe the temporal and spatial decay of foreshock probabilities, as well as decay with increasing magnitude differences. The TVZ has been analysed separately from the rest of New Zealand.

Five main properties have been found:

- The chances of a bigger event following close in time and space are the same for different magnitudes of the triggering earthquake.
- Foreshock probabilities in the TVZ exceed the values for the rest of the country by a factor of approximately 3 (22% compared to 7%).

- The magnitude distribution of the mainshock in the foreshock-mainshock pairs follows the Gutenberg-Richter relationship with a b-value of 1.3 ± 0.2 for TVZ and 1.3 ± 0.1 for Non-TVZ.

- Foreshock probabilities decrease faster with time in the TVZ with $1/t^{2.4\pm0.5}$ compared to the rest of New Zealand, where they decrease with $1/t^{1.6\pm0.2}$

- Spatial decay of foreshock probabilities is faster in the TVZ, too. It goes as $1/r^{3.63\pm0.03}$ inside and $1/r^{2.7\pm0.2}$ outside.

3.4.1 Foreshock magnitude independence

Considering that I am dealing with observational data over a relatively short time period of 40 years (which is especially short for larger events that occur less often), the agreement of the probability distributions for different foreshock magnitudes is remarkable. It justifies the assumption that foreshock probabilities and their decay behaviour are independent of the foreshock magnitude. However, we do not have enough data for high magnitudes to prove that assumption. Rather we cannot disprove it. So the best approximation at this stage is to assume foreshock magnitude independence for the whole magnitude band, which is the outcome of other regional studies as well, e.g. Nevada (**Savage and DePolo, 1993** [49]). **Jones, 1985** [25] found foreshock magnitude independence for $3 \leq M \leq 5$ foreshocks in southern California, but saw an increased probability for events greater than M=5 to be followed by a larger earthquake.

3.4.2 Higher probabilities in the TVZ

The Taupo Volcanic Zone is an area of ongoing volcanism, associated normal faults (i.e. extension) and high thermal activity. It differs in many physical properties from the rest of the country. Especially, many earthquake swarms are observed in the region (**Sherburn, 1992**, [52]), which is likely to increase foreshock probabilities, as matching intraswarm events will get counted as pairs.

The increased probabilities for the TVZ are a reproduction of **Merrifield et al.'s,**

2004 [32] findings. However, the calculated probabilities are not the same: the earlier study suggested 6% of events outside the TVZ to be followed by equal sized or larger ones, too, but found only 9% (compared to 22% in this study) of TVZ earthquakes to be foreshocks. This discrepancy could be an artifact produced by different definitions of what pairs to call located in the TVZ. This study only requires the foreshock to be located within the boundaries, not the mainshock.

Similar observations are made in other volcanic regions, e.g. foreshock probabilities are higher in the Basin and Range, an extensional region of diffuse seismicity, compared to Southern California (**Savage and DePolo, 1993** [49]).

3.4.3 *b*-value

Two aspects need noting considering the result for the b-value.

First, the b-value of 1.3 determined for events that had foreshocks is higher than the slope of the magnitude distribution of all New Zealand events above the completeness level. Generally the b-value for the country is taken to be slightly less than 1.0. However, the value of 1.3 for the TVZ agrees with the b-value of 1.3 ± 0.2 that **Smith and Webb, 1986** [55] calculated for TVZ events with minimum magnitude 4.5 between 1940 and 1983.

Secondly, it is quite surprising that the results are the same for the TVZ and the rest of the country. The TVZ shows a very high occurrence of earthquake swarms of small to moderate magnitudes. Meanwhile it does not feature faults capable of producing very large events. This would suggest the expectation of a steeper slope of events on a logarithmic magnitude distribution plot, i.e. a higher b-value for the TVZ. Earthquakes are often due to volcanic processes and therefore b-values are usually higher in volcanic regions compared to non-volcanic regions. It is remarkable that this is not the case in this data set.

Using a similar technique **Savage and DePolo, 1993** [49] found the expected higher b-value for the extensional Mammoth/Mono region (0.89 ± 0.03 compared to 0.72 ± 0.03 for Nevada).

3.4.4 Temporal decay

Other unexpected results are the exponents describing the temporal decay. Previous studies that looked into foreshock probability decay over time after an event found that foreshock probabilities behave extremly similar to the frequency decay of an aftershock sequence, modelled by a modified Omori's law (**Utsu et al., 1995** [61]):

$$R(t) = \frac{1}{(t+c)^p} \tag{3.16}$$

where c is small and p usually very close to one. **Jones, 1985** [25] and **Savage and DePolo, 1993** [49] determined p for Southern Californian and Western Nevada's foreshock probabilities, and got values of 0.9 and 1.0, respectively.

It is certainly a very interesting finding that New Zealand foreshock probabilities do not follow this generic law, at least not with the generally observed decay exponent of approximately one, but 1.6 ± 0.2 and 2.4 ± 0.5 for Non-TVZ and TVZ, respectively.

It should be examined, whether the exponents vary, if the data is discretised hourly (as in the Californian studies) rather than daily as in this study. However, the smaller amount of data in New Zealand could complicate the analysis on an hourly basis.

3.4.5 Spatial decay

More difficult to interpret are the results for the spatial decay because there are not as well established laws for distance dependence as for time dependence against which the data could be compared. The result of stronger localisation in the TVZ agrees well with the findings of high seismic attenuation in the Central Volcanic Region (**Salmon et al., 2002**) [48], i.e. the dynamic triggering effect is diminished over shorter distances than in the rest of the country. The surprising result that the probabilities' decay exponent is closer to three rather than two could be explained as a combination of spherical divergence, which is a likely candidate for explaining spatial decay patterns and decreases with radius squared, and an extra factor due the high attenuation.

For this analysis, too, it would be worthwhile to compare the results with a finer resolution of foreshock-mainshock distances (i.e. discretising on 1 km bins rather than

10 km bins).

3.5 The model in summary

Three sets of equations have been developed to model each of the observed decays for foreshock probabilities within the TVZ and outside: the decay with increasing magnitude difference, increasing time and increasing epicentral distance.

The variability in foreshock probabilities for the range of magnitude differences between the events can be modelled through equation 3.10. The temporal and spatial windows so far used for foreshock studies can be replaced by functions describing the decay that has been observed (equations 3.15 and 3.13).

Multiplying the three equations allows me to model the probabilities in all three dimensions. The time, distance and magnitude dependent foreshock probability model for New Zealand is given by:

$$\begin{aligned} fsprob(t,r,\delta mag) &= P(n|N,t=1,r=10,\delta mag=0)*10^{-b*\delta mag} \\ &\quad *\frac{1}{(t+c)^{texp}}*\frac{10^{rexp}}{r^{rexp}} \end{aligned} \tag{3.17}$$

$$fsprob_{TVZ}(t,r,\delta mag) = 0.0375*10^{-1.3\delta mag}*\frac{1}{(t+0.001)^{2.4}}*\frac{10^{3.6}}{r^{3.6}} \tag{3.18}$$

$$fsprob_{NonTVZ}(t,r,\delta mag) = 0.0049*10^{-1.3\delta mag}*\frac{1}{(t+0.005)^{1.6}}*\frac{10^{2.7}}{r^{2.7}} \tag{3.19}$$

Part II

Aftershock Probability Model

Chapter 4

International Studies

The occurrence of – sometimes big – aftershocks after large events is a well known pattern of earthquake clustering. For more than 100 years scientists around the world have been studying earthquake sequences in order to describe aftershock productivity in time and space.

This chapter summarises some of the more important results of aftershock studies of the last century.

4.1 Omori

In 1894 **Omori** [36], [37] proposed a formula describing the time decay in aftershock activity. He derived it from studying the temporal distribution of felt aftershocks following the 1891 Nobi, Central Japan, and two more Japanese earthquakes. After attempting to fit the data using the commonly observed exponential decay function, he found that the frequency of aftershocks per unit time interval $n(t)$ at a time t is better represented by a power law dependence on time:

$$n(t) = \frac{K}{(t+c)} \tag{4.1}$$

where K and c are constants.

Omori, 1894 found that the aftershock sequence of the 1889 Kumamoto earthquake could be better fitted by the first two terms of the following equation, from which equation 4.1 is the simplest approximation.

$$n(t) = \frac{K}{(t+c) + k'(t+c)^2 + k''(t+c)^3 + ...} \tag{4.2}$$

Equation 4.1, commonly known as the original Omori formula, also the hyperbolic law, has been successfully applied to many aftershock sequences worldwide. **Omori, 1902** [38] observed a good fit between model and data for the 1891 Nobi aftershocks for a time interval of ten years after the mainshock. Fig. 4.1 (top) shows the high degree of fit between Omori's felt data from Gifu, a city in the aftershock zone of the Nobi aftershock sequence and the fitted Omori formula. Additionally, the rates of felt shocks recorded at JMA's Gifu Observatory during 1900-1991 have been plotted. The bottom part of the plot shows the cumulative number of events through the century and the integrated form of Omori's formula.

The Omori formula has also been found to fit secondary aftershock sequences, i.e. the aftershock sequences of aftershocks. As one example, the secondary aftershocks of the April 1 aftershock of the Tango earthquake of March 7, 1927, were well fitted by

equation 4.1 (**Jeffreys, 1938** [23]).

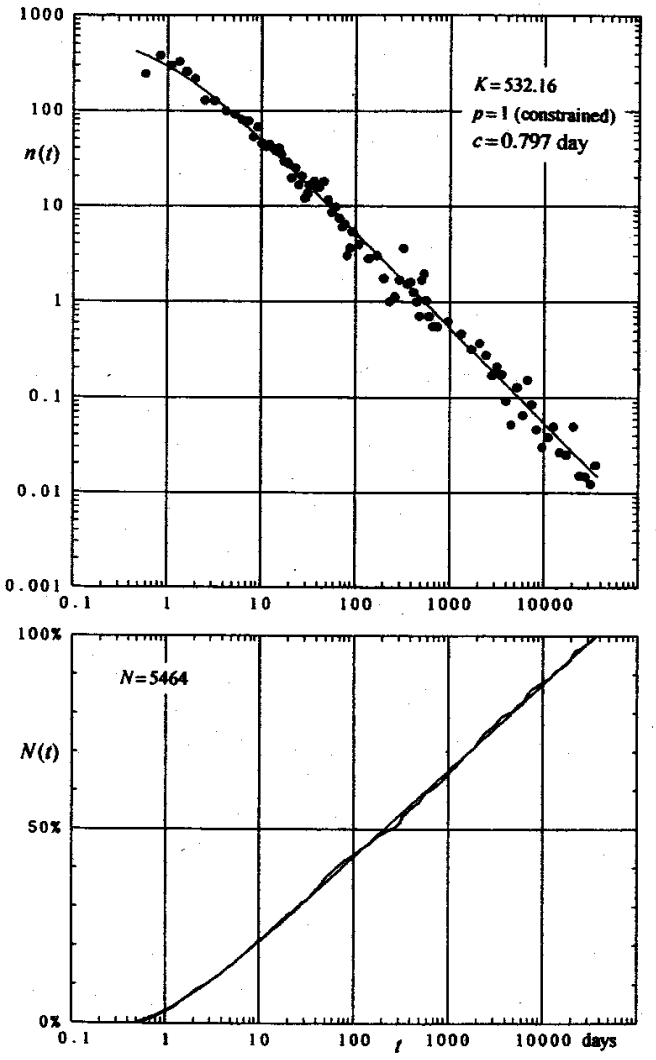

Figure 4.1: Occurrence rate (top) and cumulative number (bottom) of felt earthquakes at Gifu after the Nobi earthquake of 1891. Smooth curves represent the Omori formula fitted to the data. (Figure from **Utsu et al., 1995** [61])

4.2 Utsu

In 1957 **Utsu** showed that some aftershock sequences decay more rapidly than calculated by the original Omori formula and are better fitted by a slight modification of

equation 4.1:

$$n(t) = \frac{K}{(t+c)^p} \tag{4.3}$$

Utsu named equation 4.3 the modified Omori formula and estimated p and c values for 51 Japanese aftershock sequences. The range for p turned out to be 0.9 to 1.8, but most frequently p fell between 1.1 and 1.4. He could not find any correlation between p and the mainshock magnitude. The c values were scattered widely, from 0.01 to more than 1 day, with a median of 0.3 days. **Utsu** suggested that the p and c values are specific for each individual mainshock-aftershock sequence. (**Utsu et al., 1995** [61])

4.3 Reasenberg and Jones

Reasenberg and Jones, 1989 [42] combined the Gutenberg-Richter magnitude frequency distribution (**Gutenberg and Richter, 1944** [19]) (equation 3.6) and the modified Omori law (**Utsu et al., 1995** [61]) (equation 4.3) to calculate the probability for the occurrence of one or more aftershocks of a certain magnitude in any given time interval. They express the rate $R(t, M)$ of aftershocks of magnitude M or larger at time t after a mainshock of magnitude M_m as

$$R(t, M) = 10^{a+b(M_m - M)} \frac{1}{(t+c)^p} \tag{4.4}$$

where a, b, c and p are the constants from the Gutenberg-Richter and modified Omori laws. In 1994 **Reasenberg and Jones** [45] published a revised formula to calculate the probability P of one or more earthquakes equal to or greater than magnitude M occurring in the time range $T_1 \leq t \leq T_2$

$$P(t, M) = 1 - e^{-\int_{T_1}^{T_2} R(t,M)\, dt} \tag{4.5}$$

If $M_1 < M_2$, the difference $P(t, M_1) - P(t, M_2)$ gives the probability for occurrence of aftershocks of magnitude $M_1 \leq M \leq M_2$. For $M_2 = M_m$ this formula calculates the

probabilities for aftershocks. Setting $M_1 = M_m$ and $M_2 = \infty$, equation 4.5 produces foreshock probabilities.

The authors estimated the parameters of equation 4.4, a, b, c and p separately for 62 Californian aftershock sequences between 1933 and 1987 with a minimum mainshock magnitude of five, using the maximum likelihood method. To determine the Omori law's parameters they used all aftershocks of magnitude equal to or greater than $M_m - 3$. For parameter b all aftershocks of magnitude two and above were used. The median parameter values determined for the 62 sequences are called the "generic California" model (**Reasenberg and Jones, 1989** [42]):

$$\begin{aligned} a &= -1.67 \\ b &= 0.91 \\ c &= 0.05 \\ p &= 1.08 \end{aligned}$$

Reasenberg and Jones calculate probabilities for large aftershocks for certain time intervals at certain times after the mainshock. In their 1994 correction of the original formula from 1989 they estimate, for example that with a probability of 58% at least one $M \geq 5.5$ aftershock will follow a $M = 6.5$ within one week starting 0.01 days after the mainshock. The one-week probability drops to 5% when starting 15 days after the mainshock.

To support the validity of the generic model for earthquakes, the authors calculated the probability for larger events after a mainshock and compared the estimates with the independently obtained empirical frequency of foreshocks. For the first week after a magnitude five event, the foreshock occurrence rate suggests a probability of 5.9% for an equal or larger event to occur. The probability for the same interval calculated from the generic aftershock model is 10.1%.

Although any aftershock sequence has to be expected to depart from generic behaviour, the generic California model provides a useful starting point to estimate post-

mainshock hazard in the absence of any information but the mainshock magnitude.

4.4 Gerstenberger

Gerstenberger, 2003 [16] improved the generic California model by adding spatial information. He defines three different types of aftershock zones that require different amounts of information about the individual aftershock sequence.

The simplest model requires only knowledge of the mainshock magnitude. It assumes a circular aftershock zone which extends one fault length from the epicentre of the mainshock. This radius is calculated using the Wells and Coppersmith relationship (**Wells and Coppersmith, 1994** [65]). The model parameters a, b, c and p are used as given by the generic California model.

The second model is calculated once 100 aftershocks have been recorded. The aftershock zone is then defined based on the spatial distribution of seismicity. A two segment fault including the mainshock location is estimated from the largest spatial extent of the recorded seismicity (excluding outliers). The aftershock zone is defined to be the region of half a fault length around the constructed fault. With this sequence specific model the parameters are fitted to the ongoing aftershock sequence, which allows a more accurate modelling of the individual sequence.

The most complex model requires an externally calculated fault rupture model. Once that is available, every event within half a fault length of that model is considered an aftershock. If more detailed information about an appropriate radius is available, it gets included. This spatially varying model allows for heterogeneities in the spatial distribution of the parameters a, b, c and p. Fig. 4.2 shows a cartoon of the three possible aftershock zones for the 1992 Landers, California, earthquake.

For all three models the aftershock productivity is smoothed over the aftershock area. As no systematic study of the average spatial distribution of aftershocks within an aftershock zone has been done, **Gerstenberger, 2003** [16] based his smoothing on observations for the 1992 Landers earthquake's aftershock sequence. He found that

the aftershock density in that case decreased approximately as $\frac{1}{r^2}$ from the mainshock epicentre.

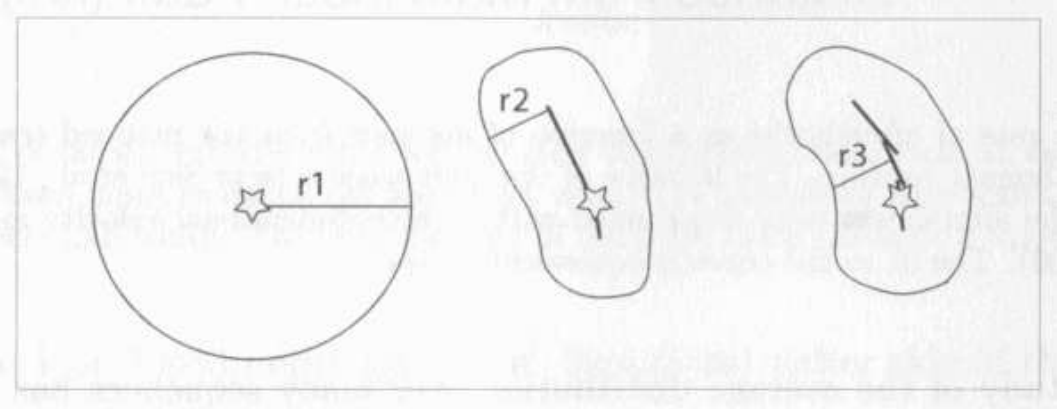

Figure 4.2: Cartoon of 3 possible aftershock zone models for Landers. Left: Simple model based on one Wells and Coppersmith radius (r1) from mainshock epicentre. Center: Synthetic fault model keeping all events within 1/2 of a Wells and Coppersmith radius (r2). Right: External model based on the slip model of **Wald and Heaton, 1994** [64] and keeping all events within radius r3. (Figure from **Gerstenberger, 2003** [16])

Gerstenberger calculates the aftershock probabilities on every node of a 0.05 degree grid overlying the above explained regions around mainshocks, following the most appropriate level of complexity depending on the availability of sequence data.

4.5 Christophersen

Christophersen, 2000 [8] established a global catalogue covering the period from 1964 to 1995 and including events of magnitude five and above to study probabilities of damaging earthquakes following damaging earthquakes on a global scale. Considering each earthquake to be a possible mainshock, she searched for related events in a circular area around the mainshock, using a magnitude dependent search radius:

$$r(M) = 4 * \sqrt{\frac{10^{1.02M-4.01}}{\pi}} \tag{4.6}$$

With each aftershock that was found in the spatial window, the temporal window

was extended by 30 days. The longest sequence using that definition was found to have a duration of 455 days.

The author fitted ellipses around the epicentre locations for each sequence, with the centre of the ellipses being the spatial mean. The ellipse fitting was designed to capture about 90% of the events associated with the mainshock by the initial search radius. One example of a fitted ellipse is shown in Fig. 4.3.

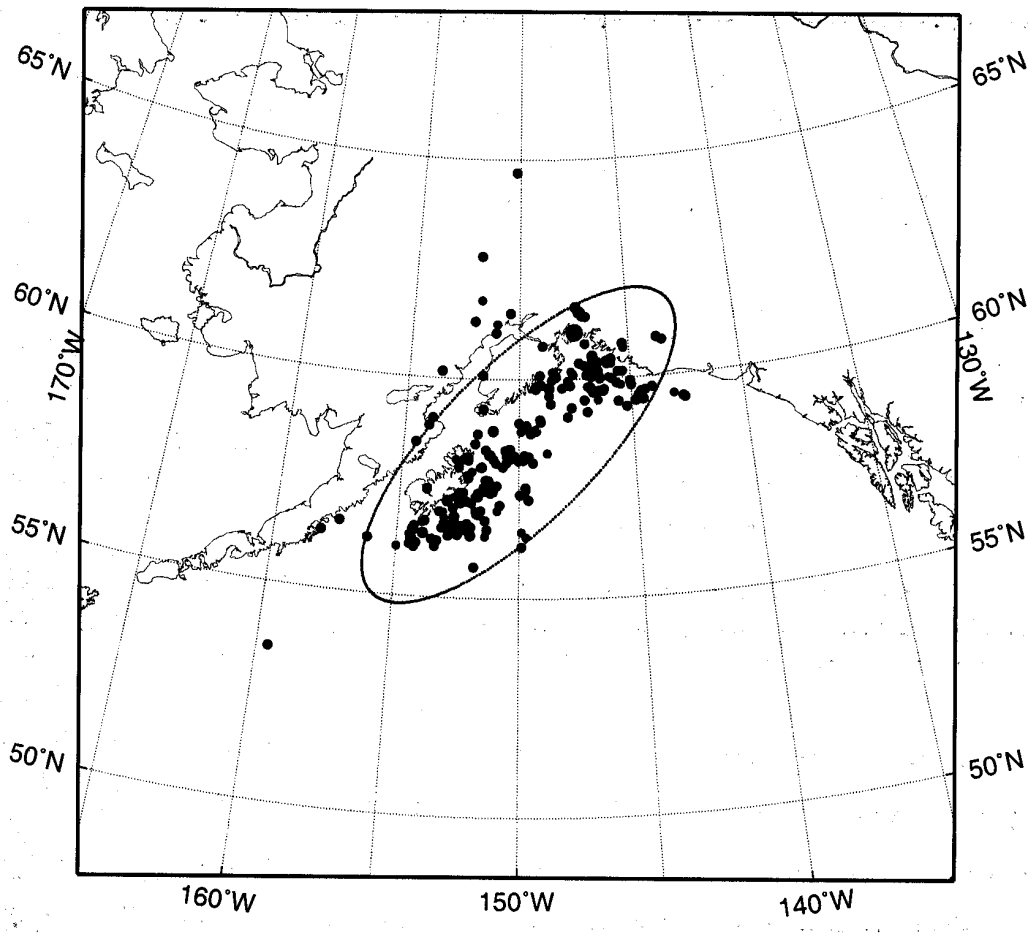

Figure 4.3: Example of a model ellipse fitted to the aftershock sequence of the 1964, M=9.2 Alaska earthquake. Epicentres of 244 earthquakes with magnitude $\geq$ 5.0 within a radius of 1098km and 10 months of the mainshock are plotted. The ellipse contains about 90% of the plotted events. (Figure from **Christophersen, 2000** [8])

Christophersen found that the epicentres of the earthquakes within the ellipses

were nearly normally distributed along the principal axes. Figure 4.4 shows the distribution of epicentres of 79 sequences including a total of 4428 earthquakes along the principal axes of the ellipses compared to a normal distribution with mean 0 and sigma 1.

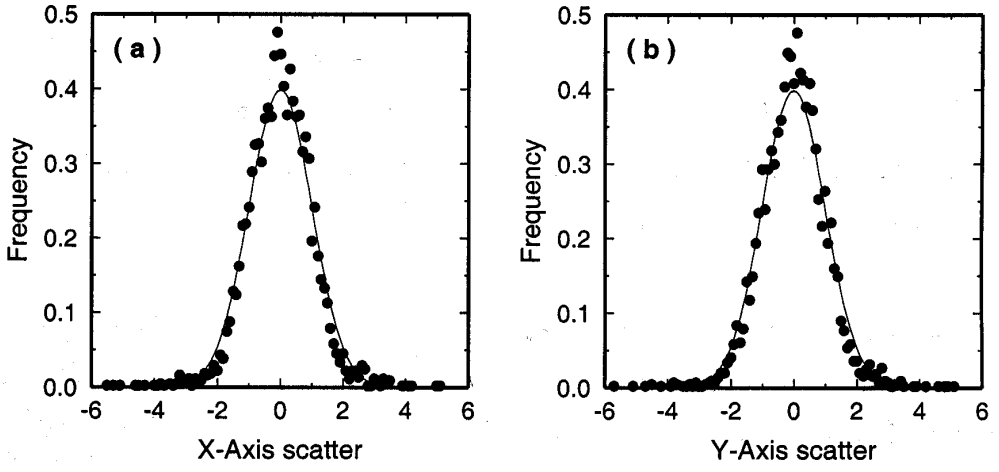

Figure 4.4: The distribution of epicentres along the x- and y-axis (solid circles) and a normal distribution as a reference (Figure from **Christophersen, 2000** [8])

In her study, **Christophersen** analysed the database separately for different tectonic settings to investigate variations in the parameters of Omori's law and the Gutenberg-Richter relationship. She found that some of them vary significantly. For example, mid-ocean ridges have a higher p-value than any other setting.

Christophersen reproduced earlier results (e.g. **Singh and Suarez, 1988** [53], **Yamanaka and Shimazaki, 1990** [67]) that the abundance of aftershocks is not a constant as assumed by the generic California model, but scales with magnitude. If a_0 is the value determined for an average mainshock magnitude M_0, then the parameter a as used in the Gutenberg-Richter relationship (equation 3.6) calculates as:

$$a(M) = a_0 + (M - M_0) \tag{4.7}$$

From that analysis, **Christphersen, 2000** [8] could predict probabilities for large events following large events as a function of tectonic setting, i.e. an aftershock with

$M_m - \delta \leq M \leq M_m$ occurring in the time interval $[t_1, t_2]$ after the mainshock of magnitude M_m. For a mainshock of magnitude eight, for example, she calculates a probability of 40% in a young subduction zone and 60% in an intracontinental zone that one or more aftershocks between magnitude 6.0 and 8.0 will be observed in the time interval 7-30 days after the mainshock. The probabilities decrease to 25% and 55%, respectively, for the time interval of the second year, i.e. days 365-730.

Chapter 5

New Zealand Parameters

The Gutenberg-Richter magnitude frequency distribution and the modified Omori law for time decay are well established empirical laws and suited to describe aftershock activity. Their parameters, however, vary between tectonic regions and need to be estimated separately for different settings.

5.1 Eberhart-Phillips

In 1998 **Eberhart-Phillips** [11] applied the empirical technique from **Reasenberg and Jones, 1989** [42] to 17 New Zealand aftershock sequences between 1987 and 1995 with a minimum mainshock magnitude of 5.5. The numbers of aftershocks per sequence varied between 25 and 579 events. As the minimum magnitude reliably detectable is not uniform throughout New Zealand, the author chose an appropriate M_{cut} for each sequence based on the b-value plot. The minimum magnitudes determined range from 2.2 to 4.6 and the magnitude range $M_m - M_{cut}$ ranged from 2.5 to 3.9.

The author found that the maximum likelihood fitted parameter values (equation 4.4) varied greatly between the individual sequences. But the median values turned out to be very similar to the generic California values: $a = -1.66$, $b = 0.91$, $c = 0.05$ and $p = 1.08$. They could be considered generic New Zealand parameters.

Eberhart-Phillips also calculated weighted averages for each model parameter, where she used weights inversely proportional to the individual sequence parameter uncertainties. The weighted averages are:

$$\begin{aligned} a &= -1.60 \\ b &= 0.98 \\ c &= 0.03 \\ p &= 1.05 \end{aligned}$$

5.2 Model adopted for this study

For the purpose of hazard calculation an aftershock model needs to be chosen to include triggering aspects in the hazard forecast. In this section I describe and justify the choice of aftershock model for this study.

In contrary to the aftershock models described earlier such as **Gerstenberger, 2003** [16], I treat foreshocks separately, as I derived more information about their spa-

tial clustering than we know about aftershocks at this stage, and found that foreshocks appear to behave differently in time compared to aftershocks. That implies that I need to avoid double counting/overpredicting of events. Aftershocks for this application therefore have to be smaller than the mainshock. Equal and larger events are covered by the foreshock probability forecasts.

In general, I use the generic model developed by **Reasenberg and Jones, 1989** [42] and given by equations 4.4 and 4.5 with the parameters determined for New Zealand by **Eberhart-Phillips, 1998** [11]. Mainly in three aspects, I go beyond the detail provided in those studies: the spatial and temporal extent of the aftershock zones, the spatial smoothing of probabilities within these zones, and a magnitude dependence in the abundance parameter a.

5.2.1 Spatial and temporal extent of the aftershock zone

A more subtle form of double counting or missing events could arise from the definition of the spatial and temporal extents of the aftershock zone. The foreshock probability model, explained in Part I, was derived from a declustered catalogue, i.e. a catalogue from which aftershocks had been removed. In order to model all seismicity, the aftershock probabilities need to allow for exactly those events that have been removed for the foreshock analysis. This means that the aftershock probabilities need to be applied to the area and times that have been used to decluster the catalogue. Those windows were modified for New Zealand by **Savage and Rupp, 2000** [50]. I modelled the windows used by **Savage and Rupp** (Table 3.1) through exponential functions to be able to calculate the appropriate radius $R(M)$ and time interval $T(M)$ for each magnitude step:

$$R(M) = 6.6182 * e^{0.4171M} \quad (5.1)$$

$$T(M) = 0.0498 * e^{1.4988M} \quad (5.2)$$

The aftershock zones range from 32.3 km and 14.8 days for a M=3.8 mainshock to

186.2 km and 8027.8 days for a magnitude eight earthquake.

5.2.2 Spatial smoothing

The probabilities estimated by equation 4.5 refer to the total number of aftershocks expected anywhere in the aftershock zone. It would not be right therefore, to apply this probability to each gridpoint within that region. That would overestimate and change the total number of expected events. Instead, the probability value needs to be smoothed over the aftershock area. **Gerstenberger, 2003** [16] based his smoothing on the observation of a $\frac{1}{r^2}$ decay of aftershock frequency distribution for the 1992 Landers earthquake. As no similar examination for a New Zealand aftershock sequence has been done, I use **Christophersen's** result from the worldwide catalogue of a normal distribution along the principal axes of the the aftershock zone circumscribing ellipse. An ellipse can be only fitted once the full sequence has been observed, so for forecast purposes the area reduces to a circle of the search radius. Accordingly, the smoothing can be performed by a 2-dimensional normal distribution. Because the search radius had initially been designed to derive foreshock probabilities and therefore removed an extremly high percentage of aftershocks, likely even non-related events in some cases, we assume that these areas will be large enough to capture 99.9% of the aftershocks that will follow a mainshock. To calculate the smoothing factor for a grid cell at distance $r \leq R$ from the mainshock, where R is the radius of the aftershock zone, the normal distribution is aggregated over the area of the grid cell. The final spatial smoothing function then is:

$$S(r) = \frac{dA}{2\pi\sigma^2} e^{-\frac{1}{2}\frac{r^2}{\sigma^2}} \tag{5.3}$$

$$\sigma = \frac{R}{3.0} \tag{5.4}$$

The definition of σ includes 99.9% of the normal distribution. The integral $\int_0^R \frac{S(r)}{dA}\, dr$ is equal to one.

5.2.3 Parameters

Parameters b, c, and p from the magnitude frequency distribution and modified Omori law (equations 3.6 and 4.3) are used as determined by **Eberhart-Phillips, 1998** [11]: $b = 0.98$, $c = 0.03$, $p = 1.05$. I chose to use the weighted values because the variation of the values between the sequences was high ($b_{min} = 0.78$, $b_{max} = 1.27$, $c_{min} = 0.01$, $c_{max} = 0.34$, $p_{min} = 0.20$, $p_{max} = 1.61$) and it might only be a coincidence that the means are so similar to the generic California values.

For parameter a I adopted the finding that it is not constant but scales with magnitude (equation 4.7). I used the value of $a = -1.6$ as calculated by **Eberhart-Phillips** as a_0 to be appropriate for the average mainshock magnitude of the sequences it had been derived from: $M_0 = 6.1$. In this study a gets calculated accordingly:

$$a(M) = -1.6 + (M - 6.1) \tag{5.5}$$

Part III

Dynamic Seismic Hazard Model

Chapter 6

Background: Probabilistic Seismic Hazard Analysis

Probabilistic Seismic Hazard Analysis (PSHA) was first developed in and for Californian engineers as a time independent measure of earthquake hazard at certain sites. Later the standardised methodology was applied to New Zealand. A new generation of PSHA starts to incorporate time dependence by including hazard due to foreshock and aftershock triggering.

6.1 Motivation

For highly industrialised societies earthquake damage is a very costly natural hazard. Earthquakes cause the destruction of buildings and transportation systems as well as business interruption. In most major earthquakes people get injured or killed, especially in less developed countries with no building regulations. Probabilistic seismic hazard analysis (PSHA) is the basis on which engineers develop safety standards that buildings need to fulfil to hopefully withstand earthquakes.

PSHA estimates the probability for exceeding various ground motion levels at a site (or a grid of sites) within a certain time period given all possible earthquakes. Traditional probabilistic seismic hazard analysis is time-independent. It assumes rates of earthquake occurrences on known faults (and off-fault) that are poissonian, i.e. time-independent, and calculates the associated ground motions from each of these events for each site based on an attenuation model. The influence of each earthquake is multiplied by the rate with which the event is assumed to occur. Summing over all events allows one to calculate, for each site, the probability of a certain ground motion being observed within a certain time. The hazard information is usually presented in maps that show the exceedance of levels of ground motion that is expected to occur with a certain probability (e.g. 10%) in a certain time (e.g. 50yrs).

This approach is completely time-independent: it does not consider information about recent activity of faults with long recurrence intervals (e.g. has a fault which is known to produce earthquakes once every 2000 years been active 20 years ago or 1900 years ago?), nor does it deal with earthquake triggering aspects. The seismic gap hypothesis on which recurrence interval concerns ultimately rest, failed tests in the early nineties where it should have forecasted areas of enhanced and reduced probability for large events in near future. Therefore, some people dispute its applicability (e.g. **Kagan and Jackson, 1991** [27]). However, time dependent information built on earthquake triggering could considerably facilitate emergency managers' decisions on rescue operations as well as temporary shut downs of gas pipes and dangerous machinery, closure of bridges and other important structures which are likely to collapse.

A new generation of PSHA is being developed (STEP model for California, see Section 6.4, this study's Dynamic Seismic Hazard Model for New Zealand) that incorporates short term hazard changes due to foreshock and aftershock triggering.

6.2 International work

The methodology of PSHA was originally developed by **Cornell, 1968** [9]. He formalised the numerical/analytical approach which should provide engineers with average return periods of certain ground motions on a building site. As minimum input data **Cornell's** algorithm needed the best estimates of average activity levels of all potential earthquake sources, i.e. the annual number of earthquakes above a certain minimum magnitude produced on each source. The algorithm then integrated over all individual influences of the various potential earthquake sources into a probability distribution of maximum annual intensity.

In 1996 geoscientists of the US Geological Survey and the California Department of Conservation (today California Geological Survey) released the 1996 California probabilistic seismic hazard maps. A detailed description of this work is given in **Frankel, 1995** [13].

The analysis developed earthquake sources from a 200 year record of historical seismicity and active fault data (geologic information about prehistoric earthquakes on active faults). The model takes into account the recurrence rates of potential earthquakes on each earthquake source and the potential ground motion that may result from each of those earthquakes.

The faults are categorised into different classes depending on slip rates and availability of paleoseismic information. Accordingly, different statistical magnitude-frequency distributions are applied. These two relationships are based on (1) the characteristic earthquake model, which implies that a typical size of earthquake ruptures repeatedly along a particular segment of the fault (**Schwartz and Coppersmith, 1984** [51]) and (2) the exponential Gutenberg-Richter relationship (**Richter, 1958** [46]).

After calculating the earthquake distributions for all faults, attenuation relationships are applied to estimate the ground motion distribution for each earthquake of a given magnitude, distance, and rupture mechanism.

The map for California (Fig. 6.1) shows the above mentioned exceedance of horizontal peak ground acceleration at 10% probability in 50 years on a uniform firm-rock site condition. The calculated acceleration values range from about 0.1g to over 1g. More than 3/4 of the state's population lives in areas that have seismic hazard above 0.4g, including San Francisco Bay and greater Los Angeles (Fig. 6.1). (**Petersen, 1996** [41])

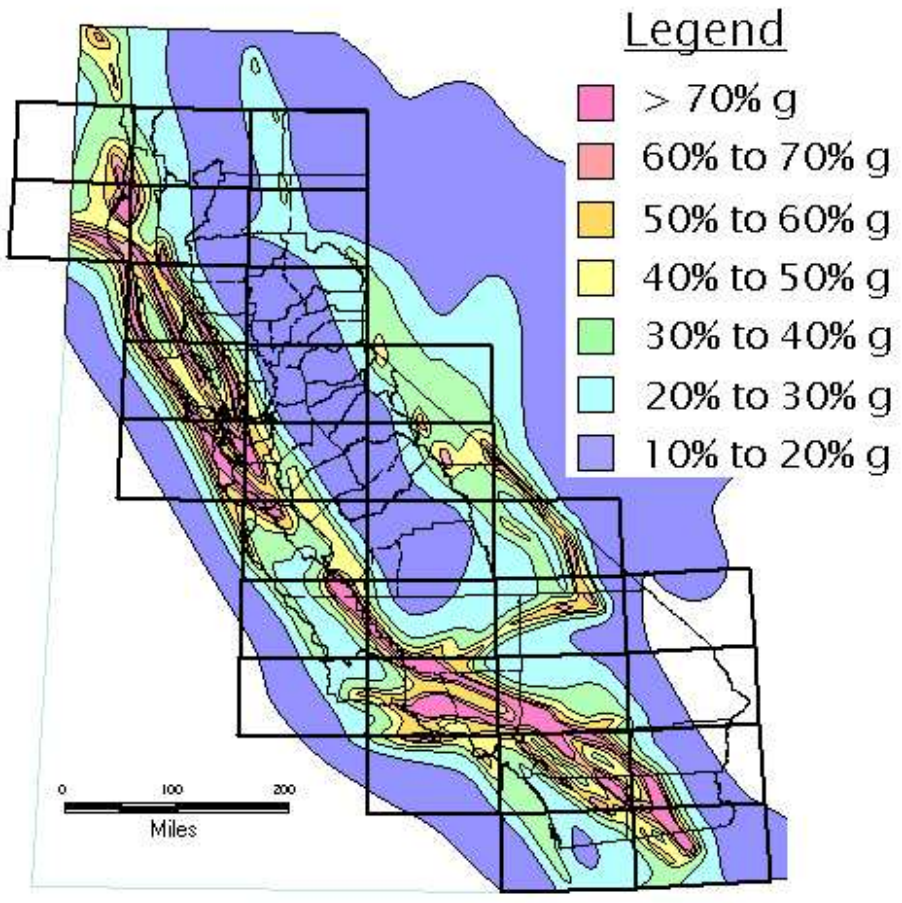

Figure 6.1: Probabilistic ground shaking (Peak Ground Acceleration [PGA], 10% probability of being exceeded in 50 years, assuming a uniform soft rock site condition) contour maps have been developed for all 1 degree by 2 degree areas of California. (Figure from **Petersen, 1996** [41])

From 2000 to 2002 the hazard model has undergone a process of revision and improvement based on new seismological, geophysical and geological information (**Frankel, 2002** [14]). Changes of some aspects of the source parameters (mean recurrence time, characteristic magnitude, spatial concentration of some place's sources of large earthquakes, rupture zone geometry, additional attenuation relations) show that the first map, for example, overestimated the hazard along a segment of the San Andreas fault and underestimated it along the Calaveras fault. The hazard along the southern San Andreas fault is unchanged although the model parameters are calculated differently. In Southern California, the hazard has changed along several faults due to modified parameter modelling. (**Cao et al., 2003** [7])

6.3 National Seismic Hazard Model for New Zealand

In the late 1990s **Stirling et al.** started to construct a probabilistic seismic hazard model for the whole of New Zealand, following the methodology developed for California. Today's New Zealand National Seismic Hazard Model — a model combining geologic data with historical seismicity data to estimate future ground shaking that will occur across a gridwork of sites in New Zealand — was developed in two stages.

The first stage, the experimental model, was finished in 1998 (**Stirling, Wesnousky and Berryman, 1998** [60]). The authors used geologic information available at that time describing 154 active faults, as well as historical observations and instrumental seismicity data for New Zealand earthquakes between 1964 and 1996. They also estimated that moderate earthquakes could occur on still unknown faults. On this basis they calculated locations, magnitudes and recurrence rates of moderate-to-large earthquakes. Using this information as input they followed the standard methodology of probabilistic seismic hazard analysis (PSHA) developed by **Cornell, 1968** [9]:

1. Calculate the annual frequencies of exceedance for several ground motion levels at each grid point as a function of the magnitude, recurrence rate and source-to-site

distance of earthquakes predicted from the source model. These plots are called hazard curves.

Do this at each site for all sources in the source model and sum the results to obtain the annual frequencies of exceedance at the site due to all sources.

2. Construct maps that show the maximum ground motion level that is expected to be exceeded with a certain probability in a certain time period at each site.

Stirling et al., 1998 [60] showed maps for expected ground accelerations that will be exceeded with a probability of 10% in 50 years.

They estimated the maximum ground motions at each site using a Poisson model, where the probability P is calculated as a function of the time of interest t (in yrs) and the annual rate of exceeding a certain ground motion r. For given P and t, the relation can be solved for the rate:

$$P(r,t) = 1 - e^{-rt} \tag{6.1}$$

$$r(P,t) = -\frac{ln(1-P)}{t} \tag{6.2}$$

For the values chosen by the authors, $P = 0.1$ and $t = 50$, the rate calculates to $r = 0.0021$. All ground motions in the hazard curves with rates of r or more will contribute to this measure of PSH.

The standard methodology of PSHA calculates the rate R_{tot} of ground motion on a particular site as follows (e.g. **Field** [12]).

Assuming a seismic source model with N earthquake scenarios, each of them having a magnitude M_n, distance from the site of interest d_n and annual rate of occurrence r_n, the attenuation model provides the distribution of possible ground motion levels for each potential earthquake source:

$$P_n(ln(PGA)) = \frac{1}{\sigma_n\sqrt{(2\pi)}} e^{-\frac{ln(PGA)-g(M_n,d_n)^2}{2\sigma_n}} \tag{6.3}$$

In this equation $g(M_n, d_n)$ and σ_n are the median and the standard deviation of $ln(PGA)$ given by the attenuation relationship. Integration of equation 6.3 gives the probability of exceeding each $ln(PGA)$, were the event n to occur:

$$P_n(> ln(PGA)) = \frac{1}{\sigma_n \sqrt{(2\pi)}} \int_{ln(PGA)}^{\infty} e^{-\frac{ln(PGA)-g(M_n,d_n)^2}{2\sigma_n}} dln(PGA) \qquad (6.4)$$

As the annual rate of occurrence of this event, r_n, is known, the annual rate of exceedence of each $ln(PGA)$, R_n is given by

$$R_n(> ln(PGA)) = r_n P_n(> ln(PGA)) \qquad (6.5)$$

The total annual rate of exceedence of $ln(PGA)$ at a site is the sum of all R_n:

$$R_{tot}(> ln(PGA)) = \sum_{n=1}^{N} R_n(ln(PGA)) \qquad (6.6)$$

This rate can be used directly to calculate the Poissonian probability of exceeding $ln(PGA)$ at this site within time T:

$$P_{poisson}(> ln(PGA), T) = 1 - e^{-R_{tot}T} \qquad (6.7)$$

A plot of R_{tot} against PGA is called a seismic hazard curve. Figure 6.2 shows seismic hazard curves of the annual rate of exceedance for various levels of peak ground acceleration for some New Zealand cities.

The hazard maps calculated by this initial model show highest levels of peak ground acceleration along the faults that accomodate most of the relative plate motion between the Australian and Pacific plates. They predict that strong earthquake shaking will occur in Wellington at least 10 times more frequently than in Auckland, Christchurch or Dunedin.

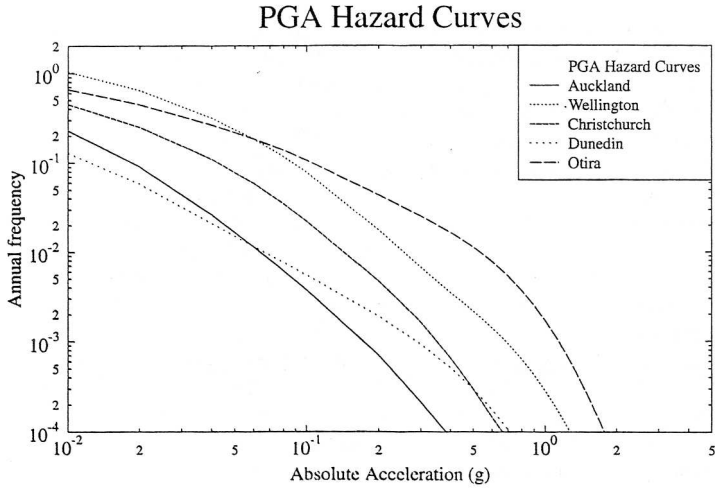

Figure 6.2: Seismic hazard curves for the centers of Auckland, Wellington, Christchurch, Dunedin, and Otira (little village in the highest seismic hazard zone in the country: South Island, Alpine Fault, close to Arthur's Pass). (Figure from **Stirling et al., 2002** [58])

Still, the model was only experimental at that stage, as the attenuation relationship used for the calculation was preliminary and unpublished and the treatment of uncertainty in the attenuation model did not follow well established procedures.

In 2002 **Stirling, McVerry and Berryman** [58] presented a new seismic hazard model for New Zealand, which became the National Seismic Hazard Model now used for the development of building codes.

Still using **Cornell's** [9] methodology as a basis, the analysis first defines the location of earthquake sources across and beneath the country, the likely magnitudes and mechanisms, and occurrence intervals for each. The new model uses an extended geologic data set and a new treatment of the historical seismicity record. Having defined all sources, the ground motions that will be produced by them are estimated for a gridwork of sites that covers the whole country with a spacing of 0.1°. In this model the value of historical earthquake information is increased and a new ground motion attenuation model for New Zealand is used for the estimates (**McVerry et al., 2000** [29]).

The new geological dataset was constructed on the basis of the one used previously, and extended with newly observed data. It contains 305 faults of determined slip type, dip, dip direction, maximum and minimum depth, slip rate, displacement, maximum magnitudes, and recurrence intervals that were first listed in **Stirling et al., 2000** [59]. To estimate the last two fault parameters, maximum magnitude, and recurrence intervals, different techniques are used, depending on the quantity and quality of available data. The maximum magnitude in this context is understood to be the most likely maximum magnitude rather than the maximum possible for the particular source. At this stage better use is made of the historical record than in earlier PSH models. If no historical observations are available, published estimates of single-event displacements and fault area are used in the equations for seismic moment and moment magnitude to derive the maximum magnitude.

The recurrence intervals are either published estimates from geological investigations or calculated using average single-event displacements and fault slip rate.

For two reasons the model additionally considers distributed seismicity. 1. A large percentage of earthquakes from the historical dataset have not occured directly on the mapped faults. 2. Earthquakes smaller than magnitude 6.5 generally do not produce surface ruptures that contribute to the geological displacement of the ground surface across major faults.

Using the recorded spatial seismicity distribution of events with magnitude greater than 5.25, likely locations and recurrence rates of distributed seismicity are estimated on a three dimensional grid of point sources across and beneath the country (spacing of 0.1° in longitude and latitude and 20 km in depth). For each grid point the recurrence rate of distributed seismicity is estimated by calculating the a and b-values from the Gutenberg-Richter relationship from a Reasenberg declustered catalogue (**Reasenberg, 1985**) [43] In the Gutenberg-Richter relationship (**Gutenberg and Richter, 1944** [19]) (equation 3.6) N is the number of events greater than or equal to magnitude M and a and b are empirical constants. Parameter, b, describing the magnitude-frequency slope,

is calculated for three different Reasenberg declustered subcatalogues covering different time periods with different completeness magnitudes (since 1964: $M_{cut} = 4$, since 1940: $M_{cut} = 5$, since 1840: $M_{cut} = 6.5$). One b is calculated for each of the 37 seismotectonic zones in New Zealand, and applied to all grid points that are located in the zone.

Once the b-values are known, for each grid cell the hypocentres found inside are summed for each of the three different subcatalogues, giving three N-values. The b-values and M_{cut} are smoothed within the horizontal grid layers.

Next the a-value is calculated for the entire catalogue, following a maximum likelihood method for the three sets of smoothed N-values. This a-value can be finally used to solve the Gutenberg-Richter distribution for the number of events with $M \geq 4$ per year:

$$log(N/yr) = a - bM \tag{6.8}$$

From there, incremental rates n/yr of magnitude M are calculated for each 0.1 increment of magnitude from $M = 5.25$ (which is the smallest magnitude the attenuation model can handle reliably) to the largest considered magnitude for that seismotectonic zone.

The lowest distributed seismicity rates that can be detected with this method with 90% certainty in the 33 year completeness period for $M \geq 4$ are approximately $8 * 10^{-4}$ events per year per 0.1° x 0.1° grid cell. Grid cells that produce rates lower than that are assigned this minimum rate (**Stirling et al., 2000** [59]).

Based on this dual input of characteristic earthquakes on known sources and distributed seismicity, the hazard analysis is calculated according to the standard methodology described above.

The new attenuation model used for this hazard analysis was developed by **McVerry et al., 2000** [29]. It accounts for the differing tectonic types of earthquakes in New Zealand (i.e. crustal, subduction interface and dipping slab) and their range of centroid depths. For crustal events, the attenuation parameters differ for different types of fault

rupture (i.e. strike-slip, normal, oblique/reverse and reverse). The attenuation model was calculated for three site classes based on the definition in the New Zealand loading code from 1992. To account for the rapid attenuation of high-frequency motions through the TVZ, an extra term was included.

Limited data from New Zealand (from 51 events of magnitudes 5.08 to 7.23 between 1966 and 1994, a total of 461 strong motion records were available, covering a range of horizontal source-to-site distances from 11 km to 573 km and centroid depths between 4 km and 149 km) required the use of some overseas attenuation models as base models to be fitted to New Zealand data. A residual analysis for data versus the forecasts from the various base models was the basis to constrain some of their parameters and allow others to be fitted especially to the New Zealand data. Two models for New Zealand data were fitted, one for crustal earthquakes and one for subduction zone earthquakes. Equations 6.9 and 6.10 calculate the expected maximum horizontal acceleration, PGA, in units of g on a soil site for crustal and subduction zone events, respectively.

$$\begin{aligned} ln(PGA)_{crustal} &= 0.59021 - 0.144(M-6) - 0.00967r - 0.48469(M-6) \\ &\quad *ln\sqrt{(r^2+5.6^2)} - 0.03279r_{vol} + 0.2CN + 0.26CR \end{aligned} \tag{6.9}$$

$$\begin{aligned} ln(PGA)_{subduction} &= 8.9856 + 1.4227(M-6) - 2.56727ln(r + 1.7818e^{0.554M}) \\ &\quad +0.0155H_c - 0.50962SI - 0.03279r_{vol}(1-DS) \end{aligned} \tag{6.10}$$

where M is the moment magnitude, r is the shortest distance in km between site and source, r_{vol} is the length in km of the part of the source-to-site path that lies in the volcanic zone (higher attenuation), $CN = -1$ for normal mechanism earthquakes, 0 otherwise, $CR = 0.5$ for reverse/oblique mechanisms, 1 for reverse mechanisms, 0 otherwise, H_c is the hypocenter depth, $SI = 1$ for subduction interface earthquakes, 0 otherwise, and $DS = 1$ for deep slab earthquakes, 0 otherwise.

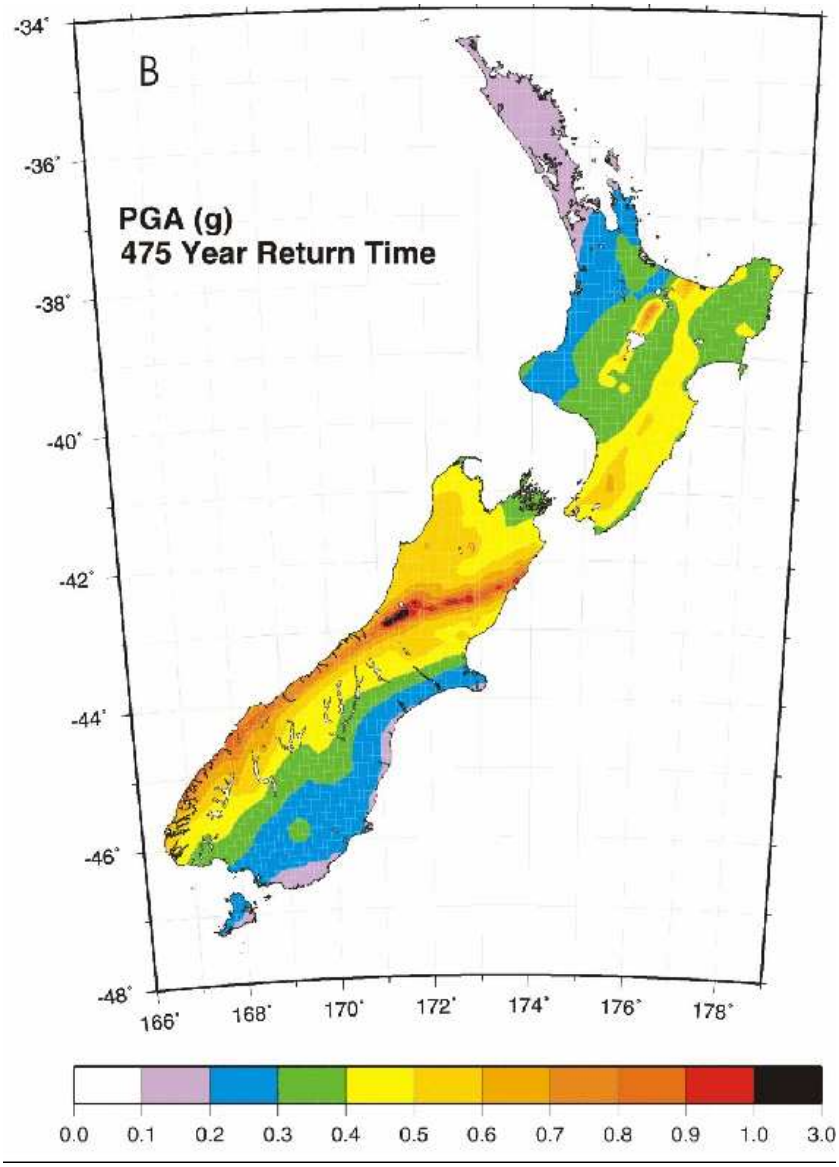

Figure 6.3: Probabilistic Seismic Hazard Map for New Zealand, showing peak ground accelerations in units of g for a 10% probability in 50 years (return time of 475 years)(Figure from **Stirling et al,2002** [58])

The PSH measure of exceedence of acceleration with a 10% probability in 50 years corresponds to a return time of 475 years (Fig. 6.3). The highest accelerations for the North Island of up to 0.6g for a one in ten chance in 50 years occur along the northeast striking faults in the eastern part above the subducting Pacific plate and in the Taupo

Volcanic Zone. In the South Island the Alpine fault displays the highest hazard with 0.8g expected to be observed. The lowest values for the whole of New Zealand are found in Northland. For the South Island the minimum hazard is estimated in southeastern Southland. In these regions the hazard might be underestimated due to seismicity rates below the smallest values that can be resolved with the method described above.

By calculating the hazard using average time-independent earthquake occurrence rates for each fault source, no attention is paid to knowledge of the time since the last event ruptured a fault, and therefore the model does not consider time-dependent processes. This is why the model is sometimes referred to as the Poissonian seismic hazard model, as it assumes a time-independent Poisson model of earthquake occurrence.

6.4 Time dependent PSHA: The STEP Model

Time-dependent probabilistic seismic hazard analysis has had limited application in the world to date. The first model ready to be used in real time (at the moment limited to California) was developed by **Gerstenberger, 2003** [16].

The model called STEP (short term earthquake probabilities) combines traditional long term background hazard analysis based on geological data and historic seismicity with short term models of different complexity. In the statistical analysis **Gerstenberger** does not distinguish between foreshocks and aftershocks as he treats a foreshock to be a mainshock whose aftershock happens to be bigger. Every single event, including those in an aftershock sequence, is considered to be a mainshock and the full aftershock probability model is applied. The calculation therefore allows for more than one event contributing to the aftershock hazard at one location, but it only shows the highest rate produced by any of the events.

Depending on the information available, **Gerstenberger** has three different aftershock models that increase in complexity and performance (see Chapter 4.4).

The simplest one is a generic model after **Reasenberg and Jones, 1989** and **1994** [42], [45] that only considers the magnitude of the mainshock to estimate the expected aftershock rate. He uses this one immediately after the event, when not much

information is available yet.

If the observed earthquake produces a sufficient number of aftershocks, a sequence-specific model is calculated which uses the a posteriori parameter values estimated for the sequence at a given time.

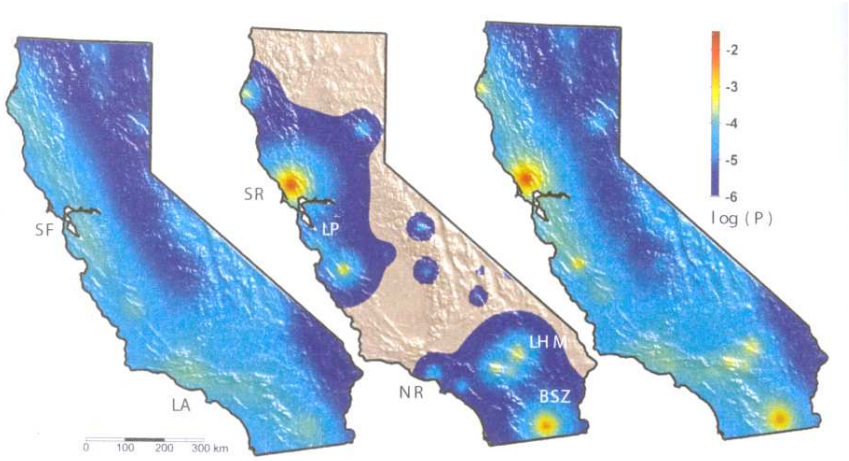

Figure 6.4: Maps of California showing the probability of exceeding MMI VI in the next 24-hr period starting from May 25, 2003, 2:07 a.m., PDT. The left frame depicts the time-independent hazard based on the 1996 USGS hazard maps for California. SF and LA are the locations of San Francisco and Los Angeles, respectively. The center frame represents the time dependent hazard which exceeds the background including contributions from several events; SR:M4.3 Santa Rosa event which occurred two hours before the calculations; BSZ: M4.2 Brawley Seismic Zone swarm that peaked 31 hours before the calculations. LHM: 1992/1993 Landers/Hector Mine events; NR: 1994 Northridge event; and LP: 1989 Loma Prieta event. The right frame is the combination of these two contributions, representing the total forecast of the likelihood of ground shaking in the next 24-hr period. (Figure from **Gerstenberger, 2003** [16])

The most complex model can be applied if the aftershock sequence develops a significant spatial heterogeneity. This most complex, spatially heterogeneous model calculates its parameters on each node of the grid covering the aftershock zone independently.

The model is designed for real-time analysis, and will be made available on the internet once the testing phase is completed. One example map is shown in Fig. 6.4

(**Gerstenberger et al., 2003**) [17]

6.5 Time dependent PSHA for New Zealand: A pilot study by Rudolf, 2003

The work presented in this thesis is the continuation of a research project that I carried out during my studies for a Graduate Diploma in 2003. (**Rudolf** (my birth name), **2003** [47]) The intention in that study was a first step towards incorporating short term hazard information into the National Seismic Hazard Model for New Zealand (**Stirling, 2002** [58]).

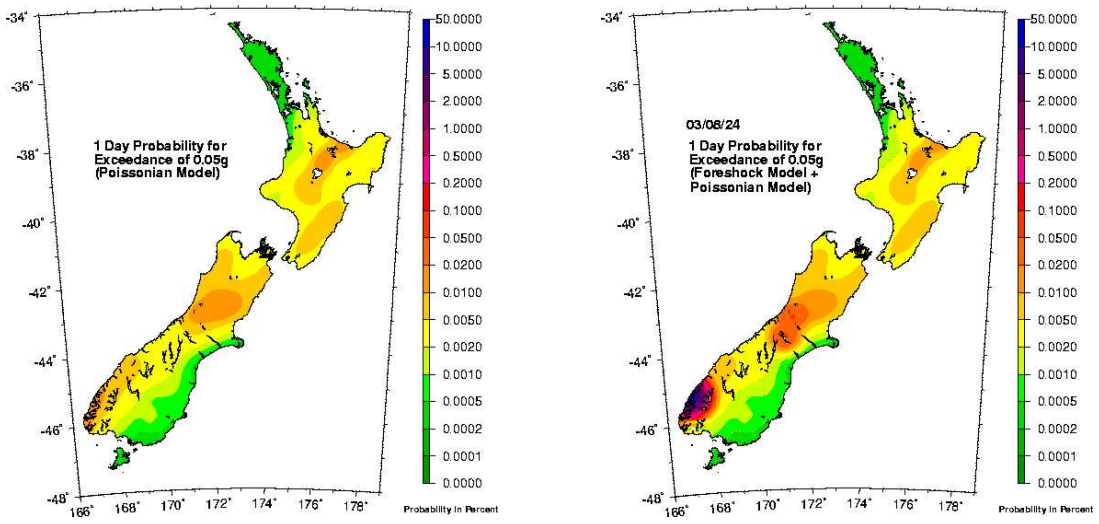

Figure 6.5: 24 hour probabilistic seismic hazard map: poissonian (left) versus foreshock hazard, here for 22 Aug 2003 (right)

I used the **Merrifield et al., 2004** [32] Foreshock Probability Model for New Zealand to augment the seismic background hazard given by **Stirling's** National Seismic Hazard Model. In one-day hazard maps I showed the foreshock hazard impact for small areas around all events younger than five days. The two examples in Fig. 6.5 demonstrate the effect. On the left hand side is the one day appearance of the National Seismic Hazard Model, showing the static probability for a ground motion of 0.05g being exceeded. The map on the right hand side shows the hazard distribution for 22

Aug 2003 taking the foreshock triggering aspect into account.

Looking at series of these daily maps produced by the Dynamic Seismic Hazard Model for New Zealand showed the fluctuations in short term hazard above the background hazard very clearly and therefore confirmed the necessity of studying time dependent hazard as an advanced form of probabilistic seismic hazard analysis.

But the model developed last year only considered the probabilities that an event would trigger bigger ones, not the chances for smaller ones to occur. Also it used simplified assumptions for the spatial and temporal behaviour of foreshock probabilities. Therefore, I continued the analysis in this thesis.

Chapter 7

Foreshock Input for Subsequent Hazard Calculation

In Part I I described the foreshock model, which provides equations that enable us to calculate foreshock probabilities as a function of time since the event, distance from the epicentre and magnitude difference between foreshock and mainshock. This information now needs to be applied to events that could still be triggering mainshocks, and transformed into the input expected by the hazard codes.

7.1 Concept

Only non-aftershock events are considered potential foreshocks. Accordingly, the foreshock probabilities will only be assigned to areas around recent events from the declustered catalogue. This study investigates shallow events only, i.e. not deeper than 40 km, and of minimum magnitue 3.8. As the maximum time window for foreshock triggering has been defined to be five days, all events younger than that will be considered.

For each event that fulfils these conditions, the probabilities of mainshocks of all magnitudes larger than or equal to the foreshock magnitude are calculated. The calculation includes the time since the potential foreshock and the distance from its epicentre. The parameters for the equations are chosen according to the foreshock location within or outside the TVZ.

A two layered grid, at 10 and 30 km depth, with 0.1° horizontal spacing is used for the calculations. The midpoints of each grid cell are the reference points for the distance from the earthquake. Foreshocks are considered to only trigger within their own depth layer, which is 0-20 km (10 km layer) or 20-40 km (30 km layer). Distances therefore are calculated horizontally only.

7.2 Application

To calulate the foreshock probability distribution for day X, the up-to-date earthquake catalogue needs to be declustered first. I use the Gardner & Knophoff algorithm (**Gardner and Knophoff, 1974** [15]) (see Chapter 3.1). From the declustered catalogue only events younger than five days from day X, shallower than 40 km and with minimum magnitude 3.8 are kept. Their depth layer gets assigned and their location is checked to determine whether they are situated within the TVZ triangle or not: N($-37.0°/175.85°$), S($-39.29°/175.55°$) , E($-37.5°/177.4°$). Accordingly, the parameters for the calculation of time, distance and magnitude dependent probabilities are chosen (see Chapter 3):

Parameter	TVZ	Non-TVZ
initial	0.0375	0.0046
b	1.3	1.3
rexp	3.6	2.7
texp	2.4	1.6

If the actual time difference in days between the potential foreshock and 00.00 am day X, $\delta tdays$, is less than one, it is set to one as this is the minimum time difference studied in this model. Because the model forecasts probabilities for one whole day, not a moment at 00.00am, the equations are integrated over time, i.e. from 00.00am to 12.00pm of day X:

$$timedecay(t_{start}) = \int_{t_{start}}^{t_{finish}} \frac{1}{t^{texp}}\, dt \tag{7.1}$$

$$timedecay(t_{start}) = \frac{t_{finish}^{1-texp} - t_{start}^{1-texp}}{1 - texp} \tag{7.2}$$

$$t_{start} = \delta tdays$$

$$t_{finish} = t_{start} + 1$$

For each event, the appropriate layer of the rectangular grid ($-34.00°$ to $-48.00°$ latitude and $166°$ to $179°$ longitude) is searched for grid points closer than 50 km to the potential foreshock. For each grid point found, the actual horizontal distance from the earthquake, dis, is calculated. Since the closest distance studied in the foreshock probability model was 10 km, again every distance less than that is set to 10 km. The probabilities given by the model are those for the full concentric rings. To get the probability per grid cell, the value needs to be divided by the number of grid points within the same concentric ring, $\#gridpoints_{disring}$.

$$disdecay(dis) = \frac{10^{rexp}}{dis^{rexp}} * \frac{1}{\#gridpoints_{disring}} \tag{7.3}$$

The hazard code needs an input file that for each affected grid cell provides the expected annual number of events of magnitudes 5.3, 5.4, 5.5,..., M_{max}. The fact that the code only uses events of magnitude 5.3 (actually 5.25) and higher, originates from limitations in the attenuation model. M_{max} is the maximum possible magnitude to be expected at any point in the country. The value is defined for each of the 37 seismotectonic zones of New Zealand and then smoothed over the edges.

For an event to be called a mainshock following a foreshock, the magnitude by definition has to be at least the same as the foreshock magnitude. Therefore, for this section of pure foreshock hazard calculation, in the array of all annual numbers of events, those of magnitudes less than the foreshock magnitude are set to zero. For all magnitudes *mags* equal to and greater than the foreshock magnitude M_f, the magnitude decay is calculated as:

$$startprob(mags) = initial * 10^{-b(mags-Mf)} \tag{7.4}$$

The foreshock probability on a grid point at day X for each expected magnitude is the product of equations 7.2, 7.3, and 7.4. The annual number of expected events is the number of days per year times the one day probability.

$$prob(t, d, M) = startprob(M) * timedecay(t) * disdecay(d) \tag{7.5}$$

$$annualnumber(t, d, M) = 365 * prob(t, d, M) \tag{7.6}$$

After the hazard calculation, the timespan is reduced back to one day.

If any grid points are affected by more than one potential foreshock, the probabilities are added assuming independence of the effects:

$$prob_{tot}(t, d, M) = 1 - \prod_{i=1}^{N} (1 - prob_i(t, d, M)) \tag{7.7}$$

where N is the number of potential foreshocks affecting the grid point.

7.3 Interface

This thesis did not intend to develop the best possible foreshock probability model, but a first one providing temporal and spatial decay parameters. So if a new foreshock model should be developed, the effort needed to feed it into the same short term hazard calculations is relatively small. Either the parameters for the equations can be changed in the existing code, or if necessary the equations themselves can be changed too. Perhaps more regional features could be added than just the distinction in TVZ and Non-TVZ, or a new bit of code could be written that produces the same format of output: a table of all grid cells (on the grid specified above), giving the expected annual numbers of events of each magnitude.

Chapter 8

Aftershock Input for Subsequent Hazard Calculation

The aftershock model chosen for this study is applied to recent events to produce an output format that can be used by the subsequent hazard codes.

8.1 Concept

The aftershock model is designed to calculate all chances that a recent earthquake will trigger smaller events close in time and space. In contrast to the foreshock assumptions, every event, even one that is part of an aftershock sequence itself, is considered to produce aftershocks of its own. The calculation of the aftershock probability distribution at a certain time is therefore based on the raw catalogue. But the model is still restricted to shallow events of magnitude 3.8 or more.

For aftershock triggering, as in foreshock triggering, maximum time and space windows are defined. In the case of aftershocks though, these windows are magnitude dependent. So all events that are still possible aftershock sources according to their maximum time windows are considered in the analysis.

As no study of aftershock probabilities in New Zealand has investigated any systematic differences between geographic regions, all events are treated the same; no distinction between TVZ and Non-TVZ is made.

Again, as in the foreshock model, the earthquakes are assumed to trigger only in the same depth layer, and all distances are calculated purely horizontally. The probabilities are calculated on the same two layered grid as the foreshock probabilities.

8.2 Application

The aftershock probability distribution for day X is calculated from the raw catalogue of shallow events greater than or equal to magnitude 3.8. For each M $\geq$ 3.8, all earthquakes that are younger than the magnitude dependent time window (in days) given by

$$timewindow(M) = 0.0498e^{1.4988M} \tag{8.1}$$

(see section 5.2.1) are included in the calculation. They are searched for in 0.1 magnitude increments from magnitude 3.8 to 8.0. The actual time between potential

aftershock source and 00.00am day X, $\delta tdays$, is calculated, and the temporal decay factor integrated for the full day:

$$timedecay(t_{start}) = \int_{t_{start}}^{t_{finish}} \frac{1}{t^p}\, dt \tag{8.2}$$

$$timedecay(t_{start}) = \frac{t_{finish}^{1-p} - t_{start}^{1-p}}{1-p} \tag{8.3}$$

$$t_{start} = \delta tdays$$

$$t_{finish} = t_{start} + 1$$

where $p = 1.05$ (see Chapter 5).

For each potential aftershock source found through the time window search, all those points of the two layered grid that are in the appropriate depth layer and closer than the magnitude dependent radius (see section 5.2.1)

$$radius(M) = 6.6182e^{0.4171M} \tag{8.4}$$

are determined. The aftershock probabilities are "artificially" spread over the aftershock area, as their spatial distribution has not yet been systematically analysed for New Zealand. A two dimensional normal distribution is used for the spreading (see Chapter 5):

$$areadistribution(dis) = \frac{dA}{2\pi\sigma^2} e^{-\frac{dis^2}{\sigma^2}} \tag{8.5}$$

where $dA = 95$ is the area of each grid cell, $\sigma = \frac{radius}{3}$ is the scaling factor of the standard deviation, so that 99.9% of all aftershocks can be assumed to occur within the area defined by $radius$, and dis being the horizontal distance between the earthquake's epicentre and the grid point.

The hazard code, as previously discussed, expects the annual numbers of events of all magnitudes between 5.3 and M_{max}. In most models aftershocks are allowed to be bigger than the mainshock to allow for foreshock probabilities. As foreshock probabilities are accounted for separately in this study, aftershocks in this case are restricted to be smaller than the triggering event. Therefore all probabilities of events equal to or bigger than the mainshock are set to zero. The probabilities for smaller magnitudes are calculated using the Reasenberg and Jones model. Unfortunately, the aftershock probabilities in this study were calculated from the original model of **Reasenberg and Jones, 1989** [42] as I only found out later about the 1994 update and the revised formula ([45]). Although changing the formula within the hazard code is simple, the computational time involved in rerunning the models requires several months and is not feasible to be done in the time span available for the MSc thesis. Therefore, in the hazard calculations that were run for this thesis, the probabilities are calculated as an integral over a small magnitude band around each tenth of a magnitude $mags$:

$$\begin{aligned} prob(mags,t,dis) &= (1-e^{10^{a+bM}\frac{1}{\beta}(exp(-\beta(mags+0.05))-exp(-\beta(mags-0.05)))*timedecay(t)}) \\ &\quad *areadistribution(dis) \end{aligned} \tag{8.6}$$

In this equation M is the magnitude of the potentially triggering event, $b = 0.98$ and $a = a_0 + (M - 6.1)$ with $a_0 = -1.6$ (see Chapter 5 for explanations). $\beta = b * ln(10)$ is a term evolving from the integration over magnitude.

Just as in the procedure for the foreshock model, for grid points which are affected by more than one potentially triggering event, the probabilities of each are added assuming they are independent (equation 7.7). Again, for computational reasons within the hazard code, the daily probabilities are turned into annual numbers of expected events by multiplying them by 365.

8.3 Interface

Again, the emphasis in this thesis was the construction of a first short term hazard model for New Zealand, not the development of the best possible aftershock model. The interface to insert a different aftershock model into the hazard calculations is the same as for the foreshock model: either editing the parameters and/or equations in the existing code or writing a new code which produces the same list of expected annual numbers of events of each mangitude for all affected grid points.

Chapter 9

Methodology for Short Term Hazard Calculation

The seismic hazard for day X is the combined influence of poissonian background hazard, foreshock probability influence, and aftershock hazard.

The hazard is calculated following standard PSHA methodology (**Cornell, 1968** [9]) as described earlier. It takes into account the uncertainty in estimates of ground motion from the attenuation equation by assuming the value for each site to be the median value of a log-normal distribution with an associated standard deviation. The estimate of the probability of exceedence of a certain ground motion is calculated as the appropriate integral over the probabilities for a suite of ground motion levels up to three standard deviations above and below the median.

The hazard code with the input files created by the methodolgy described above, allows one to calculate four different categories of hazard: the pure Poissonian background hazard on a daily basis (this map looks the same every day), the hazard resulting from foreshock probabilities (this map shows zero probability everywhere except the areas affected by foreshock probabilities), the hazard due to aftershock probabilities (this map shows zero probability everywhere except the areas affected by aftershock probabilities), and the conditional hazard, which is understood as the combined influences of foreshock probabilities and aftershock probabilities (this map shows zero probability everywhere except the areas affected by foreshock or aftershock or both probabilities).

The foreshock, aftershock or conditional hazard can be added to the Poissonian hazard, the latter giving the total 24 hour hazard distribution for the country.

The Poissonian hazard is the equivalent of the National Seismic Hazard Model. The only difference is the fairly short return time of one day (in contrast to usually 475 years). It calculates the hazard for each site due to all 305 known fault sources and the distributed seismicity file that assigns distributed seismicity rates greater than zero to every grid point.

The output I chose to produce is the probability at each point with which to expect a peak ground acceleration of 0.05 g at this location within the next 24 hours. 0.05 g is considered the lowest ground motion that could potentially cause damage. Though some small earthquakes reach it for very short durations, it is usually correlated with

the ground motion caused in the near field of a magnitude 5.5 earthquake.

The value that is calculated by the attenuation model is actually not the total peak ground acceleration that would hit the location, i.e. the vector of the three components of motion (two orthogonal horizontal and one vertical), but the maximum of the two horizontal components. The reason for that lies within the purposes of the attenuation model's development for engineering. Building responses to ground motions are uncoupled for horizontal and vertical motions and depend on the largest ground motion along one of the principal horizontal axes.

Foreshock and aftershock hazard are calculated on the basis of the annual numbers of events expected due to foreshock and aftershock probabilities, respectively. As positive probability values are only assigned to restricted areas around recent events, these maps show large areas of zero hazard, contrasted by fluctuating spots of increased foreshock/aftershock hazard.

Not every earthquake does actually produce a visible change in hazard: the hazard model only includes events of magnitude 5.25 and more in the calculations. If events smaller than that threshold produce foreshock hazard for the higher magnitudes that are considered, a small event can alter the hazard. Aftershock hazard increase is only produced by events of at least magnitude 5.4, since the smallest aftershock included will have to be smaller than the mainshock but bigger than 5.25.

The conditional hazard is the combined influence of foreshock and aftershock probabilities on the country's hazard. It is calculated by combining the two lists of affected grid cells and adding the foreshock and aftershock probabilities according to equation 7.7 for those cells that are influenced by both foreshock and aftershock probabilities.

From this combined file the hazard code calculates the total hazard distribution of increased hazard. It, too, is calculated in probabilities to observe 0.05 g within the next day.

The total hazard of day X is the sum of Poissonian background hazard and conditional hazard for that day. The two sets of probabilities of 0.05 g ground motion to be expected are again assumed to be independent and are therefore added using equation 7.7:

$$P_{tot} = 1 - \prod_{i=1}^{N}(1 - P_i) \tag{9.1}$$

Chapter 10

Results

The Dynamic Seismic Hazard Model for New Zealand produces two kinds of output: daily hazard maps on the one hand and hazard values for specific sites on the other hand.

10.1 Daily hazard maps

Figure 10.1 shows an example of one day hazard. The day chosen for the calculations is August 22nd, 2003. Just under 12 hours earlier a magnitude 7.2 earthquake occured in Fiordland (south-western part of the South Island). The map shows the probability at each point to observe a ground motion of 0.05g or more during the next 24 hours. The colour scale covers the full range of theoretically possible probabilities, 0% to 100% on a logarithmic type scale. The highest hazard value on this plot is a chance of about 13% to observe 0.05g in the blue area in Fiordland.

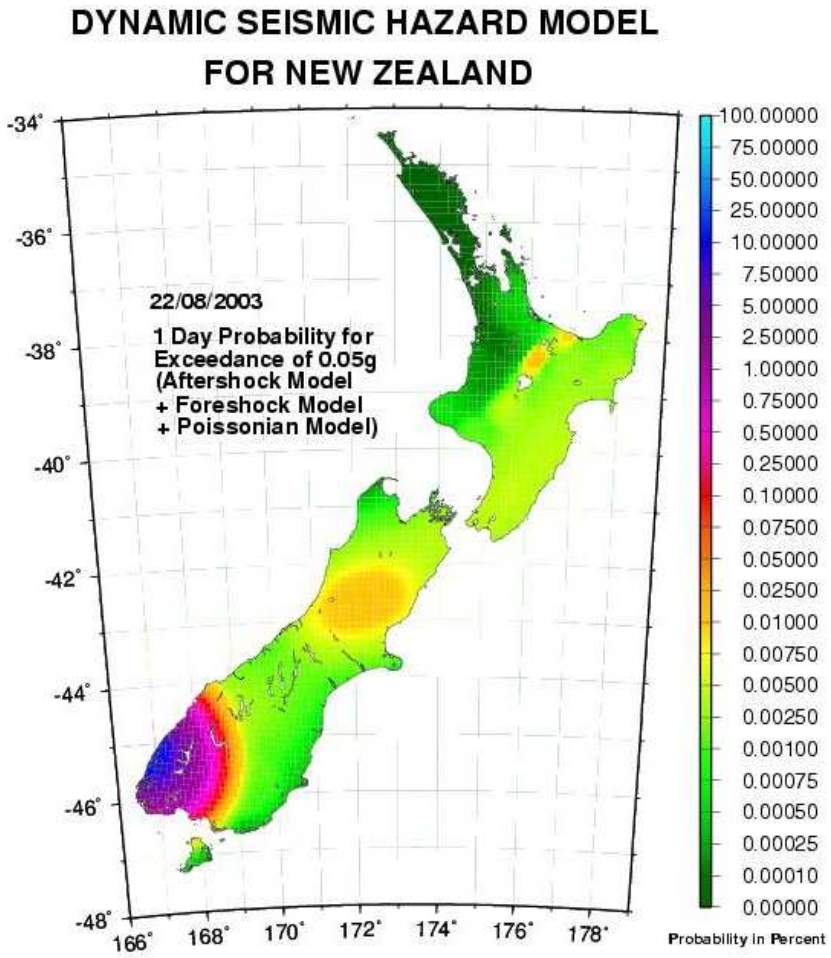

Figure 10.1: 24 hour hazard for 22 August 2003. 12 hours earlier a magnitude 7.2 earthquake ruptured in Fiordland.

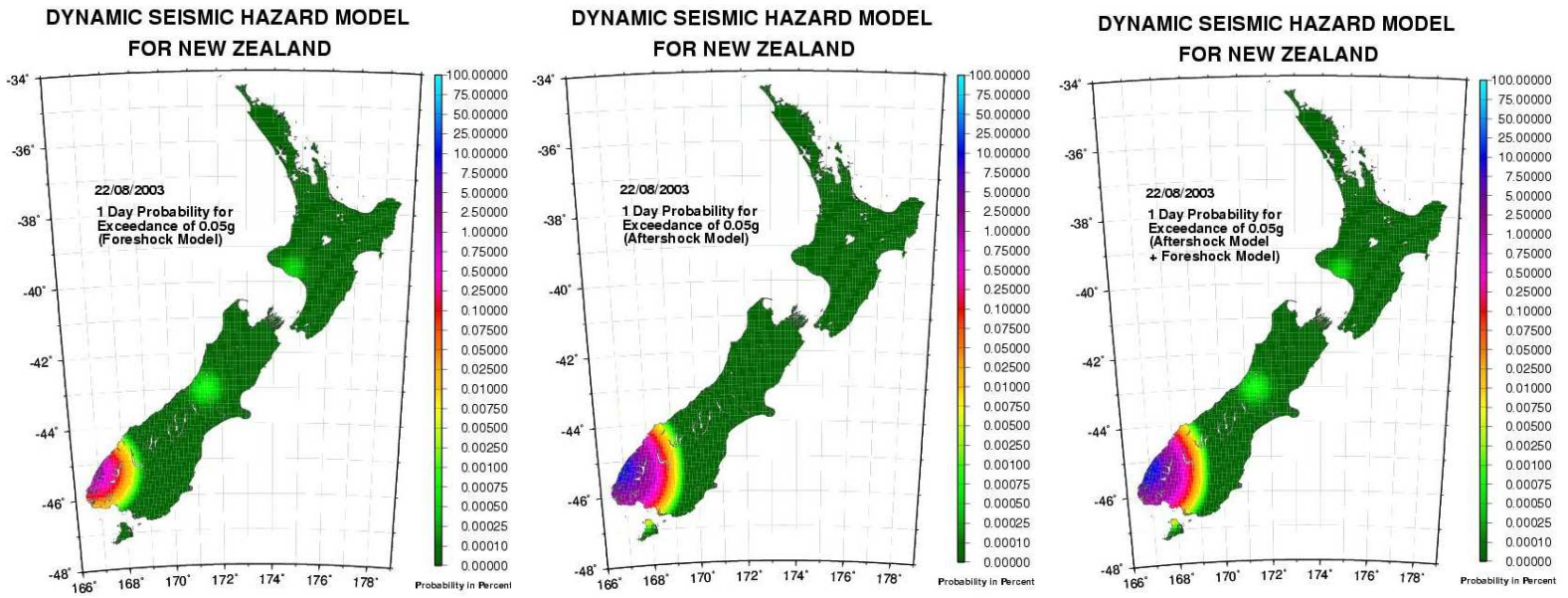

Figure 10.2: 24 hour foreshock hazard (left), aftershock hazard (center), and combined conditional hazard (right) for 22 August 2003. 12 hours earlier a magnitude 7.2 earthquake ruptured in Fiordland.

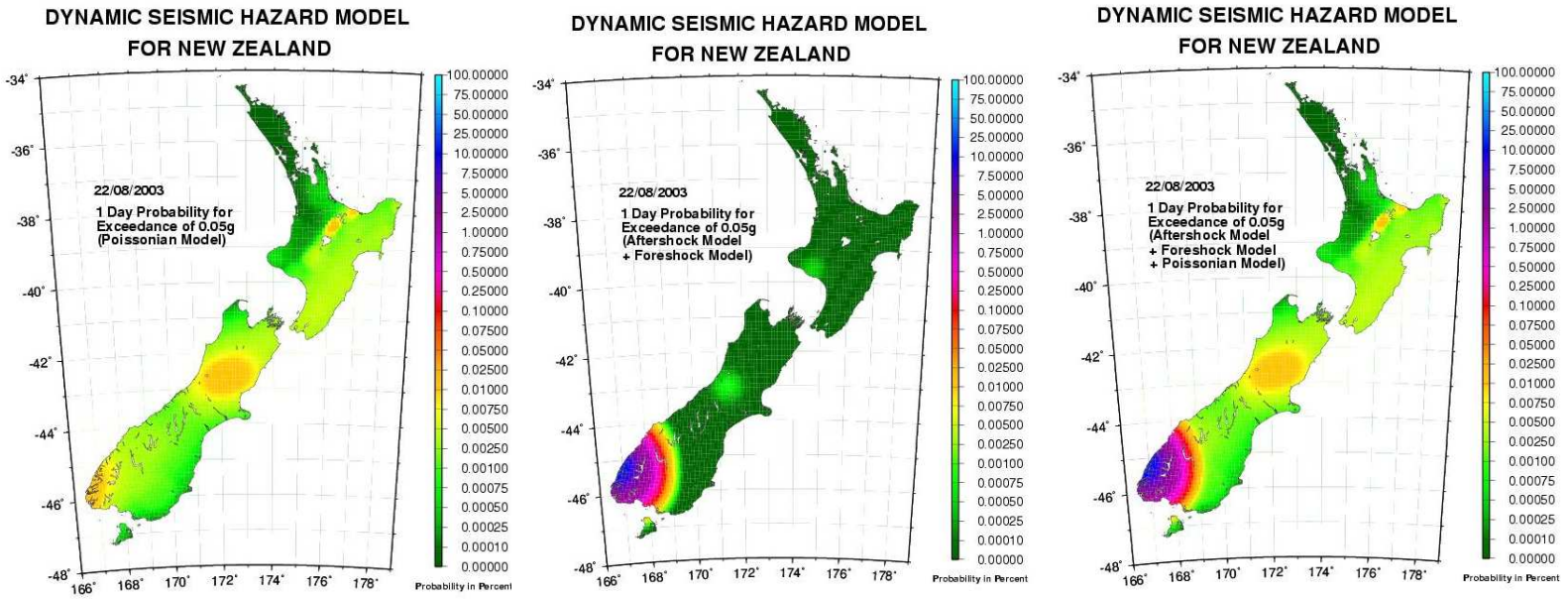

Figure 10.3: 24 hour poissonian hazard (left), conditional hazard (center), and combined total hazard (right) for 22 August 2003. 12 hours earlier a magnitude 7.2 earthquake ruptured in Fiordland.

Figures 10.2 and 10.3 visualise the above mentioned procedure of calculating total one day hazard: Fig. 10.2 shows foreshock and aftershock hazard, added together to conditional hazard. Fig. 10.3 shows the Poissonian background and the conditional hazard added together to total hazard.

The foreshock hazard will decrease rapidly with time and vanish after five days, covering the same area for the whole time. The aftershock hazard will decrease with time, too, but will increase the hazard for a much longer period than will a foreshock. The area covered by the aftershock hazard depends on the mainshock magnitude, but stays constant over the entire time window of the increased hazard, unless smaller aftershocks temporarily widen the region of the mainshock induced hazard.

The plots on the next four pages show the foreshock, aftershock, and total hazard evolution in the vicinity of the 21 August 2003, $M = 7.2$ Fiordland earthquake for eight days, starting with the forecast for the day on which the mainshock occurred.

The example shown in figure 10.4 is a forecast for three consecutive days approximately eleven months after the Fiordland event. In that region the still lasting aftershock hazard shows up. All other hazard on these plots is pure foreshock hazard (no aftershock hazard is produced by these events, because they are all smaller than 5.4, see Chapter 9). The "high" hazard area on the North Island is caused by an earthquake swarm (magnitudes 4 to 5) in the TVZ.

Foreshock Hazard
21/08/2003

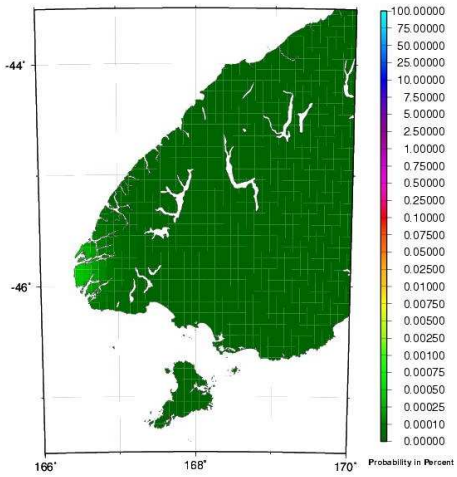

Foreshock Hazard
22/08/2003

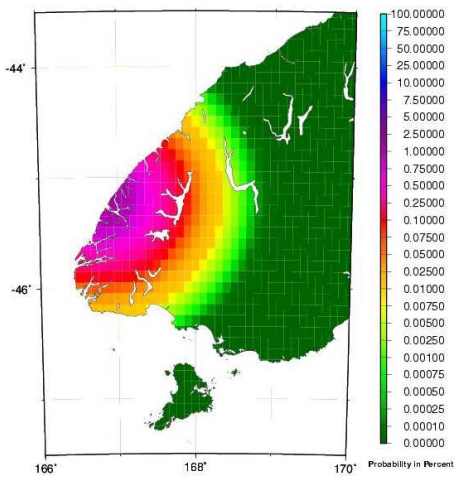

Aftershock Hazard
21/08/2003

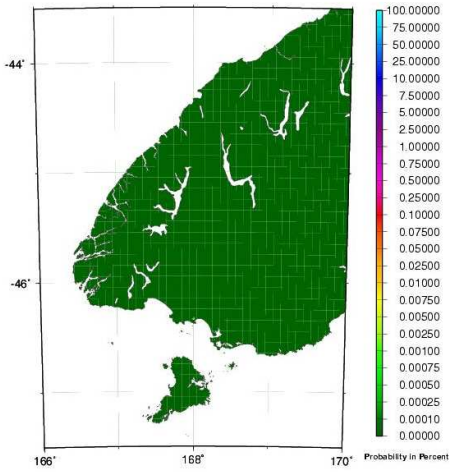

Aftershock Hazard
22/08/2003

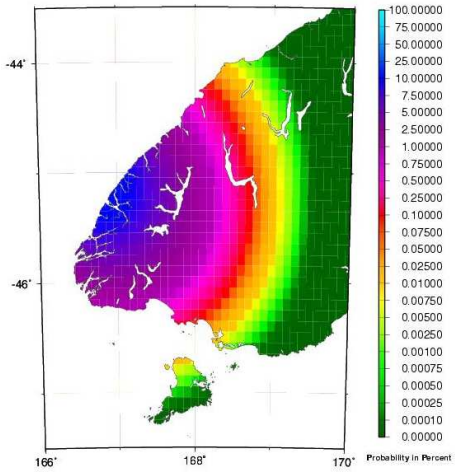

Total Hazard
21/08/2003

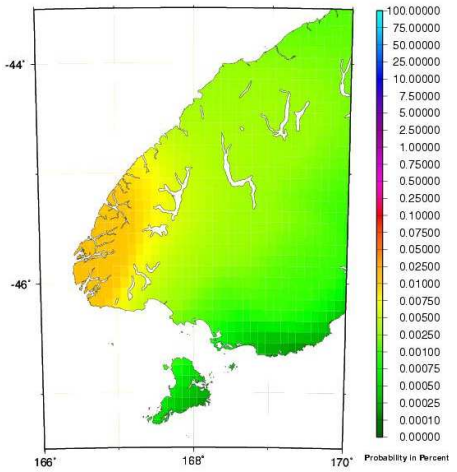

Total Hazard
22/08/2003

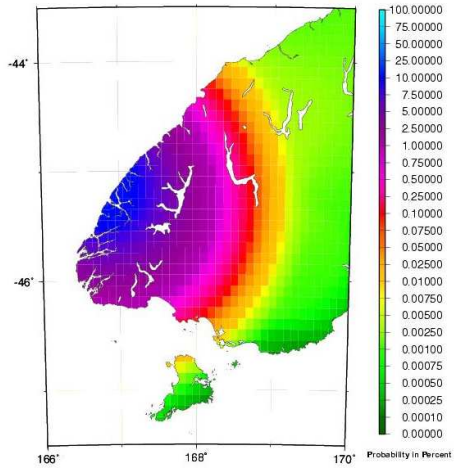

Foreshock Hazard
23/08/2003

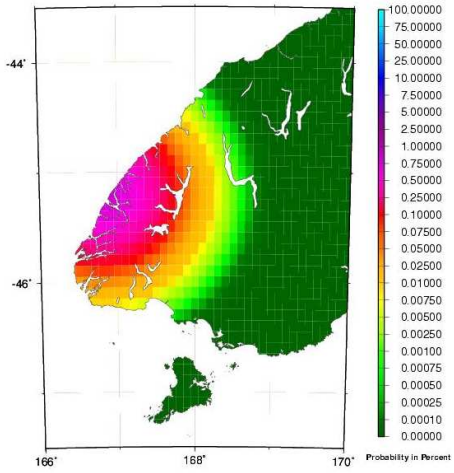

Foreshock Hazard
24/08/2003

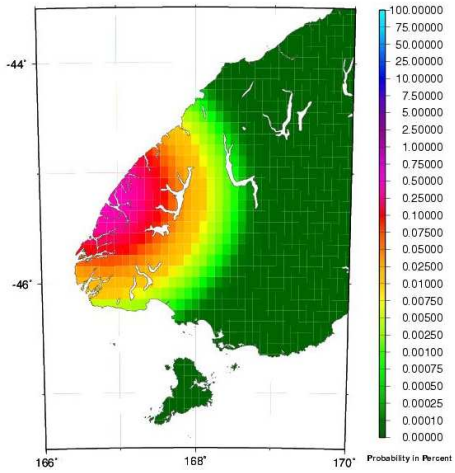

Aftershock Hazard
23/08/2003

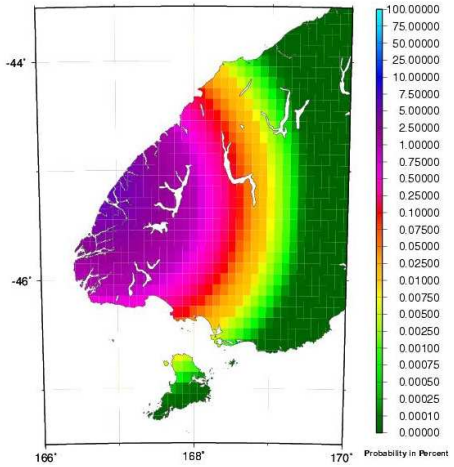

Aftershock Hazard
24/08/2003

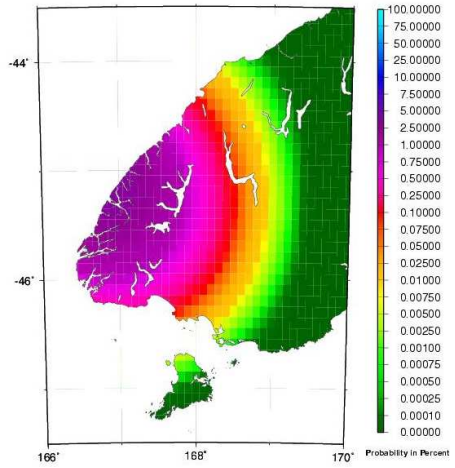

Total Hazard
23/08/2003

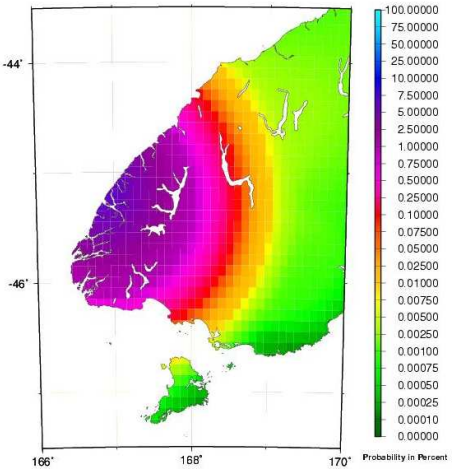

Total Hazard
24/08/2003

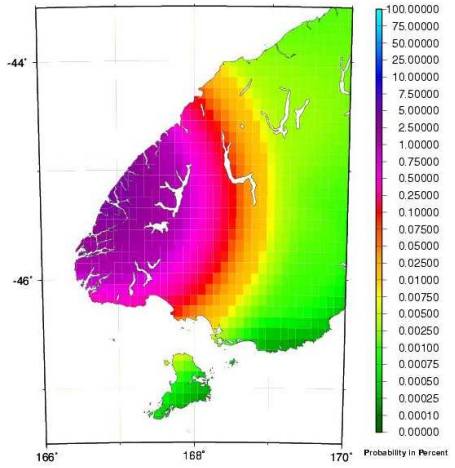

Foreshock Hazard
25/08/2003

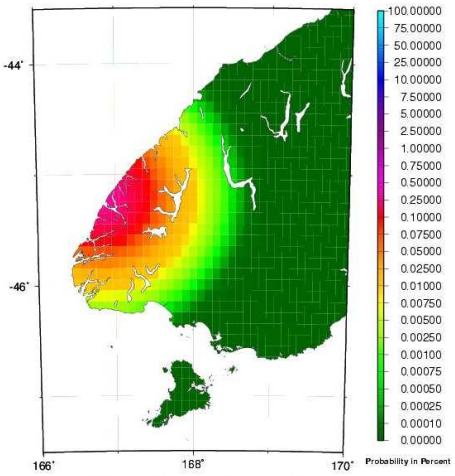

Foreshock Hazard
26/08/2003

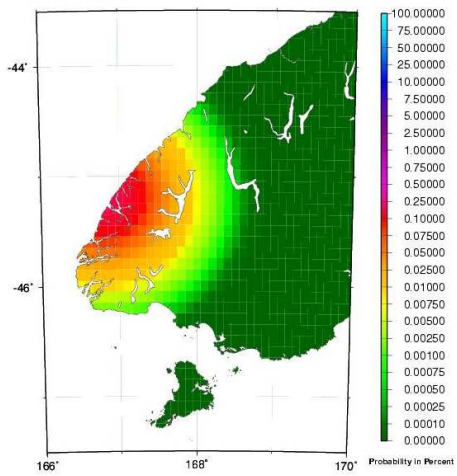

Aftershock Hazard
25/08/2003

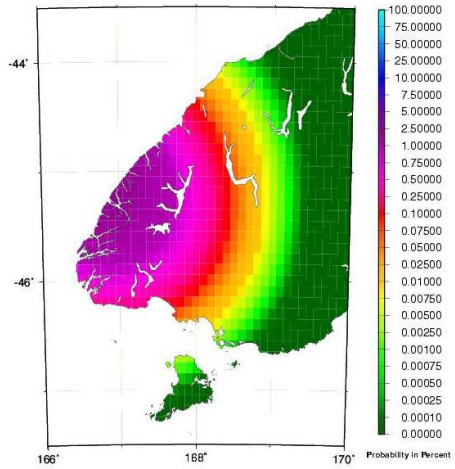

Aftershock Hazard
26/08/2003

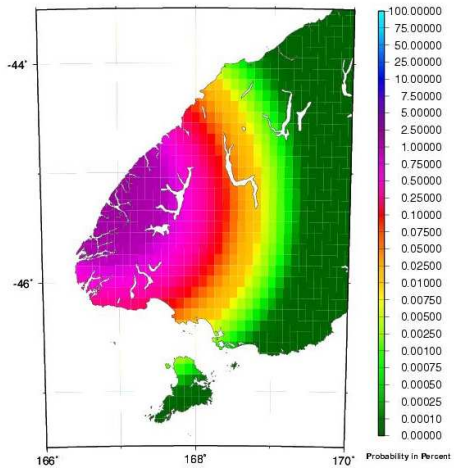

Total Hazard
25/08/2003

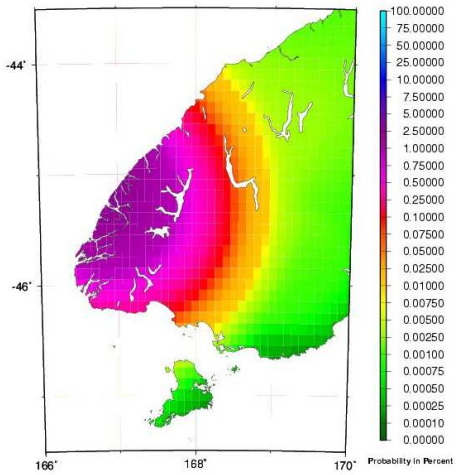

Total Hazard
26/08/2003

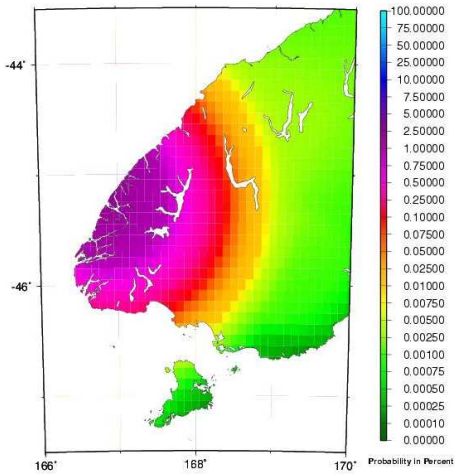

Foreshock Hazard
27/08/2003

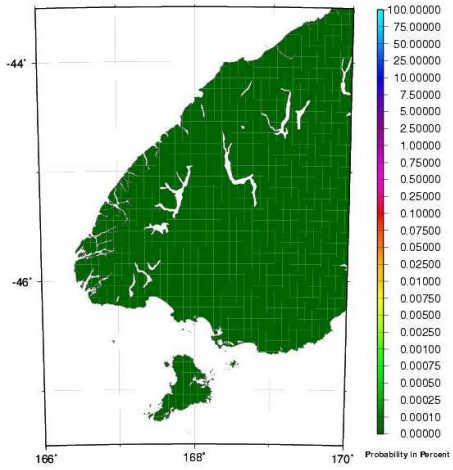

Foreshock Hazard
28/08/2003

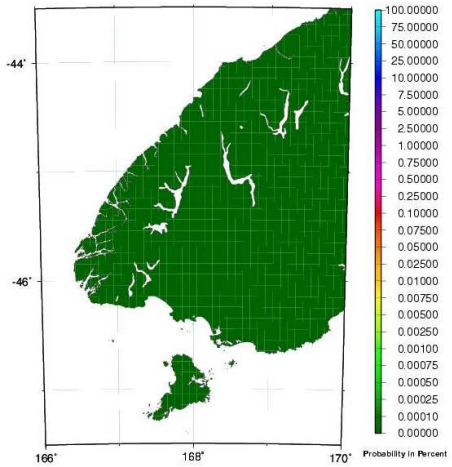

Aftershock Hazard
27/08/2003

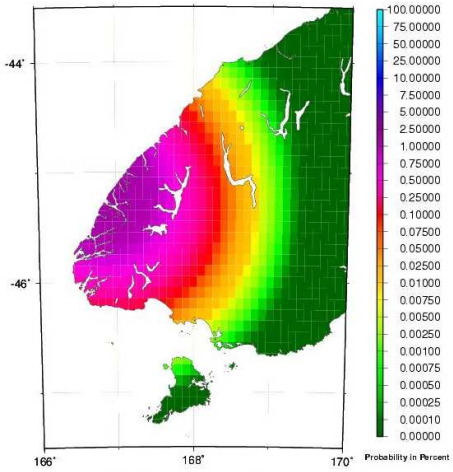

Aftershock Hazard
28/08/2003

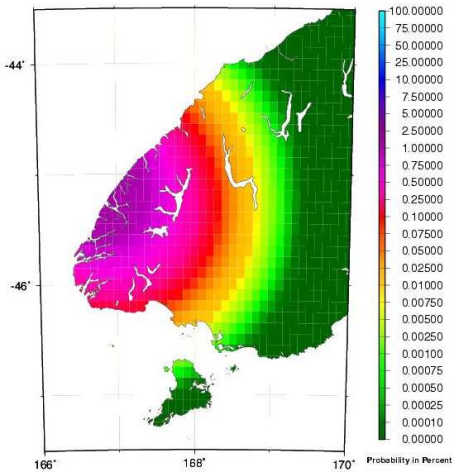

Total Hazard
27/08/2003

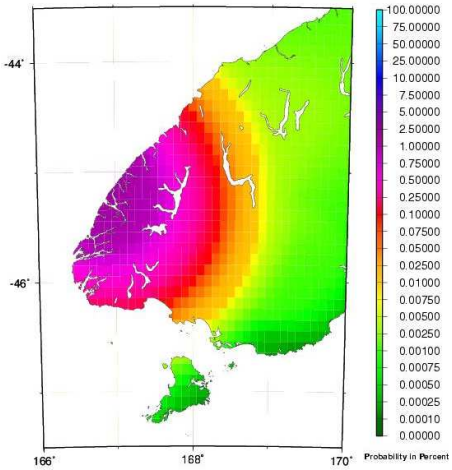

Total Hazard
28/08/2003

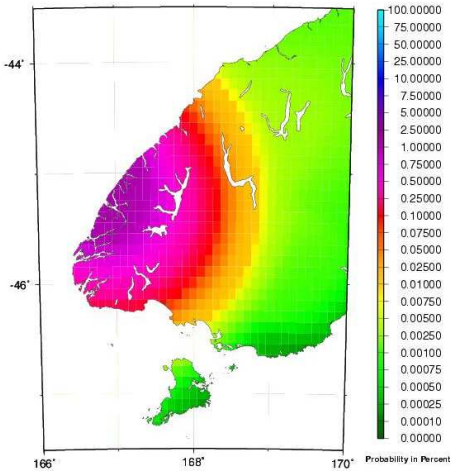

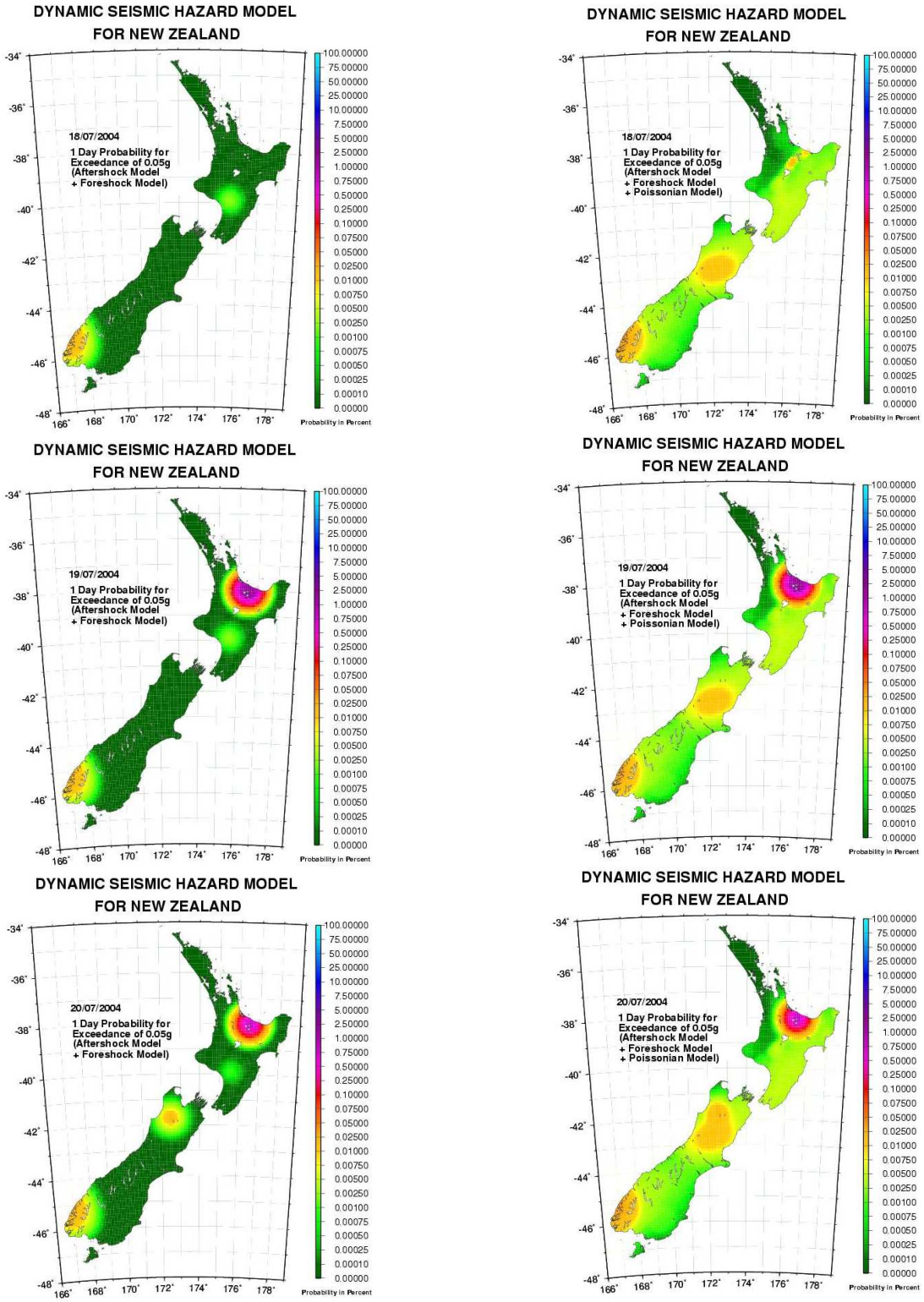

Figure 10.4: Conditional (left) and total (right) hazard forecasts for 18-20 July 2004. The hazard increase in Fiordland is still aftershock hazard due to the 7.0 event on 21 August 2003. All other hazard increase is due to foreshock probabilities. The big spot on the North Island is caused by an earthquake swarm in the TVZ (magnitudes 4 to 5).

10.2 Daily hazard for specific sites

Additionally to the computation of hazard maps for the entire country or parts of New Zealand, I have calculated the daily hazard forecasts for a certain length of time on several sites throughout New Zealand.

I display them as plots of time histories for each site. Each plot covers one year of ground motion probability forecasts. Figure 10.5, 10.6 and 10.7 show three examples of these plots. The locations of the sites are the locations of strong ground motion instruments at Iwitahi Forestry Headquarters ($-38.8333°/176.267°$), Queenstown Telephone Exchange ($-45.0335°/168.658°$), and Hamner Springs Fire Station ($-42.5217°/172.825°$), respectively. Figure 10.8 shows a comparison of 2003's seismic hazard in Christchurch and Wellington.

The right hand part of the plots displays the hazard forecasts in probability of 0.05g exceedance (in numbers between 0 and 1). For each day the total hazard (i.e. Poissonian plus foreshock plus aftershock hazard) is plotted. The possible minimum is always the Poissonian background hazard for that specific site. If no additional effects due to foreshock or aftershock triggering probabilities influence the site, the hazard shows as a straight line on the daily background hazard level. Each yearly plot is scaled to the maximum probability during the time shown. The scale on the X-axis therefore changes from plot to plot.

If there were any, the left hand part shows the actually observed cases of exceeding this level of ground motion on these days, i.e. triggers of the instrument with maximum horizontal PGA of more than 0.05g. The triggers are shown as star shaped symbols on the day of observation at the magnitude of the earthquake they have been caused by. The size of the symbol reflects the strength of PGA in g that was registered by the instrument for this particular trigger.

These examples display the different features that can occur in the forecasts.

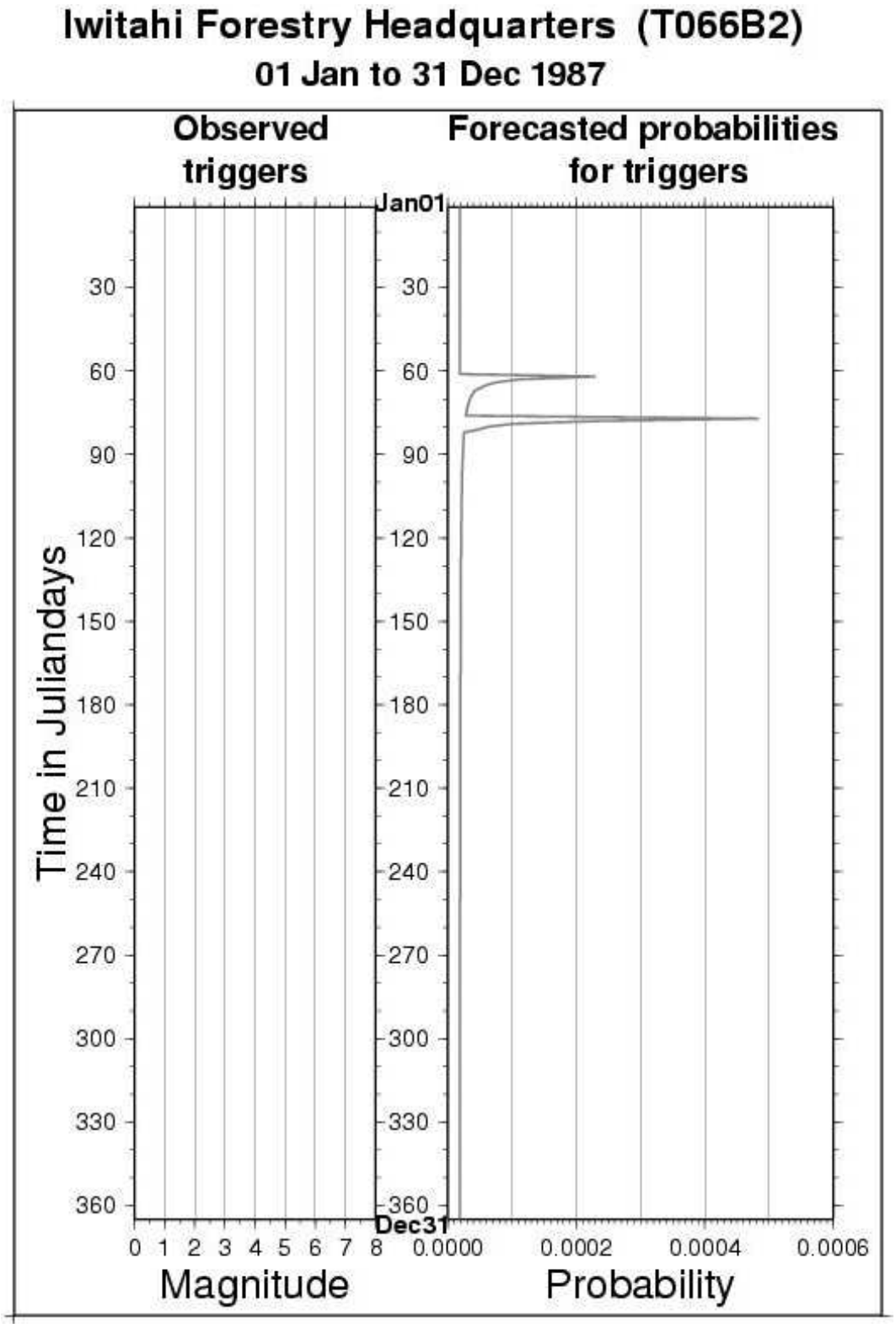

Figure 10.5: Daily hazard forecasts of exceedence of 0.05g for 1987 at Iwitahi Forestry Headquarters. Forecasts based on Poissonian, foreshock and aftershock hazard on the right hand side, observed triggers of that ground motion on the left hand side.

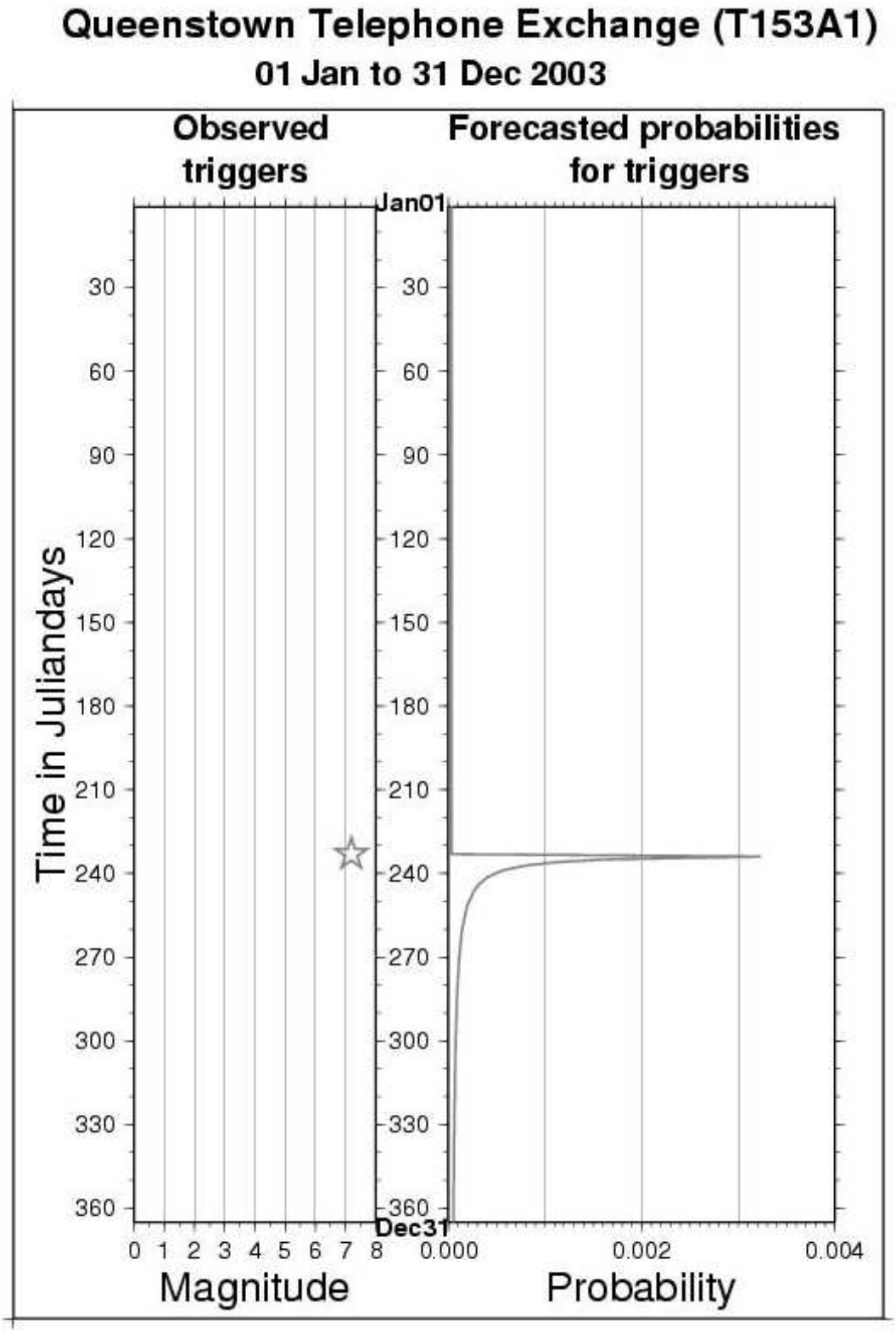

Figure 10.6: Daily hazard forecasts of exceedence of 0.05g for 2003 at Queenstown Telephone Exchange. Forecasts based on Poissonian, foreshock and aftershock hazard on the right hand side, observed triggers of that ground motion on the left hand side.

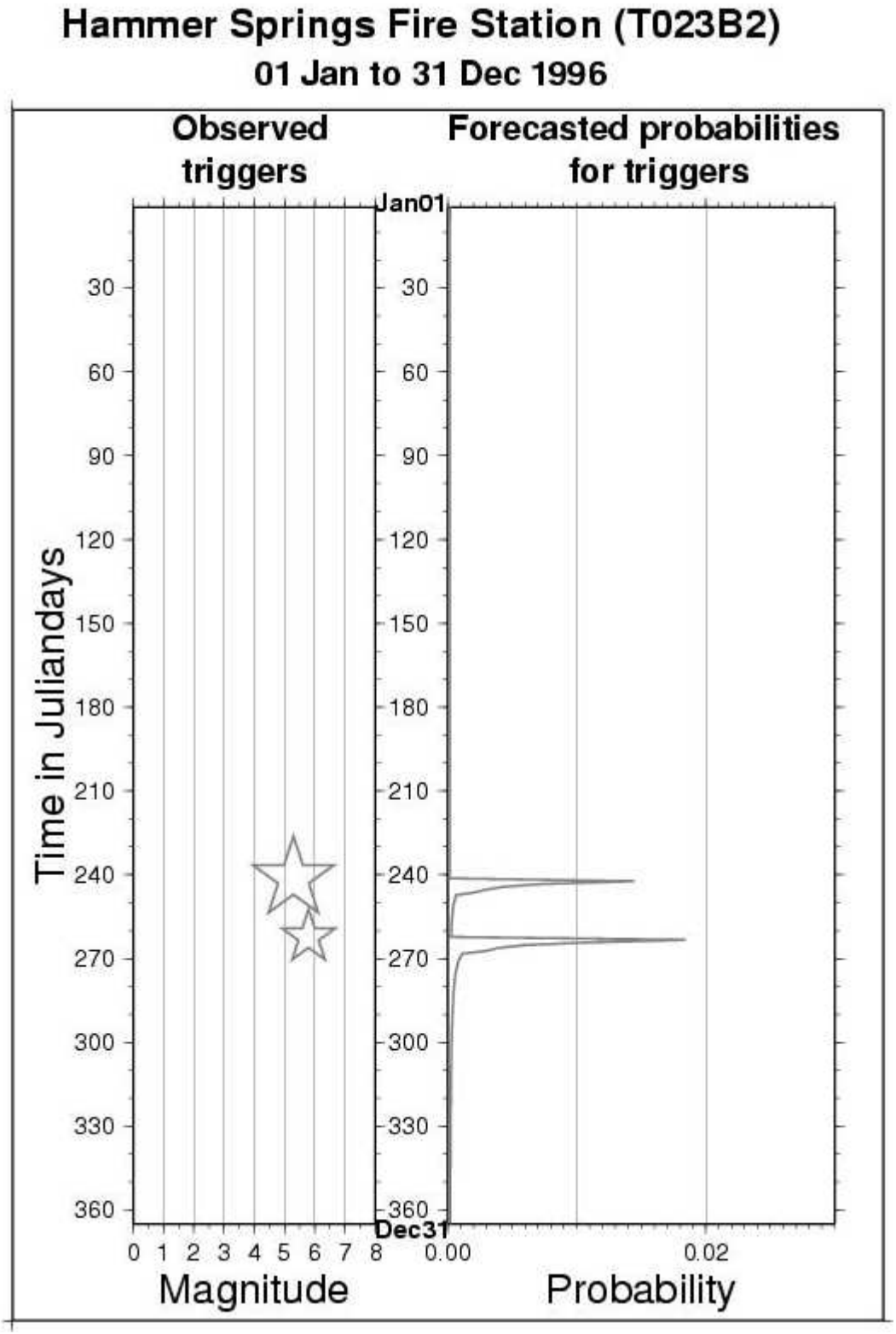

Figure 10.7: Daily hazard forecasts of exceedence of 0.05g for 1996 at Hamner Springs Fire Station. Forecasts based on Poissonian, foreshock and aftershock hazard on the right hand side, observed triggers of that ground motion on the left hand side.

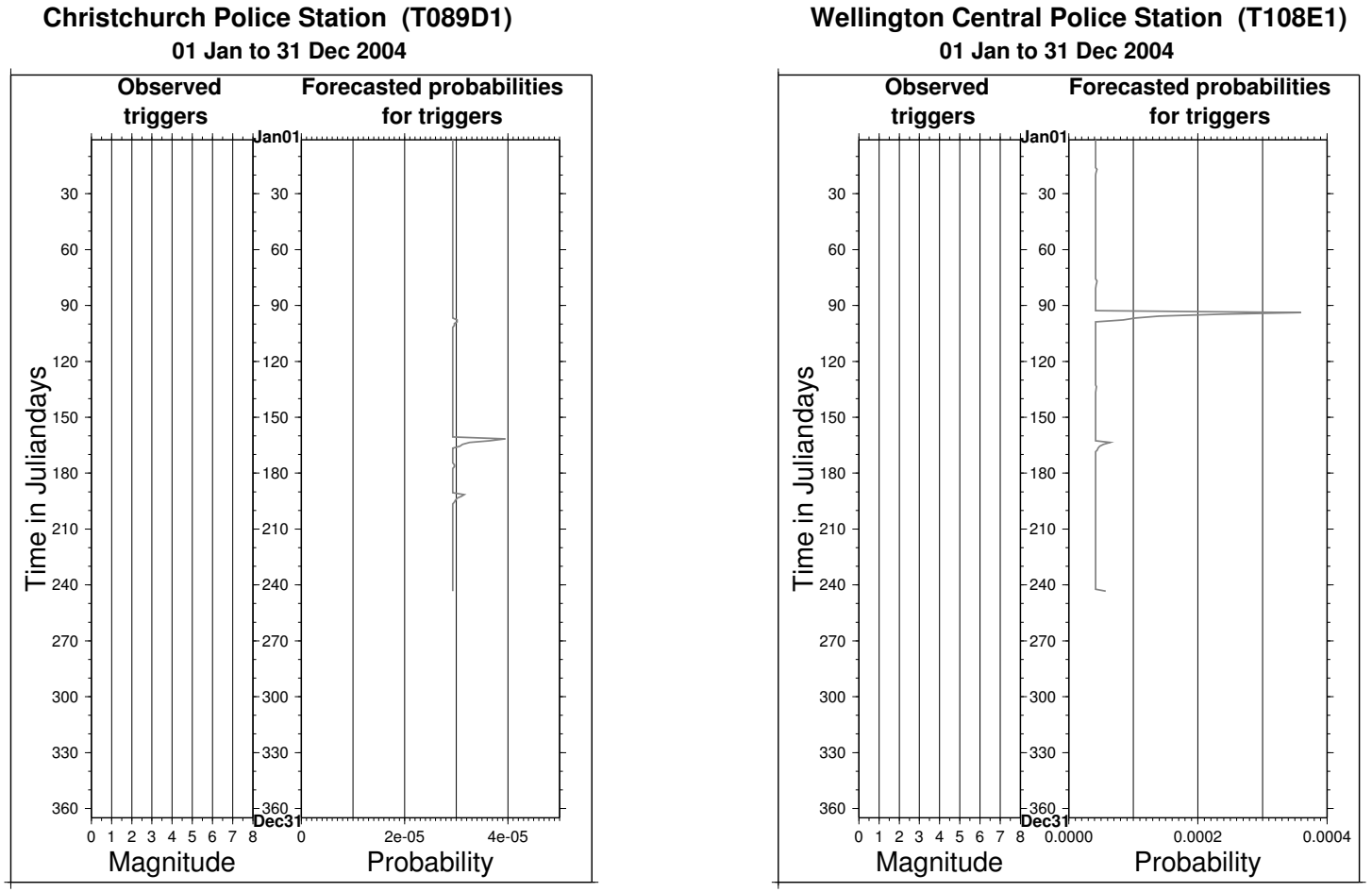

Figure 10.8: Daily hazard forecasts of exceedence of 0.05g for 1st Jan to 31st Aug 2004 in Christchurch (left) and Wellington (right). Forecasts based on Poissonian, foreshock and aftershock hazard on the right hand side of each plot, observed triggers of that groundmotion on the left hand side.

The peaks in figure 10.5 exhibit the two types of decays for aftershock and pure foreshock hazards. The first peak has a much longer duration than the second, it is still decaying when the second peak finishes. This first peak is an aftershock peak, i.e. the event that caused the hazard to increase for this period was at least a magnitude 5.4 earthquake. The second peak occurs while the aftershock hazard is ongoing. It increases the hazard further for five days, which is the foreshock time window. This second peak is a foreshock peak with no aftershock hazard component, which implies that it is caused by an earthquake smaller than magnitude 5.4. There is a sudden jump to zero additional probability after the smooth decay for the first five days. The aftershock peak in that plot is the hazard increase due to a magnitude 6.1 event on 2 March 1987 ($-37.9°/176.8°$), the foreshock peak due to a magnitude 4.0 event on 17 March 1987 ($-38.9°/175.9°$), which was too far from the M=6.1 earthquake location to be an aftershock. Neither of the events caused 0.05g ground motion at the site of the instrument.

The station in Queenstown (Fig. 10.6) was triggered by the event that caused the hazard increase. That event was the 21 August 2003 Fiordland earthquake of magnitude 7.2 ($-45.2°/166.8°$). The strong motion instrument recorded a maximum horizontal acceleration of 0.09g. The hazard after the event shows the slowly decaying shape of aftershock hazard. For the day the instrument was triggered, the hazard forecast was solely background hazard, i.e. the chance for exceeding 0.05 g on this particular day had been estimated 0.003%. Even at that distance, the Fiordland earthquake still increased the hazard by a factor of 100 to 0.3% for the next day.

Figure 10.7 shows two triggers at a station in Hamner Springs. Both causative events were big enough to create aftershock hazard (magnitudes 5.8 and 5.7). The second event occured 21 days after the first earthquake and at a time of increased hazard of about a factor of two above background hazard, thus the second trigger occurred on a day when the probability of a trigger was 0.02%. Due to the second event the probability increases again to just under 2%, but no further strong events followed.

The last plot (Fig. 10.8) compares the hazard in the capital Wellington and the biggest city on the South Island, Christchurch, from 01 January to 31 August 2004. The time was seismically calm at both sites; for most of the time only background hazard was forecast. The horizontal scales are different, thus the hazard level was lowest in Christchurch.

The question of how well the model forecasts reality is addressed in Part IV.

Part IV

Testing Conditional Seismic Hazard Models

Chapter 11

Introduction

Seismic hazard models produce estimates of exceedance of ground motions that are expected within a certain return period. Testing seismic hazard models should therefore be testing their ground motion forecasts against actually observed ground motions. However, no such methods have been standardised yet; most tests still concentrate on the models' components, mainly the seismicity rate forecasting.

11.1 General thoughts

It is unquestioned that every scientific model claiming to describe processes of one kind or the other needs to be tested to find out whether the output is true. Testing probabilistic seimic hazard forecasts is difficult for several reasons: as for any forecast that estimates measures with more than two possible values, there is no obvious line of when a forecast was wrong (e.g. if the weather forecast predicts 15 degrees and the temperature reaches 16, was that wrong or pretty close? What if it is only 8 degrees instead?). Additionally, seismic hazard analysis is only probabilistic and the forecast probabilities of expected exceedance of ground motions are low, much less than 1% for most days, with maximum values after large events between 20% and 50%. Finally, the greatest hazard is caused by large events, which are relatively rare. Therefore only tests covering very many forecasts over a long time period can reveal whether the low probabilities are of the right order.

It is difficult to decide whether a model performs well enough, at what point a forecast is wrong enough to call the model 'bad' or 'useless' or 'dangerous', and when it is still more benefit having it with its faults than not having it at all. This makes it difficult to design an absolute test for one probabilistic model. If more than one model is available, it is easier to test them against each other and each against the data and formulate a measure of their relative goodness in describing observed data.

To test the seismic hazard model, it is desireable to demand a check of the final output: the forecast strengths of shaking that are planned to be made available to the public once they have been proved to be reliable. But there are several problems connected with testing ground motions. For one, the model is calculating expected levels of ground motions on a grid of 0.1 degree, which is about 11 km spacing between the points and produces thousands of forecast exceedance values each day. For now (and for a long time into the future) we do not have ground motion data for all or at least most or even very many of these sites in the country. Instead, the set of data points (strong motion seismometers and with some additional effort broadband stations, too)

is very small, only a few hundred, and those are not even randomly chosen, but concentrate in seismically active areas. This already implies that one cannot test all data produced by the model.

Testing ground motions is obviously limited by the problems just discussed. But there is another aspect about them that commonly makes it even less attractive to use this final output for testing: the biggest uncertainties in hazard calculations are mostly thought to originate from the choice of the attenuation model. Different models have been developed to adequately describe attenuation relations for different countries, but still none is completely satisfying. To not blur the visibility of hazard impact due to foreshock and aftershock earthquake triggering, some researchers decided to test only the input to the hazard calculation, i.e. the seismicity rates.

11.2 Statistical tests for the STEP model

To validate his STEP model (previously discussed in Chapter 6.4), **Gerstenberger, 2003** [16] developed three statistical tests: a parameter optimisation test, a consistency test and a ratio test. All three tests investigate seismicity rate forecasts rather than the actual ground motion forecasts. The tests use likelihood, which is a statistical tool that gives a measure of consistency between a model and observed data. In contrast to the least square method, which gives the actual distances between prediction and datapoints, the likelihood gives the probability of making those particular observations given the model parameters.

The parameter optimisation test is designed to test various sets of parameters and allows a selection of the set that best fits the data. For each set the model's forecasts are calculated and retrospectively compared to observed earthquake data. The consistency test uses only one parameter set and investigates whether the forecasts are consistent with the data or can be rejected with a given significance. This test is performed with the real earthquake data as well as with simulated catalogues. The ratio test finally decides whether one model can be rejected on the basis of another, i.e. whether one

model is better than another. In all tests, daily 24 hour seismicity rate forecasts were computed and compared with the earthquake numbers observed in the exact same locations and time periods.

The results of the consistency test showed that the STEP model for the short 250 days testing period had to be rejected for days with no earthquakes, while it could not be rejected for days with activity. This is to be expected as the model's resolution forces probability smoothing over larger areas than where earthquakes will actually occur. The ratio test was performed for a three year period, testing the STEP model against three other models: the poissonian background model, the generic California model and a composite model including the generic California model and sequence specific models. On days with no earthquake occurrences, the models could not be rejected over the STEP forecasts. But on days where events have been observed, the STEP model did always do significantly better.

11.3 Precarious rock studies

A methodology to test long term seismic hazard forecasts in terms of ground motions has been developed by **Brune, 1996** [6] and **Stirling and Anooshehpoor, 2004** [57] and recently been applied to New Zealand in a pilot study by **Stirling and Anooshehpoor, 2004** [57]. **Brune** and **Stirling** use ancient precariously balanced rocks to constrain maximum ground motion levels that could have occured since their formation, i.e. for periods of thousands of years.

Precariously balanced rocks are rocks that appear unstable with respect to ground shaking and therefore could be toppled by low PGAs. Once toppled into a stable position the rocks cannot reach their unstable state again through further shaking. From the formation's geometry it is possible to estimate the ground acceleration that is necessary to topple a certain precariously balanced rock formation. It is also possible to estimate the age of those formations. Combined, this information gives an estimate of upper limit ground motions that can have occurred during those long periods, i.e. during previous large earthquakes.

Brune, 1996 [6] did precarious rock surveys in Southern California, with special effort in regions near historic large earthquakes. He compared the occurrence zones with long term seismic hazard maps (return times of 1000 and 5000 years, 90% probability of exceedence). He found that the maps produced by the modern methodology of **Wesnousky, 1986** [66], which incorporates uncertainties in the attenuation model into estimates of ground motions, showed excellent agreement in zones of low acceleration and occurrence of precariously balanced rocks. Comparison with other models showed that the assumption of random earthquakes occurring on unknown faults tends to overestimate the hazard in certain areas, compared with what the rocks show.

Stirling and Anooshehpoor, 2004 [57] surveyed precarious rocks in three areas on the South Island of New Zealand: central Otago, eastern Fiordland and northwest Nelson. They did not find any unstable rocks in Fiordland (probably a reflection of alpine erosion and regular strong earthquake shaking), but the formations were abundant in central Otago and northwest Nelson. All sites in central Otago were very close to major active fault sources (less than 5 km). According to the geologically derived fault parameters, all these faults should have produced several large earthquakes in the time span during which the nearby precariously balanced rocks have been in existance. The test field in northwest Nelson is located nearly 100 km from the nearest active fault, which leaves the PGA calculations of the seismic hazard model to be estimated from distributed seismicity alone.

The 28 rocks used in the study have estimated ages of 10,000 to 55,000 years. Their toppling accelerations range from 0.11g to 0.73g. A comparison between the precarious rock data and the seismic hazard curves of the New Zealand National Seismic Hazard Model shows lower hazard from the near field Otago rocks than the model predicts, suggesting either fault parameter problems for these particular sources or issues in the near field attenuation relationship. In northwest Nelson, data and model agreed well, strengthening the procedures of hazard calculation from multiple earthquake sources.

11.4 Goal for this test

As discussed in Section 11.2, there are many counterarguments for attempting ground motion tests. However, ground motions are seismic hazard models' output and it is important to try to test this final information. It is one thing to test all components of a model and prove them right. That still does not prove the sum of their influences to be right, too. Releasing ground motion forecasts to the public at some point requires them to have been tested.

Precarious rock studies provide a measure for estimates of PSHA for long return periods and have shown that this is potentially useful information. Short term time-dependent models need to be tested differently to achieve a temporal resolution that the rocks cannot provide. Strong motion records do provide this resolution, but are very limited in the time span and spatial density they cover.

The attempts I offer in this thesis build a basis of relatively simple checks on which different models could be compared in terms of ground motion forecasting success. I compare my conditional model with the Poissonian model and show some unexpected results for the latter. I also show that the most problematic part of the hazard forecasting machinery is not necessarily the attenuation model.

At this stage, without more future earthquake and strong motion data, this test should be slightly circular in the sense that much of the data that is used to test the code was also used to develop it. The foreshock and aftershock probabilities were developed from the same catalogue data that was used to develop the attenuation model and test the accelerations. Therefore, for as long as not much more earthquake data is available, this test is more of a consistency test. However, the model is so complex that the test is worthwhile, and the unexpected results described in the next chapter show that it was very important to do.

Chapter 12

Ground Motion Tests

I test the seismic hazard model in terms of the ground motion acceleration data that it forecasts every day for any point. I compare the forecasts to the observed triggers of strong motion instruments.

12.1 Data

12.1.1 Stations

To test the model's peak ground acceleration forecasts I need ground motion information. This is available on sites of strong motion seismometers, the first of which were installed in New Zealand in the mid 1960s. The network has grown to the present distribution of more than 200 stations in the country. Since 1999 GeoNet has installed a new additional network of about 150 Etna strong motion stations. As the data of the original network are available fully processed and the Etna network data come in an inconvenient raw format, I decided to concentrate on the original network for this first approach of ground motion testing.

To build a reliable database of stations and triggers, I tried to use only stations for which the records are complete for the time they have been running. I only used data from stations that triggered at least once. The trigger did not need to be of the level I am interested in; it could be the lowest acceleration above the trigger threshold (which is mostly 0.001 g and well below the level I use). I assumed that an instrument that had triggered at all would be unlikely to miss the stronger triggers I use for the test, while a station that did not trigger might not be working.

Furthermore, I only used data from one station in locations where two or more instruments were simultanously running in the same place, i.e. in the same building. Wherever I had the choice I used only data from stations located in the basement or first floor of buildings and neglected the ones located on higher stories.

I am left with 156 stations with running times per station of a few months to more than 38 years. The total running time of all stations sums up to just under 2500 years. Figure 12.1 shows the regional distribution of the instruments' locations. Apart from the dense cluster in and around Wellington, the instruments are distributed evenly over most parts of the country.

Table B.1 in the Appendix lists all 156 stations I have used with information about their location, time span of recording, name and original network station codes. I have

renamed the stations and aggregated under those new names formerly differently named stations, i.e. when an instrument at a location was replaced and the new one continued recording at the same location, the new one would get a new code in the original network. I combined those datasets to one per location (if they recorded continuously). The last column in table B.1 lists what original stations are aggregated on each of the locations I kept. Apart from numbering the stations (T plus 3 digit number), the code I assigned to the locations indicates how many original stations there were at that location (letter) and how many of them I used (last digit).

To get a minimal regional resolution, I additionally divide the stations into two subsets: low hazard sites (<0.3g based on the national seismic hazard map showing exceedence levels for 10% in 50yrs) and high hazard sites ($\geq$ 0.3g). See Fig. 12.2 for the locations of the low and high hazard sites.

12.1.2 Triggers

Fully processed strong motion data for the original network has just recently become available on the GeoNet website (www.geonet.org.nz). The information includes the time and instrument for each trigger, the peak acceleration in mm/s^2 of the two orthogonal horizontal and the vertical components, the magnitude and depth of the triggering event as well as the distance between its epicenter and the instrument.

Most of the instruments trigger at accelerations as low as 0.001g. I need all those triggers that exceeded the threshold of the Dynamic Seismic Hazard Model, i.e. 0.05g. As explained earlier, the PGA defined in the dynamic model is the maximum peak acceleration measured on the horizontal components. I therefore transformed the provided acceleration information for each trigger into that measure of PGA: I chose the maximum value of the horizontal acceletations in mm/s^2 and divided it by 9810 to get a value in unit g. I then kept only triggers for which that value was 0.05g or more.

Because the model's forecasts are only based on earthquakes of minimum magnitude 5.25 and maximum depth 40km, I eliminated all triggers whose initiating events did not fulfil these conditions. Also I only kept triggers from the stations I chose as discussed

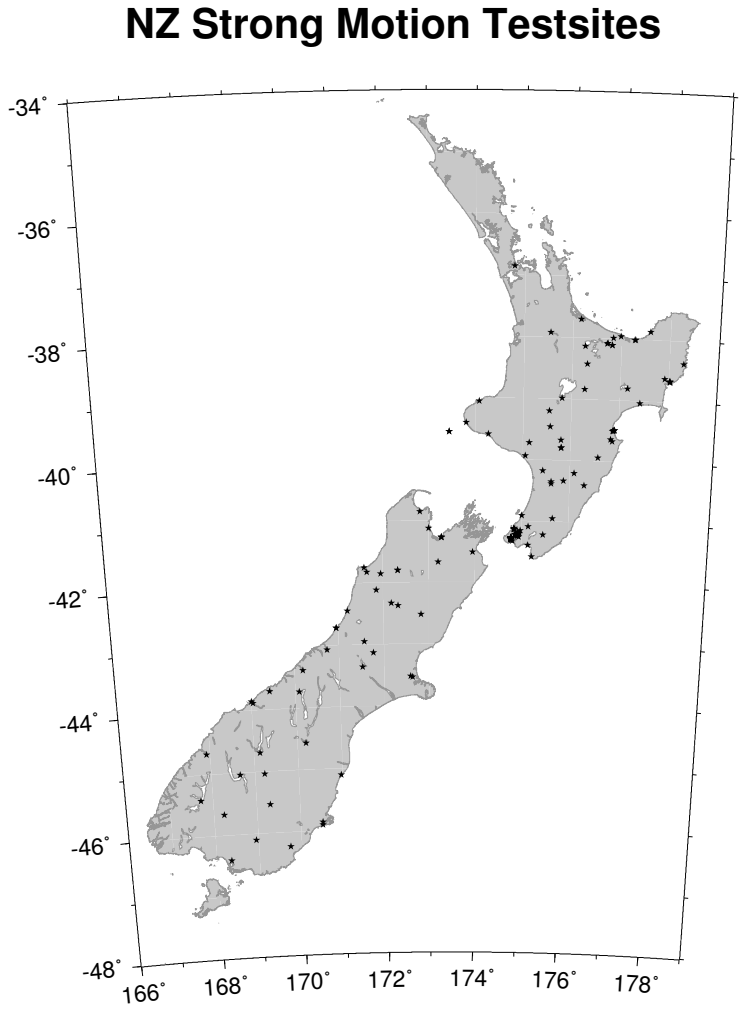

Figure 12.1: Locations of strong motion instruments in New Zealand used as test sites for the ground motion test of the Dynamic Seismic Hazard Model

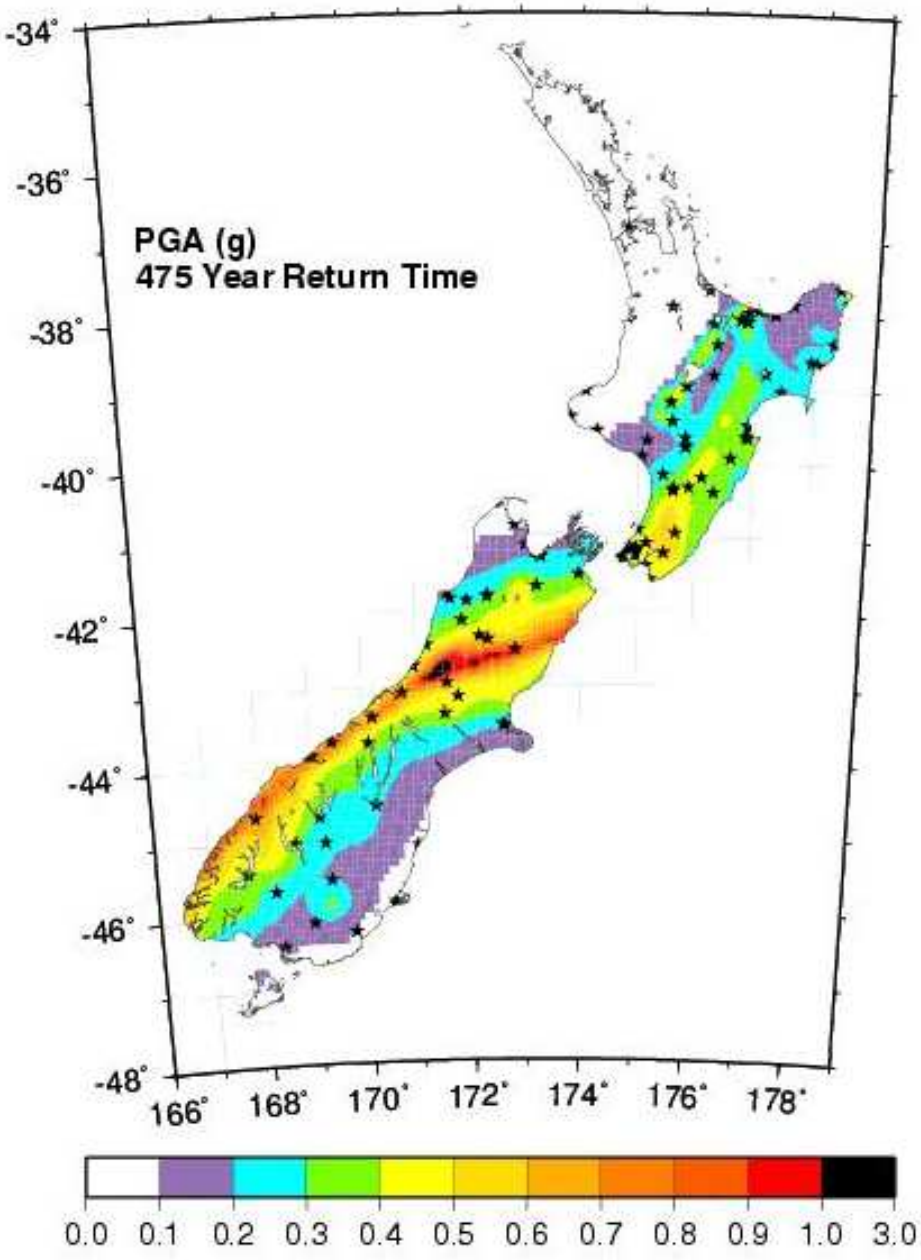

Figure 12.2: Low and high hazard locations of strong motion instruments in New Zealand used as test sites for the ground motion test of the Dynamic Seismic Hazard Model. All stations in areas of less than 0.3g exceedence in 475 years return period (white/purple/blue areas) have been classified low hazard stations. All stations in the green/yellow/red/black areas are classified as high hazard stations.

above, i.e. I eliminated those of simultanously recording instruments at the same location.

The number of remaining triggers for the last 39 years is 74. Many of the triggers were multiple triggers from several stations recording the same earthquake. These 74 triggers were caused by 34 separate events.

A list of all triggers with information about the time, measured maximum horizontal acceleration and the instrument of recording, as well as the magnitude, depth and distance to the associated earthquake, can be found in table B.2. The earthquake information given in the processed trigger file in many cases varies in magnitude and depth information from the values given by the GeoNet earthquake catalogue for New Zealand for the earthquakes in question. But the trigger file includes the best available magnitude and location information, which was not necessarily supplied by the online catalogue (**J. Cousins** personal communication, 2004). For this reason I use the information from the trigger file.

By choosing all triggers above 0.05g, the models' forecasts of probability of ground motion exceeding 0.05g in a given period can be interpreted as probabilities for triggers to be recorded.

12.2 Test I: general test

The first test is designed to give a general idea about whether the Poissonian and/or the Dynamic Seismic Hazard Model correctly forecast the overall numbers of occasions of 0.05g exceedence expected in a certain time for a certain set of locations.

12.2.1 Method

For each station I compute daily hazard forecasts for its whole running time. Each forecast is the probability that the instrument might trigger within a single day. To calculate the number of expected triggers per station I add up the forecast probabilities for all days. For the Poissonian model, the probability at a station will be the same

every day, so the total number of expected 0.05g exceedences at a station, $N_{poisson}$, is the product of the number of days that the station has been recording, $days$, times the location specific Poissonian probability, $P_{poisson}$.

$$N_{poisson}(station) = days * P_{poisson}(station) \tag{12.1}$$

The number expected by the Dynamic Seismic Hazard Model, N_{total}, is the sum of all daily forecasts. Each forecast is at least the Poissonian value, depending on nearby seismic activity, which increased foreshock and/or aftershock hazard.

$$N_{total}(station) = \sum_{i=1}^{days} P_{total,i}(station) \tag{12.2}$$

12.2.2 Results

Adding the numbers of expected triggers of all stations for a total of 902,499 station days, the Poissonian model predicts 33.65 observations of 0.05g or more PGA, while the combined background, foreshock and aftershock model forecasts 53.03 triggers. 74 triggers were actually observed.

The subset of 59 stations on low hazard sites had a total running time of 347,981 station days. 27 triggers were recorded; the Poissonian model forecast 8.38 and the new time-dependent model 15.01.

The 97 stations on high hazard sites covered 554,518 station days and recorded 47 triggers. The Poissonian forecast was 25.27 and the total forecast 38.02.

These numbers are discussed in Section 12.4.

12.3 Test II: specific test

Although at first sight the results above suggest the new model performs better, it is necessary to check whether the triggers actually tend to occur on days of increased hazard or whether a random addition of hazard would do equally well/poorly.

This second test is designed to provide some statistics that can be interpreted to answer the question.

12.3.1 Method

This test analyses the hazard forecasts for those days and for those stations on which triggers have been recorded. For each trigger I calculate the Poissonian and total hazard forecasts and compute by how many times the total hazard exceeds the Poissonian hazard:

$$factor(station, day) = \frac{P_{total}(station, day)}{P_{poisson}(station, day)} \tag{12.3}$$

By construction, the total probability cannot be less than the Poissonian probability, and therefore $factor \geq 1$. I round all factors to integers and then bin the $factor$ information on a logarithmic scale: one times the background hazard being all $factor < 1.5$, ten times the background hazard being all $1.5 \leq factor < 15$, one hundred times the background hazard being all $15 \leq factor < 150$, etc.

Out of the set of 902,499 24-hour forecasts I count the total number of days on which the new model forecast probabilities within each bin, i.e. how many days had probability forecasts of just the background hazard ($factor < 1.5$), how many days of ten times the background hazard ($1.5 \leq factor < 15$), etc. For each bin I add up the probabilities that were forecast, getting the number of expected triggers in those bins, and compare those numbers to the actually observed triggers.

A further similar check is performed on the actual daily probabilities: I divided all 902,499 forecasts into 46 classes depending on the total probability P predicted for each day. The classes are defined on a logarithmic scale again.

Class 1	$P \leq 0.00001$
Class 2	$0.00001 < P \leq 0.00002$
...	...
Class 10	$0.00009 < P \leq 0.0001$
Class 11	$0.0001 < P \leq 0.0002$
...	...
Class 19	$0.0009 < P \leq 0.001$
Class 20	$0.001 < P \leq 0.002$
...	...
Class 28	$0.009 < P \leq 0.01$
Class 29	$0.01 < P \leq 0.02$
...	...
Class 37	$0.09 < P \leq 0.1$
Class 38	$0.1 < P \leq 0.2$
...	...
Class 46	$0.9 < P \leq 1.0$

For each class I compare the predicted number of 0.05g exceedences for the total time with the actually observed numbers of triggers. This gives a rough idea of whether the frequencies of certain probability forecasts are right.

12.3.2 Results

Out of the 74 triggers observed by the whole set of strong motion instruments during the last 40 years, 49 occured on days of pure Poissonian hazard forecasts, in other words, they were not caused by associated events based on the definitions used for aftershocks and foreshocks in this thesis. Another 16 occurred with so little foreshock/aftershock hazard increase that the total hazard is still rounded to one times the background level, i.e. total hazard is less than 1.5 times the background on that station. The count results are listed in Table 12.1.

Numbers of triggers	Forecast hazard at time of triggers (in rounded multiples of the background)
65 out of 74	1*background
2 out of 74	2*background
1 out of 74	6*background
1 out of 74	8*background
1 out of 74	48*background
1 out of 74	90*background
1 out of 74	171*background
1 out of 74	5748*background
1 out of 74	12428*background

Table 12.1: Hazard forecasts for the days and locations of all 74 triggers.

As described earlier, this data has been binned into logarithmic intervals of multiples of background hazard. Table 12.2 lists, for each interval, the number of days for which the hazard forecast of the Dynamic Model fell within, the numbers of triggers that have been observed on those days, and the predicted number of triggers on those days. The forecast from the total model is listed as well as the Poissonian part of the hazard for those days.

Forecast hazard at time of triggers (numbers of days)	Observed Numbers of triggers	Predicted Numbers of triggers (Poissonian)	Predicted Numbers of triggers (Total)
1*background (853,476)	65 out of 74	31.57 out of 33.65	32.13 out of 53.03
10*background (44,001)	4 out of 74	1.88 out of 33.65	6.97 out of 53.03
100*background (4,591)	2 out of 74	0.18 out of 33.65	6.76 out of 53.03
1000*background (403)	1 out of 74	0.01 out of 33.65	5.28 out of 53.03
10000*background (28)	2 out of 74	0.0007 out of 33.65	1.91 out of 53.03

Table 12.2: Predicted versus observed numbers of triggers at certain hazard levels. The hazard forecasts per day have been binned logarithmically, the Poissonian forecast is the Poissonian fraction of each total daily forecast.

The same analysis has been done for the two subsets of stations in low and high hazard locations, respectively. Out of the 27 triggers at low hazard sites 18 happened on days of pure background hazard. For high hazard sites this figure is 31 out of 47. The binned results are presented in Tables 12.3 and 12.4.

Forecast hazard at time of triggers (numbers of days)	Observed Numbers of triggers	Predicted Numbers of triggers (Poissonian)	Predicted Numbers of triggers (Total)
1*background (327,782)	23 out of 27	7.85 out of 8.34	7.99 out of 15.01
10*background (17,478)	1 out of 27	0.46 out of 8.34	1.80 out of 15.01
100*background (2,443)	0 out of 27	0.06 out of 8.34	2.16 out of 15.01
1000*background (257)	1 out of 27	0.006 out of 8.34	1.92 out of 15.01
10000*background (21)	2 out of 27	0.0003 out of 8.34	1.15 out of 15.01

Table 12.3: Predicted versus observed numbers of triggers at certain hazard levels for low hazard sites. The hazard forecasts per day have been binned logarithmically, the Poissonian forecast is the Poissonian fraction of each total daily forecast.

Forecast hazard at time of triggers (numbers of days)	Observed Numbers of triggers	Predicted Numbers of triggers (Poissonian)	Predicted Numbers of triggers (Total)
1*background (525,694)	42 out of 47	23.71 out of 25.27	24.14 out of 38.02
10*background (26,523)	4 out of 47	1.42 out of 25.27	5.16 out of 38.02
100*background (2,148)	1 out of 47	0.12 out of 25.27	4.60 out of 38.02
1000*background (146)	0 out of 47	0.009 out of 25.27	3.36 out of 38.02
10000*background (7)	0 out of 47	0.0004 out of 25.27	0.76 out of 38.02

Table 12.4: Predicted versus observed numbers of triggers at certain hazard levels for high hazard sites. The hazard forecasts per day have been binned logarithmically, the Poissonian forecast is the Poissonian fraction of each total daily forecast.

The results for the probability class test are summarised in Figure 12.3. For each class, the numbers of observed and forecast triggers from the Poissonian and total model have been normalised by the numbers of days for which probabilities in each interval

have been counted. The plot therefore shows the average daily rates of observed and predicted triggers in each probability class. By construction of the intervals, the total probability will show as an approximate line of 45° on a log-log plot.

For low daily probabilities of up to 0.1% (=0.001 label in the plot) the model slightly underestimates the daily numbers of actual triggers. On days of probability forecasts between 0.1% and 10% (=0.1 label in the plot) the model overestimates by much, as no triggers were observed in these categories. For high hazard days of more than 10% there is a rough agreement between model and data again.

The actual numbers underlying this plot are given in Table B.3 in the Appendix.

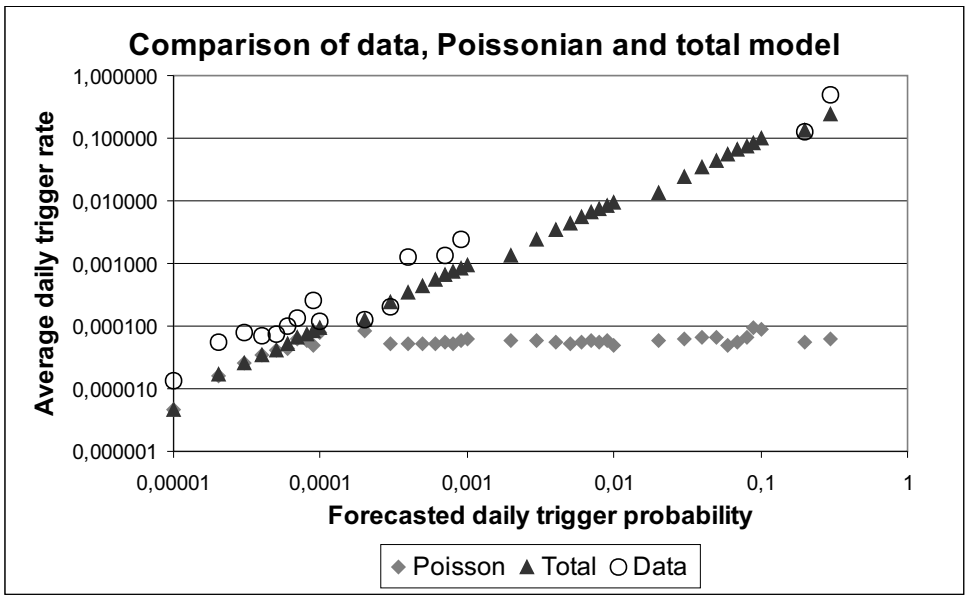

Figure 12.3: Data versus Poissonian and total forecasts in terms of daily trigger probability rates.

12.4 Discussion

The test results presented in the previous section are to some extent unexpected and raise many questions. It is certainly not appropriate to expect a model like the Poissonian or the Dynamic Seismic Hazard Model to be 100% right, but the discrepancies shown in the above results need discussion and some further investigation.

In this section I start to address some of the problems and offer suggestions as to

where they may originate and how they might be explained. As I will explain in each case though, it is beyond the scope of this thesis to finalise the interpretation, which needs substantially more time and effort (see "Recommendations for further work").

While the Poissonian model and its test results are not affected, the Dynamic model's results would probably be different, if the corrected formula for aftershock probabilities had been used. A comparison of the probabilities produced by the original versus the revised formula showed that the later predicts more events for small magnitude differences between mainshock and aftershock (up to a factor of 2.2 for 0.1 units of magnitude difference) and smaller probabilities for large magnitude differences. Therefore, it is difficult to estimate the changes in the test results that one would expect for the corrected model.

It needs to be kept in mind for all the tests that, although the set of strong motion instruments reaches a total running time of more than 900,000 days, they cover less than 40 years. If these last 40 years happened to be seismically unusually active or inactive, or showed other temporal extremes, the Poissonian model, which has been developed from longer term seismicity information, might mispredict the seismicity of the last 40 years. Also, the small number of only 74 observations of ground motion exceedence of 0.05g does not allow very detailed analysis or strong conclusions on statistical significance.

To develop an understanding of how both models could underpredict the number of triggers so greatly (74 observations, 34 predicted by Poissonian model and 53 predicted by Dynamic Model) the attenuation model was tested for the triggers observed. One hypothesis for the discrepancies is that some or many of the recorded triggers showed ground motions that were stronger than the ones expected by the attenuation model for an earthquake of that magnitude at that distance. That would lead to more 0.05g exceedence observations than the attenuation model, and therefore the Poissonian and

Dynamic model, would predict.

The test was done by calculating the attenuation curves for each event that caused one or more of the observed 74 triggers. The attenuation model tested (**McVerry et al., 2000** [29]) was used in the National Seismic Hazard Model (**Stirling, McVerry and Berryman, 2002** [58]) as well as in the new Dynamic Seismic Hazard Model described in this thesis. To compute the ground motion forecasts from the attenuation equation as a function of distance from the earthquake, only the magnitude and slip type of the event need to be known. The magnitudes are provided in the trigger file. The slip type has been assigned according to which seismotectonic zone (defined by **Stirling,McVerry and Berryman, 2002** [58]) the earthquakes occurred in. The attenuation curves are plotted with a 3σ standard error and the observed peak ground accelerations at the stations' distances. One plot is produced for each slip type and each magnitude. If more than one earthquake of a certain slip type and magnitude combination triggered stations, all those triggers will be shown in one plot. One example is shown in Fig. 12.4. The information is plotted on both linear and logarithmic scales. Two different symbols for the data show whether ground motion information from the causative earthquake (not necessarily the particular trigger itself) was used to develop the attenuation model in the first place (circles) or whether it is new independent information valuable for testing (diamond).

This example is very typical; the fit between data and model is exceptionally high for the complete trigger set. The attenuation plots for all 28 different slip type magnitude combinations for which ground motion data were included into the test dataset are shown in Appendix C.

Although only two thirds of the earthquakes in my dataset have been used for the development of the attenuation model, only 13 out of the 74 triggers are due to the new events. Still, comparing the average absolute residuals between model and data for the whole and the new trigger datasets suggests that the new data subset is fitted even better by the model than the complete set of triggers, and certainly not worse:

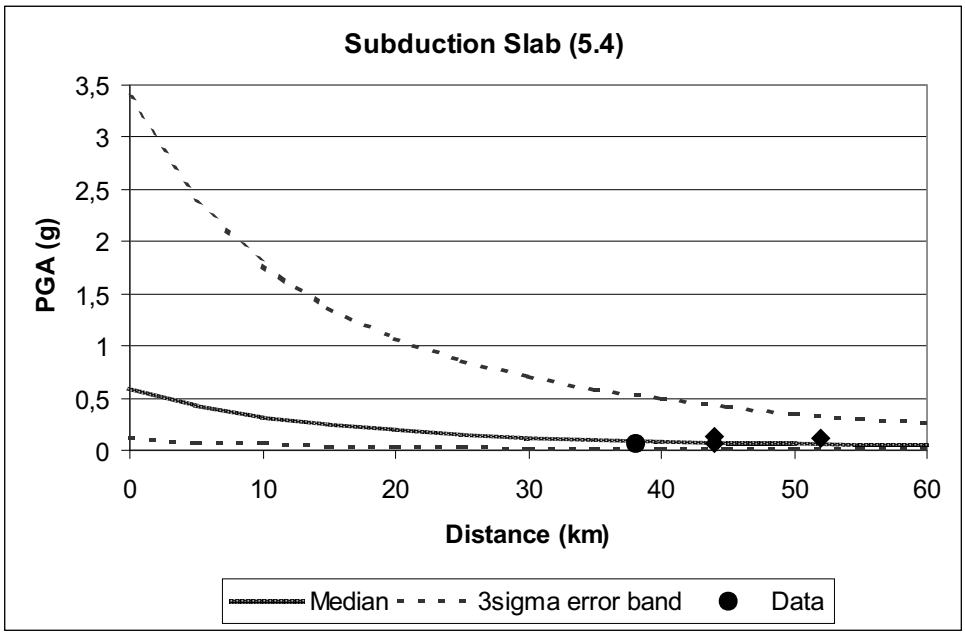

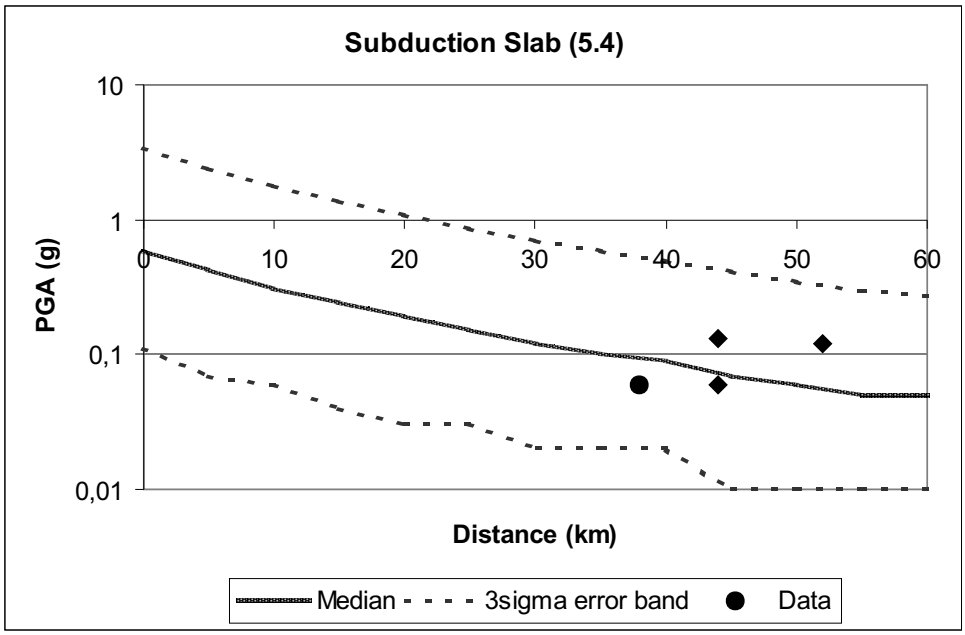

Figure 12.4: Comparison of observed ground motions versus predicted by the McVerry attenuation model. Attenuation curve and trigger data for M=5.4 subduction slab earthquakes. Circles are data used to develop the model, diamonds are new data.

$$\widehat{Res}_{all} = 0.13 \tag{12.4}$$

$$\widehat{Res}_{new} = 0.07 \tag{12.5}$$

The residual distributions are shown in Figures 12.5 and 12.6.

Only one out of the 74 triggers showed a much stronger ground motion than modelled (outside the 3σ error band) and this one has a plausible explanation: it was recorded by a station on top of Matahina Dam and therefore may have experienced considerable amplification from the dam structure.

The residual plots (Fig. 12.5 and 12.6) show more stations recording accelerations below the forecast than above the forecast. This is a reasonable observation as the model calculates ground motions expected at free-field sites, while most of the instruments are located in buildings. Several studies (e.g. **McVerry, 1984** [28], **Zhao, 1998** [68]) show that records in a building are considerably attenuated compared to remote sites due to high frequency filtering by the building's dimensions.

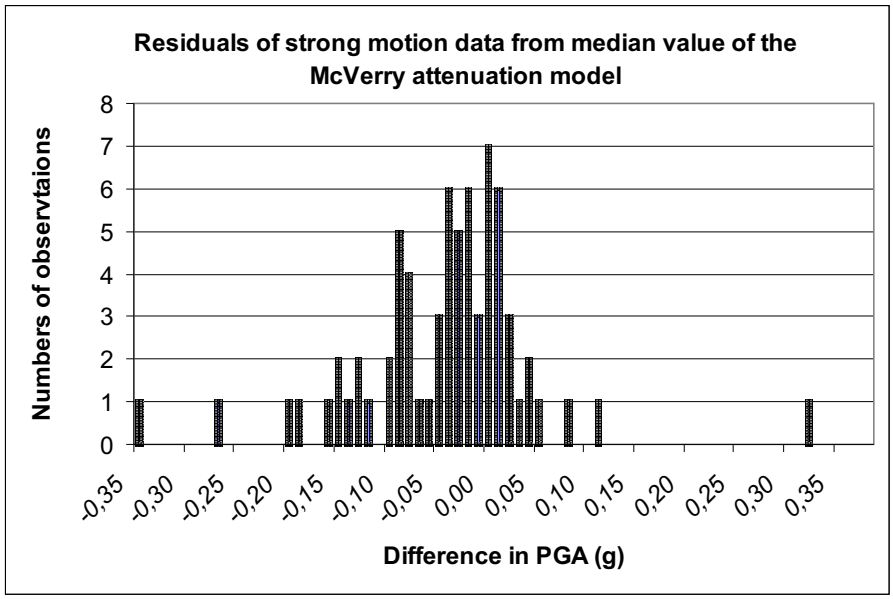

Figure 12.5: Residual distribution for the McVerry attenuation model test using all triggers.

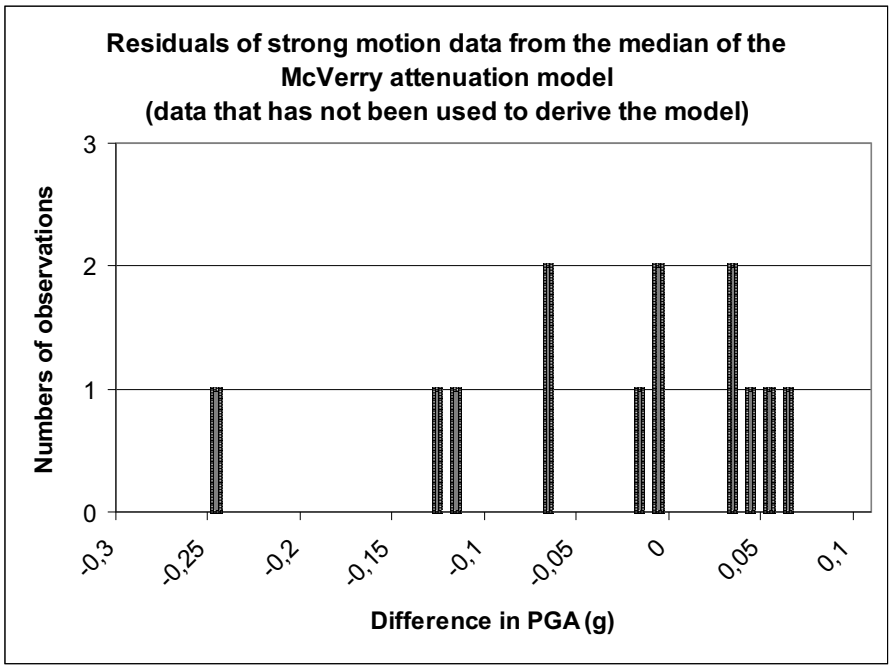

Figure 12.6: Residual distribution for the McVerry attenuation model test using only new triggers, i.e. caused by events that have not been used to contrain the model.

These results clearly show that issues in this attenuation model are not the cause of the discrepancies observed between the hazard models' forecasts and the ground motion observations.

The problem in this case must originate earlier in the process of the hazard calculation, i.e. somewhere on the forecast seismicity rate level. To get a clearer picture of the relative successes and failures of the Poissonian versus the total model, the results as listed in Table 12.2 are shown in Fig. 12.7. The log-log plot shows the numbers of observed/predicted triggers for different classes of days, separated by the magnitude of hazard predicted for them (in multiples of background hazard). The Poissonian model underpredicts for all forecast hazard levels, and the new model overpredicts on the days for which it adds hazard. By construction, the Poissonian model is progressively worse on days with greater forecast hazard. In contrast, the total hazard predicts the same order of magnitude of trigger numbers as the data, for all hazard levels. Therefore, it appears to be a reasonably good average prediction tool.

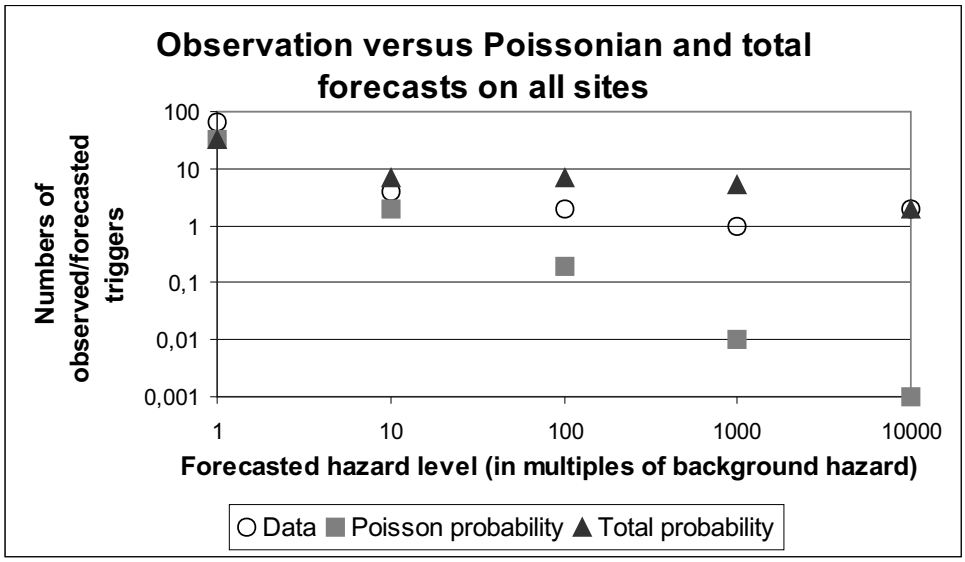

Figure 12.7: Numbers of observed versus predicted triggers on different hazard levels. The unit for the x-axis is multiples of the background hazard (hazard has been rounded on a logarithmic scale, see text).

Assuming that the chances of any particular trigger falling into any of the hazard levels is independent, the Poisson distribution can be used to calculate the significance of the forecast versus the observed numbers of triggers. The Poisson distribution for the forecast number of events is presented in the form of the probability that a particular value for the number of triggers should be observed (Figures 12.8 to 12.10), i.e. if the forecast was right, how likely would any particular observation be? The actual numbers of triggers are shown on the same diagram. For instance, in Figure 12.8, for the Poissonian background forecast level of 34, there is a 0.07 (7%) probability that exactly 34 triggers will be observed, 4% chance that 40 triggers would be observed, etc. The three markers show the real observations of all triggers (74), triggers that occurred on days of less than 1.5 times the background hazard (65), and non-aftershock triggers that occurred on days of pure background hazard (49). None of the observations is close to the centre of the distribution: there is a 0.005 (0.5%) probability that 49 triggers would be observed, and the observed number of 74 triggers is much higher than would be predicted from the straight Poissonian model.

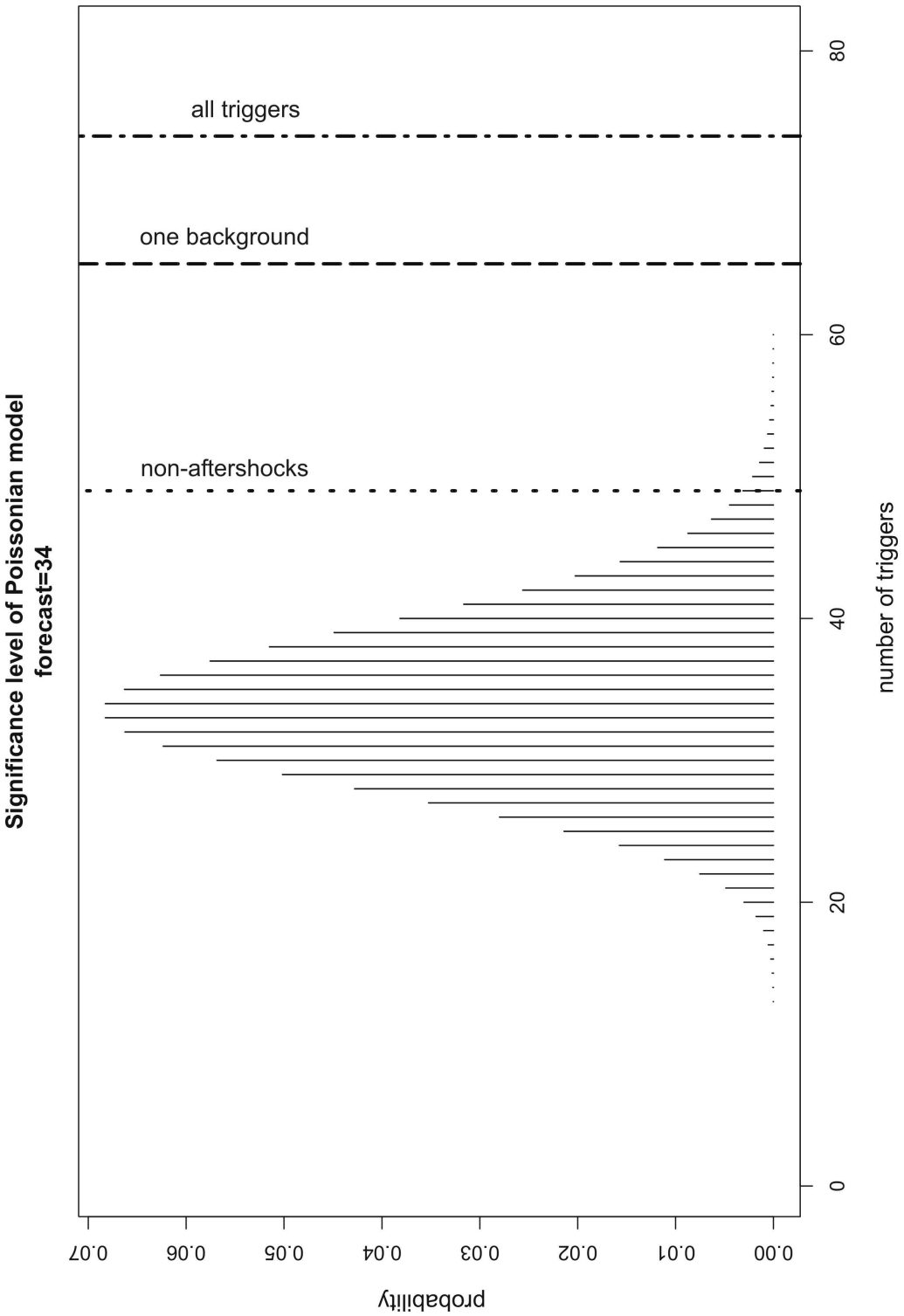

Figure 12.8: Poisson probability distribution for forecast number of 34 triggers (Poissonian background model). Markers show how many triggers have been observed: "non-aftershock" triggers being triggers observed on days of pure background hazard, "one background" triggers having occurred on days of < 1.5 times the background hazard.

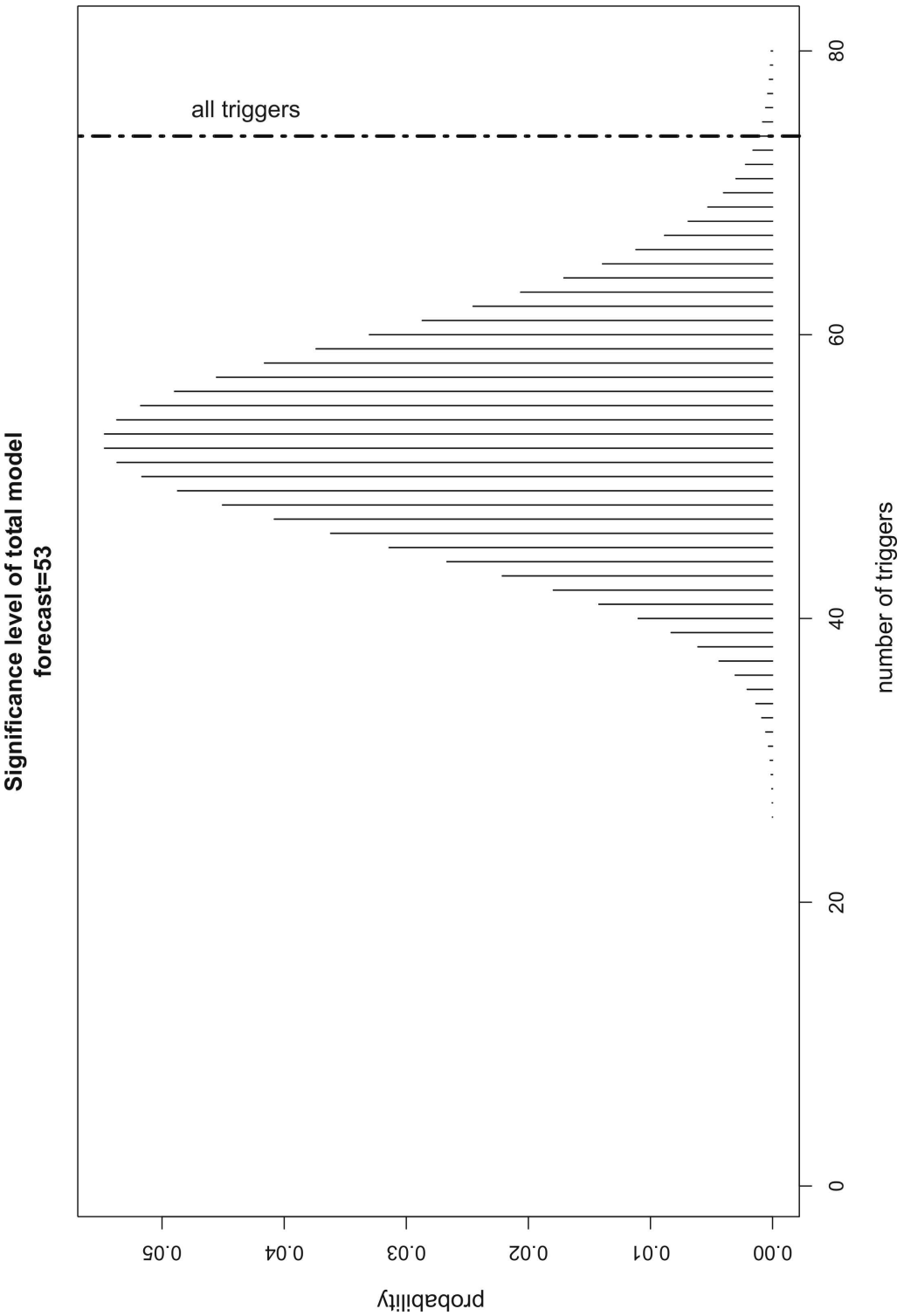

Figure 12.9: Poisson probability distribution for forecast number of 53 triggers (total model). Marker shows how many triggers have been observed.

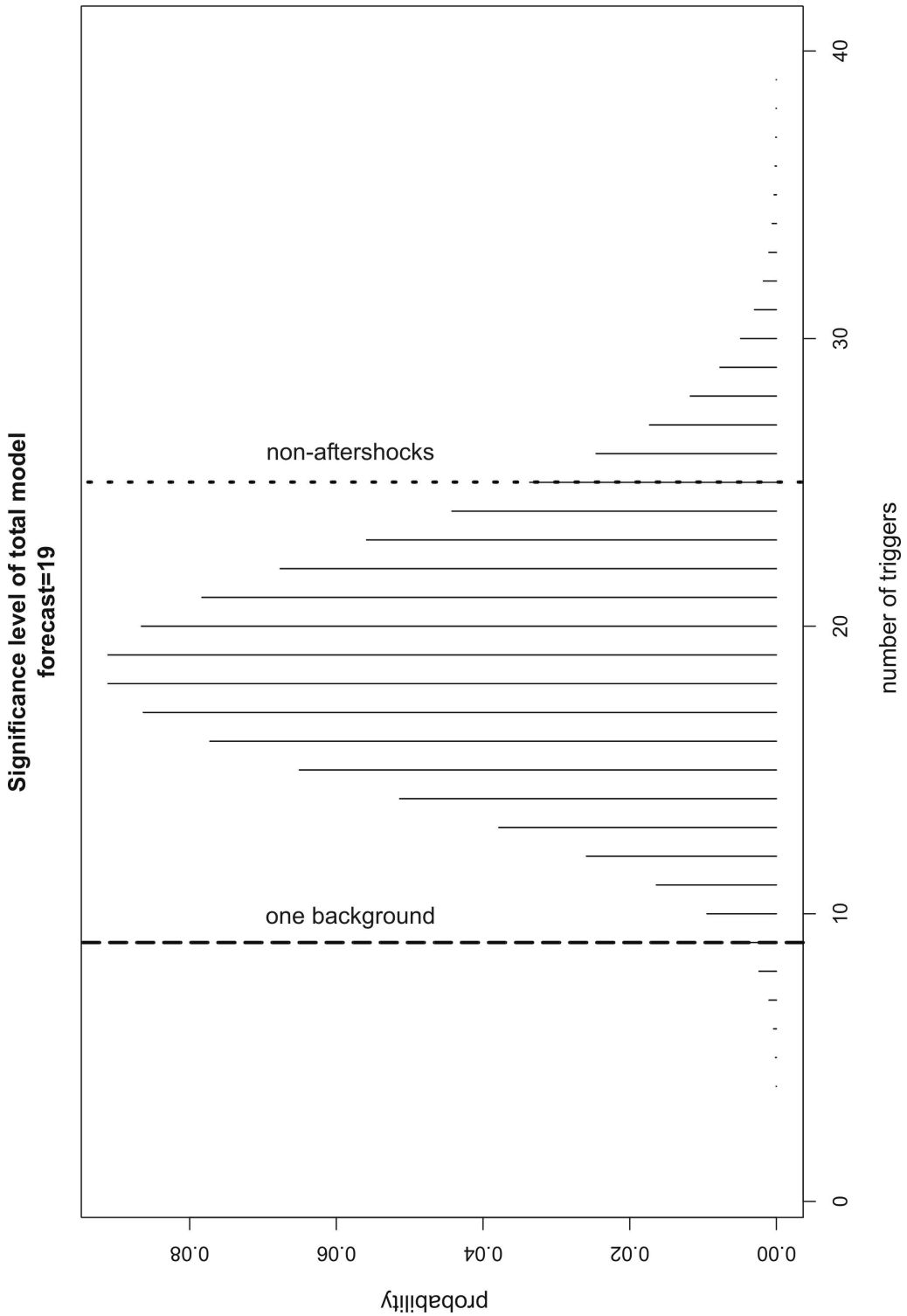

Figure 12.10: Poisson probability distribution for forecast number of 19 triggers (foreshock/aftershock model). Markers show how many triggers have been observed: "non-aftershock" triggers being triggers observed on days of pure background hazard, "one background" triggers having occurred on days of < 1.5 times the background hazard.

Sites	Model	Forecast	Observation	Probability	σ level	99.9% confidence level
	Poissonian	34 (total)	74 (all triggers)	$0.0027 * 10^{-10}$	6.9σ	significant
A	Poissonian	34 (total)	65 ($< 1.5 * B$ triggers)	$7.5349 * 10^{-10}$	5.3σ	significant
L	Poissonian	34 (total)	49 (pure background triggers)	0.006	2.6σ	not significant
L	Total	53 (total)	74 (all triggers)	0.0025	2.9σ	not significant
	Total	19 (additional)	9 ($\geq 1.5 * B$ triggers)	0.0089	2.3σ	not significant
	Total	19 (additional)	25 (>background triggers)	0.1067	1.1σ	not significant
	Poissonian	25 (total)	47 (all triggers)	$2.8278 * 10^{-5}$	4.4σ	significant
H	Poissonian	25 (total)	42 ($< 1.5 * B$ triggers)	0.0007	3.4σ	significant
I	Poissonian	25 (total)	31 (pure background triggers)	0.1001	1.2σ	not significant
G	Total	38 (total)	47 (all triggers)	0.0657	1.5σ	not significant
H	Total	13 (additional)	5 ($\geq 1.5 * B$ triggers)	0.0107	2.2σ	not significant
	Total	19 (additional)	16 (>background triggers)	0.1645	0.7σ	not significant
	Poissonian	8 (total)	27 (all triggers)	$2.9256 * 10^{-8}$	6.7σ	significant
L	Poissonian	8 (total)	23 ($< 1.5 * B$ triggers)	$3.7255 * 10^{-6}$	5.3σ	significant
O	Poissonian	8 (total)	18 (pure background triggers)	0.0007	3.5σ	significant
W	Total	15 (total)	27 (all triggers)	0.0025	3.1σ	not significant
	Total	7 (additional)	9 ($\geq 1.5 * B$ triggers)	0.1695	0.8σ	not significant
	Total	7 (additional)	4 (>background triggers)	0.173	1.1σ	not significant

Table 12.5: Significance levels of forecasts, probabilities of observing the actual numbers of triggers given the models' forecasts. 'High' and 'low' refer to the two sets of strong motion stations in high and low Poissonian background hazard locations (>0.3g and $\leq$0.3g with 10% in 50yrs, respectively)

Similarly, the 65 triggers that occurred on days on which the hazard was less than 1.5 times background is higher than expected from the pure Poissonian model (see Table 12.5 for more details). For the total model, which predicted 53 events, there is a 0.25% probability that the observed 74 triggers would have occurred by chance (Fig. 12.9). Finally, if we consider only the 19 triggers (53-34=19) expected on days when hazard above background was predicted, the observed numbers of 25 events (74-49=25), with 9 (74-65=9) occurring on days when the hazard was less than or equal to 1.5 times the background, are reasonably consistent with the model (Fig. 12.10). The number of 25 observed versus 19 predicted triggers for days of no pure background hazard has a probability of about 11%, which is 1.1σ and the best result achieved by the models.

Table 12.5 lists, for all forecasts of the three different sets of stations, the probability of observing the real number of triggers and states whether the discrepancy is significant on a 99.9% confidence level.

Dividing the set of strong motion stations into two subsets, those on high hazard sites and those on low hazard sites, showed that the Poissonian model's problem of underpredicting the numbers of background triggers is a general problem, not restricted to either set. It suggests that the model is doing a little worse for low hazard sites: on those stations it only forecasts about one third of the triggers, while it captures nearly half of the observations on the high hazard sites. This result might be biased by the numbers of stations in each subset (about one third in the low hazard areas, two thirds in the high hazard areas).

As the test result is similarly poor on both subsets, one can conclude that the overall outcome is not biased by a few stations with extreme site conditions. If non-standard site conditions are the reason for the general misprediction, then they are more or less evenly distributed over the two subsets.

The diagram in Figure 12.11 shows a cartoon of the forecast and observed trigger distribution for three cases: days of pure background hazard, days of hazard increases

that are greater than 1.5 times background ('high hazard = peak'), and days of hazard increase in between background and 1.5 times background ('medium hazard = tail'). The dynamic hazard model yields 5% of the time with high hazard (shown as the body of the peak in Fig. 12.11), 16% of days with medium hazard (shown as the tail of the peak), and 79% of days with pure background hazard (horizontal background line). For pure background days, the Poissonian model predicts 25 triggers, while 49 have been observed. For "tail" days, the Poissonian hazard model forecasts 6 events, the total model 7, and 16 were observed. During peak times the Dynamic Model's forecast is 21, 2 of which have been produced by the Poissonian Model's influence during that time. 9 triggers were actually recorded on those days.

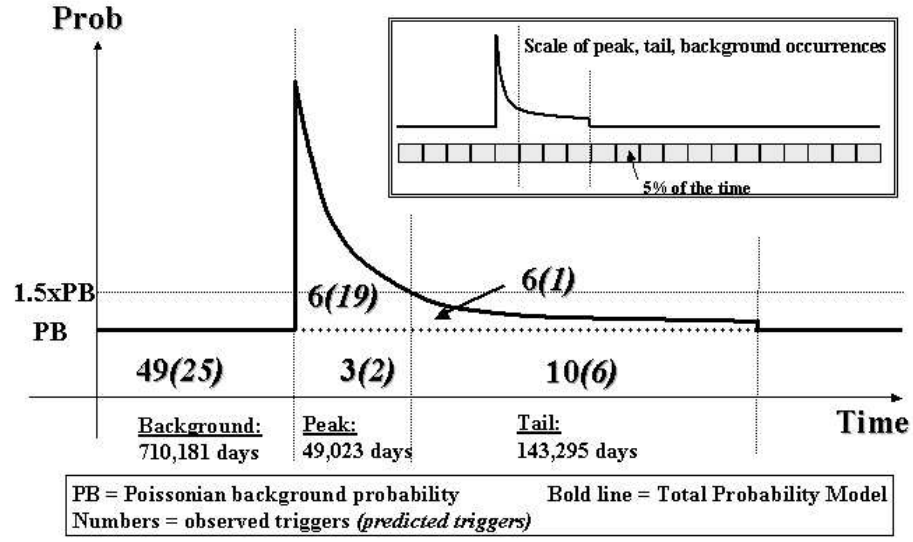

Figure 12.11: Cartoon comparing forecasts and observations for background, low hazard and high hazard days. See text for further explanation of the numbers.

These pairs of numbers are of some concern: great underprediction on background days, huge overprediction in the peak period and a strong underprediction again at tail

times.

To try to understand the trigger data better, the relative fractions of time of the peak and tail compared to the background allows one to calculate the expected number of background events during peak and tail times based on the observations during background time. Neglecting the peak times for a moment, the total time would be tail days plus background days. The percentage of tail days calculates to 17% of the time, the background 83%. This and the number of known background triggers during background times can be used to calculate how many background events are expected to have happened during the tail times:

$$\frac{tail}{background} = \frac{17}{83} = \frac{N_{expected}}{49} \tag{12.6}$$

$$N_{expected} = 10 \tag{12.7}$$

The same method predicts 3 background triggers during peak times. That leaves only 6 of the 9 events during highly increased hazard times to actually be aftershock related, compared to 19 forecast by the model. At the same time, the model only predicts one trigger during tail times, but 6 non-background events have been recorded. Thus there is an imbalance between over and underprediction in the Dynamic Seismic Hazard model that looks much like a problem with the decay function: too high in the beginning, too low in the end. But aftershock decay in time at least is very well established to follow the Omori decay of 1/time. Varying the lengths and dimensions of the total time and space windows for the aftershock model would influence the results shown in Fig. 12.11. The windows used in the model were assumed to be on the high end of reasonable windows, especially in space (see discussion in Section 5.2.1). But decreasing the radii would increase the maximum values in the centre and probably change the forecasts as shown in the cartoon in the wrong direction. If one would replace the unusual results obtained for foreshock probability decay in time and space in New Zealand with the Californian relationships (see Chapter 3.5), one would decrease

the exponents, i.e. slow the decay and increase the number of expected triggers in the first few days. This would be the opposite effect to the one needed. On the other hand, slowing the decay would increase the number of predicted events in the medium hazard tail, which would be closer to the data.

To understand the causes for the misprediction in the Dynamic Model it will be necessary to separate foreshock and aftershock related hazard forecasts and do a similar analysis with each set in the future.

The Poissonian model on the other hand seems to consistently underpredict by a factor of approximately 2, which has to originate in the modelled seismicity rates.

A likely candidate for causing wrong seismicity rate forecasts in the Poissonian model would be the choice of declustering algorithm. Background hazard is calculated from a declustered catalogue. Should the decluster algorithm remove too many non-aftershock earthquakes, the Poissonian rate will be too low. Additionally, if the declustering removed more aftershocks than the dynamic model is putting back in, the total number of predicted events will consistently be less than the total number of observed events. A rough comparison of the number of events removed by the Reasenberg decluster algorithm (1291 out of 3188 in the raw catalogue of crustal events with $M \geq 4$) with the number of triggered events put back by the Dynamic Seismic Hazard Model (960) confirms this kind of problem: an over-removing/underpredicting by a quarter.

Other possible reasons for the wrong forecasts could be errors in the fault parameters in the geological database that is used in the calculations for the Poissonian model.

12.5 Conclusion

With the ground motion tests I showed that the Poissonian model for the low acceleration threshold of 0.05g in the last 40 years on the locations of easily accessible strong motion records underestimated the hazard by a factor of 2. This does not mean, however, that the model during either the same time period looking at stronger ground motions, or with the same acceleration level looking at longer or different time periods,

would necessarily mispredict in the same manner.

The Dynamic Seismic Hazard Model developed in the course of this thesis has been found to increase the total hazard by approximately 36% and therefore seemingly compensate parts of the Poissonian underprediction. Analysis of the temporal distribution of hazard increase versus trigger occurrence showed, however, that the model is overpredicting for high hazard times (i.e. shortly after events) and underpredicting during low hazard times (i.e. in the tail of the increase functions, long after events).

This analysis shows the need for further research to investigate the possibility of problems in the Poissonian model as well as to determine more successful short term hazard forecast models (see "Recommendations for further work").

Recommendations for Further Work

This study has touched many aspects of seismic hazard analysis, but could not investigate all questions worthy of being answered. In this remark I summarise what I consider important additional work to further the process of successful short term seismic hazard analysis in New Zealand.

Foreshock Model

My analysis of spatial and temporal foreshock probability decay was done on bins of single days and 10km spacing. Comparable studies for California have used a finer hourly and 1km spacing scale. I suspect that the application of that scale to New Zealand data will be limited by the relatively small amount of data, but it should be tried nevertheless to confirm the difference in parameters between New Zealand and California foreshock data as observed in this study.

The foreshock model presented in this thesis did not investigate any depth dependence between foreshock-mainshock pairs, neither did it study intermediate and deep earthquakes (earlier studies found major differences in foreshock behaviour of shallow earthquakes), nor did it analyse whether foreshock-mainshock pairs are usually events very close in depth or whether the triggering process works over large vertical distances, too. If the pairs are not well constrained in depth, the question whether a model could describe the depth distribution of mainshocks following foreshocks would be very helpful to refine the hazard calculation (e.g. predominantly up dip triggering?). Currently the hazard model assumes that foreshocks will only trigger in the same depth layer, which is either 10 to 20 km or 20 to 40 km. This is probably an oversimplification.

A worthwhile study would be an analysis of the effects of earthquake clusters, e.g. probabilities for triplets or quadruples to occur instead of pairs.

Aftershock Model

The aftershock model used in this study is a rough approach, as limited information about New Zealand aftershock probabilities is available at this time. A detailed study of spatial aftershock probability behaviour with increasing distance from the mainshock

(3D) and possible parameter changes for different seismotectonic zones would be very valuable.

Short Term Hazard Calculation

The short term hazard calculation itself is currently limited by two factors:

The calculations of one day hazard are set up to be updating only once every 24 hours. Most earthquake triggering phenomena evolve rapidly with time. For example, foreshock-mainshock pairs are often only a few minutes apart and are rarely more than a few hours apart. Thus they change the hazard while the map is showing a constant state for 24 hours. If this or other models should be developed to a state that they might be considered to be published on a web page, the 24 hour calculations would need to be updated every hour to provide a better time resolution of hazard evolvement during foreshock and aftershock sequences.

The second factor that very much limits the quality of hazard forecasts at the moment is the fact that the attenuation model only allows one to consider earthquakes of magnitude 5.25 or more to contribute to the hazard. Many smaller earthquakes are found to produce ground motions of 0.05g, too. Although they are less hazardous as they have shorter durations, they should be included into the hazard calculations down to magnitude 4, if only to increase the set of triggers usable for the ground motion test. This would require a new or additional attenuation model for small magnitude earthquakes, i.e. magnitudes 4 to 5.25. It might be worthwhile considering a new attenuation model to calculate not the maximum of two horizontal components but the vector sum of the two horizontal components at least, possibly even including the vertical component and therewith actually forecasting the total peak ground accelerations for each point.

Testing Short Term Time Dependent Hazard Models

The methodology and results of ground motion tests of short term seismic hazard forecasts as described in this thesis show the importance of this kind of test. The results

are still limited by the small amount of data. One way to enlarge the dataset would follow up the suggestion made for improvement of the hazard model itself: including smaller magnitudes into forecasts and tests. Many triggers of 0.05g were caused by earthquakes between magnitudes 4 and 5.25 and had to be removed for this test. It would be good to be able to use them in a similar procedure.

A second way to increase the test data is to expand the ground motion dataset by including recordings from the new Etna network installed by GeoNet over the last five years. This would increase the number of recordings, especially improving the regional coverage, but would not increase the total time span. This is obviously a fault that reduces every day, and as there is no more information accessible further back in time, the only way to increase the length of the seismicity data set and ground motion recordings for New Zealand, is to wait. As this is a long term problem it might be more attractive to perform ground motion data tests for other regions, e.g. for California. California is covered by a very dense network of seismometers and models have been developed that forecast daily hazard, e.g. the STEP model. It should be possible without great effort to analyse those data in a similar manner to the New Zealand ones.

If enough data is available, an important modification to the ground motion test suggested by this study is to calculate forecasts for various levels of peak ground acceleration and test them separately. That would investigate whether the model performs differently for different hazard levels.

Bibliography

[1] D.C. Agnew and L.M. Jones. Prediction Probabilities from Foreshocks. *Journal of Geophysical Research*, Vol. 96 (No. B7): pp. 11959–11971, July 1991.

[2] J.G. Anderson et al. Seismicity in the Western Great Basin Apparently Triggered by Landers, California, Earthquake, 28 June 1992. *Bulletin of the Seismological Society of America*, Vol. 84(3): pp. 863–891, 1994.

[3] K.R. Berryman and S. Beanland. The Rate of Tectonic Movement in New Zealand from Geological Evidence. *Transactions of the Institute of Professional Engineering, New Zealand*, Vol. 15: pp. 25–35, 1988.

[4] J. Bowman and C. Kisslinger. A Test of Foreshock Occurrence in the Aleutian Arc. *Bulletin of the Seismological Society of America*, Vol. 74: pp. 181–198, 1984.

[5] E. Brodsky, V. Karakostas, and H. Kanamori. A New Observation of Dynamically Triggered Regional Seismicity: Earthquakes in Greece Following the August, 1999 Izmit, Turkey Earthquake. *Geophysical Research Letters*, Vol. 27: pp. 2741–2744, 2000.

[6] J.N. Brune. Precariously Balanced Rocks and Ground-Motion Maps for Southern California. *Bulletin of the Seismological Society of America*, Vol. 86(No. 1A): pp. 43–54, 1996.

[7] T. Cao et al. The Revised 2002 California Probabilistic Seismic Hazard Maps. Revision, California Geological Survey, June 2003.

[8] A. Christophersen. *The Probability of a Damaging Earthquake Following a Damaging Earthquake.* PhD thesis, Victoria University of Wellington, 2000.

[9] C.A. Cornell. Engineering Seismic Risk Analysis. *Bulletin of the Seismological Society of America*, Vol. 58: pp. 1583–1606, 1968.

[10] J.H Dieterich and B. Kilgore. Implications of Fault Constitutive Properties for Earthquake Prediction. *Proceedings of the National Academy of Sciences USA*, Vol. 93: pp. 3787–3794, 1996.

[11] D. Eberhart-Phillips. Aftershock Sequence Parameters in New Zealand. *Bulletin of the Seismological Society of America*, Vol. 88 (No. 4): pp. 1095–1097, August 1998.

[12] E.H. Field. Probabilistic Seismic Hazard Analysis (PSHA). A Primer. http://www.relm.org/tutorial_materials.

[13] A.D. Frankel. Mapping Seismic Hazard in the Central and Eastern United States. *Seismological Research Letters*, Vol. 66: pp. 8–21, 1995.

[14] A.D. Frankel et al. Documentation for the 2002 Update of the National Seismic Hazard Maps. Open-file Report 02-420, US Geological Survey, 2002.

[15] J. Gardner and L. Knopoff. Is the Sequence of Earthquakes in Southern California, with Aftershocks Removed, Poissonian? *Bulletin of the Seismological Society of America*, Vol. 64 (No. 5): pp. 1363–1367, 1974.

[16] M. Gerstenberger. *Earthquake Clustering and Time-Dependent Probabilistic Seismic Hazard Analysis for California.* PhD thesis, Swiss Federal Institute of Technology, 2003.

[17] M. Gerstenberger, S. Wiemer, L.M. Jones, and P. Reasenberg. Realtime Forecasts of Tomorrow's Earthquakes in California. will be submitted to *Science*, July 2003.

[18] J. Gomberg et al. Earthquake Triggering by Seismic Waves Following the Landers and Hector Mine Earthquakes. *Nature*, Vol. 411: pp. 462–466, 2001.

[19] B. Gutenberg and C.F. Richter. Frequency of Earthquakes in California. *Bulletin of the Seismological Society of America*, Vol. 34: pp. 185–188, 1944.

[20] J.L. Hardebeck. Stress Triggering and Earthquake Probability Estimates. *Journal of Geophysical Research*, Vol. 109, 2004.

[21] R.A. Harris. Earthquake Stress Trigger, Stress Shadows, and Seismic Hazard. *Current Science*, Vol. 79(No. 9): pp. 1215–1225, 2000.

[22] S.C. Jaumé. Stress Transfer, Dynamic Triggering, and Stress Correlations: How Earthquake Occurrence Affects the Timing and Slip of Subsequent Earthquakes. *ACES Inaugural Workshop Proceedings*, 1999.

[23] H. Jeffreys. Aftershocks and Periodicity in Earthquakes. *Gerlands Beitr. Geophys.*, Vol. 56: pp. 111–139, 1938.

[24] L.M. Jones. Foreshocks (1966-1980) in the San Andreas System, California. *Bulletin of the Seismological Society of America*, Vol. 74: pp. 1361–1380, 1984.

[25] L.M. Jones. Foreshocks and Time-Dependent Earthquake Hazard Assessment in Southern California. *Bulletin of the Seismological Society of America*, Vol. 75 (No. 6): pp. 1669–1679, December 1985.

[26] L.M. Jones, R. Console, F. Di Luccio, et al. Are Foreshocks Mainshocks Whose Aftershocks Happen to Be Big? in press *Bulletin of the Seismological Society of America*, February 1999.

[27] Y.Y. Kagan and D.D. Jackson. Seismic Gap Hypothesis: Ten Years After. *Journal of Geophysical Research*, Vol. 96: pp. 419–21,431, 1991.

[28] G.H. McVerry. Comparison of Remote Site and Basement Records as Excitation of the Vogel Building. *Bulletin of the New Zealand National Society for Earthquake Engineering*, Vol. 17(No. 1): pp. 3–14, 1984.

[29] G.H. McVerry et al. Crustal and Subduction Zones Attenuation Relations for New Zealand Earthquakes. In *Proceedings of the 12th World Conference of Earthquake Engineering 2000, Auckland, New Zealand*, 2000.

[30] A. Mendenhall, D.D. Wackerly, and R. L. Scheaffer. *Mathematical Statistics with Applications*. Duxbury Press, Belmont, California, fourth edition, 1994.

[31] A. Merrifield. An Examination of Prospective Foreshock Probabilities in New Zealand. Thesis, Master of Science, Victoria University of Wellington, July 2000.

[32] A. Merrifield, M.K. Savage, and D. Vere-Jones. Geographical Distributions of Prospective Foreshock Probabilities in New Zealand. *New Zealand Journal of Geology and Geophysics*, Vol. 47: pp. 327–339, 2004.

[33] K. Mogi. Relationship between the Occurrence of Great Earthquakes and Tectonic Structure. *Bulletin of the Earthquake Research Intitute, Tokyo University*, Vol. 47: pp. 429–451, 1969.

[34] H. Motulsky and A. Christopoulus. *Fitting Models to Biological Data Using Linear and Nonlinear Regression. A Practical Guide to Curve Fitting.* GraphPad Software, Inc., San Diego, California, 4.0 edition, 2003.

[35] Y. Ogata, T. Utsu, and K. Katsura. Statistical Features of Foreshocks in Comparison with other Earthquake Clusters. *Geophysical Journal International*, Vol. 121: pp. 233–254, 1995.

[36] F. Omori. On After-Shocks. *Rep. Imp. Earthq. Inv. Com.*, Vol. 2: pp. 103–138, 1894. (in Japanese).

[37] F. Omori. On After-Shocks of Earthquakes. *J. Coll. Sci. Imp. Univ. Tokyo*, Vol. 7: pp. 111–200, 1894.

[38] F. Omori. Note on the After-Shocks of the Mino-Owari Earthquake of Oct. 28th, 1891. *Pub. Imp. Earthq. Inv. Com.*, Vol. 7: pp. 27–51, 1902.

[39] B.C. Papazachos. Foreshocks and Earthquake Prediction. *Tectonophysics*, Vol. 28: pp. 213–226, 1975.

[40] T. Parsons. Global Omori Law Decay of Triggered Earthquakes: Large Aftershocks Outside the Classical Aftershock Zone. *Journal of Geophysical Research*, Vol. 107(No. B9): pp. 2199–2219, 2002.

[41] M. D. Petersen et al. Probabilistic Seismic Hazard Assessment for the State of California. Open-file Report 96-08/96-706, California Department of Conservation & US Geological Survey, 1996.

[42] P. A. Reasenberg and L. M. Jones. Earthquake Hazard after a Mainshock in California. *Science*, Vol. 243: pp. 1173–1176, 1989.

[43] P.A. Reasenberg. Second-Order Moment of Central California Seismicity, 1969-1982. *Journal of Geophysical Research*, Vol. 90 (No. B7): pp. 5479–5495, 1985.

[44] P.A. Reasenberg. Foreshock Occurrence before Large Earthquakes. *Journal of Geophysical Research*, Vol. 104 (No. B3): pp. 4755–4768, March 1999.

[45] P.A. Reasenberg and L.M. Jones. Earthquake Aftershocks: Update. *Science*, Vol. 265: pp. 1251–1252, 1994.

[46] C.F. Richter. *Elementary Seismology.* W. H Freeman and Company, 1958.

[47] T. Rudolf. Dynamic Seismic Hazard Model for New Zealand. Thesis, Graduate Diploma of Science, Victoria University of Wellington, December 2003.

[48] M. Salmon, S. Bannister, M.K. Savage, et al. Seismic Attenuation in the Central North Island, New Zealand. *Poster at 2002 Western Pacific Geophysics Meeting*, 2002.

[49] M.K. Savage and D.M. DePolo. Foreshock Probabilities in the Western Great-Basin Eastern Sierra Nevada. *Bulletin of the Seismological Society of America*, Vol. 83 (No. 6): pp. 1910–1938, December 1993.

[50] M.K. Savage and S.H. Rupp. Foreshock Probabilities in New Zealand. *New Zealand Journal of Geology and Geophysics*, Vol. 43: pp. 461–469, 2000.

[51] D.P. Schwartz and K.J. Coppersmith. Fault Behaviour and Characteristic Earthquakes: Examples from the Wasatch and San Andreas Faults. *Journal of Geophysical Research*, Vol. 89: pp. 5873–5890, 1984.

[52] S. Sherburn. Characteristics of Earthquake Sequences in the Central Volcanic Region, New Zealand. *New Zealand Journal of Geology and Geophysics*, Vol. 35: pp. 57–68, 1992.

[53] S.K. Singh and Suarez. Regional Variation in the Number of Aftershocks ($m_b \geq 5$) of Large, Subduction-Zone Earthquakes ($m_w \geq 7.0$). *Bulletin of the Seismological Society of America*, Vol. 78(1): pp. 230–242, 1988.

[54] E.G.C. Smith. Foreshocks of Shallow New Zealand Earthquakes. *New Zealand Journal of Geology and Geophysics*, Vol. 24: pp. 579–584, November 1981.

[55] E.G.C. Smith and T.H. Webb. The Seismicity and Related Deformation of the Central Volcanic Region, North Island, New Zealand. *Royal Society of New Zealand Bulletin*, Vol. 23: pp. 112–133, 1986.

[56] R.S. Stein. The Role of Stress Transfer in Earthquake Occurrence. *Nature*, Vol. 402: pp. 605–609, 1999.

[57] M.W. Stirling and R. Anooshehpoor. Use of Precariously-Balanced Rocks to Test the New Zealand Seismic Hazard Model: A Pilot Study. Client Report 2004/158, Institute of Geological & Nuclear Sciences, November 2004.

[58] M.W. Stirling, G.H. McVerry, and K.R. Berryman. A New Seismic Hazard Model for New Zealand. *Bulletin of the Seismological Society of America*, Vol. 92 (No. 5): pp. 1878–1903, June 2002.

[59] M.W. Stirling, G.H. McVerry, K.R. Berryman, et al. Probabilistic Seismic Hazard Assessment of New Zealand: New Active Fault Data, Seismicity Data, Attenuation

Relationships, and Methods. Client Report 2000/53, Institute of Geological & Nuclear Sciences, May 2000.

[60] M.W. Stirling, S.G. Wesnousky, and K.R. Berryman. Probabilistic Seismic Hazard Analysis of New Zealand. *New Zealand Journal of Geology and Geophysics*, Vol. 41: pp. 355–375, 1998.

[61] T. Utsu, Y. Ogata, and R.S. Matsu'ura. The Centenary of the Omori Formula for a Decay Law of Aftershock Activity. *Journal of the Physics of the Earth*, Vol. 43: pp. 1–33, 1995.

[62] D. Vere-Jones, S. Turnovsky, and G. Eiby. A Statistical Survey of Earthquakes in the Main Seismic Region of New Zealand. *New Zealand Journal of Geology and Geophysics*, Vol. 7: pp. 722–744, 1964 .

[63] C. Voisin, F. Cotton, and S. Di Carli. A Unified Model for Dynamic and Static Stress Triggering of Aftershocks, Antishocks, Remote Seismicity, Creep Events, and Multisegmented Rupture. *Journal of Geophysical Research*, Vol. 109, 2004.

[64] D.J. Wald and T.H. Heaton. Spatial and Temporal Distribution of Slip for the 1992 Landers, California, Earthquake. *Bulletin of the Seismological Society of America*, Vol. 84: pp. 668–691, 1994.

[65] D.L. Wells and K.J. Coppersmith. New Empirical Relationships Among Magnitude, Rupture Length, Rupture Width, Rupture Area, and Surface Displacement. *Bulletin of the Seismological Society of America*, Vol. 84(4): pp. 974–1002, 1994.

[66] S.G. Wesnousky. Earthquakes, Quaternary Faults, and Seismic Hazard in California. *Journal of Geophysical Research*, Vol. 91: pp. 12587–12631, 1986.

[67] Y. Yamanaka and K. Shimazaki. Scaling Relationship Between the Number of Aftershocks and the Size of the Mainshock. *Journal of the Physics of the Earth*, Vol. 38: pp. 305–324, 1990.

[68] J.X. Zhao. Estimating Kinematic Interaction of Raft Foundations from Earthquake Records and its Effects on Structural Response. *Soil Dynamics and Earthquake Engineering*, Vol. 17: pp. 73–88, 1998.

Appendix A

Foreshock probability model

A1. Lookup tables for New Zealand foreshock probabilities (Non-TVZ)

A2. Lookup tables for New Zealand foreshock probabilities (TVZ)

Non-TVZ	$1^{st}day$	2^{nd} day	3^{rd} day	4^{th} day	5^{th} day
0-10 km	0.021	0.004	0.0015	0.0021	0.0009
	± 0.002	± 0.001	± 0.0007	± 0.0008	± 0.0005
10-20 km	0.008	0.0018	0.0012	0.00002	0.0012
	± 0.002	± 0.0008	± 0.0006	± 0.00007	± 0.0006
20-30 km	0.007	0.0021	0.0015	0.0012	0.0009
	± 0.001	± 0.0008	± 0.0007	± 0.0006	± 0.0005
30-40 km	0.0021	0.0006	0.00002	0.0003	0.0009
	± 0.0008	± 0.0004	± 0.00007	± 0.0003	± 0.0005
40-50 km	0.0018	0.0018	0.0021	0.0024	0.0009
	± 0.0008	± 0.0008	± 0.0008	± 0.0009	± 0.0005

Table A.1: Foreshock probabilities for all foreshock mainshock pairs (Non-TVZ)

Non-TVZ	$1^{st}day$	2^{nd} day	3^{rd} day	4^{th} day	5^{th} day
0-10 km	0.00458	0.00154	0.00032	0.00062	0.00032
	± 0.00118	± 0.00068	± 0.00031	± 0.00044	± 0.00031
10-20 km	0.00184	0.00062	0.00062	0.00002	0.00002
	± 0.00075	± 0.00044	± 0.00044	± 0.00007	± 0.00007
20-30 km	0.00214	0.00123	0.00062	0.00032	0.00002
	± 0.00081	± 0.00061	± 0.00044	± 0.00031	± 0.00007
30-40 km	0.00123	0.00002	0.00002	0.00002	0.00062
	± 0.00061	± 0.00007	± 0.00007	± 0.00007	± 0.00044
40-50 km	0.00002	0.00032	0.00032	0.00093	0.00062
	± 0.00007	± 0.00031	± 0.00031	± 0.00053	± 0.00044

Table A.2: Foreshock probabilities for foreshock and mainshock of the same magnitude (Non-TVZ)

Non-TVZ	1^{st}*day*	2^{nd} day	3^{rd} day	4^{th} day	5^{th} day
0-10 km	0.004	0.00002	0.0003	0.0003	0.0003
	± 0.001	± 0.00007	± 0.0003	± 0.0003	± 0.0003
10-20 km	0.0012	0.0003	0.00002	0.00002	0.0003
	± 0.0006	± 0.0003	± 0.00007	± 0.00007	± 0.0003
20-30 km	0.0018	0.00002	0.00002	0.00002	0.00002
	± 0.0008	± 0.00007	± 0.00007	± 0.00007	± 0.00007
30-40 km	0.00002	0.0003	0.00002	0.00002	0.00002
	± 0.00007	± 0.0003	± 0.00007	± 0.00007	± 0.00007
40-50 km	0.00002	0.0006	0.0003	0.0009	0.00002
	± 0.00007	± 0.0004	± 0.0003	± 0.0005	± 0.00007

Table A.3: Foreshock probabilities for foreshock and mainshock 0.1 magnitudes apart (Non-TVZ)

Non-TVZ	1^{st}*day*	2^{nd} day	3^{rd} day	4^{th} day	5^{th} day
0-10 km	0.004	0.0009	0.0003	0.0012	0.0003
	± 0.001	± 0.0005	± 0.0003	± 0.0006	± 0.0003
10-20 km	0.0012	0.00002	0.00002	0.00002	0.0006
	± 0.0006	± 0.00007	± 0.00007	± 0.00007	± 0.0004
20-30 km	0.0012	0.0003	0.0003	0.0003	0.0003
	± 0.0006	± 0.0003	± 0.0003	± 0.0003	± 0.0003
30-40 km	0.0003	0.00002	0.00002	0.00002	0.00002
	± 0.0003	± 0.00007	± 0.00007	± 0.00007	± 0.00007
40-50 km	0.0006	0.00002	0.00002	0.00002	0.0003
	± 0.0004	± 0.00007	± 0.00007	± 0.00007	± 0.0003

Table A.4: Foreshock probabilities for foreshock and mainshock 0.2 magnitudes apart (Non-TVZ)

Non-TVZ	$1^{st}day$	2^{nd} day	3^{rd} day	4^{th} day	5^{th} day
0-10 km	0.0025	0.0003	0.0003	0.00002	0.00002
	± 0.0009	± 0.0003	± 0.0003	± 0.00007	± 0.00007
10-20 km	0.0015	0.00002	0.00032	0.00002	0.0003
	± 0.0007	± 0.00007	± 0.00031	± 0.00007	± 0.0003
20-30 km	0.0009	0.0006	0.00002	0.0003	0.00002
	± 0.0005	± 0.0004	± 0.00007	± 0.0003	± 0.00007
30-40 km	0.0003	0.00002	0.00002	0.00002	0.0003
	± 0.0003	± 0.00007	± 0.00007	± 0.00007	± 0.0003
40-50 km	0.0003	0.0003	0.0006	0.0003	0.00002
	± 0.0003	± 0.0003	± 0.0004	± 0.0003	± 0.00007

Table A.5: Foreshock probabilities for foreshock and mainshock 0.3 magnitudes apart (Non-TVZ)

Non-TVZ	$1^{st}day$	2^{nd} day	3^{rd} day	4^{th} day	5^{th} day
0-10 km	0.0015	0.00002	0.00002	0.00002	0.00002
	± 0.0007	± 0.00007	± 0.00007	± 0.00007	± 0.00007
10-20 km	0.00002	0.00002	0.00002	0.00002	0.00002
	± 0.00007	± 0.00007	± 0.00007	± 0.00007	± 0.00007
20-30 km	0.0003	0.00002	0.00002	0.00002	0.00002
	± 0.0003	± 0.00007	± 0.00007	± 0.00007	± 0.00007
30-40 km	0.00002	0.00002	0.00002	0.00002	0.00002
	± 0.00007	± 0.00007	± 0.00007	± 0.00007	± 0.00007
40-50 km	0.0006	0.00002	0.00002	0.0003	0.00002
	± 0.0004	± 0.00007	± 0.00007	± 0.0003	± 0.00007

Table A.6: Foreshock probabilities for foreshock and mainshock 0.4 magnitudes apart (Non-TVZ)

Non-TVZ	1^{st}*day*	2^{nd} day	3^{rd} day	4^{th} day	5^{th} day
0-10 km	0.0018	0.0003	0.00002	0.00002	0.00002
	± 0.0008	± 0.0003	± 0.00007	± 0.00007	± 0.00007
10-20 km	0.00002	0.00002	0.00002	0.00002	0.00002
	± 0.00007	± 0.00007	± 0.00007	± 0.00007	± 0.00007
20-30 km	0.0003	0.00002	0.00002	0.00002	0.00032
	± 0.0003	± 0.00007	± 0.00007	± 0.00007	± 0.00031
30-40 km	0.00002	0.00002	0.00002	0.00002	0.00002
	± 0.00007	± 0.00007	± 0.00007	± 0.00007	± 0.00007
40-50 km	0.00002	0.00002	0.00002	0.00002	0.00002
	± 0.00007	± 0.00007	± 0.00007	± 0.00007	± 0.00007

Table A.7: Foreshock probabilities for foreshock and mainshock 0.5 magnitudes apart (Non-TVZ)

Non-TVZ	1^{st}*day*	2^{nd} day	3^{rd} day	4^{th} day	5^{th} day
0-10 km	0.00002	0.00002	0.0003	0.00002	0.00002
	± 0.00007	± 0.00007	± 0.0003	± 0.00007	± 0.00007
10-20 km	0.00002	0.00002	0.00002	0.00002	0.00002
	± 0.00007	± 0.00007	± 0.00007	± 0.00007	± 0.00007
20-30 km	0.00002	0.00002	0.00062	0.00002	0.00002
	± 0.00007	± 0.00007	± 0.00044	± 0.00007	± 0.00007
30-40 km	0.00002	0.00002	0.00002	0.00002	0.00002
	± 0.00007	± 0.00007	± 0.00007	± 0.00007	± 0.00007
40-50 km	0.00002	0.00002	0.00002	0.00002	0.00002
	± 0.00007	± 0.00007	± 0.00007	± 0.00007	± 0.00007

Table A.8: Foreshock probabilities for foreshock and mainshock 1.0 magnitudes apart (Non-TVZ)

Non-TVZ	$1^{st}day$	2^{nd} day	3^{rd} day	4^{th} day	5^{th} day
0-10 km	0.0003	0.00002	0.00002	0.00002	0.00002
	± 0.0003	± 0.00007	± 0.00007	± 0.00007	± 0.00007
10-20 km	0.00002	0.00002	0.00002	0.00002	0.00002
	± 0.00007	± 0.00007	± 0.00007	± 0.00007	± 0.00007
20-30 km	0.0003	0.00002	0.00002	0.00002	0.00002
	± 0.0003	± 0.00007	± 0.00007	± 0.00007	± 0.00007
30-40 km	0.00002	0.00002	0.00002	0.00002	0.00002
	± 0.00007	± 0.00007	± 0.00007	± 0.00007	± 0.00007
40-50 km	0.00002	0.00002	0.00002	0.00002	0.00002
	± 0.00007	± 0.00007	± 0.00007	± 0.00007	± 0.00007

Table A.9: Foreshock probabilities for foreshock and mainshock 1.5 magnitudes apart (Non-TVZ)

Non-TVZ	$1^{st}day$	2^{nd} day	3^{rd} day	4^{th} day	5^{th} day
0-10 km	0.00002	0.00002	0.00002	0.00002	0.00002
	± 0.00007	± 0.00007	± 0.00007	± 0.00007	± 0.00007
10-20 km	0.00002	0.00002	0.00002	0.00002	0.00002
	± 0.00007	± 0.00007	± 0.00007	± 0.00007	± 0.00007
20-30 km	0.00002	0.00002	0.00002	0.00002	0.00002
	± 0.00007	± 0.00007	± 0.00007	± 0.00007	± 0.00007
30-40 km	0.00002	0.00002	0.00002	0.00002	0.00002
	± 0.00007	± 0.00007	± 0.00007	± 0.00007	± 0.00007
40-50 km	0.00002	0.00002	0.00002	0.00002	0.00002
	± 0.00007	± 0.00007	± 0.00007	± 0.00007	± 0.00007

Table A.10: Foreshock probabilities for foreshock and mainshock 2.0 magnitudes apart (Non-TVZ)

TVZ	$1^{st}day$	2^{nd} day	3^{rd} day	4^{th} day	5^{th} day
10-20 km	0.12	0.011	0.011	0.006	0.011
	± 0.02	± 0.008	± 0.008	± 0.005	± 0.008
20-30 km	0.03	0.011	0.0003	0.0003	0.0003
	± 0.01	± 0.008	± 0.001	± 0.001	± 0.001
30-40 km	0.011	0.0003	0.0003	0.006	0.0003
	± 0.008	± 0.001	± 0.001	± 0.005	± 0.001
40-50 km	0.0003	0.0003	0.0003	0.0003	0.006
	± 0.001	± 0.001	± 0.001	± 0.001	± 0.005
40-50 km	0.0003	0.0003	0.0003	0.0003	0.006
	± 0.001	± 0.001	± 0.001	± 0.001	± 0.005

Table A.11: Foreshock probabilities for all foreshock mainshock pairs (TVZ)

TVZ	$1^{st}day$	2^{nd} day	3^{rd} day	4^{th} day	5^{th} day
0-10 km	0.04	0.006	0.0003	0.0003	0.011
	± 0.01	± 0.005	± 0.001	± 0.001	± 0.008
10-20 km	0.006	0.006	0.0003	0.0003	0.0003
	± 0.005	± 0.005	± 0.001	± 0.001	± 0.001
20-30 km	0.006	0.0003	0.0003	0.006	0.0003
	± 0.005	± 0.001	± 0.001	± 0.005	± 0.001
30-40 km	0.0003	0.0003	0.0003	0.0003	0.0003
	± 0.001	± 0.001	± 0.001	± 0.001	± 0.001
40-50 km	0.0003	0.0003	0.0003	0.0003	0.0003
	± 0.001	± 0.001	± 0.001	± 0.001	± 0.001

Table A.12: Foreshock probabilities for foreshock and mainshock of the same magnitude (TVZ)

TVZ	1^{st}*day*	2^{nd} day	3^{rd} day	4^{th} day	5^{th} day
0-10 km	0.02	0.006	0.006	0.0003	0.0003
	± 0.01	± 0.005	± 0.005	± 0.001	± 0.001
10-20 km	0.006	0.0003	0.0003	0.0003	0.0003
	± 0.005	± 0.001	± 0.001	± 0.001	± 0.001
20-30 km	0.0003	0.0003	0.0003	0.0003	0.0003
	± 0.001	± 0.001	± 0.001	± 0.001	± 0.001
30-40 km	0.0003	0.0003	0.0003	0.0003	0.0003
	± 0.001	± 0.001	± 0.001	± 0.001	± 0.001
40-50 km	0.0003	0.0003	0.0003	0.0003	0.0003
	± 0.001	± 0.001	± 0.001	± 0.001	± 0.001

Table A.13: Foreshock probabilities for foreshock and mainshock 0.1 magnitudes apart (TVZ)

TVZ	1^{st}*day*	2^{nd} day	3^{rd} day	4^{th} day	5^{th} day
0-10 km	0.016	0.0003	0.0003	0.0003	0.0003
	± 0.009	± 0.001	± 0.001	± 0.001	± 0.001
10-20 km	0.0003	0.0003	0.0003	0.0003	0.0003
	± 0.001	± 0.001	± 0.001	± 0.001	± 0.001
20-30 km	0.0003	0.0003	0.0003	0.0003	0.0003
	± 0.001	± 0.001	± 0.001	± 0.001	± 0.001
30-40 km	0.0003	0.0003	0.0003	0.0003	0.0003
	± 0.001	± 0.001	± 0.001	± 0.001	± 0.001
40-50 km	0.0003	0.0003	0.0003	0.0003	0.006
	± 0.001	± 0.001	± 0.001	± 0.001	± 0.005

Table A.14: Foreshock probabilities for foreshock and mainshock 0.2 magnitudes apart (TVZ)

TVZ	$1^{st}day$	2^{nd} day	3^{rd} day	4^{th} day	5^{th} day
0-10 km	0.02	0.0003	0.006	0.0003	0.0003
	± 0.01	± 0.001	± 0.005	± 0.001	± 0.001
10-20 km	0.011	0.0003	0.0003	0.0003	0.0003
	± 0.008	± 0.001	± 0.001	± 0.001	± 0.001
20-30 km	0.006	0.0003	0.0003	0.0003	0.0003
	± 0.005	± 0.001	± 0.001	± 0.001	± 0.001
30-40 km	0.0003	0.0003	0.0003	0.0003	0.0003
	± 0.001	± 0.001	± 0.001	± 0.001	± 0.001
40-50 km	0.0003	0.0003	0.0003	0.0003	0.0003
	± 0.001	± 0.001	± 0.001	± 0.001	± 0.001

Table A.15: Foreshock probabilities for foreshock and mainshock 0.3 magnitudes apart (TVZ)

TVZ	$1^{st}day$	2^{nd} day	3^{rd} day	4^{th} day	5^{th} day
0-10 km	0.0003	0.0003	0.0003	0.006	0.0003
	± 0.001	± 0.001	± 0.001	± 0.005	± 0.001
10-20 km	0.0003	0.006	0.0003	0.0003	0.0003
	± 0.001	± 0.005	± 0.001	± 0.001	± 0.001
20-30 km	0.0003	0.0003	0.0003	0.0003	0.0003
	± 0.001	± 0.001	± 0.001	± 0.001	± 0.001
30-40 km	0.0003	0.0003	0.0003	0.0003	0.0003
	± 0.001	± 0.001	± 0.001	± 0.001	± 0.001
40-50 km	0.0003	0.0003	0.0003	0.0003	0.0003
	± 0.001	± 0.001	± 0.001	± 0.001	± 0.001

Table A.16: Foreshock probabilities for foreshock and mainshock 0.4 magnitudes apart (TVZ)

TVZ	1^{st}*day*	2^{nd} day	3^{rd} day	4^{th} day	5^{th} day
0-10 km	0.006	0.0003	0.0003	0.0003	0.0003
	± 0.005	± 0.001	± 0.001	± 0.001	± 0.001
10-20 km	0.006	0.0003	0.0003	0.0003	0.0003
	± 0.005	± 0.001	± 0.001	± 0.001	± 0.001
20-30 km	0.0003	0.0003	0.0003	0.0003	0.0003
	± 0.001	± 0.001	± 0.001	± 0.001	± 0.001
30-40 km	0.0003	0.0003	0.0003	0.0003	0.006
	± 0.001	± 0.001	± 0.001	± 0.001	± 0.005
40-50 km	0.0003	0.0003	0.0003	0.0003	0.0003
	± 0.001	± 0.001	± 0.001	± 0.001	± 0.001

Table A.17: Foreshock probabilities for foreshock and mainshock 0.5 magnitudes apart (TVZ)

TVZ	1^{st}*day*	2^{nd} day	3^{rd} day	4^{th} day	5^{th} day
0-10 km	0.0003	0.0003	0.0003	0.0003	0.0003
	± 0.001	± 0.001	± 0.001	± 0.001	± 0.001
10-20 km	0.0003	0.0003	0.0003	0.0003	0.0003
	± 0.001	± 0.001	± 0.001	± 0.001	± 0.001
20-30 km	0.0003	0.0003	0.0003	0.0003	0.0003
	± 0.001	± 0.001	± 0.001	± 0.001	± 0.001
30-40 km	0.0003	0.0003	0.0003	0.0003	0.0003
	± 0.001	± 0.001	± 0.001	± 0.001	± 0.001
40-50 km	0.0003	0.0003	0.0003	0.0003	0.0003
	± 0.001	± 0.001	± 0.001	± 0.001	± 0.001

Table A.18: Foreshock probabilities for foreshock and mainshock 1.0 magnitudes apart (TVZ)

TVZ	$1^{st}day$	2^{nd} day	3^{rd} day	4^{th} day	5^{th} day
0-10 km	0.0003	0.0003	0.0003	0.0003	0.0003
	± 0.001	± 0.001	± 0.001	± 0.001	± 0.001
10-20 km	0.0003	0.0003	0.0003	0.0003	0.0003
	± 0.001	± 0.001	± 0.001	± 0.001	± 0.001
20-30 km	0.0003	0.0003	0.0003	0.0003	0.0003
	± 0.001	± 0.001	± 0.001	± 0.001	± 0.001
30-40 km	0.0003	0.0003	0.0003	0.0003	0.0003
	± 0.001	± 0.001	± 0.001	± 0.001	± 0.001
40-50 km	0.0003	0.0003	0.0003	0.0003	0.0003
	± 0.001	± 0.001	± 0.001	± 0.001	± 0.001

Table A.19: Foreshock probabilities for foreshock and mainshock 1.5 magnitudes apart (TVZ)

TVZ	$1^{st}day$	2^{nd} day	3^{rd} day	4^{th} day	5^{th} day
0-10 km	0.0003	0.0003	0.0003	0.0003	0.0003
	± 0.001	± 0.001	± 0.001	± 0.001	± 0.001
10-20 km	0.0003	0.0003	0.0003	0.0003	0.0003
	± 0.001	± 0.001	± 0.001	± 0.001	± 0.001
20-30 km	0.0003	0.0003	0.0003	0.0003	0.0003
	± 0.001	± 0.001	± 0.001	± 0.001	± 0.001
30-40 km	0.0003	0.0003	0.0003	0.0003	0.0003
	± 0.001	± 0.001	± 0.001	± 0.001	± 0.001
40-50 km	0.0003	0.0003	0.0003	0.0003	0.0003
	± 0.001	± 0.001	± 0.001	± 0.001	± 0.001

Table A.20: Foreshock probabilities for foreshock and mainshock 2.0 magnitudes apart (TVZ)

Appendix B

Testing Conditional Seismic Hazard Models

B1. List of stations used for the ground motion test

B2. List of triggers used in the ground motion test

B3. Results of the probability class test

B4. Results of the attenuation model test

Table B.1: List of NZ strong motion instruments used for ground motion test

Code	Latitude	Longitude	Start date			End date			Name	Network Station Codes		
T001B2	-36.8530	174.778	1996	05	22	2002	09	03	Auckland University School of Engineering	012A	012B	
T002A1	-39.2012	175.539	1995	09	25	1996	05	26	Chateau Tongariro	013A		
T003A1	-39.5010	176.872	1991	07	30	2002	04	23	Napier Civil Defence	014A		
T004A1	-39.4880	176.892	1991	07	30	1999	07	05	Napier Hospital	015A		
T005A1	-38.6743	178.025	1991	08	01	2002	07	31	Gisborne Kaiti Hill	016A		
T006A1	-38.6675	178.020	1989	08	10	1999	06	17	Gisborne 2ZG	017A		
T007D1	-38.6597	178.022	1974	04	06	2004	08	31	Gisborne Chief Post Office	018A		
T008B2	-38.8052	177.150	1966	01	24	2004	08	31	Tuai Power Station	020A	020B	
T009A1	-38.4228	176.309	1991	09	16	2002	08	02	Reporoa Anchor Dairy Factory	021A		
T010A1	-39.0553	174.071	1969	12	03	2003	07	08	New Plymouth Post Office	024A		
T011A1	-39.5853	174.271	1994	09	19	2002	03	13	Hawera High School	025A		
T012C3	-39.5038	176.892	1966	01	24	1988	04	12	Napier Telephone Exchange Marewa	027A	027C	027D
T013C3	-39.4875	176.918	1988	04	12	2002	04	22	Napier Museum	027E	027F	027G
T014A1	-38.0060	177.284	1991	08	03	1994	12	11	Opotiki Shell Service Station	028A		
T015A1	-39.6418	176.839	1989	08	08	2002	04	24	Hastings Civil Defence Headquarters	029A		
T016A1	-38.0067	177.268	1994	12	11	2002	08	01	Opotiki Fruit Bowl	030A		
T017A1	-39.9400	176.586	1981	07	01	2004	08	31	Waipawa Post Office	032A		
T018C3	-40.2063	176.093	1980	03	24	2002	07	02	Dannevirke Telephone Exchange	033A	033B	033C
T019A1	-40.4000	176.308	1990	02	20	1995	08	07	Weber School	034A		
T020D3	-40.9500	175.656	1966	09	21	2002	08	29	Masterton Telephone Exchange	039A	039C	039D
T021A1	-41.5735	175.223	1990	10	16	2001	12	12	Ngawihi Fish Processing Factory	040A		
T022A1	-41.3880	175.141	1990	10	16	1990	11	15	Lake Ferry Fire Station	041A		
T023B2	-42.5217	172.825	1990	10	12	2002	02	24	Hammer Springs Fire Station	042A	042B	
T024B2	-45.8587	170.508	1990	10	10	2002	06	09	Dunedin GNS	043A	043B	
T025A1	-45.9000	170.506	1990	10	10	2002	06	08	Dunedin St Kilda Fire Station	044A		

continued on next page

Table B.1 – continued from previous page

Code	Latitude	Longitude	Start date	End date	Name	Network Station Codes
T026A1	-41.2703	173.276	1970 05 26	2002 10 07	Nelson Coucil Building	045A
T027D4	-41.5095	173.954	1969 11 04	2002 10 24	Blenheim Post Office	048A 048B 048C 048D
T028A1	-41.1225	173.006	1993 03 03	2002 10 09	Motueka DOC	050A
T029D4	-41.7545	171.593	1966 11 16	2002 04 16	Westport Telephone Exchange	051A 051B 051C 051D
T030A1	-42.1178	171.856	1971 08 19	1995 04 06	Reefton Forestry Headquarters	052A
T031A1	-42.3748	172.326	1969 11 02	1979 02 18	Maruia Springs Hotel	053A
T032A1	-43.8838	169.039	1993 11 06	2002 04 11	Haast DOC Workshop	054A
T033A1	-42.4505	171.207	1991 10 11	2002 04 19	Greymouth Telecom	055A
T034A1	-41.2732	173.284	1993 11 01	2002 10 07	Nelson Substation	056A
T035A1	-42.7185	170.958	1969 10 31	1989 03 03	Hokitika Post Office	057A
T036A1	-42.7177	170.958	1989 03 03	1992 06 19	Hokitika Telecom Line Depot	057B
T037B2	-43.0703	170.735	1997 10 17	2003 09 07	Waitaha Valley	061A 061B
T038A1	-43.3873	170.186	1997 10 17	2002 04 14	Franz Joseph DOC	062A
T039A1	-43.7347	170.090	1983 05 21	2002 07 03	Mount Cook National Park Headquarters	064A
T040B2	-43.7042	169.423	1997 10 18	2003 01 10	Lake Paringa	066A 066B
T041A1	-45.4175	167.718	1970 02 22	2002 02 13	Te Anau Fire Station	070A
T042A1	-46.2350	169.737	1996 02 20	2002 03 22	Balclutha Telecom	075A
T043B2	-46.4085	168.341	1970 02 24	2004 03 22	Invercargill Telephone Exchange	077A 077B
T044A1	-43.8572	169.004	1969 11 01	1993 03 05	Haast Telephone Exchange Generator Room	078A
T045B2	-44.6715	167.923	1970 02 23	1981 05 04	Milford Sound Hotel Fiordland	080A 080B
T046C3	-38.9887	175.804	1970 03 20	2002 09 06	Turangi Fire Station	081A 081B 081C
T047A1	-41.8263	171.656	1968 06 07	2004 03 18	Te Kuha	083A
T048G1	-44.5673	170.191	1967 08 22	1993 06 17	Benmore Dam	084D
T049F1	-38.1098	176.810	1967 08 09	1996 12 08	Matahina Dam (I)	085A
T050F1	-38.1098	176.809	1994 04 18	2004 08 31	Matahina Dam (II)	085G
T051D1	-39.7180	175.136	1967 07 05	2004 08 31	Atene Valley	087C

continued on next page

Table B.1 – continued from previous page

Code	Latitude	Longitude	Start date	End date	Name	Network Station Codes
T052B1	-39.6737	175.801	1996 06 17	2001 11 27	Taihape Primary School	088A
T053A1	-44.6912	169.139	1973 06 29	2002 07 02	Wanaka National Park Headquarters	089A
T054A1	-41.8543	171.952	1975 02 26	1994 07 28	Inangahua NZED Substation	090A
T055A1	-39.8020	175.804	1975 05 29	1981 10 14	Manaweka Carroll's Woolshed	092A
T056A1	-39.0348	177.421	1980 10 29	2002 08 21	Wairoa Telephone Exchange	096A
T057A1	-41.2183	175.456	1980 10 28	1999 06 04	Martinborough Post Office	098A
T058B2	-38.3712	178.292	1994 09 14	2002 08 01	Tolaga Bay	099A 099B
T059B1	-37.6347	178.359	1977 07 22	1993 07 12	Te Araroa District High School	100A
T060C1	-39.5540	173.443	1978 01 31	2001 02 15	Maui A Offshore Tower (I)	101A
T061A1	-39.5540	173.443	1998 04 22	2004 08 31	Maui A Offshore Tower (II)	101D
T062A1	-39.4595	175.567	1978 03 30	2004 08 31	Karioi Pulp Mill	102A
T063B1	-42.3347	172.175	1979 02 18	1995 04 05	Springs Junction Ranger Station	103A
T064B2	-39.4013	173.807	1980 07 21	2004 08 31	Oaonui Gas Processing Plant	106A 106B
T065C1	-39.7915	175.806	1981 12 04	2001 12 03	South Rangitikei Rail Bridge	110C
T066B2	-38.8333	176.267	1982 08 05	1991 09 16	Iwitahi Forestry Headquarters	111A 111B
T067B1	-43.1340	171.768	1982 09 18	1995 03 01	Flock Hill Station	112A
T068A1	-37.8718	177.584	1982 10 15	2001 06 14	Maraenui Primary School	113A
T069C3	-40.1753	175.425	1982 10 17	2003 07 07	Ohakea RNZAF Avionics Department	114A 114B 114C
T070A1	-40.8500	172.819	1983 02 08	2002 10 10	Takaka Scott's Farm	115A
T071A1	-38.1362	176.252	1983 04 21	1999 06 16	Rotorua Police Station	117B
T072C1	-45.0375	169.218	1983 05 23	2004 03 20	Cromwell Bridge	118B
T073B2	-40.3353	175.868	1983 07 20	1999 06 04	Woodville Post Office	120A 120B
T074A1	-41.8025	172.322	1984 05 23	1996 04 02	Murchison MWD Depot Office	122A
T075C1	-41.0843	175.140	1984 09 27	2004 08 31	Te Marua Dam	123A
T076A1	-41.8010	172.323	1991 10 09	2002 02 27	Murchison Area School	129A
T077B1	-41.6695	173.202	1985 08 20	2004 08 31	Branch River Power Station	130A

continued on next page

Table B.1 – continued from previous page

Code	Latitude	Longitude	Start date	End date	Name	Network Station Codes
T078A1	-40.9097	175.002	1993 06 30	2001 10 17	Paraparaumu Primary School	131A
T079A1	-41.2930	174.775	1993 07 28	1997 05 05	Wellington Car Stereo Co.	132A
T080A1	-45.5385	169.308	1995 06 20	2004 03 23	Roxburgh Hydro	133A
T081A1	-40.3543	175.609	1970 06 22	2003 06 27	Palmerston North Telephone Exchange	301A
T082A1	-39.9347	175.052	1989 04 17	2004 08 31	Wanganui Post Office	302A
T083D1	-40.3863	175.610	1972 02 11	2004 08 31	Massey University	340A
T084A1	-41.2042	174.940	2001 11 17	2004 08 31	Lower Hutt Collett St	465A
T085A1	-41.2347	174.918	1991 04 05	1993 03 17	Lower Hutt Gracefield Library Centre	466A
T086A1	-41.2398	174.901	1991 04 12	2004 08 31	Lower Hutt Croft Combined Carriers Seaview	467A
T087A1	-41.2017	174.953	1991 06 27	2004 08 31	Lower Hutt Naenae Substation	468A
T088A1	-41.2053	174.902	1996 05 08	2001 10 29	Lower Hutt Emergency Management Office	469A
T089D1	-43.5337	172.626	1974 02 26	2004 08 31	Christchurch Police Station	501A
T090D1	-43.5222	172.583	1974 10 04	2004 08 31	Christchurch Cant. Univ. Arts Block	502A
T091A1	-46.1002	168.941	1997 06 17	2004 03 22	Gore Civic Centre	504A
T092A1	-42.9500	171.567	1992 02 14	2001 11 12	Arthurs Pass Police Station	505A
T093A1	-45.1010	170.968	1994 02 24	2002 06 28	Oamaru North Otago Museum	507A
T094F1	-43.3593	171.523	1994 07 31	2004 03 19	Coleridge Power Station	508A
T095A1	-41.2237	174.870	1969 12 16	1981 11 11	Petone Gear Meatworks	601A
T096C3	-41.1887	174.923	1968 11 20	2004 08 31	Lower Hutt Belmont Substation	602A 602B 602C
T097B2	-41.2217	174.856	1970 07 03	2004 08 31	Petone Woollen Mills Substation	603A 603B
T098A1	-41.2262	174.905	1968 11 20	1994 07 07	Lower Hutt Elizabeth St Pumping Station Moera	604A
T099B2	-41.2057	174.938	1971 09 27	2004 08 31	Lower Hutt Naenae Reservoir	605A 605B
T100B1	-41.2343	174.919	1968 05 16	2004 01 28	Lower Hutt INS DSIR	606A
T101A1	-41.2223	174.874	1986 05 14	2004 08 31	Petone Municipal Building	608A
T102C1	-41.2353	174.909	1997 11 10	2004 08 31	Lower Hutt GNS Hutton Building	640A
T103B1	-41.2333	174.917	1996 02 01	1997 11 04	Lower Hutt GNS Sunbeam Building	641A

continued on next page

Table B.1 – continued from previous page

Code	Latitude	Longitude	Start date			End date			Name	Network Station Codes		
T104K3	-41.2353	174.917	1965	06	12	2002	08	14	Lower Hutt PEL DSIR	642A	642B	642C
T105B1	-41.1518	174.974	1967	12	20	2001	10	01	Lower Hutt Haywards Substation	643A		
T106D2	-41.2187	174.876	1991	01	10	2004	08	31	Petone Wellington Newspapers	644A	644C	
T107F2	-41.2553	174.942	1991	07	02	2004	08	31	Wainuiomata Bush Fire Station	646A	646B	
T108E1	-41.2867	174.773	1991	11	07	2004	08	31	Wellington Central Police Station	647C		
T109A1	-41.2742	174.771	1992	07	31	1995	05	23	Wellington Parliament Buildings	648A		
T110A1	-41.2038	174.921	2003	07	15	2004	08	31	Lower Hutt Hospital	651A		
T111A1	-37.9225	175.537	1995	05	18	2004	08	31	Karakiro Hydro	700A		
T112A1	-41.1333	174.837	1990	09	21	1991	07	09	Porirua Art Gallery	704A		
T113B2	-41.1377	174.850	1990	09	21	1992	03	04	Porirua Hall	705A	705B	
T114A1	-41.1252	174.836	1991	07	09	1993	08	25	Porirua Components and Instruments	706A		
T115A1	-41.1380	174.850	1992	03	04	2001	08	01	Porirua Free Ambulance Depot	707A		
T116B1	-41.1333	174.837	1993	12	01	2001	10	16	Porirua Library	708A		
T117A1	-38.6242	177.919	1993	12	07	2002	04	17	Gisborne Waipaoa Water Treatment Plant	709A		
T118A1	-38.6725	178.022	1994	04	14	2003	12	02	Gisborne Pumping Station	710A		
T119A1	-41.2258	174.903	1994	10	31	2002	12	12	Lower Hutt Randwick Rd Substation	711A		
T120A1	-37.9577	176.984	1994	12	12	2001	12	04	Whakatane High School	712A		
T121B1	-41.1228	174.837	1998	07	28	2004	08	31	Porirua Whitireia Polytechnic Array	713A		
T122C2	-41.2883	174.774	1989	03	21	2002	03	06	Wellington Museum of NZ	900A	900C	
T123D1	-41.2750	174.774	1969	08	01	2004	08	31	Wellington Vodele Building	902A		
T124D1	-41.2840	174.772	1968	01	25	2004	08	31	Wellington Morrison Morpeth House	903B		
T125F2	-41.2838	174.771	1970	07	06	2004	08	31	Wellington Dalmuir House	904A	904D	
T126D1	-41.2758	174.774	1970	10	12	1989	05	17	Wellington Postal Centre	905A		
T127C1	-41.2753	174.772	1972	09	05	2004	08	31	Wellington Reserve Bank	906A		
T128D1	-41.2752	174.774	1973	10	26	1987	12	11	Wellington Rutherford House	907A		
T129D1	-41.2730	174.771	1976	05	10	1981	05	27	Wellington Charles Fergusson Building	910B		

continued on next page

Table B.1 – continued from previous page

Code	Latitude	Longitude	Start date	End date	Name	Network Station Codes
T130B2	-41.2920	174.773	1969 12 22	2002 10 24	Wellington Central Library	911A 911B
T131A1	-41.3237	174.805	1970 09 16	2001 09 28	Wellington International Airport	912A
T132A1	-41.2870	174.770	1969 05 01	2002 12 12	Wellington Church St Substation	913A
T133C3	-41.2913	174.771	1974 01 23	2004 08 31	Wellington Southern Cross Medical	914A 914B 914C
T134B2	-41.2910	174.772	1975 05 08	1997 04 01	Wellington ANZ Bank	915A 916A
T135A1	-41.2850	174.767	1970 04 13	1975 03 24	Wellington Seismological Observatory (I)	918A
T136B2	-41.2850	174.768	1989 05 30	2004 08 31	Wellington Seismological Observatory (II)	918B 918C
T137A1	-41.2905	174.773	1969 04 22	1974 07 17	Wellington Te Aro Post Office	919A
T138A1	-41.3063	174.775	1979 07 19	2003 04 14	Wellington Hospital O&G Block	920A
T139B1	-41.2747	174.773	1981 09 09	2003 01 15	Wellington Beehive	922A
T140B1	-41.3073	174.774	1982 01 07	1997 02 25	Wellington Hospital Ward Spt Block	923B
T141F1	-41.2717	174.773	1982 10 28	2000 11 23	Wellington Wm Clayton Bldg (I)	924A
T142E1	-41.2717	174.773	2000 07 07	2004 08 31	Wellington Wm Clayton Bldg (II)	924I
T143B2	-41.2672	173.273	1994 07 26	2002 10 08	Nelson Depot	925A 925B
T144A1	-39.4873	176.917	1994 12 06	2001 06 14	Napier Telecom	926A
T145B2	-39.6703	176.875	1994 12 07	2002 04 26	Havelock North St Lukes School	928A 928B
T146A1	-37.9875	176.824	1987 03 03	1995 01 23	Edgecumbe Substation Electricorp	930A
T147A1	-38.0740	176.720	1987 03 03	1992 03 23	Kawerau Substation Electricorp	931A
T148B1	-38.0858	176.702	1992 03 23	1993 07 25	Kawerau Police Station	931B
T149A1	-37.7005	176.155	1995 01 23	2002 09 02	Tauranga Telephone Exchange	933A
T150C2	-41.2405	174.905	1987 08 11	2001 09 29	Lower Hutt Shell Oil	934A 934B
T151C1	-41.2075	174.903	1987 08 12	1995 10 12	Lower Hutt Chiropractic Services	935A
T152A1	-41.2708	174.771	1987 08 11	2004 08 31	Wellington Pottery Association	937A
T153A1	-45.0335	168.658	1988 10 31	2004 03 22	Queenstown Telephone Exchange	940A
T154A1	-41.2897	174.774	1990 05 04	1990 11 05	Wellington Taranaki St Police Station	941A
T155B2	-45.6680	168.236	1995 06 17	2002 06 15	Mossburn School	964A 946B

continued on next page

Table B.1 – continued from previous page

Code	Latitude	Longitude	Start date	End date	Name	Network Station Codes
T156A1	-41.2888	174.768	2002 12 11	2004 08 31	Victoria University	954A

Table B.2: List of triggers used for ground motion test ($PGA \geq 0.05g$, $mag \geq 5.25$, $depth \leq 40km$ registered by instruments from Table B.1)

Date	Time	Magnitude	Depth (km)	Distance (km)	PGA (g)	Network Station Codes	Name of Station
10.08.1993	09:46:39	6.19	36	17	0.14	016A	Gisborne Kaiti Hill
10.08.1993	09:46:39	6.19	36	16	0.18	017A	Gisborne 2ZG
10.08.1993	09:46:39	6.19	36	16	0.18	018A	Gisborne Chief Post Office A (car park)
21.02.1973	14:42:00	5.4	12R	25	0.12	027A	Napier Telephone Exchange Marewa
05.10.1980	15:32:50	5.66	36R	23	0.12	027C	Napier Telephone Exchange Marewa
02.09.1982	15:58:54	5.46	31R	26	0.09	027C	Napier Telephone Exchange Marewa
07.11.1997	22:30:01	5.4	16	87	0.06	029A	Hastings Civil Defence Headquarters
13.05.1990	04:23:10	6.37	12	94	0.06	029A	Hastings Civil Defence Headquarters
02.09.1982	15:58:54	5.46	31R	37	0.07	032A	Waipawa Post Office
11.04.1993	06:59:49	5.63	35	25	0.13	032A	Waipawa Post Office
19.02.1990	05:34:37	6.23	24	58	0.15	032A	Waipawa Post Office
13.05.1990	04:23:10	6.37	12	54	0.19	032A	Waipawa Post Office
19.02.1990	05:34:37	6.23	24	21	0.15	033A	Dannevirke Telephone Exchange
13.05.1990	04:23:10	6.37	12	19	0.27	033C	Dannevirke Post Office
02.03.1992	09:05:56	5.54	24	17	0.08	034A	Weber School
19.09.1996	12:16:34	5.8	11	5	0.15	042A	Hammer Springs Fire Station
29.08.1996	04:47:02	5.3	10	5	0.23	042A	Hammer Springs Fire Station
25.05.1968	23:49:16	5.3	12R	23	0.08	051A	Westport Telephone Exchange
24.05.1968	20:57:27	5.78	12R	32	0.06	051A	Westport Telephone Exchange
28.01.1991	18:00:54	5.93	17	17	0.14	051B	Westport Telephone Exchange
15.02.1991	10:48:10	5.42	7	31	0.11	051B	Westport Telephone Exchange
28.01.1991	12:58:46	5.79	0	15	0.14	051B	Westport Telephone Exchange
18.06.1994	03:25:15	6.81	11	140	0.05	051D	Westport Buller District Council

continued on next page

Table B.2 – continued from previous page

Date	Time	Magnitude	Depth (km)	Distance (km)	PGA (g)	Network Station Codes	Name of Station
28.01.1991	18:00:54	5.93	17	29	0.18	052A	Reefton Forestry Headquarters
15.02.1991	10:48:10	5.42	7	24	0.14	052A	Reefton Forestry Headquarters
28.01.1991	12:58:46	5.79	0	34	0.06	052A	Reefton Forestry Headquarters
13.08.1971	14:42:41	5.7	12R	34	0.06	053A	Maruia Springs Hotel
13.08.1971	14:42:41	5.7	12R	114	0.05	057A	Hokitika Post Office
10.08.1993	00:51:51	6.81	5R	82	0.06	070A	Te Anau Fire Station
31.05.1989	05:54:23	6.33	23R	68	0.1	070A	Te Anau Fire Station
20.09.1974	19:48:39	5.55	12R	101	0.05	078A	Haast Telephone Exchange Generator Room
04.05.1976	13:56:29	6.51	12R	38	0.09	080B	Milford Sound Hotel Fiordland
05.03.1984	02:07:17	5.27	9R	8	0.11	081A	Turangi Telephone Exchange
28.01.1991	18:00:54	5.93	17	7	0.13	083A	Te Kuha
28.01.1991	12:58:46	5.79	0	9	0.21	083A	Te Kuha
02.03.1987	01:42:35	6.53	10R	26	0.39	085A	Matahina Dam A (top southwest)
19.02.1990	05:34:37	6.23	24	118	0.08	087C	Atene C (valley)
13.05.1990	04:23:10	6.37	12	117	0.09	087C	Atene C (valley)
28.01.1991	18:00:54	5.93	17	24	0.19	090A	Inangahua NZED Substation
15.02.1991	10:48:10	5.42	7	36	0.08	090A	Inangahua NZED Substation
28.01.1991	12:58:46	5.79	0	31	0.11	090A	Inangahua NZED Substation
10.06.1975	10:11:20	5.62	33R	61	0.05	092A	Mangaweka Carroll's Woolshed
13.05.1990	04:23:10	6.37	12	113	0.05	102A	Karioi Pulp Mill
16.04.1983	21:29:45	5.3	12R	18	0.11	106A	Oaonui Gas Processing Plant
18.06.1994	03:25:15	6.81	11	28	0.12	112A	Flock Hill Station
15.12.1994	11:20:20	6.31	12R	67	0.08	113A	Maraenui Primary School
10.08.1993	09:46:39	6.19	36	81	0.08	113A	Maraenui Primary School
19.02.1990	05:34:37	6.23	24	30	0.15	120A	Woodville Post Office

continued on next page

Table B.2 – continued from previous page

Date	Time	Magnitude	Depth (km)	Distance (km)	PGA (g)	Network Station Codes	Name of Station
13.05.1990	04:23:10	6.37	12	31	0.17	120A	Woodville Post Office
28.01.1991	18:00:54	5.93	17	54	0.22	122A	Murchison MWD Depot Office
28.01.1991	12:58:46	5.79	0	61	0.1	122A	Murchison MWD Depot Office
19.02.1990	05:34:37	6.23	24	51	0.05	301A	Palmerston North Telephone Exchange
13.05.1990	04:23:10	6.37	12	110	0.06	302A	Wanganui Post Office
05.02.1982	17:51:37	5.36	33R	38	0.06	340A	Massey University A (tunnel)
10.06.1975	10:11:20	5.62	33R	27	0.06	340A	Massey University A (tunnel)
19.02.1990	05:34:37	6.23	24	51	0.05	340A	Massey University A (tunnel)
18.06.1994	03:25:15	6.81	11	11	0.37	505A	Arthurs Pass Police Station
24.11.1995	06:18:57	6.24	7	21	0.12	505A	Arthurs Pass Police Station
29.05.1995	10:06:42	5.5	4	3	0.32	505A	Arthurs Pass Police Station
18.01.1977	05:41:48	6.02	33R	75	0.07	604A	Lower Hutt Elizabeth St Pumping Station Moera
01.11.1968	01:32:25	5.35	33R	44	0.06	606A	Lower Hutt INS DSIR
01.11.1968	01:32:25	5.35	33R	44	0.13	642A	Lower Hutt PEL DSIR
18.01.1977	05:41:48	6.02	33R	75	0.06	642A	Lower Hutt PEL DSIR
23.04.1966	06:49:39	5.75	22	61	0.05	642A	Lower Hutt PEL DSIR
01.11.1968	01:32:25	5.35	33R	52	0.12	643A	Lower Hutt Haywards Substation
18.01.1977	05:41:48	6.02	33R	64	0.08	902A	Wellington Vogel Building A (remote)
18.01.1977	05:41:48	6.02	33R	63	0.07	904A	Wellington Dalmuir House A (basement)
18.01.1977	05:41:48	6.02	33R	64	0.06	905A	Wellington Postal Centre A (basement)
18.01.1977	05:41:48	6.02	33R	64	0.05	906A	Wellington Reserve Bank A (basement)
18.01.1977	05:41:48	6.02	33R	64	0.09	907A	Wellington Rutherford House A (car park)
18.01.1977	05:41:48	6.02	33R	64	0.08	910B	Wellington Charles Fergusson Building B (basement)
18.01.1977	05:41:48	6.02	33R	63	0.05	913A	Wellington Church Street Substation
18.01.1977	05:41:48	6.02	33R	62	0.07	914A	Wellington Gray and Elliot Ltd 167 Vivian st

continued on next page

Table B.2 – continued from previous page

Date	Time	Magnitude	Depth (km)	Distance (km)	PGA (g)	Network Station Codes	Name of Station
21.08.2003	12:12:49	7.2	18	136	0.09	940A	Queenstown Telephone Exchange

Table B.3: Results of testing forecast performance for different probability classes (as defined in Chapter 12.3)

Probability class	Days	Poissonian Prediction	Total Prediction	Observed Triggers
Class 1	74999	0.3512	0.3546	1
Class 2	70591	1.1571	1.1698	4
Class 3	88419	2.2653	2.3096	7
Class 4	155280	5.4254	5.5155	11
Class 5	381371	15.9506	16.1440	29
Class 6	19683	0.8701	1.0577	2
Class 7	43489	2.7029	2.8643	6
Class 8	9807	0.5789	0.7331	0
Class 9	3890	0.1881	0.3292	1
Class 10	8462	0.6602	0.7983	1
Class 11	31596	2.6975	3.9363	4
Class 12	5049	0.2658	1.2207	1
Class 13	2415	0.1229	0.8375	3
Class 14	1532	0.0823	0.6830	0
Class 15	931	0.0488	0.5090	0
Class 16	738	0.0408	0.4779	1
Class 17	547	0.0290	0.4096	0
Class 18	420	0.0240	0.3571	1
Class 19	344	0.0212	0.3269	0
Class 20	1547	0.0902	2.1265	0
Class 21	503	0.0288	1.2299	0
Class 22	265	0.0146	0.9141	0
Class 23	156	0.0083	0.6987	0
Class 24	88	0.0050	0.4817	0

continued on next page

Table B.3 – continued from previous page

Probability class	Days	Poissonian Prediction	Total Prediction	Observed Triggers
Class 25	57	0.0033	0.3692	0
Class 26	43	0.0024	0.3194	0
Class 27	44	0.0026	0.3712	0
Class 28	32	0.0015	0.3043	0
Class 29	112	0.0067	1.5407	0
Class 30	35	0.0022	0.8396	0
Class 31	16	0.0011	0.5476	0
Class 32	10	0.0007	0.4427	0
Class 33	6	0.0003	0.3341	0
Class 34	3	0.0002	0.1946	0
Class 35	5	0.0003	0.3720	0
Class 36	1	0.0001	0.0821	0
Class 37	3	0.0003	0.2939	0
Class 38	8	0.0004	1.0657	1
Class 39	2	0.0001	0.4710	1
Class 40	0	0	0	0
Class 41	0	0	0	0
Class 42	0	0	0	0
Class 43	0	0	0	0
Class 44	0	0	0	0
Class 45	0	0	0	0
Class 46	0	0	0	0

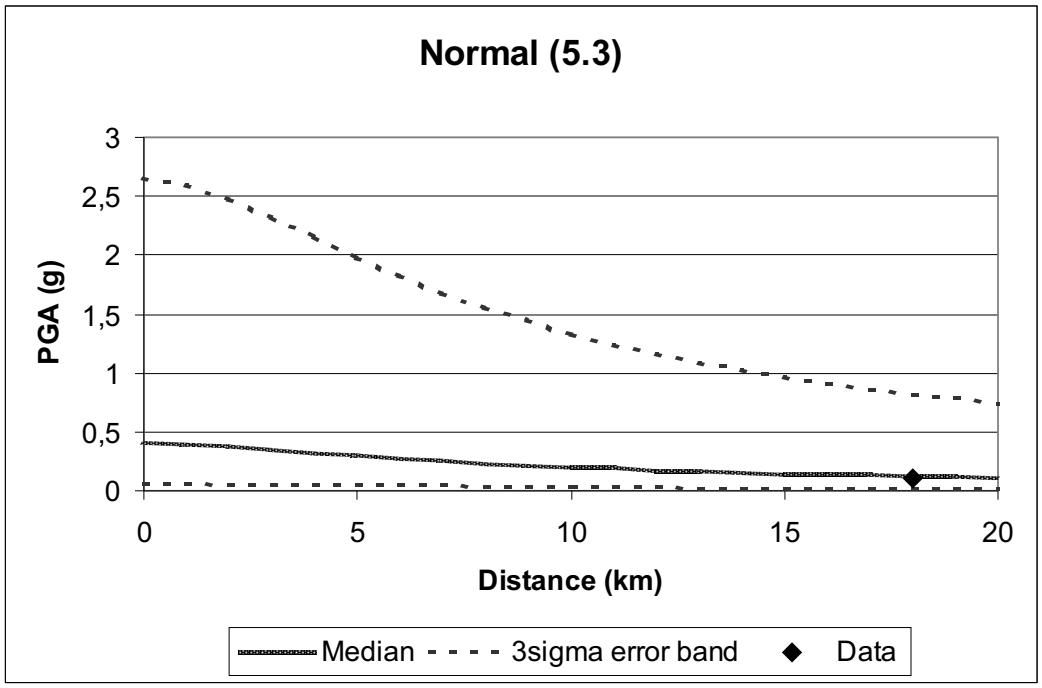

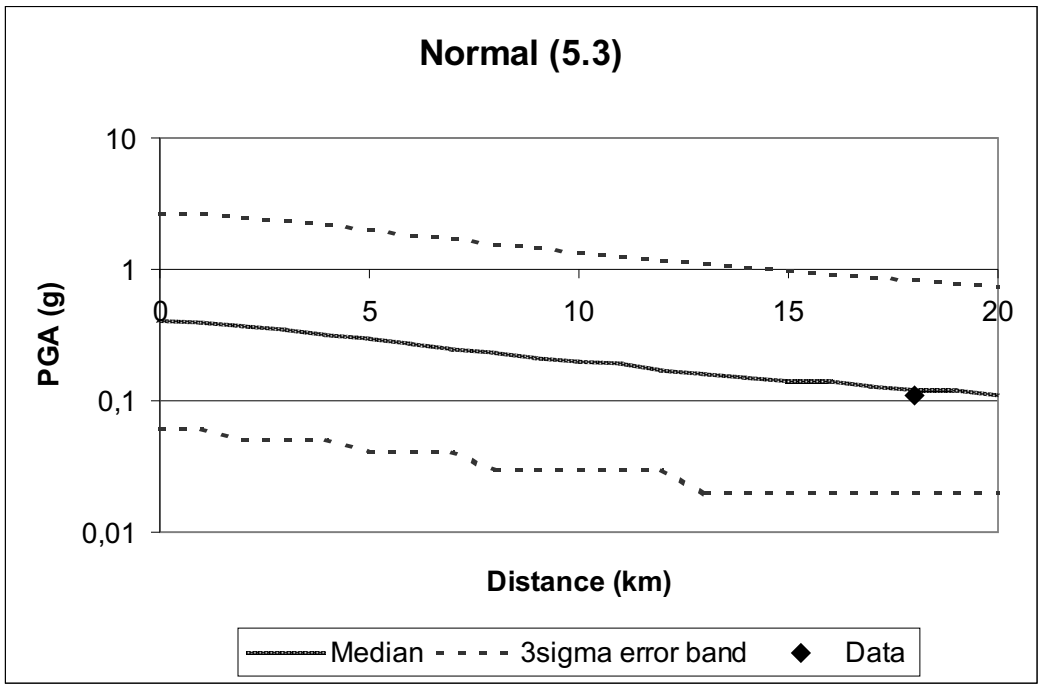

Figure B.1: Attenuation curve and test data for M=5.3, slip type: normal.

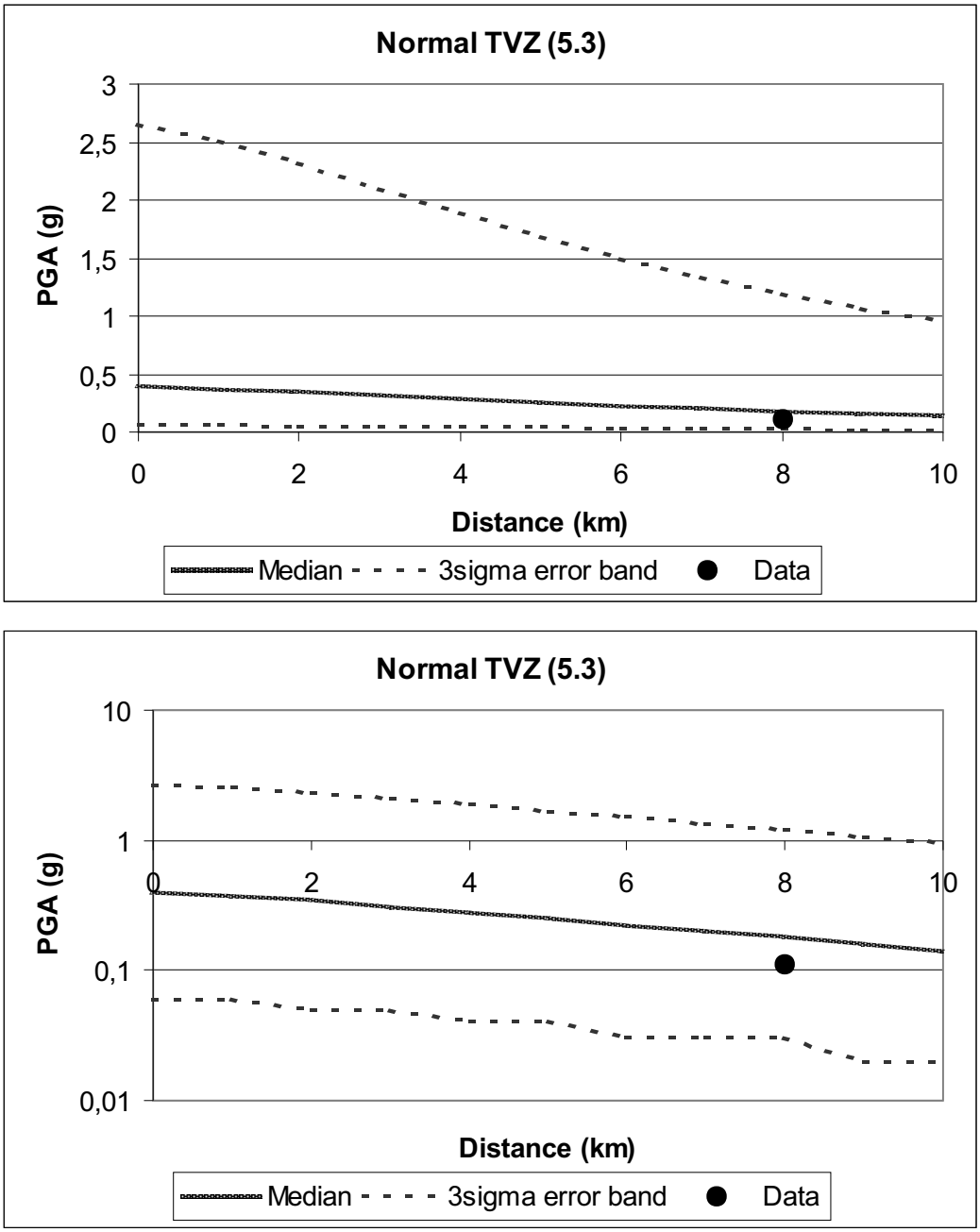

Figure B.2: Attenuation curve and test data for M=5.3, slip type: normal in TVZ.

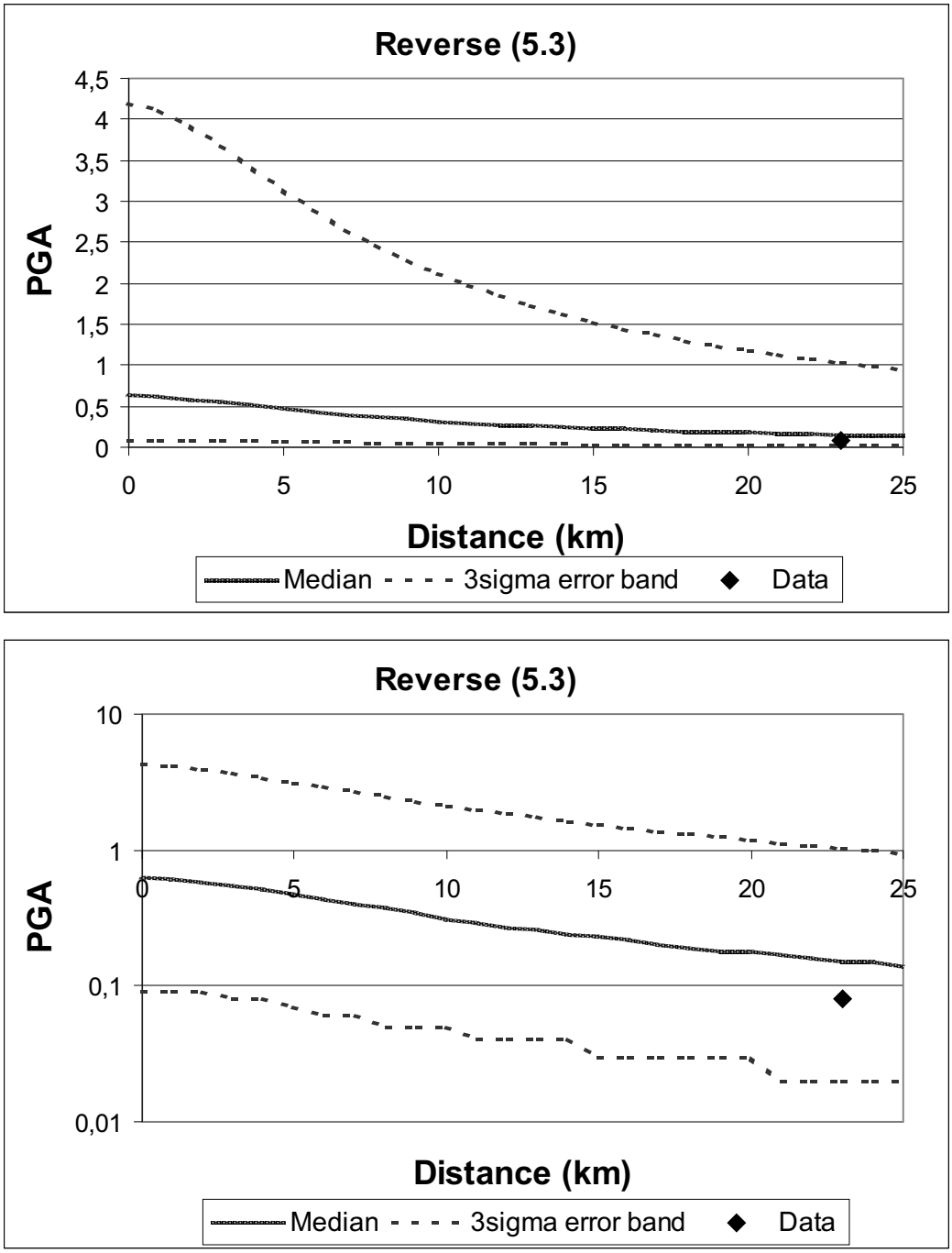

Figure B.3: Attenuation curve and test data for M=5.3, slip type: reverse.

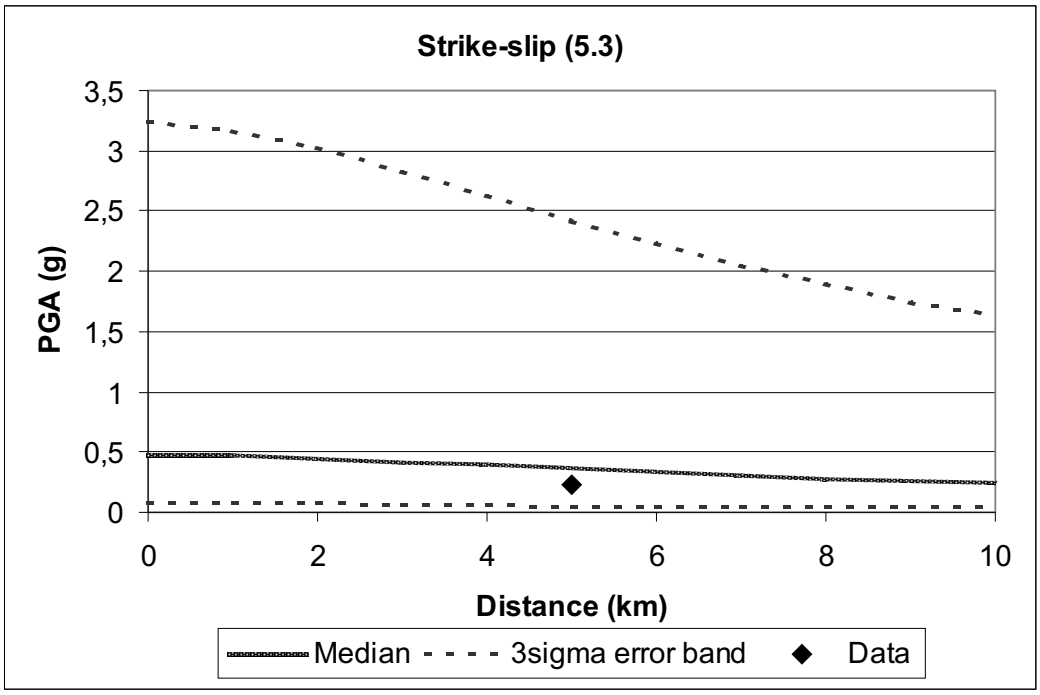

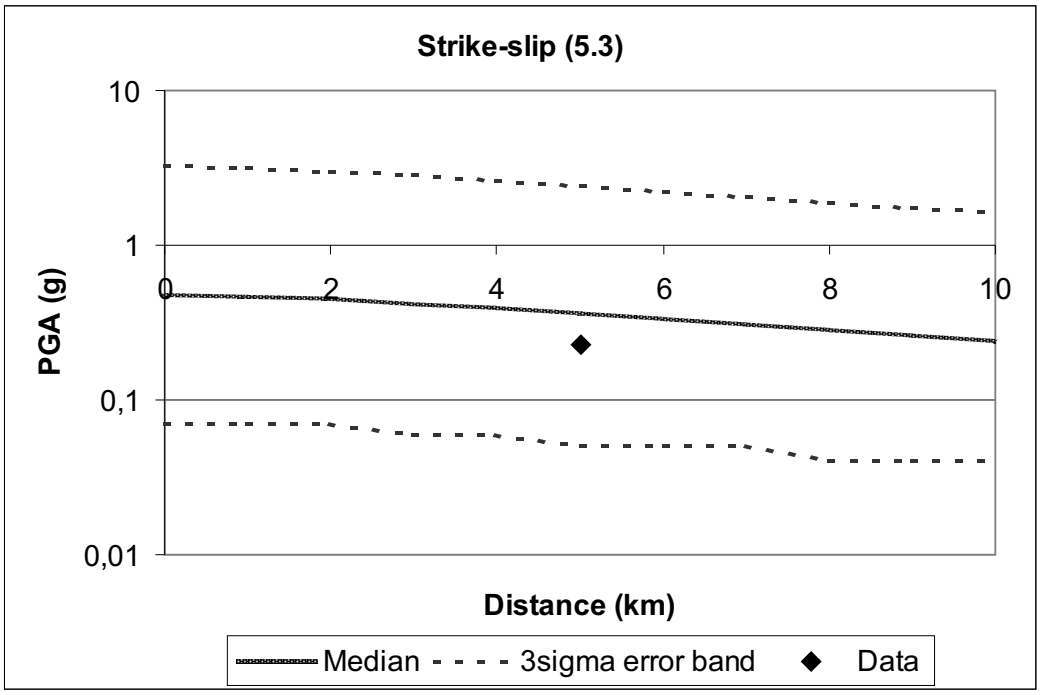

Figure B.4: Attenuation curve and test data for M=5.3, slip type: strike-slip.

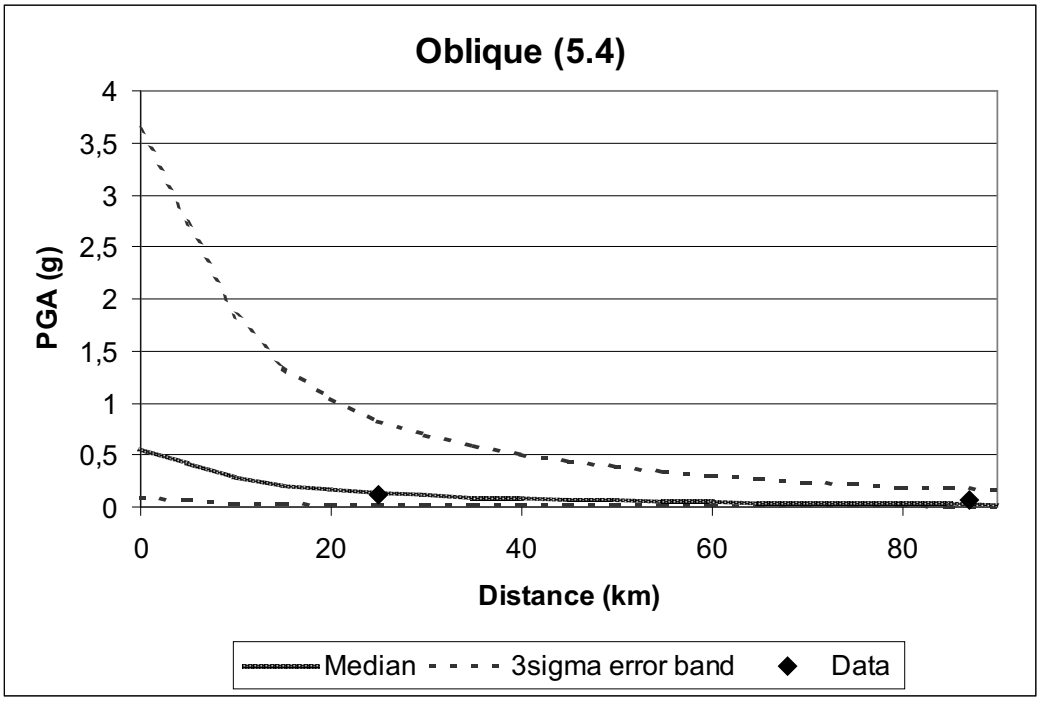

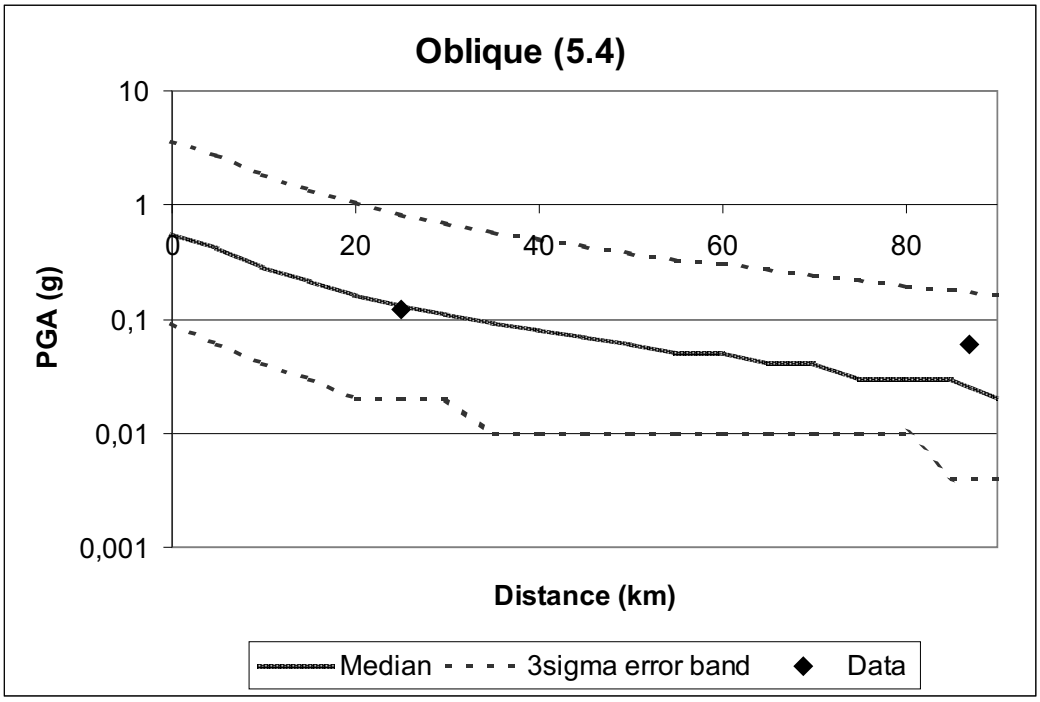

Figure B.5: Attenuation curve and test data for M=5.4, slip type: oblique.

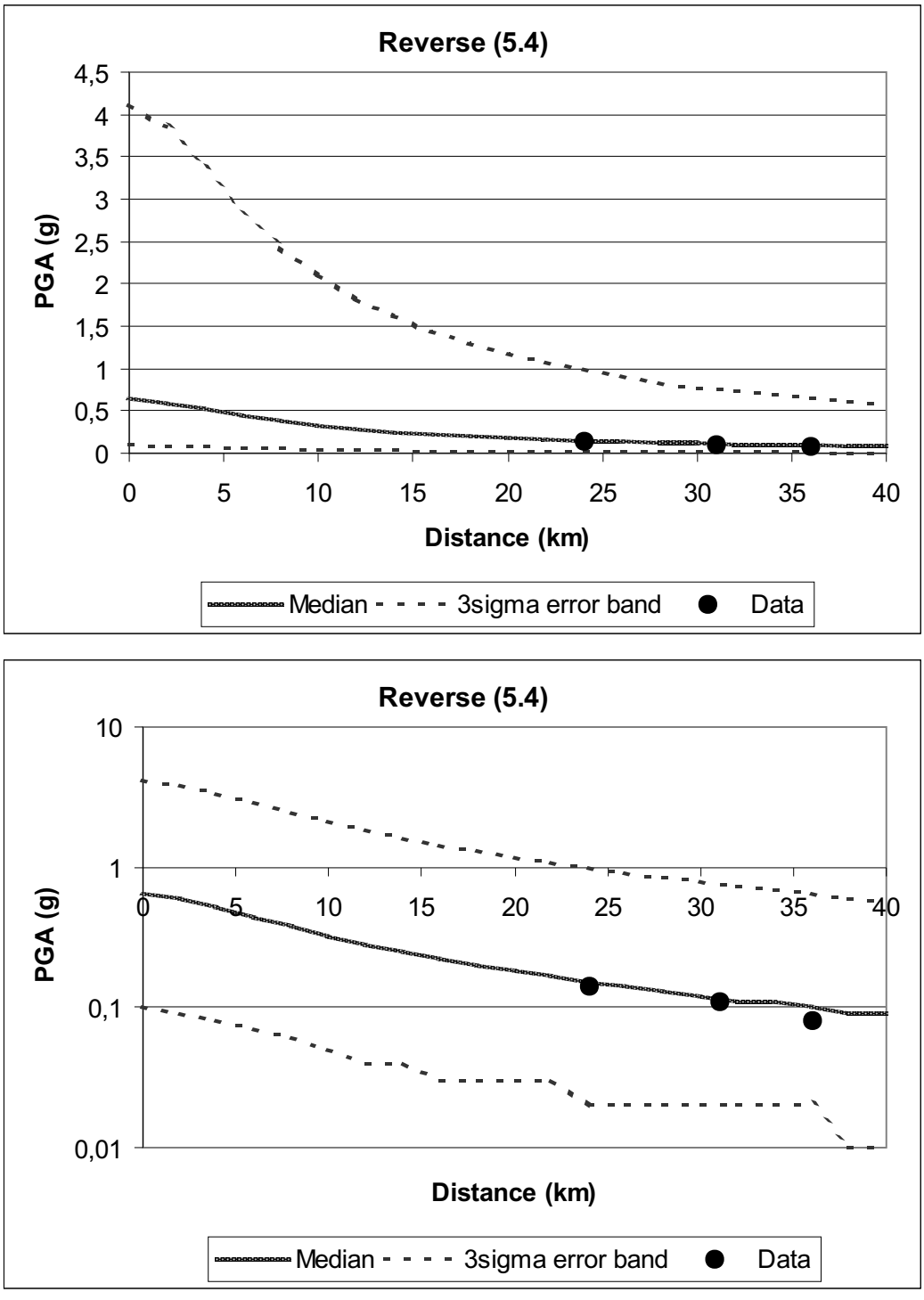

Figure B.6: Attenuation curve and test data for M=5.4, slip type: reverse.

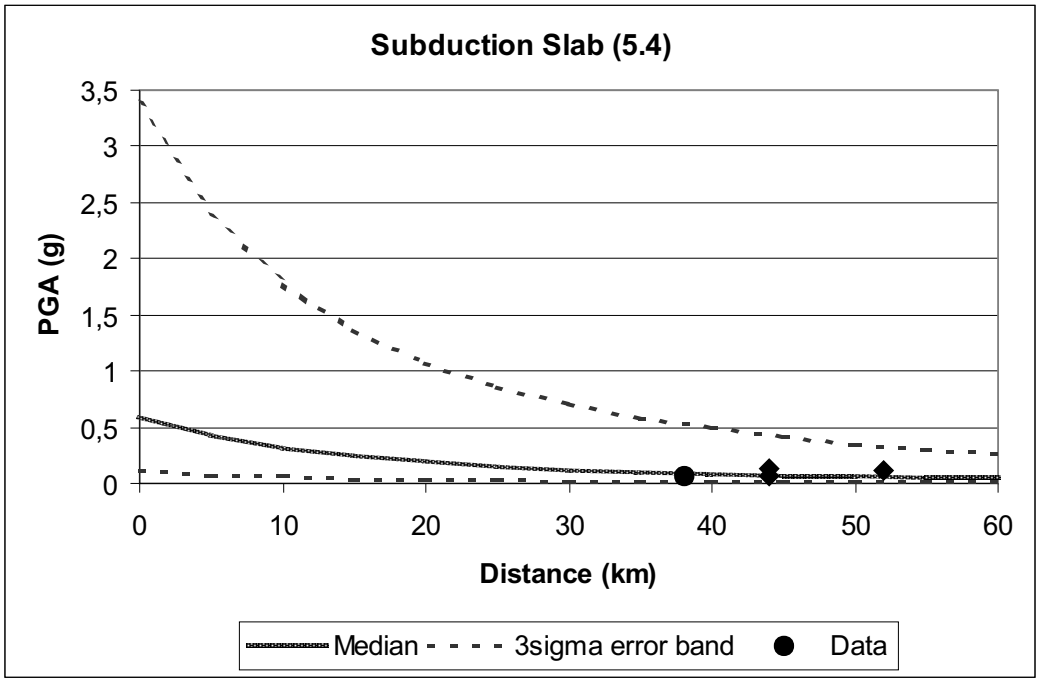

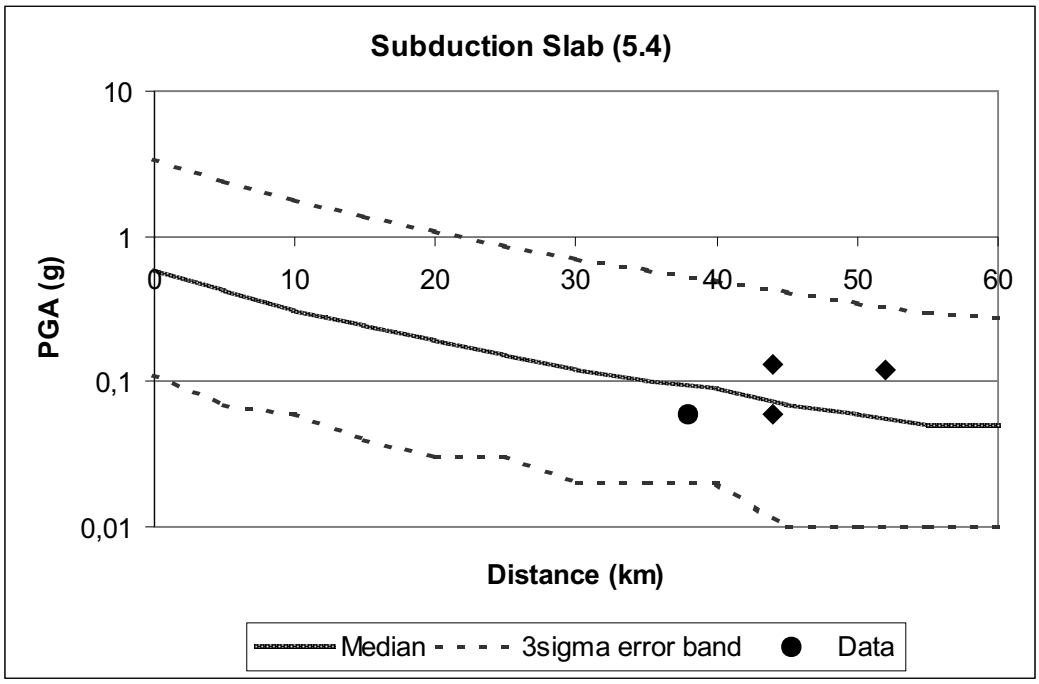

Figure B.7: Attenuation curve and test data for M=5.4, slip type: subduction slab.

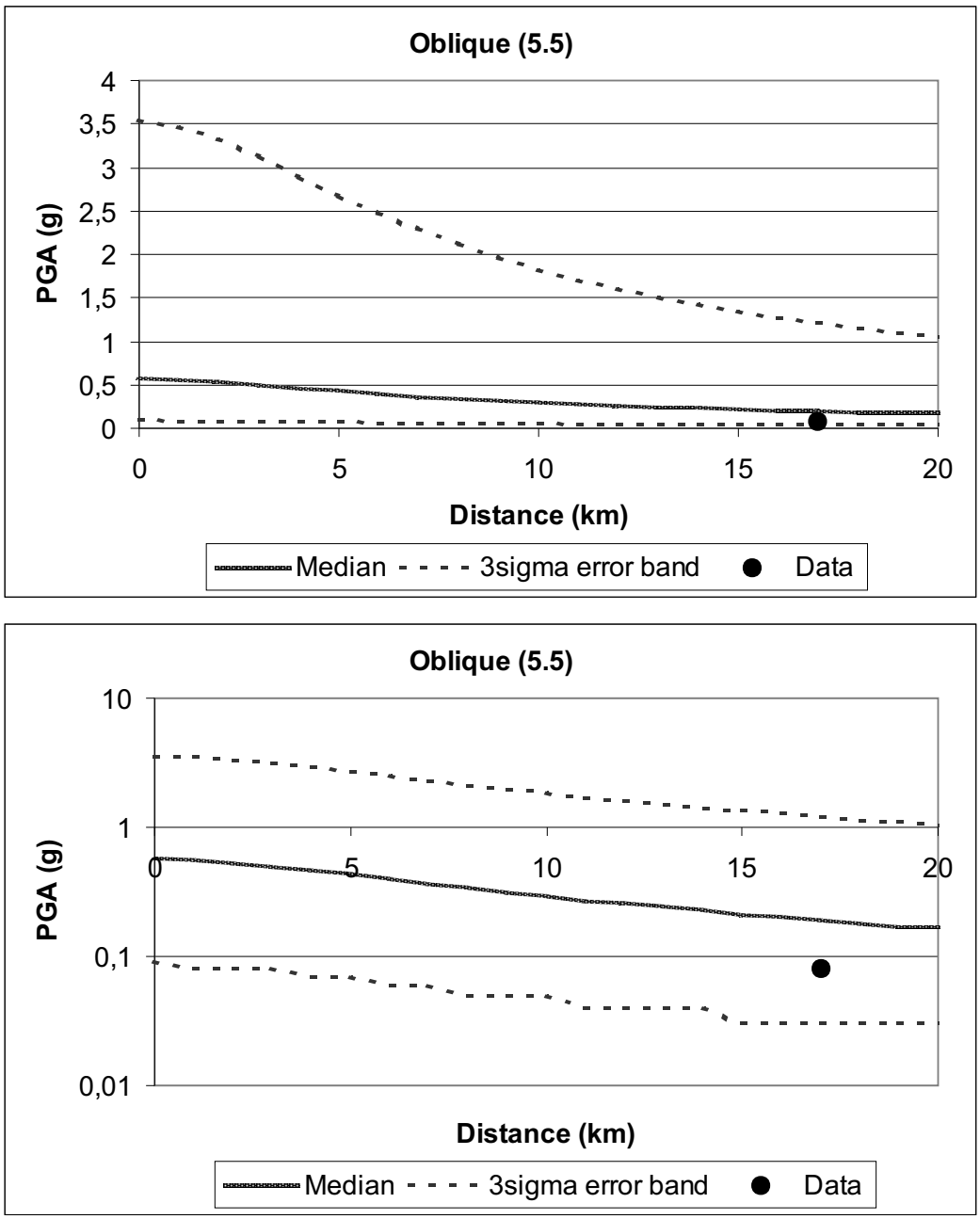

Figure B.8: Attenuation curve and test data for M=5.5, slip type: oblique.

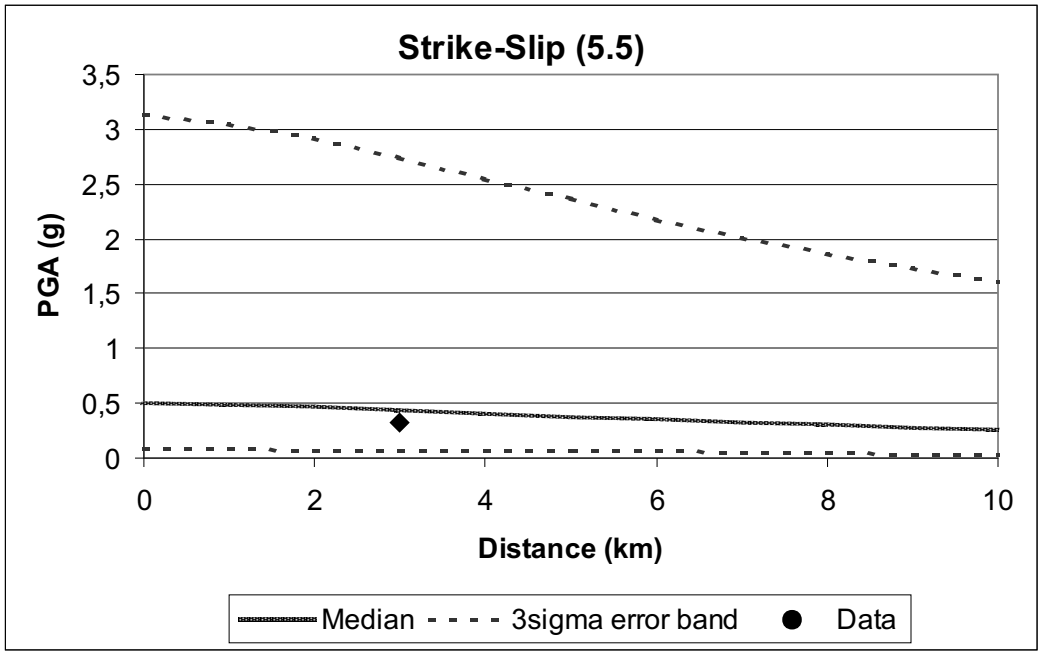

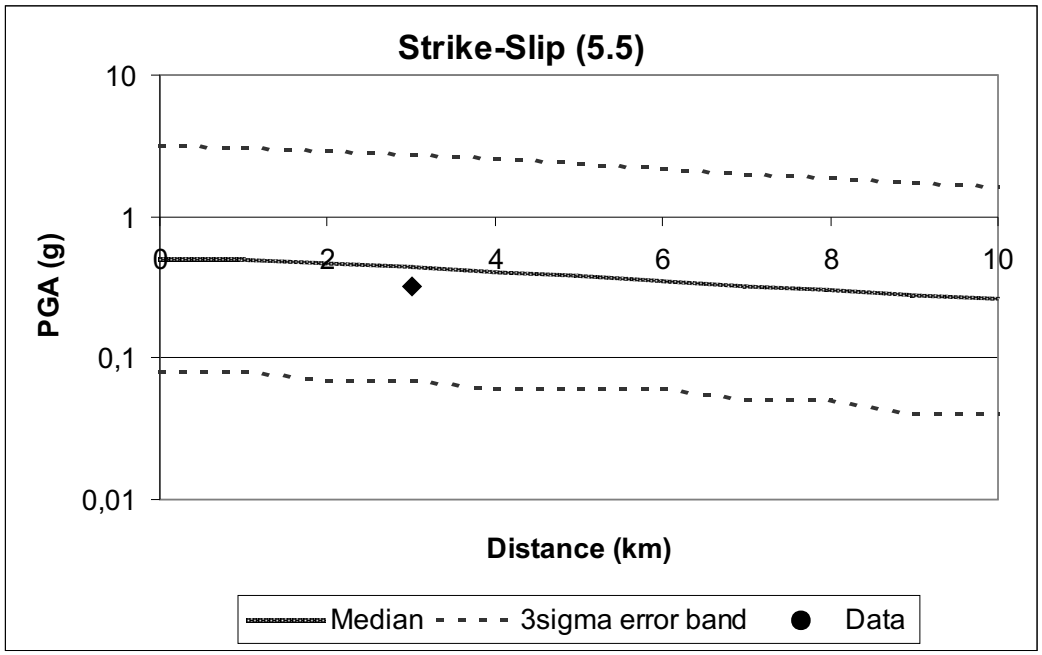

Figure B.9: Attenuation curve and test data for M=5.5, slip type: strike-slip.

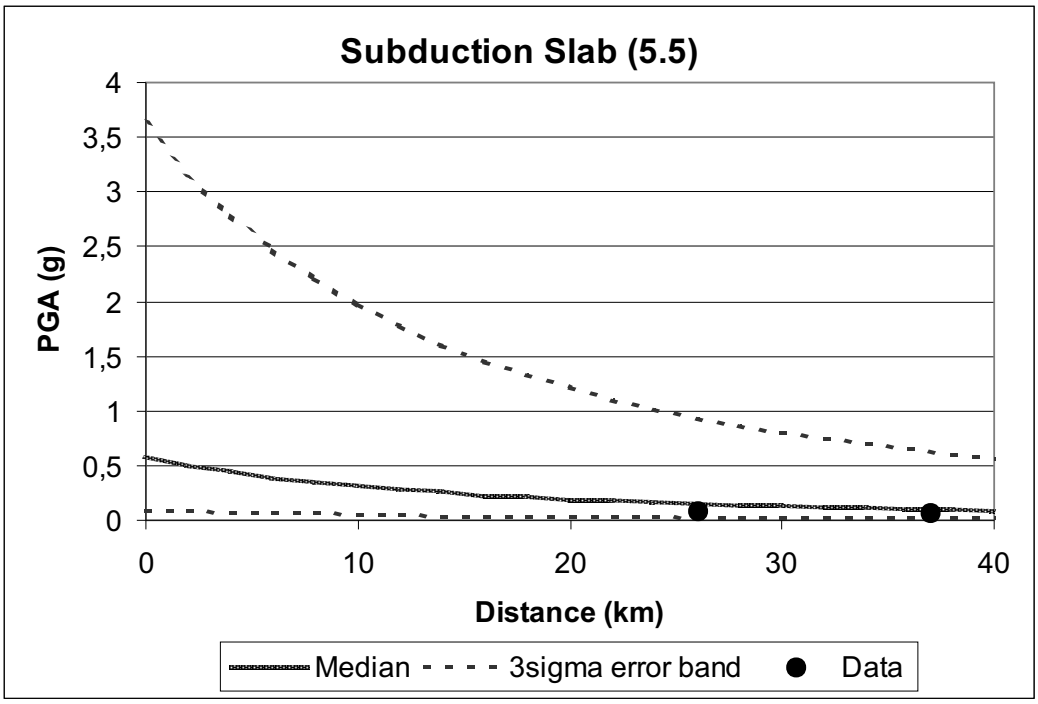

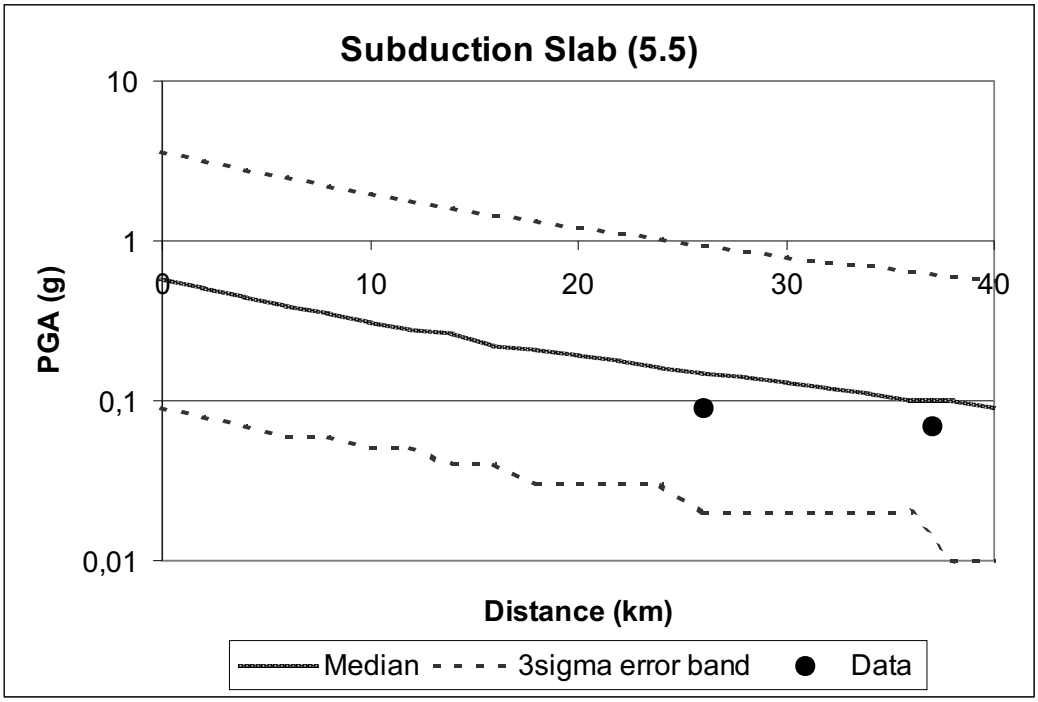

Figure B.10: Attenuation curve and test data for M=5.5, slip type: subduction slab.

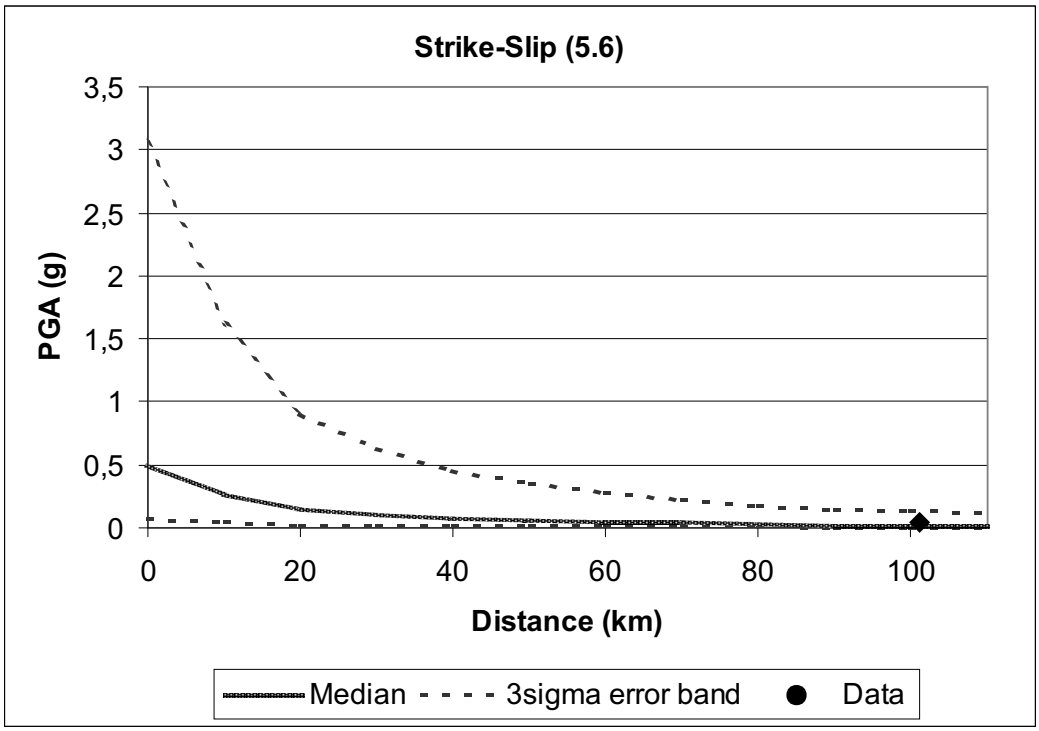

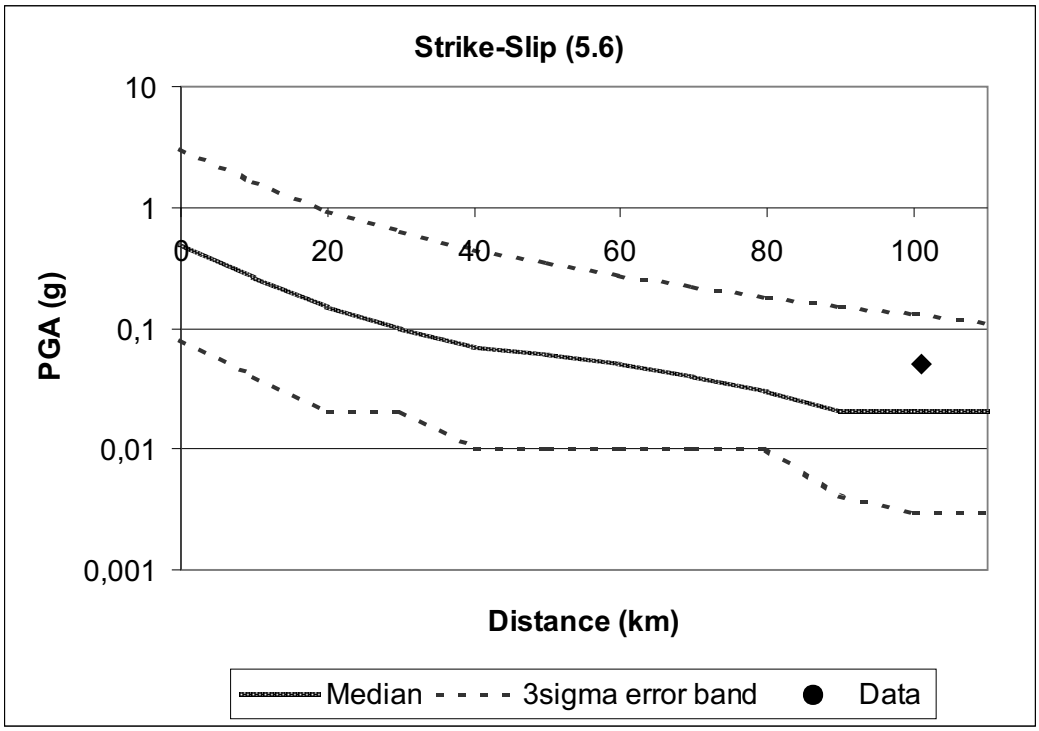

Figure B.11: Attenuation curve and test data for M=5.6, slip type: strike-slip.

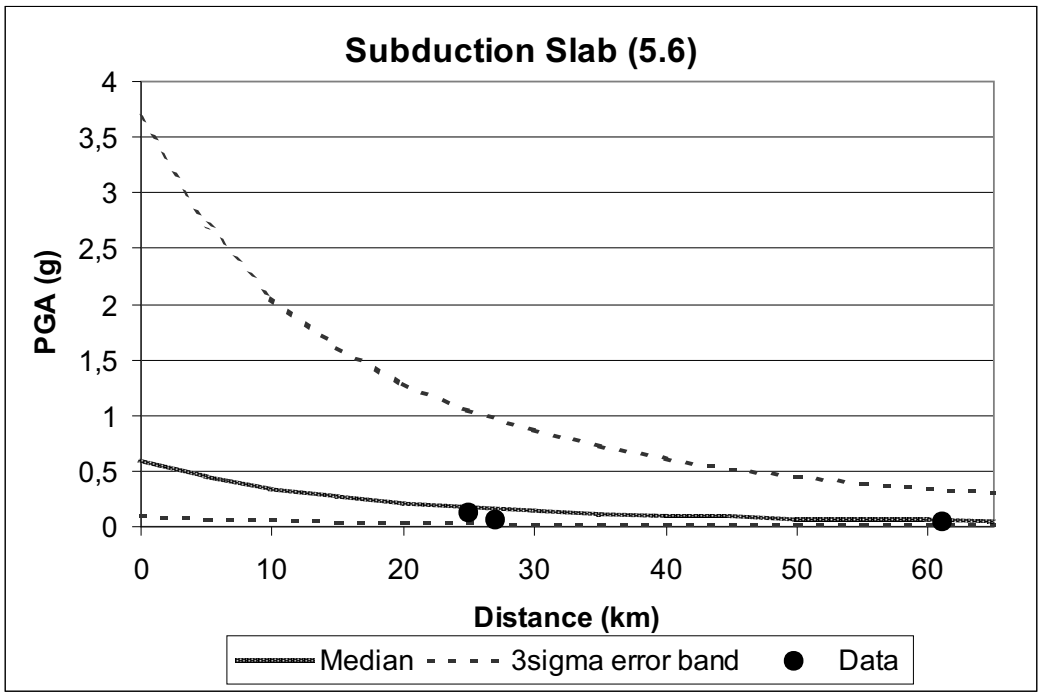

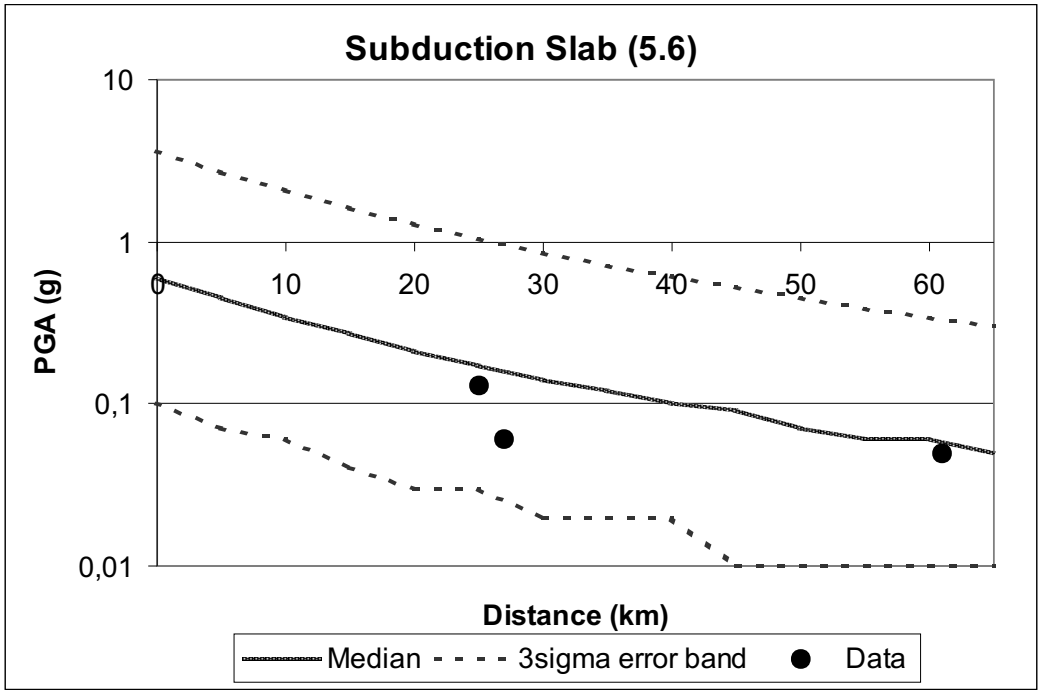

Figure B.12: Attenuation curve and test data for M=5.6, slip type: subduction slab.

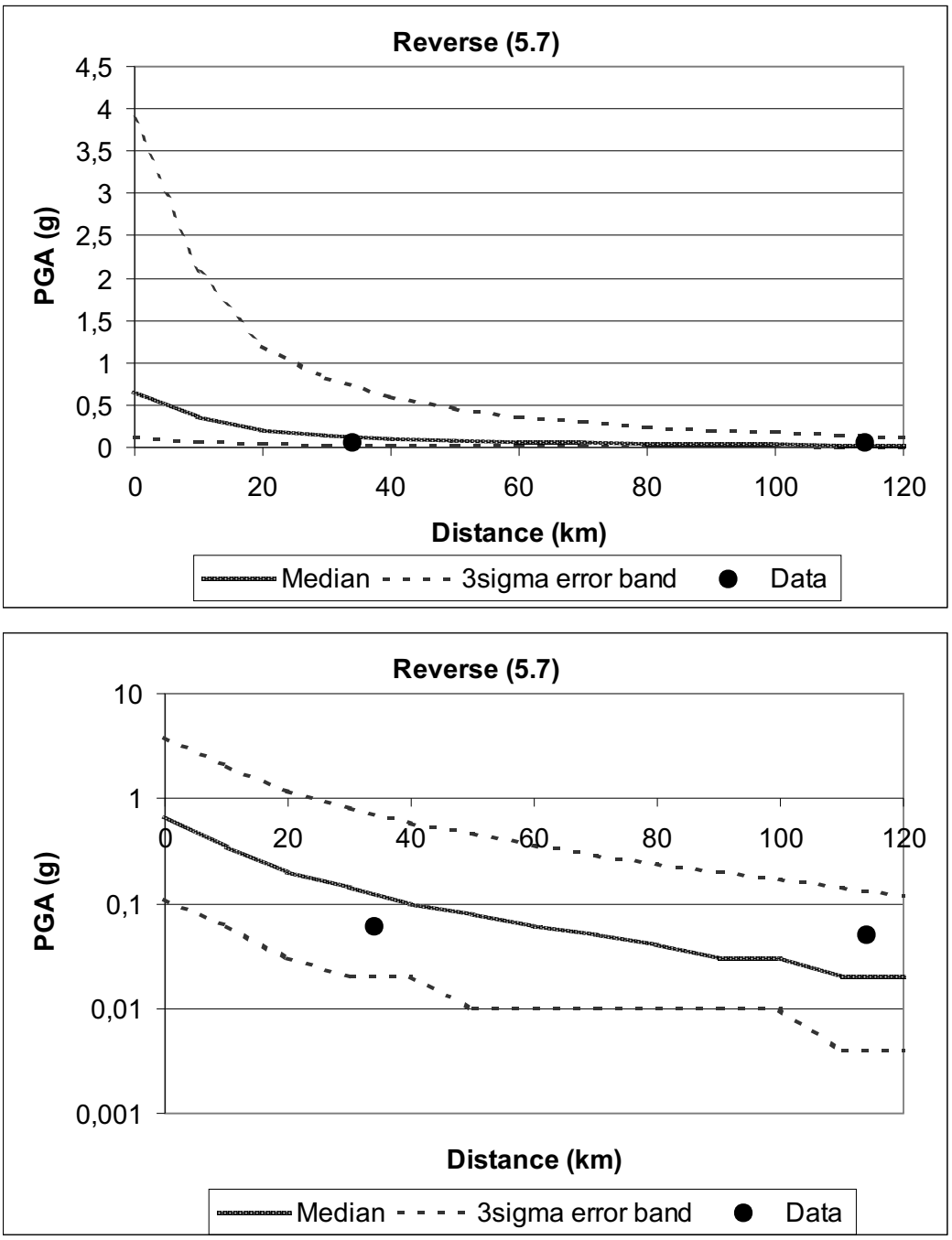

Figure B.13: Attenuation curve and test data for M=5.7, slip type: reverse.

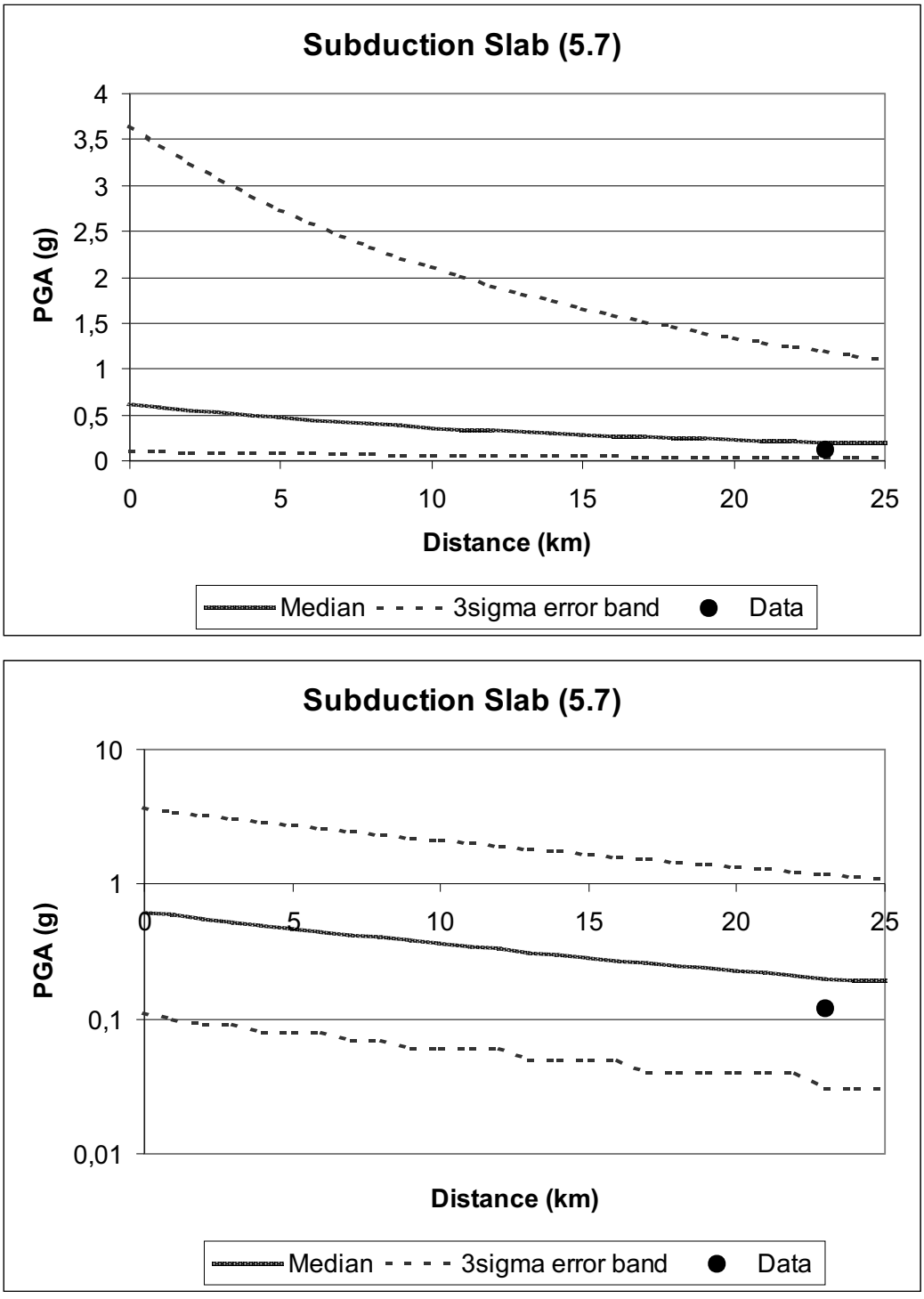

Figure B.14: Attenuation curve and test data for M=5.7, slip type: subduction slab.

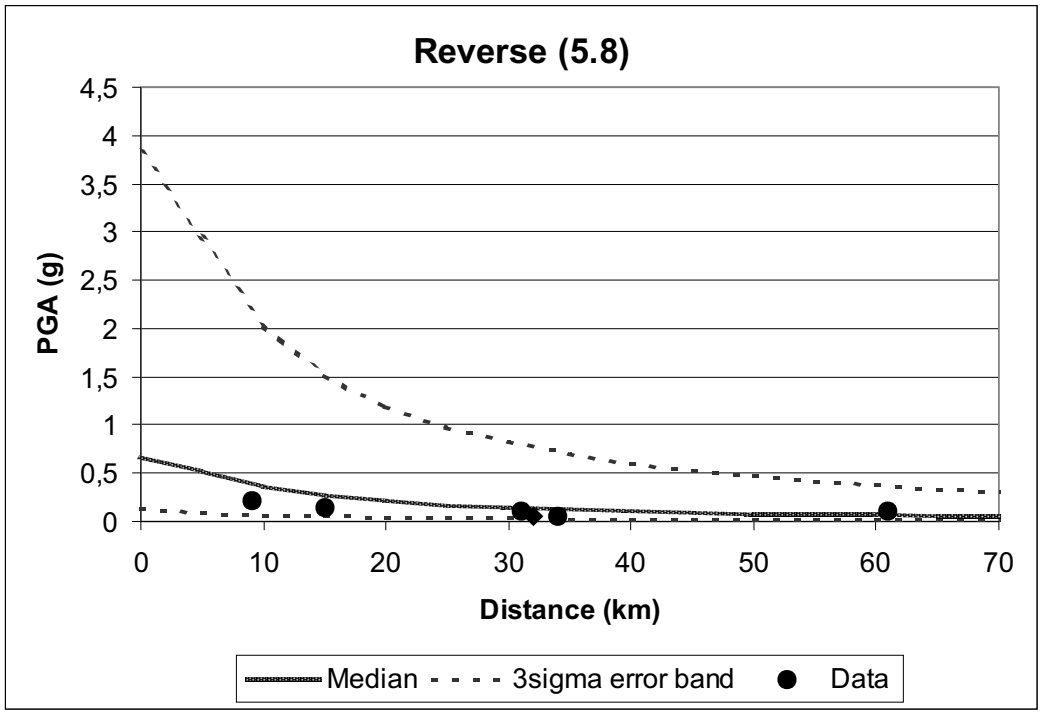

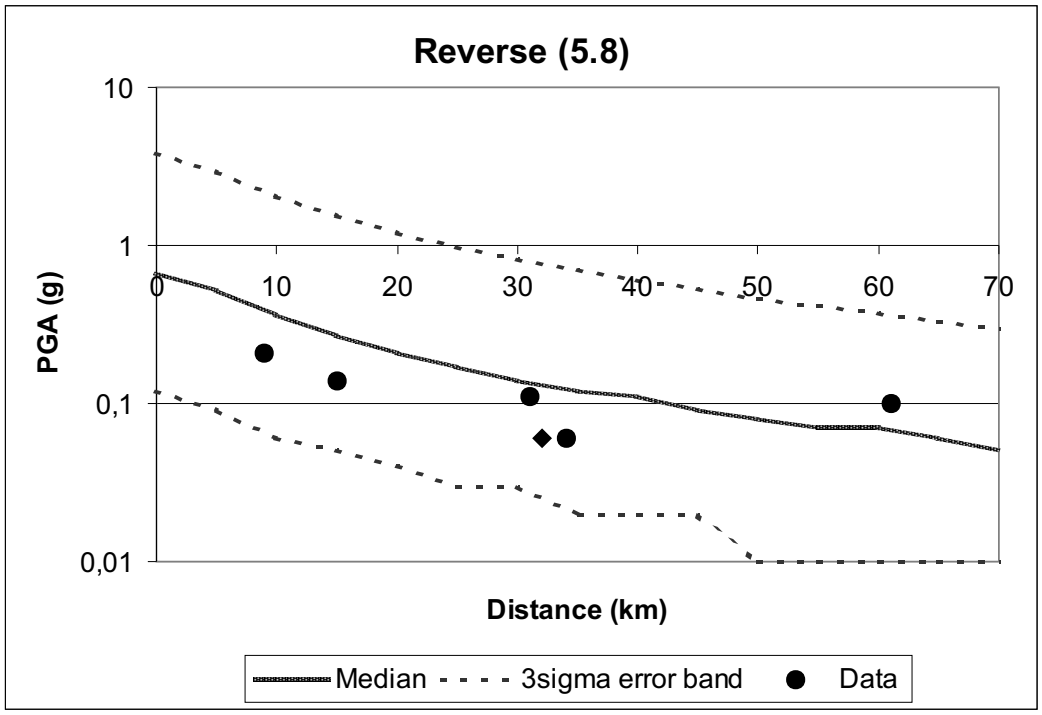

Figure B.15: Attenuation curve and test data for M=5.8, slip type: reverse.

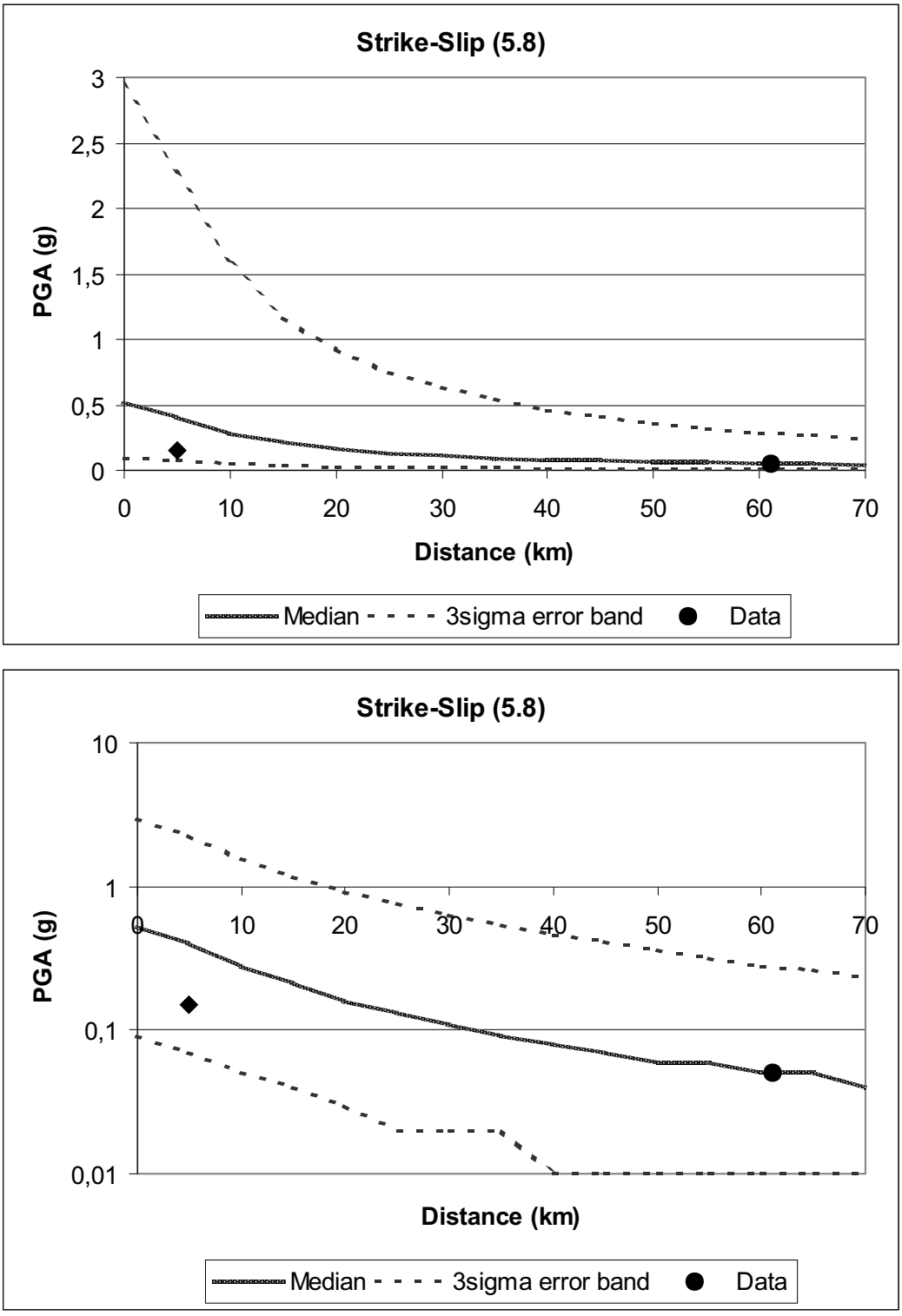

Figure B.16: Attenuation curve and test data for M=5.8, slip type: strike-slip.

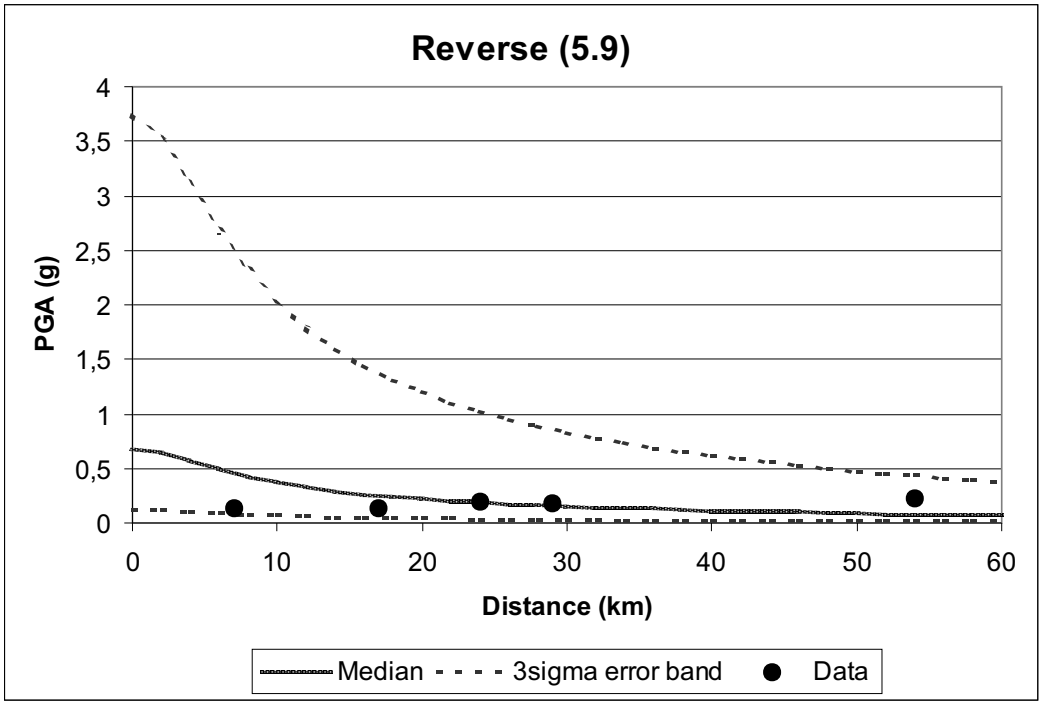

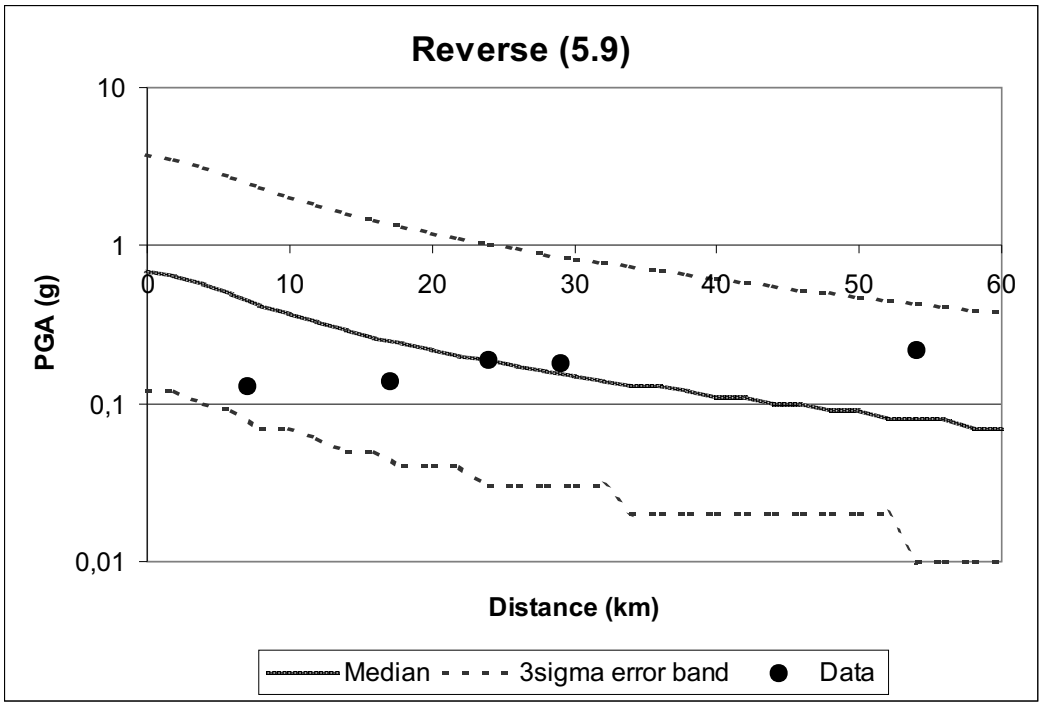

Figure B.17: Attenuation curve and test data for M=5.9, slip type: reverse.

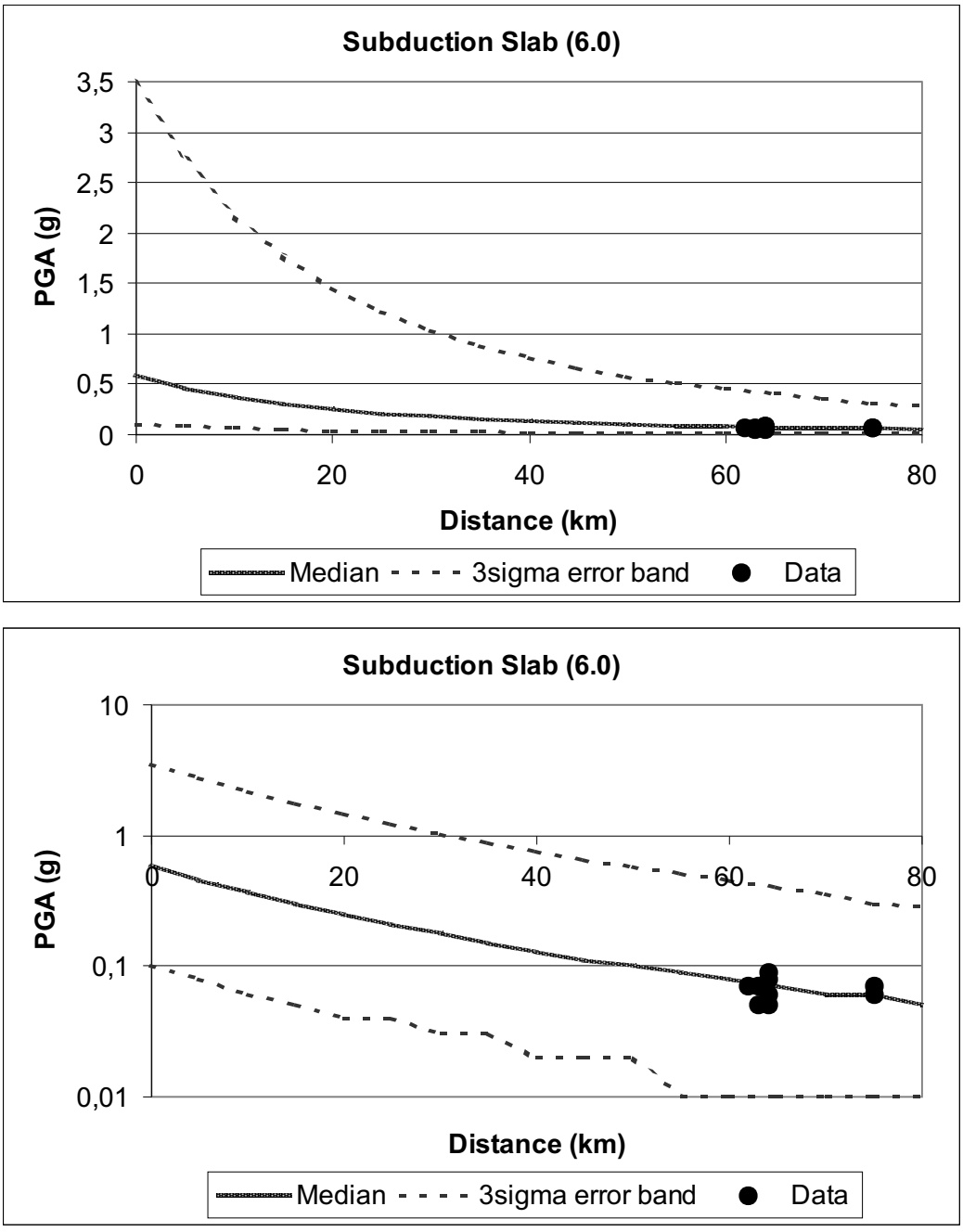

Figure B.18: Attenuation curve and test data for M=6.0, slip type: subduction slab.

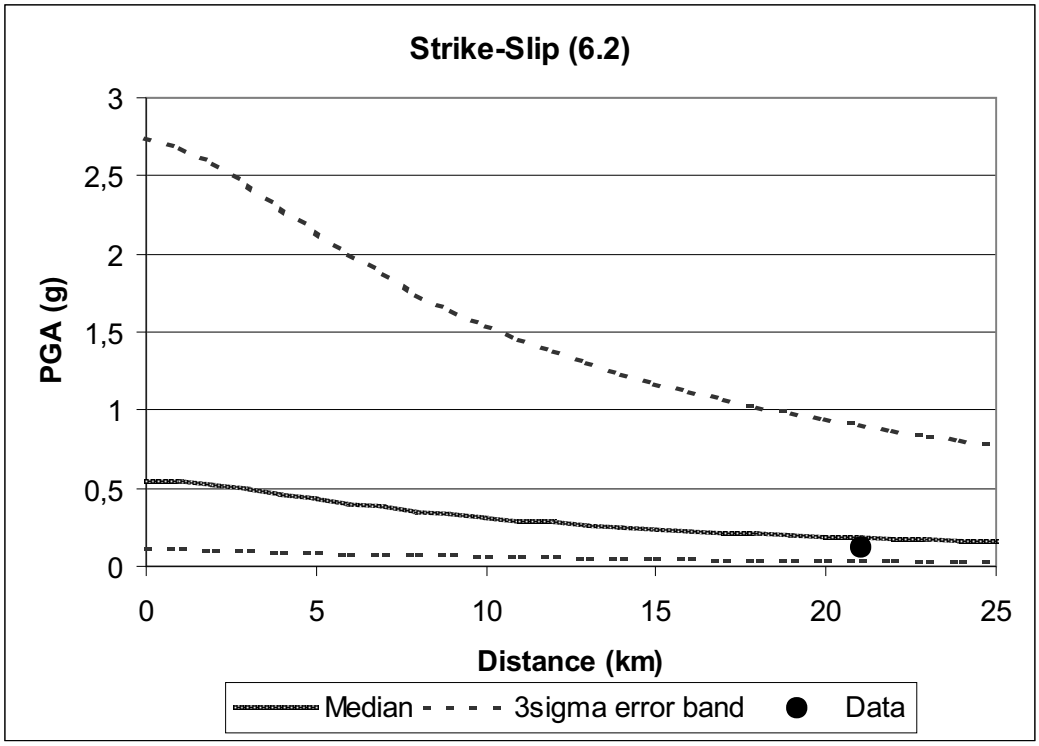

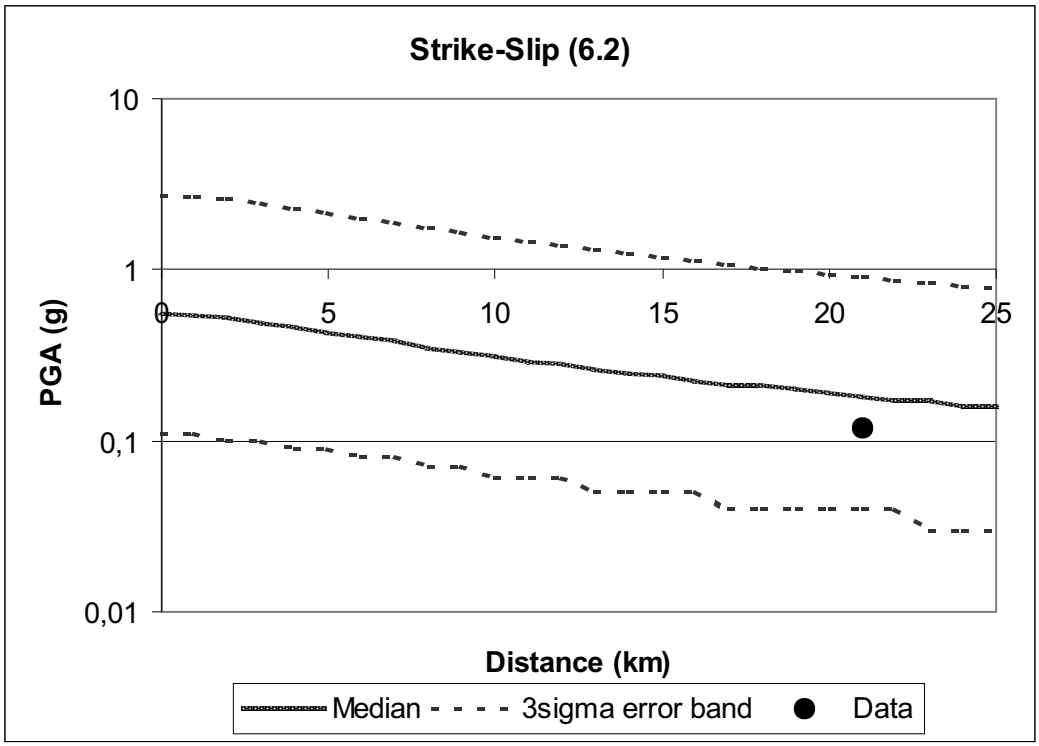

Figure B.19: Attenuation curve and test data for M=6.2, slip type: strike-slip.

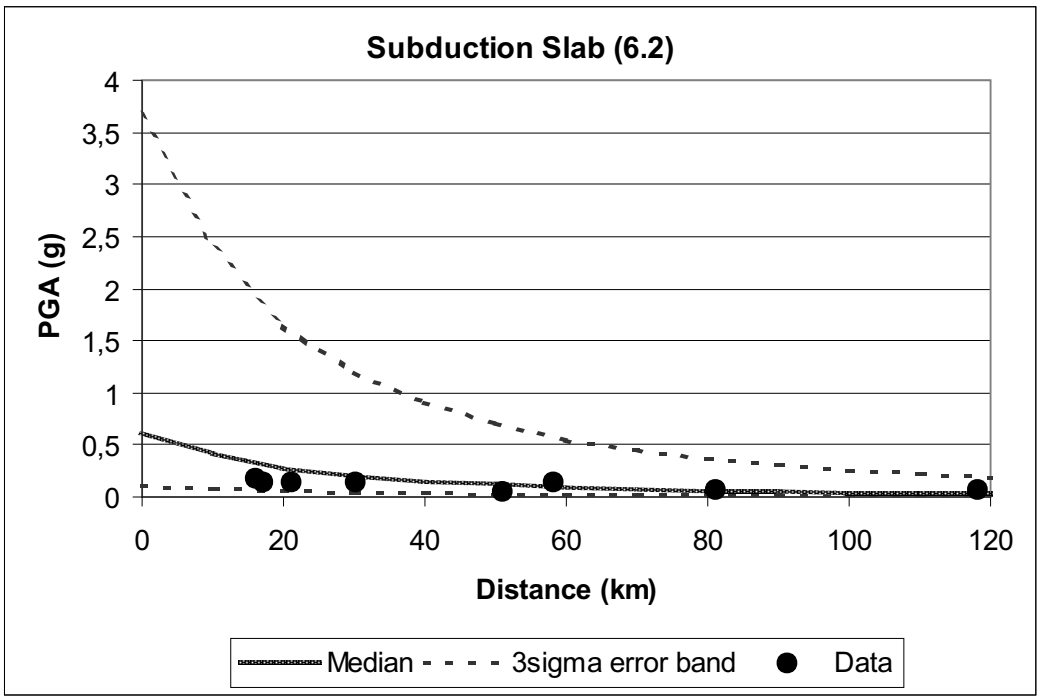

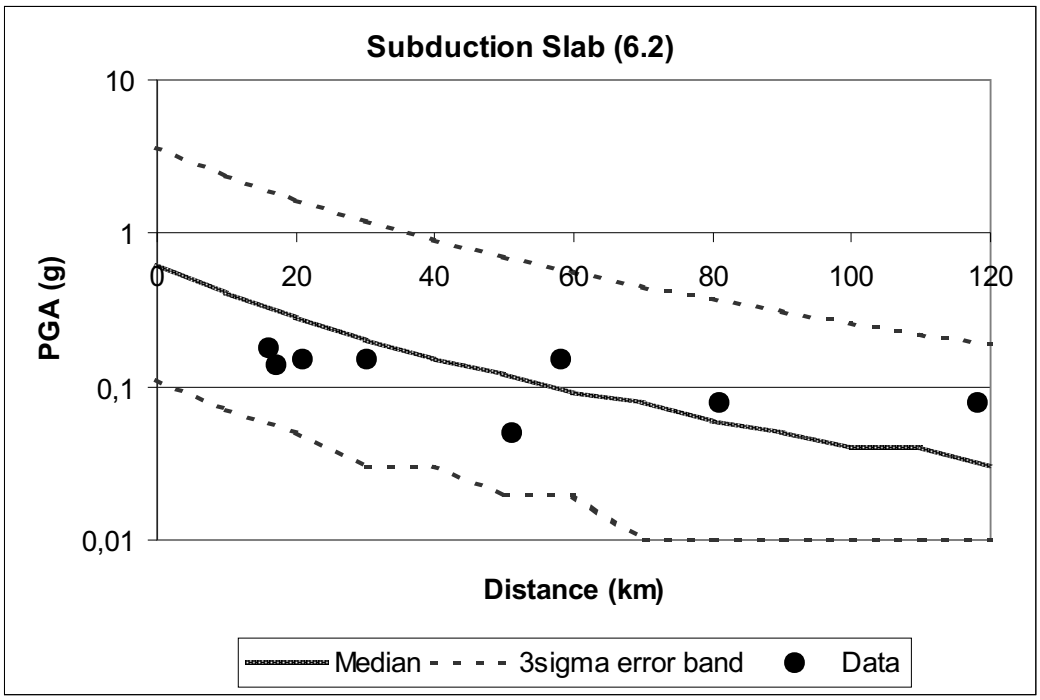

Figure B.20: Attenuation curve and test data for M=6.2, slip type: subduction slab.

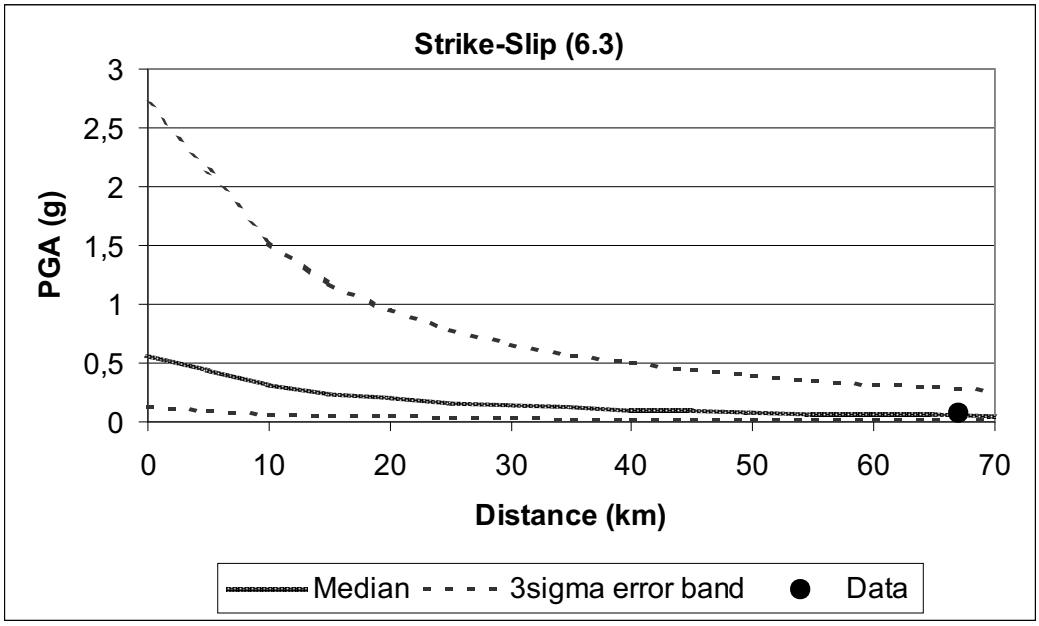

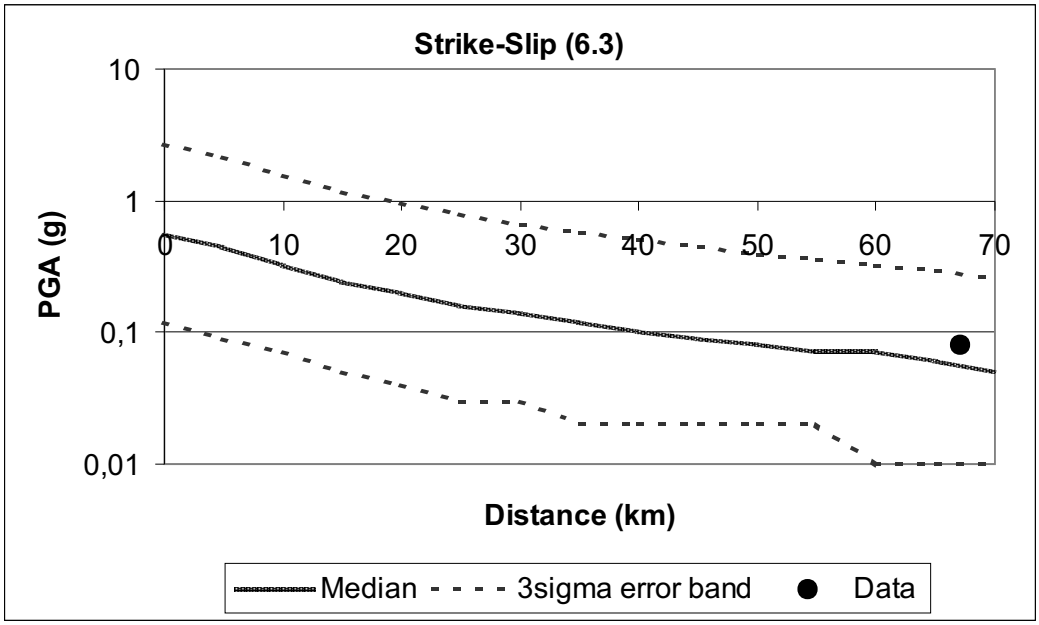

Figure B.21: Attenuation curve and test data for M=6.3, slip type: strike-slip.

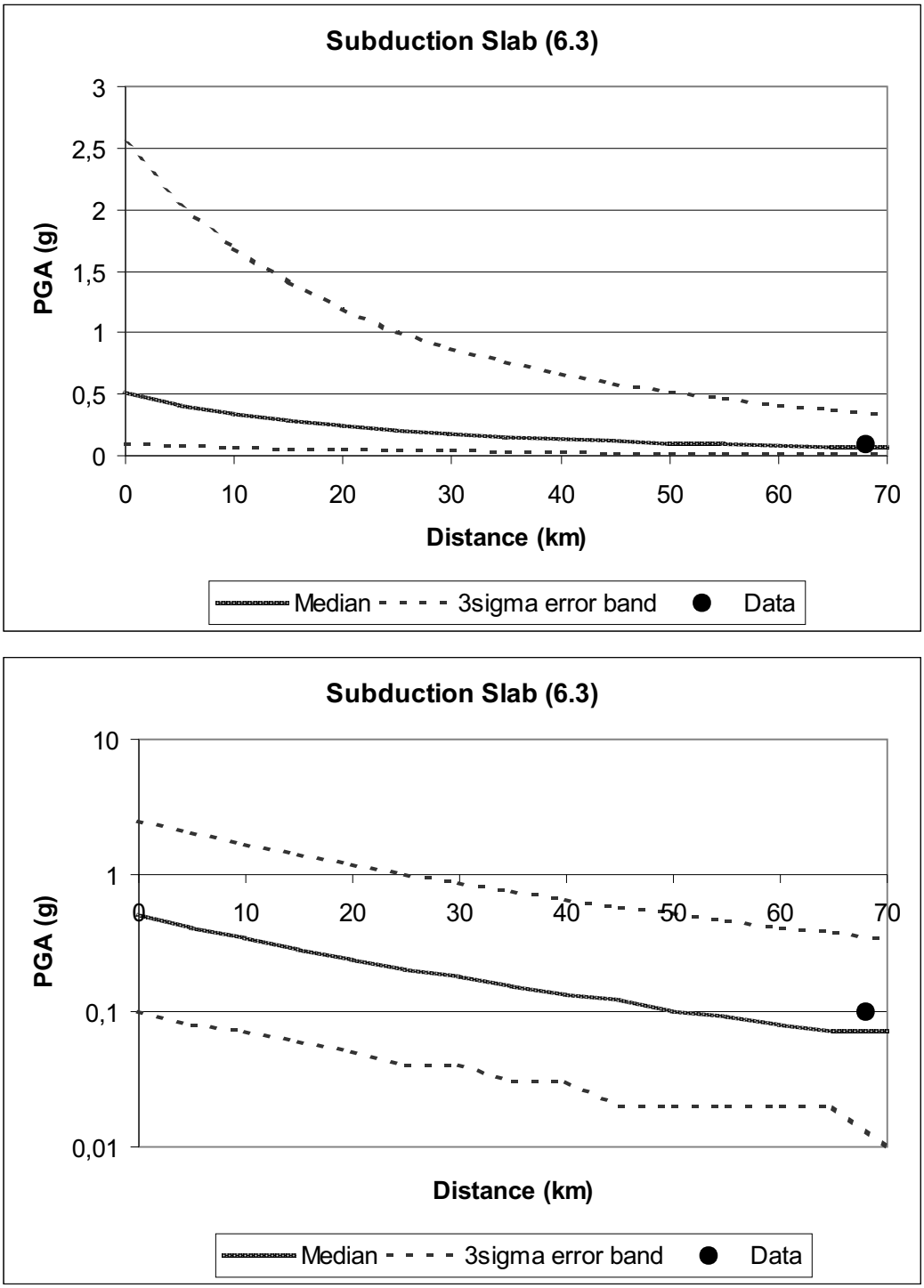

Figure B.22: Attenuation curve and test data for M=6.3, slip type: subduction slab.

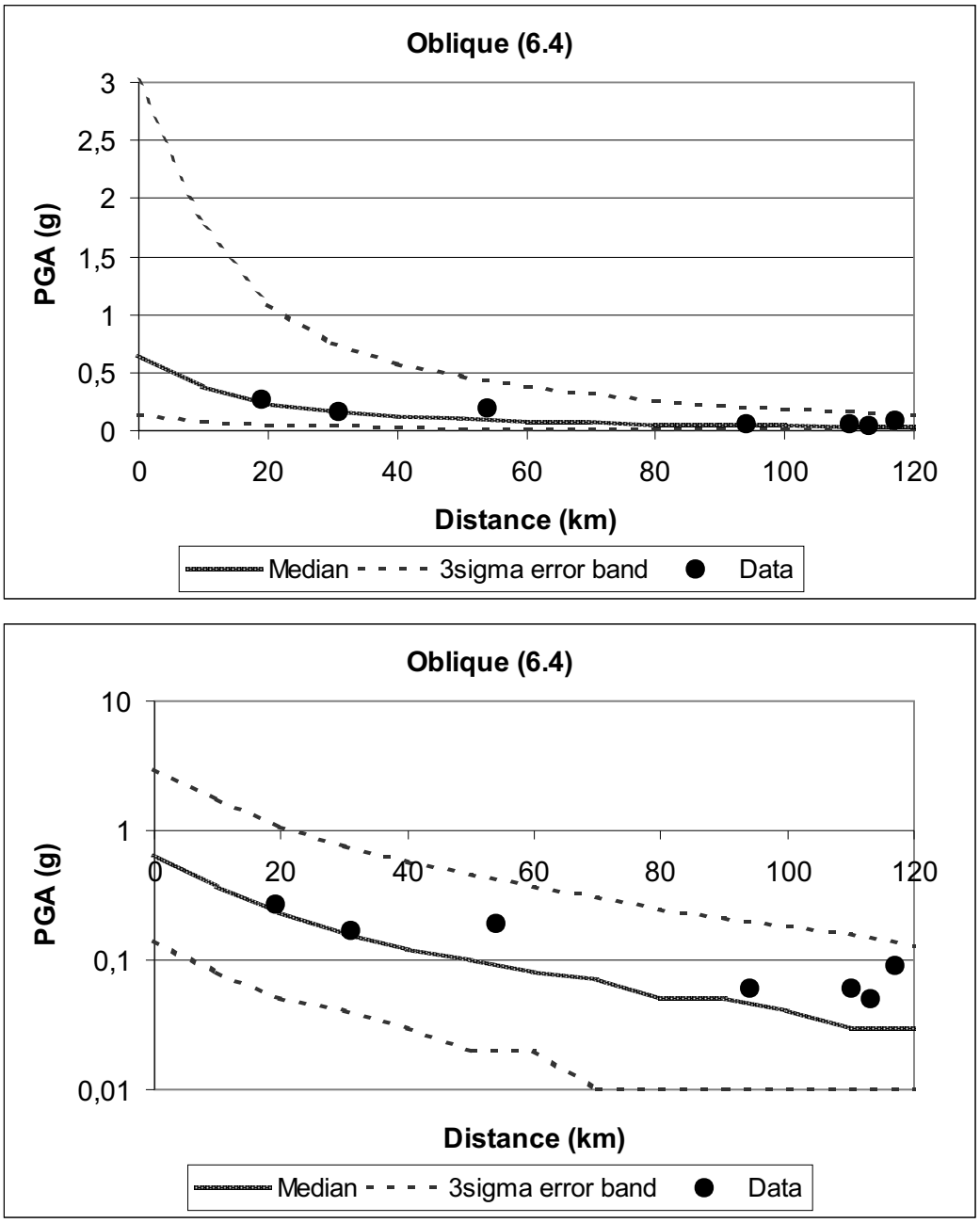

Figure B.23: Attenuation curve and test data for M=6.4, slip type: oblique.

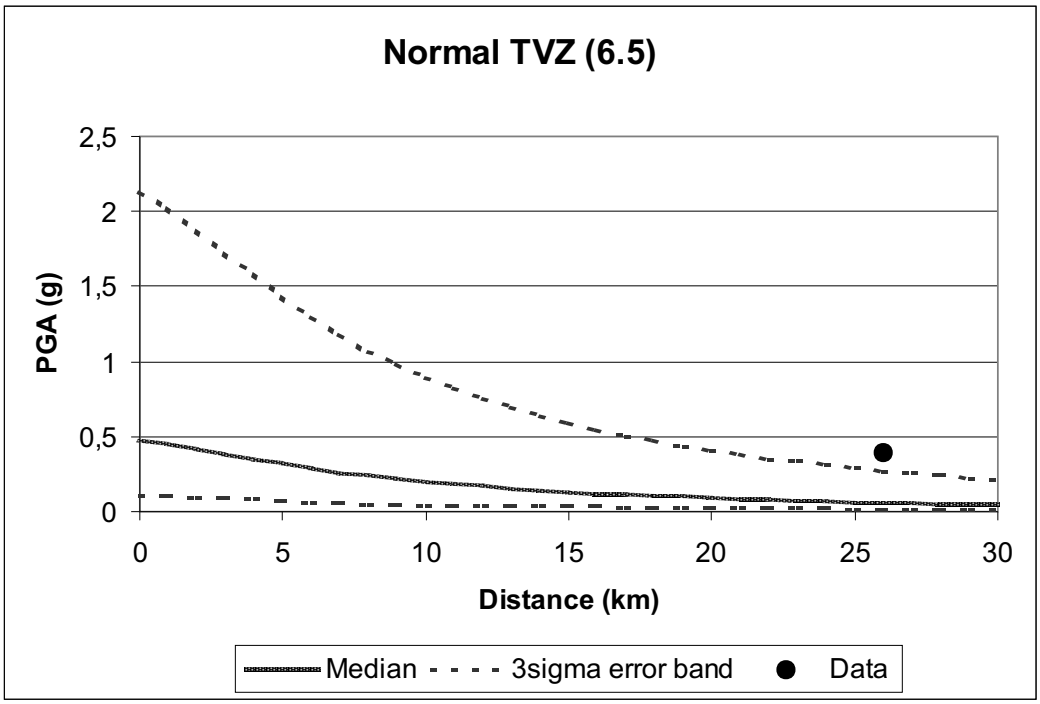

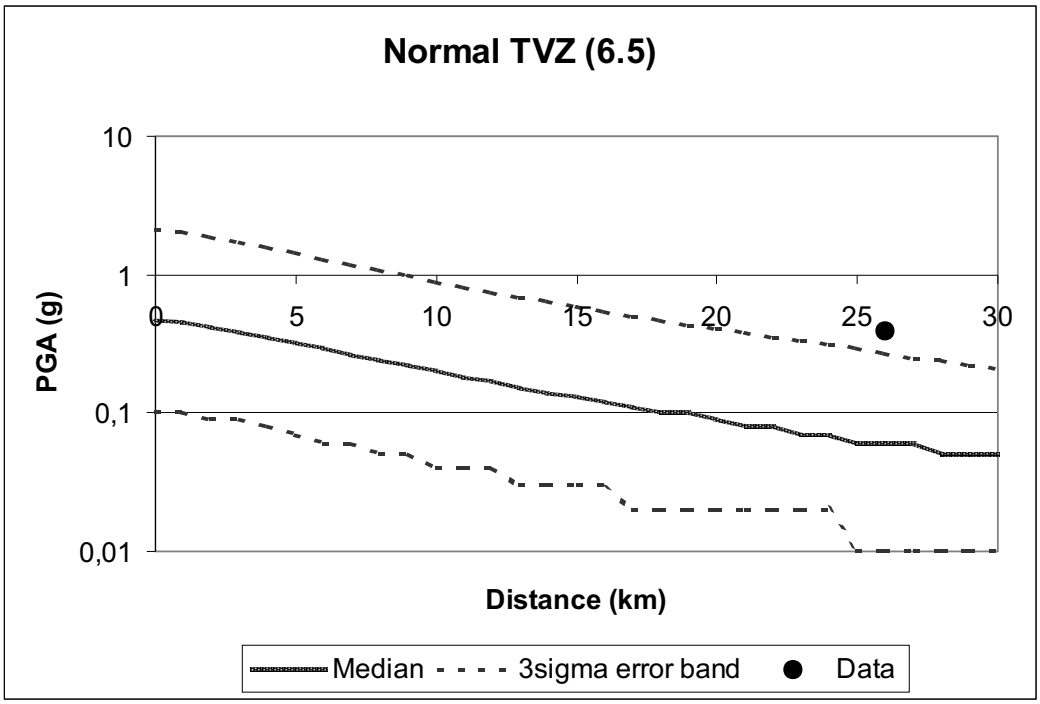

Figure B.24: Attenuation curve and test data for M=6.5, slip type: normal in TVZ.

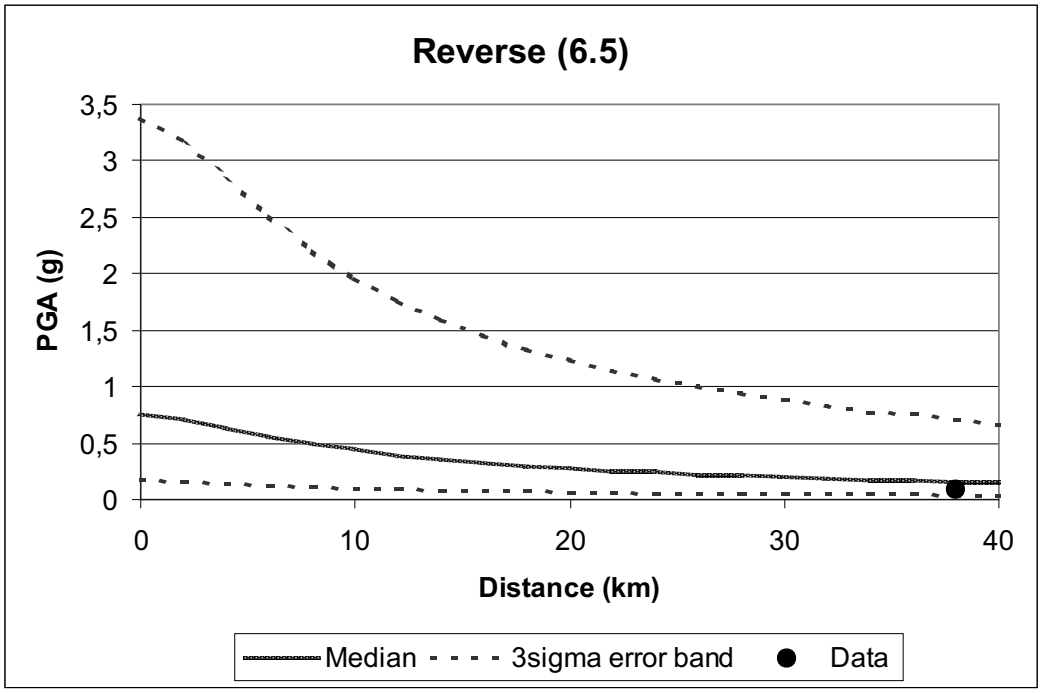

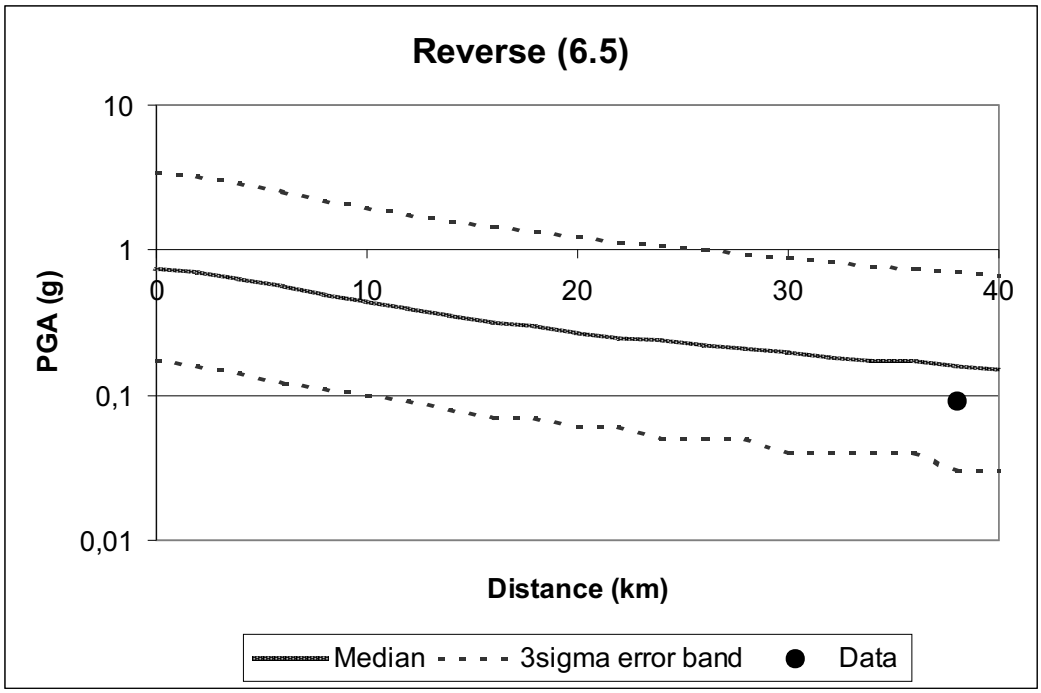

Figure B.25: Attenuation curve and test data for M=6.5, slip type: reverse.

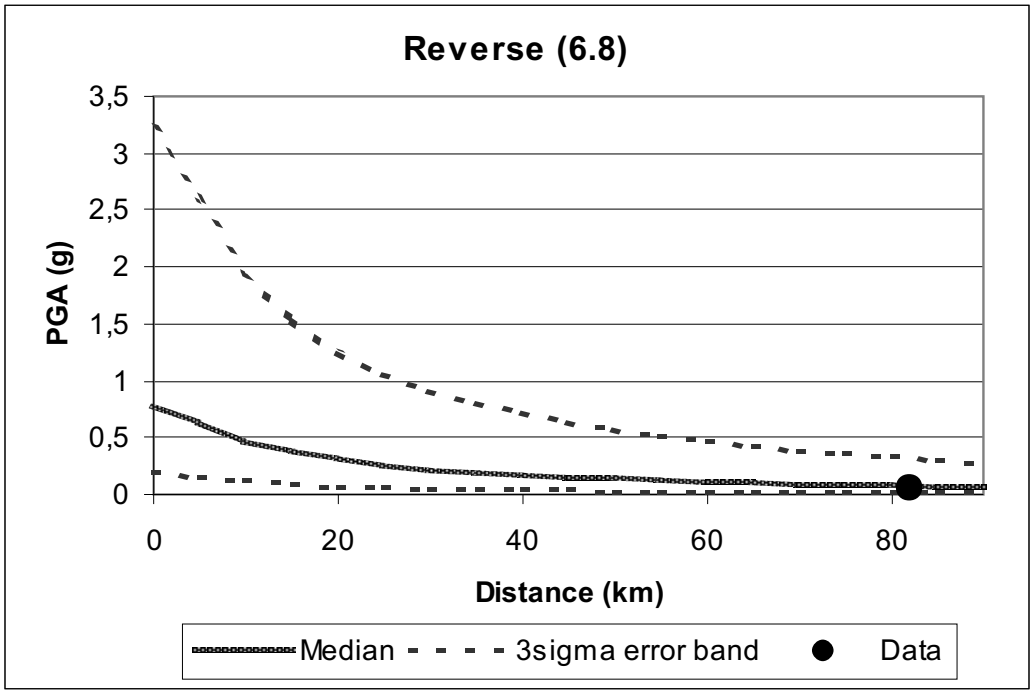

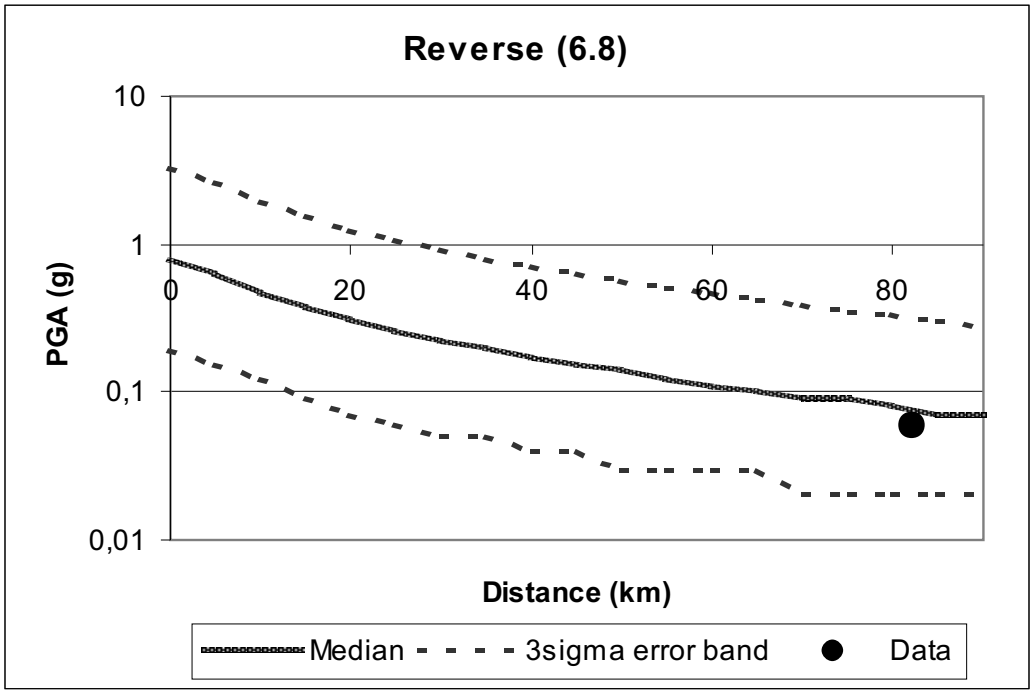

Figure B.26: Attenuation curve and test data for M=6.8, slip type: reverse.

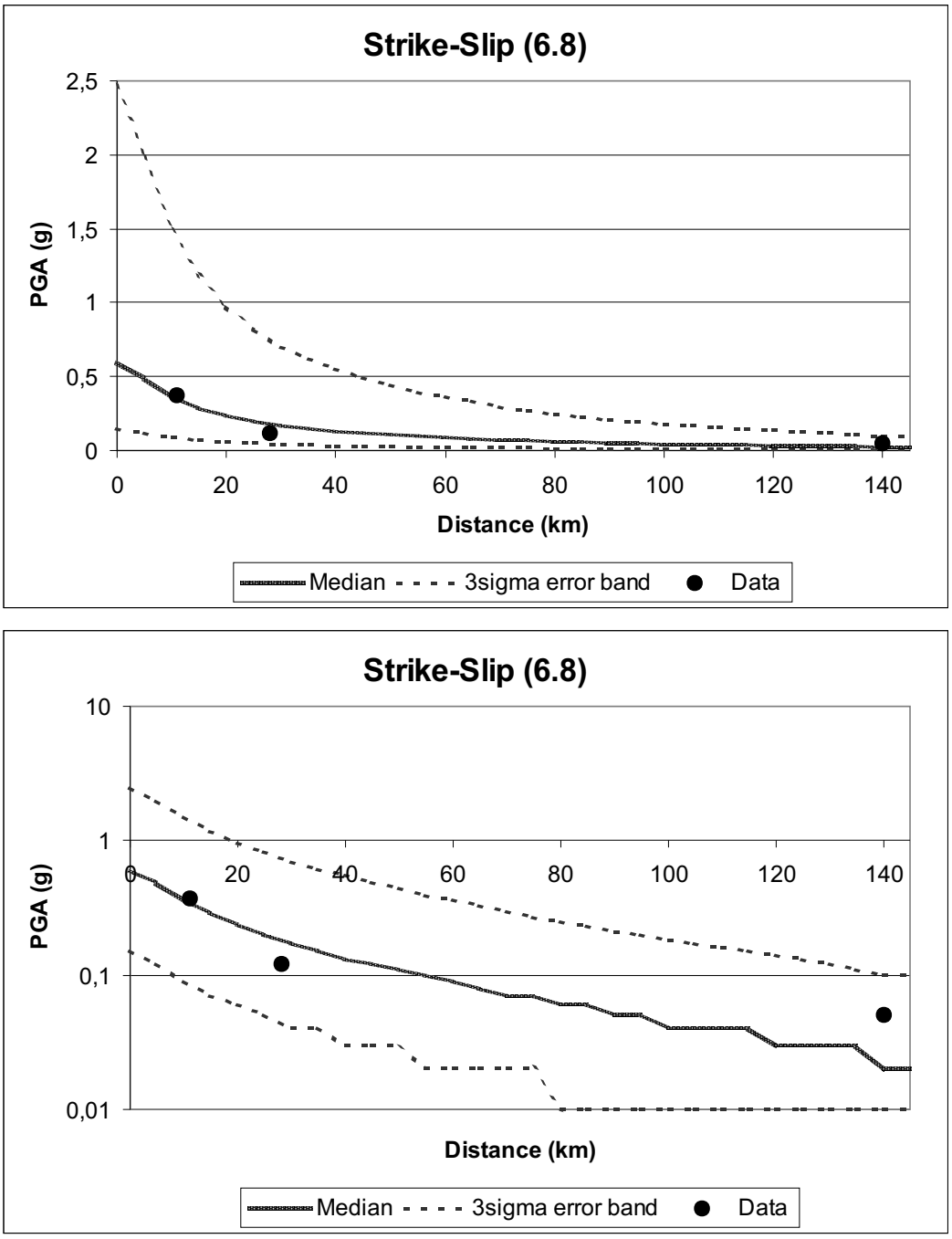

Figure B.27: Attenuation curve and test data for M=6.8, slip type: strike-slip.

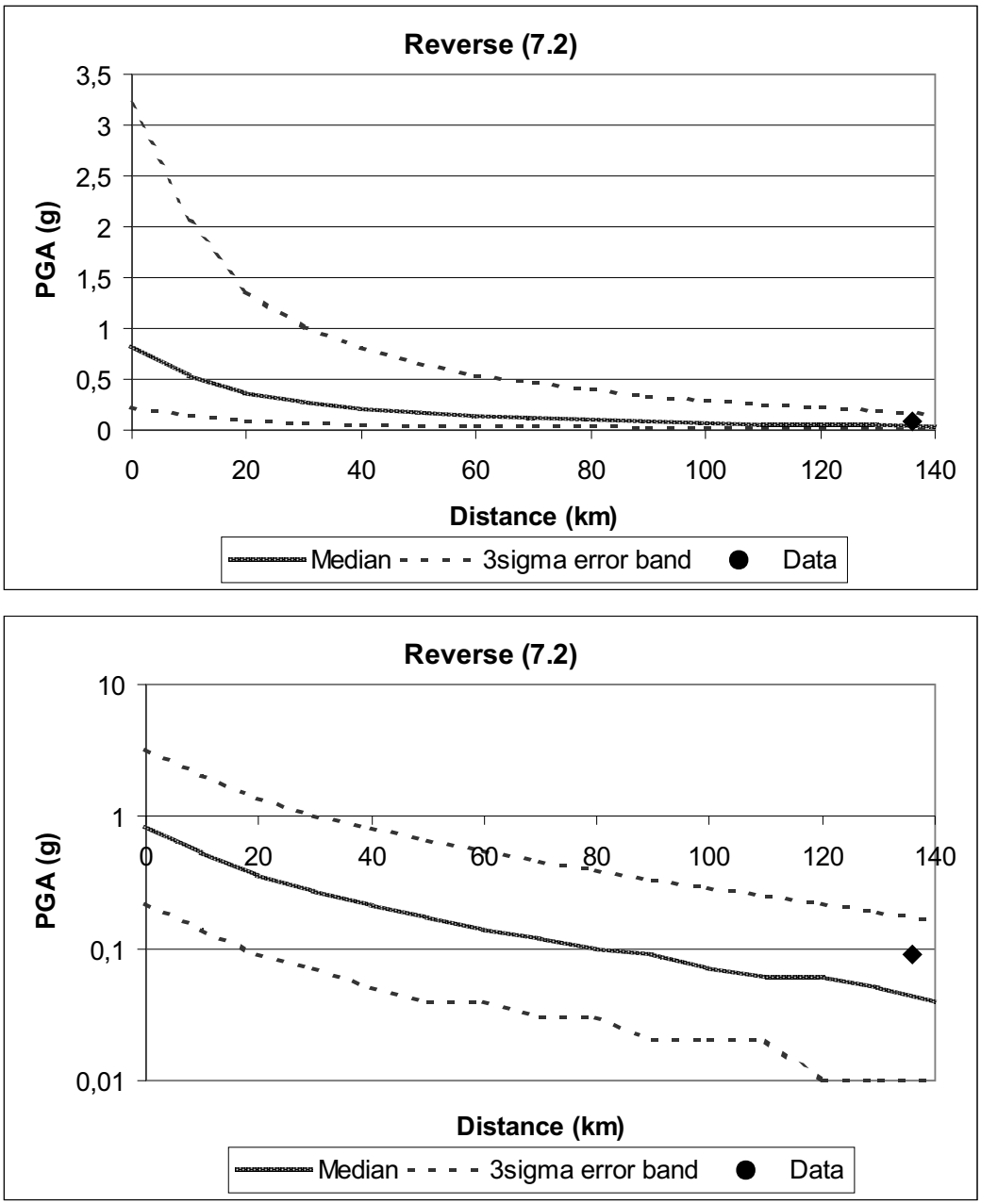

Figure B.28: Attenuation curve and test data for M=7.2, slip type: reverse.